WRAP MODEL DEVELOPMENT

In Support of

Final Dominguez Channel and Greater Los Angeles and Long Beach Harbor Waters Toxic Pollutants Total Maximum Daily Load

Final Report

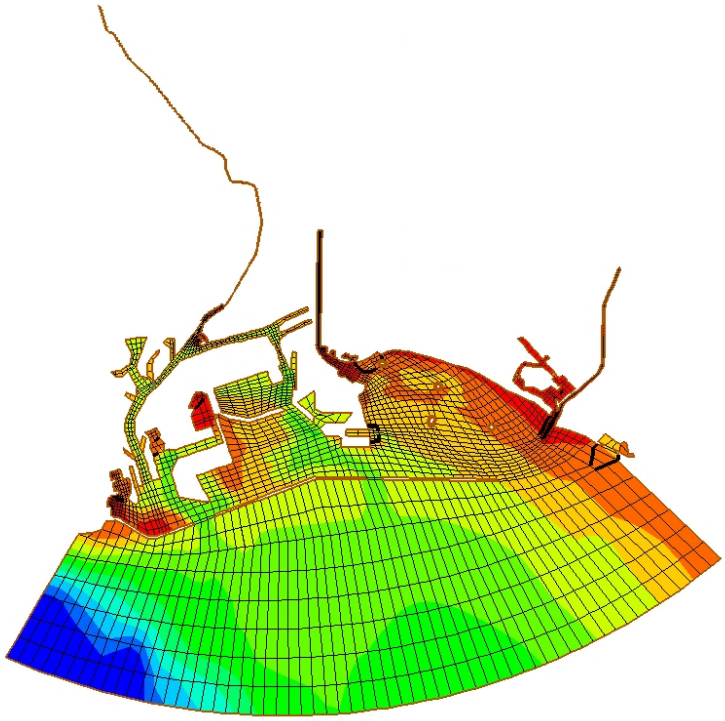

Prepared for

Port of Long Beach

Port of Los Angeles

Prepared by

Everest International Consultants, Inc.

EVEREST

February 2017

WRAP MODEL DEVELOPMENT

In Support of

Final Dominguez Channel and Greater Los Angeles and Long Beach Harbor Waters Toxic Pollutants Total Maximum Daily Load

Final Report

Prepared For

Port of Long Beach
4801 Airport Plaza Drive
Long Beach, CA 90815

Port of Los Angeles
425 South Palos Verdes Street
San Pedro, CA 90731

Prepared By

Everest International Consultants, Inc.
444 West Ocean Boulevard. Suite 1104
Long Beach, CA 90802

Contact: Ying Poon

Under Contract to

Anchor QEA
27201 Puerta Real, Suite 350
Mission Viejo, CA 92691

February 2017

TABLE OF CONTENTS

LIST OF FIGURES

LIST OF TABLES

LIST OF ACRONYMS AND ABBREVIATIONS

°C	degrees Celsius
3D	three-dimensional
ADCP	acoustic Doppler current profilers
BASINS	Better Assessment Science Integrating Point and Nonpoint Sources
BC	Ballona Creek
BPTCP	Bay Protection and Toxic Cleanup Program
CC	Coyote Creek
cm	centimeter
CP	Cabrillo Pier
CS	Consolidated Slip
CSM	Conceptual Site Model
DC	Dominguez Channel
DCEM	Dominguez Channel Estuary Model
DCEMS	Dominguez Channel Estuary Model Study
DDT	dichlorodiphenyltrichloroethane
DDX	dichlorodiphenyltrichloroethane-related compounds
DOC	dissolved organic carbon
EFDC	Environmental Fluid Dynamics Code
EPA	Environmental Protection Agency
FFT	Fast Fourier Transform
FH	Fish Harbor
f_{oc}	fraction organic carbon
hr	hour
HTWG	Harbor Technical Work Group
in	inch
K_{doc}	dissolved organic carbon partition coefficient
kg	kilogram

km	kilometer
K_{poc}	particulate organic carbon partition coefficient
L	liter
LA/LB Harbor	Los Angeles and Long Beach Harbor
LACDPW	Los Angeles County Department of Public Works
LAR	Los Angeles River
LARE	Los Angeles River Estuary
LDL	Low Detection Limit
LSPC	Loading Simulation Program in C++
m	meter
MDL	Minimum Detection Limit
mg	milligram
MLLW	mean lower low water
mm	millimeter
MSC	Main Ship Channel (or Main Channel)
ND	Non-detect
NEIBP	North Energy Island Borrow Pit
ng	nanogram
NHDPlus	National Hydrography Dataset Plus
NOAA	National Oceanic Atmospheric Administration
NOS	National Ocean Service
NPDES	National Pollutant Discharge Elimination System
NTDE	National Tidal Datum Epoch
PCB	polychlorinated biphenyl
PE	polyethylene
POC	particulate organic carbon
POLA	Port of Los Angeles
POLB	Port of Long Beach
Ports	Port of Long Beach and Port of Los Angeles
PORTS®	Physical Oceanographic Real-Time Systems

ppb	parts per billion
PSU	Practical Salinity Units
R^2	correlation coefficient
RWQCB	Regional Water Quality Control Board
s (or sec)	second
SARWQCB	Santa Ana Regional Water Quality Control Board
SCCWRP	Southern California Coastal Water Research Project
SEIBP	South Energy Island Borrow Pit
SGR	San Gabriel River
SGRE	San Gabriel River Estuary
SPE	Solid Phase Extraction
SPME	solid-phase microextraction
SQO	Sediment Quality Objective
SRB	Scientific Review Board
SWRCB	State Water Resources Control Board
TDDX	total dichlorodiphenyltrichloroethane-related compounds (4,4'-DDT, 4,4'-DDE, 4,4'-DDD, 2,4'-DDT, 2,4'-DDE, and 2,4'-DDD)
TIWRP	Terminal Island Water Reclamation Plant
TMDL	total maximum daily load
TOC	total organic carbon
TPCB	total polychlorinated biphenyl
TSS	total suspended solids
ug	microgram
USACE	U.S. Army Corps of Engineers
WDR	Waste Discharge Requirements
WRAP	Water Resources Action Plan
yr	year

1. INTRODUCTION

1.1 BACKGROUND

The Total Maximum Daily Load for Toxic Pollutants in Dominguez Channel and Greater Los Angeles and Long Beach Harbor Waters (Harbor Toxics TMDL) sets water, sediment, and fish tissue targets designed to protect beneficial uses and aquatic life (RWQCB 2011). The Harbor Toxics TMDL applies to impaired receiving waterbodies of the Dominguez Channel (DC), Los Angeles and Long Beach Harbor (LA/LB Harbor), Los Angeles River Estuary (LARE), and Eastern San Pedro Bay, as shown in Figure 1.1. The Harbor Toxics TMDL, which became effective March 2012, includes discharge limits for total polychlorinated biphenyls (TPCB) and total dichlorodiphenyltrichloroethane-related compounds (TDDX), both of which are bioaccumulative compounds. Phase I of the implementation plan concludes with a TMDL re-opener that includes an option for adjustments to the TMDL based on updated information or new State policies. This TMDL re-opener is scheduled for 2018, at which time the Los Angeles Regional Water Quality Control Board (RWQCB) may consider special studies completed by stakeholders, including those described in these report, to support refinement of source assessments, allocations, and targets of the TMDL. Examples of special studies include stressor identification studies, air deposition studies, evaluation of watershed loadings to the Harbor, sediment and fish tissue linkage studies, and additional monitoring studies of harbor waters.

The Port of Long Beach (POLB) and Port of Los Angeles (POLA) (or Ports) are developing a TMDL compliance approach that will utilize logistically feasible management options to comply with the Harbor Toxics TMDL, as well as to provide technically sound support for proposed changes as part of the TMDL re-opener. In October 2012, the Ports selected a team of consultants led by Anchor QEA to design and implement tasks to develop a TMDL compliance strategy and special studies to be considered during the TMDL re-opener, and to support TMDL revisions and compliance requirements. The Anchor QEA team is working with oversight from the Harbor Technical Work Group (HTWG). Members of the HTWG include the POLB, POLA, RWQCB, State Water Resources Control Board (SWRCB), and Southern California Coastal Water Research Project (SCCWRP). The HTWG has reviewed and approved the methodologies used for the calibration of the Water Resources Action Plan (WRAP) Model, which is the focus of this report.

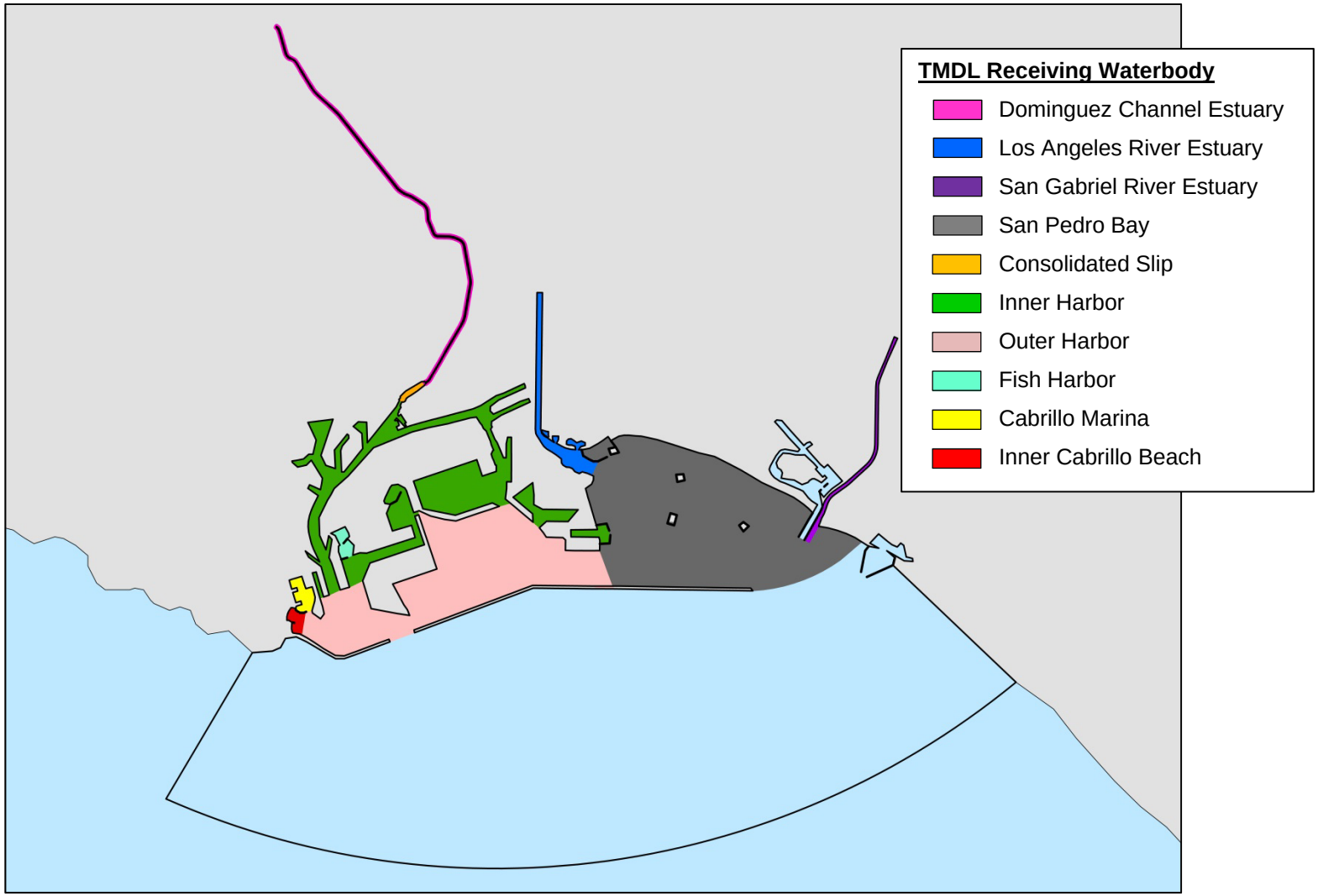

Figure 1.1 Harbor Toxics TMDL Receiving Waterbodies

The LA/LB Harbor is a unique, hydrodynamically complex system with one of the world's largest combined port operations, a confluence of urban discharges from several major watersheds, and widespread distribution of legacy pollutants. In order to balance potential ecological benefits and financial costs, the Ports' compliance approach includes development of a site-specific model to understand chemical fate and transport in the harbor. The site-specific model is also a part of a proposed Sediment Quality Objective (SQO) indirect effects Tier III assessment and consists of a chemical fate and transport model linked with a food chain bioaccumulation model (Linked Model) that will be used to evaluate potential management scenarios to attain TMDL targets.

A schematic of the Linked Model is provided in Figure 1.2. This report documents the development and calibration of the site-specific hydrodynamic, sediment transport and chemical fate model for the LA/LB Harbor known as the WRAP Model. As illustrated in Figure 1.2, outputs from the WRAP Model are used as inputs to the bioaccumulation model component of the Linked Model. A companion report documents the development and calibration of a site-specific bioaccumulation model for the LA/LB Harbor (Anchor QEA 2016).

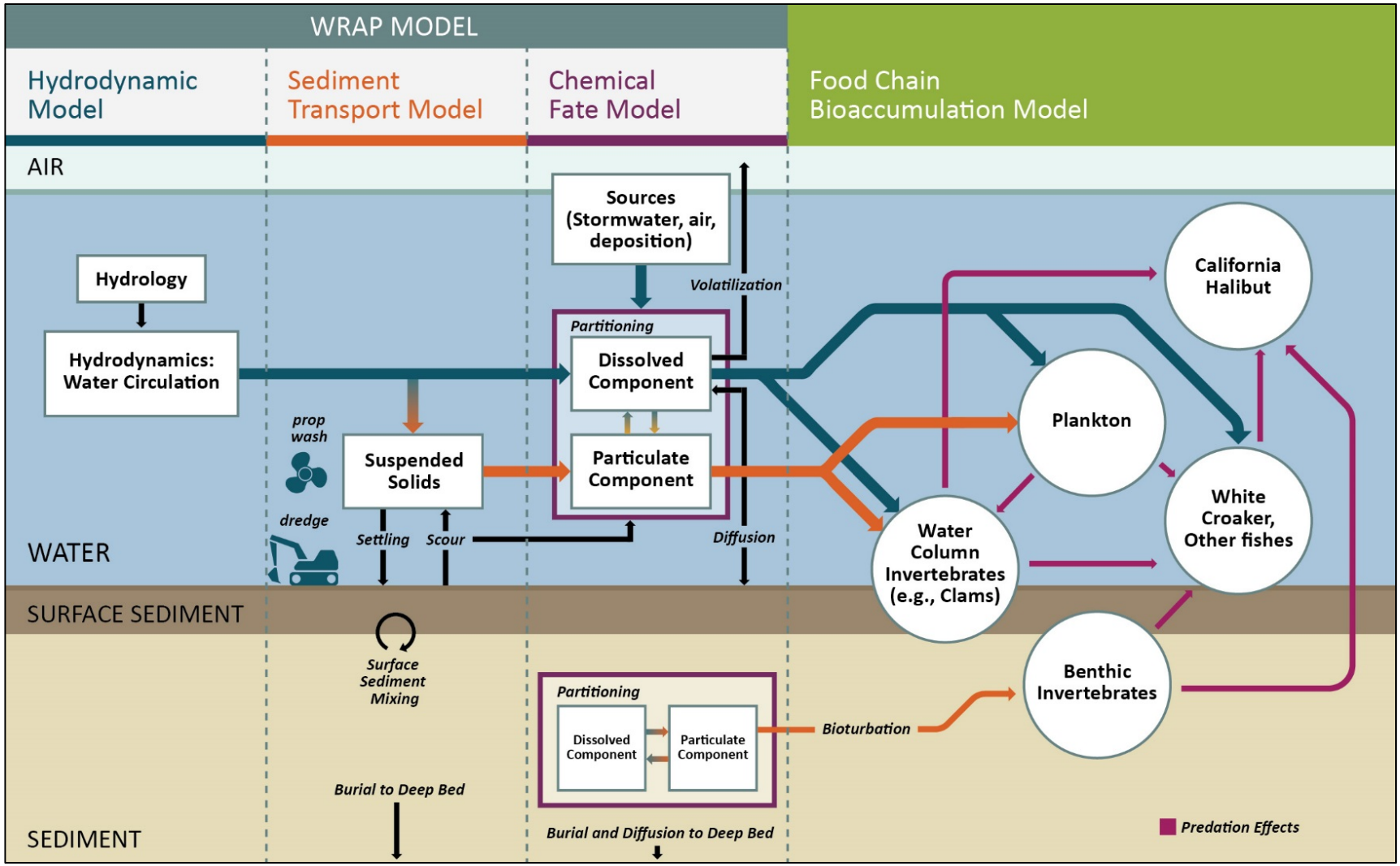

Figure 1.2 Linked Model Schematic

1.2 PURPOSE AND OBJECTIVES

The WRAP Model is a three-dimensional (3D) hydrodynamic, sediment transport, and chemical fate model of the LA/LB Harbor and San Pedro Bay. The model was calibrated to accurately simulate the complex hydrodynamic and transport conditions in the harbor and account for the harbor layout, exchange between TMDL receiving waterbodies, and anthropogenic mechanisms of transport. Ultimately, the WRAP Model will be linked with a bioaccumulation model, generating long-term organic chemical (TPCB and TDDX) water column and sediment bed concentrations as input to the bioaccumulation model. It is anticipated that the WRAP Model will be used in conjunction with the bioaccumulation model to evaluate TMDL compliance scenarios, as well as for technical support in the TMDL re-opener.

The WRAP Model development and calibration objectives included:

- Obtain and assemble prior hydrodynamic and water quality data for model calibration
- Conduct special studies to collect necessary data for developing and calibrating the WRAP Model, particularly for organic chemicals
- Update the previously developed WRAP Model with existing and anticipated changes to the harbor layout (e.g. new land areas and channel deepening)
- Confirm that previously calibrated hydrodynamic and mixing parameters still apply with the updated harbor layout
- Update WRAP Model capabilities to include volatilization of organic chemicals and propwash effects on sediment resuspension
- Calibrate WRAP Model for sediment transport
- Calibrate WRAP Model for organic chemicals (TPCB and TDDX)
- Develop methodology to estimate organic chemical loadings to LA/LB Harbor from upstream watersheds
- Provide linkage of organic chemical concentrations for bioaccumulation model

1.3 REPORT OVERVIEW

The WRAP Model development was based on updating an earlier version of the model to include the fate and transport of organic chemicals. A brief history of the WRAP Model development, model updates and model setup are presented in Section 2. Characterization of organic chemical loadings to the LA/LB Harbor and San Pedro Bay is important for the evaluation of potential TMDL management scenarios using the linked WRAP Model and bioaccumulation model. Section 3 provides a detailed discussion on the data and methodology used to estimate organic chemical loadings to the harbor from upstream watersheds. The model calibration was conducted based on the best available data from

multiple prior and new studies to provide the greatest spatial coverage and coverage of both dry and wet weather conditions. The approach for calibrating the WRAP Model is provided in Section 4. Overall, the calibration proceeded in the following sequence: hydrodynamics, mixing, sediment transport, and chemical fate. The hydrodynamic calibration, discussed in Section 5, evaluates the WRAP Model capabilities to simulate water levels and velocities throughout the harbor system. For the mixing calibration described in Section 6, the WRAP Model was evaluated based on salinity and dye concentration simulations in the harbor. For the sediment transport calibration discussed in Section 7, the WRAP Model was evaluated based on sediment deposition. A summary of the chemical fate calibration based on organic chemical water column concentrations is provided in Section 8. Section 9 examines the sensitivity of model-predicted concentrations to model parameters, as well the uncertainty in model inputs to model predictions. Lastly, a summary of the WRAP Model development and the linkage of the WRAP Model to the bioaccumulation model is provided in Section 10.

2. WRAP MODEL DEVELOPMENT AND SETUP

2.1 DEVELOPMENT HISTORY

The predecessor of the WRAP Model was the Dominguez Channel Estuary Model (DCEM) which was developed as part of the DCEM Study conducted by the POLA through a Proposition 13 Grant from the SWRCB. The DCEM Study was conducted from September 2004 through August 2006 to develop and calibrate a hydrodynamic and water quality model (referred to as the DCEM) to predict water elevations, velocities, and pollutant transport in the estuarine portion of the DC. The DCEM Study involved coordination and oversight from the POLA, RWQCB, U.S. Environmental Protection Agency (EPA), and a Scientific Review Board (SRB). The SRB was comprised of members from academia, consulting professionals, and federal and local government agencies. The DCEM Study included an extensive, one-year field program to collect data for the DCEM calibration. The DCEM was calibrated and verified for water elevations, velocities, salinity, dye, total suspended solids (TSS), and metals (Everest 2007). At the time that the DCEM was developed, it was anticipated that the RWQCB would utilize the DCEM for development and implementation of the TMDL for the LA/LB Harbor. However, a separate receiving water model was used for the Harbor Toxics TMDL, though both models use the same Environmental Fluid Dynamics Code (EFDC) modeling platform.

In 2009, the Ports collaborated on an effort to develop the WRAP aimed at protecting and improving water and sediment quality in order to achieve their respective environmental policy goals. The DCEM was updated to provide the Ports with a tool to understand existing harbor circulation and transport conditions in the LA/LB Harbor, as well as to evaluate effectiveness of control measures proposed in the WRAP (POLA and POLB 2009). The initial WRAP Model development expanded the DCEM and refined the model grid in the harbor, San Pedro Bay, LARE, and San Gabriel River Estuary (SGRE). After the updates to the grid resolution and bathymetry data, the WRAP Model was verified with hydrodynamic and water quality data from other areas of the harbor and San Pedro Bay. The WRAP Model was also verified for sediment transport based on a sediment tracer study conducted by the U.S. Army Corps of Engineers (USACE) for the Los Angeles River (Everest 2010). The WRAP Model has since been used to evaluate dredging activities, stormwater discharges, and to characterize transport conditions in the harbor to support comments provided on the Harbor Toxics TMDL development.

2.2 EFDC OVERVIEW

The EFDC modeling platform was selected to support the Harbor Toxics TMDL development (EPA and RWQCB 2011a) for the following reasons:

- EFDC contains all the appropriate modeling components (hydrodynamics, sediment transport, and contaminant fate and transport) required for simulating the LA/LB Harbor system
- EFDC is a non-proprietary model (public domain source code) supported by EPA
- EFDC has previously been utilized for numerous surface water modeling applications including metal and organic contaminant fate and transport at conventional and Superfund sites
- EFDC has been used for numerous TMDL studies by EPA

EFDC is a surface water modeling system developed and distributed by the EPA Center for Exposure Assessment Modeling. The model was originally developed by Dr. John Hamrick at the Virginia Institute of Marine Science. EFDC has been designed to quantify movement and concentrations of contaminants in lakes, rivers, stratified estuaries, and coastal environments to support environmental assessment, management, and regulatory requirements. The EFDC modeling system includes hydrodynamic, sediment, contaminant, and eutrophication components that can simulate geometrically and dynamically complex water bodies (EPA 2007a). The WRAP Model utilizes the dynamically-coupled hydrodynamic, sediment, and contaminant components of EFDC. The EFDC equations are formulated based on curvilinear-orthogonal horizontal coordinates and sigma vertical coordinates. Details of the EFDC model formulation and governing equations are provided in Appendix A.

The hydrodynamic component is similar to the Princeton Ocean Model (Blumberg and Mellor 1987). EFDC solves the 3D Reynold-Averaged Navier-Stokes equations assuming incompressible flow and hydrostatic pressure distribution with dynamically coupled salinity and temperature transport, which accounts for density variations. A second moment turbulence closure scheme relates turbulent viscosity and diffusivity to the turbulence intensity and length scale. Transport equations for salinity, dye, sediment, and contaminants are solved using a fractional step scheme with implicit vertical diffusion and explicit advection and horizontal diffusion. EFDC is capable of simulating time and spatially varying environmental forcing functions such as tides and winds, as well as an arbitrary number of inflows (e.g., rivers and storm drain discharges). User-specified inputs can be generated to allow integration of inputs from other models such as a watershed model (EPA 2007b).

The hydrodynamic component provides the dynamics for the sediment transport and contaminant components. EFDC is capable of simulating multiple sediment classes of cohesive and noncohesive sediments. Sediment transport processes include sediment

settling, deposition, resuspension, and bed consolidation mechanisms. The dynamic coupling between the sediment and hydrodynamics components account for both changes in bed topography and water depth due to sediment deposition or erosion. Sediment erosion is computed based on sediment properties (e.g., sediment size or critical shear stress) and hydrodynamic shear stresses induced by tidal currents, riverine flows, or wind-induced currents (EPA 2007c).

The sediment transport component is linked with the contaminant transport component, which can simulate an arbitrary number of toxics (e.g., metals or organic chemicals). Chemical interactions can be specified for sediments, dissolved organic carbon (DOC), or particulate organic carbon. The contaminant transport is based on the same advection-diffusion scheme used for salinity and temperature. The sorbed contaminant transport formulation uses equilibrium partitioning between adsorption and desorption components. For organic chemicals, EFDC can be specified to use a three-phase partitioning for freely dissolved, dissolved organic carbon, and particulate phases (EPA 2007c).

2.3 MODEL UPDATES

The DCEM and original WRAP Model have been calibrated with extensive field data for hydrodynamics (water levels, velocities), mixing (salinity and dye), sediment transport (sediment tracer) and metals (copper, zinc and lead). However, the WRAP Model had not been developed or calibrated for the simulation of organic chemicals (TPCB and TDDX), which are required for modeling fish tissue concentrations using the bioaccumulation model. Special studies were conducted by the Ports to collect TPCB and TDDX concentrations in storm water inflows, as well as in the harbor waters. These data were used for the calibration of WRAP Model for organic chemicals described in Section 8.

Volatile emissions between the water column and atmosphere can be an important process in the fate and transport of persistent organic chemicals (e.g., TPCB and TDDX). A study of atmospheric fluxes in the LA/LB Harbor determined that the net flux direction of TPCB and TDDX is from water to air (Sabin et al. 2011). In a Conceptual Site Model (CSM) developed to investigate the relative importance between different sources or mechanisms affecting the organic concentrations in the LA/LB Harbor, the air-water gas exchange was estimated to be a moderate sink for both TPCB and TDDX (Anchor QEA 2014a). Thus, volatilization was considered a necessary process to be included in the WRAP Model. Since EFDC—which the development of the WRAP Model was based on—does not account for volatilization, the EFDC source code needed to be enhanced to simulate TPCB and TDDX losses due to volatilization. In modifying the EFDC code, the process of volatilization was simulated based on a two-layer film resistance approach in which the contaminant flux is proportional to the concentration gradient between the water and air and a mass transfer coefficient (Liss and Slater 1974). The volatilization flux estimation was simplified based on the assumption that

TPCB and TDDX concentrations in the air are much less than concentrations in the water (Bopp 1983). Details on the incorporation of volatilization in the WRAP Model are provided in Appendix B.

In addition to volatilization, another update to the WRAP Model was the incorporation of propeller induced re-suspension of sediment (propwash), which occurs when currents from vessel propellers generate high bed shear stresses sufficient to re-suspend sediment. Consequently, sediment and associated contaminants are eroded from the bed and re-suspended into the water column, enabling the movement and redistribution of sediment and organic chemicals. Combined, the LA/LB Port complex is the busiest port in the United States with widespread deposition of legacy pollutants. Due to the frequent vessel traffic within the harbor and potential transport of contaminants, the propwash effects were incorporated into the WRAP Model. Although EFDC is capable of simulating the typical processes involved in chemical fate and transport, the standard code does not account for anthropogenic mechanisms of transport. Propwash was incorporated into the WRAP Model by simulating the hydrodynamic effects of propwash as pulses of high bed shear stresses. Temporally and spatially varying pulses of high bed shear stress were applied along frequently used vessel routes in the harbor. The propwash bed shear stresses of different vessels were quantified based on vessel characteristics (e.g., engine power, propeller diameter, vessel draft) and water depths along vessel routes. Representative time series of the high bed shear stress were then determined based on the frequency, duration, and locations of vessel traffic. EFDC then simulated the pulses of high bed shear stresses to determine the re-suspension of sediment and contaminant transport effects. The effects of propwash were included in the WRAP Model organic chemical calibration. Details on the procedures to incorporate propwash into the WRAP Model are provided in Appendix C.

2.4 MODEL GRID SETUP

The WRAP Model grid, as shown in Figure 2.1, extends from the tidally influenced portions of the DC, LAR, SGR, and through the LA/LB Harbor and eastern San Pedro Bay. The estuary portion of the DC runs 13.3 km (8.26 mi) from Vermont Avenue to Henry Ford Avenue where it discharges into the Consolidated Slip (CS). The tidally influenced portion of the LAR extends approximately 4 km (2.5 mi) from Willow Street to Ocean Boulevard and flows into Queensway Bay. The SGRE stretches about 3 km (1.88 mi) from Spring Street just downstream of the SGR and Coyote Creek (CC) confluence to the Pacific Ocean. The estuarine portions of these rivers are earth bottom channels with riprap sides that discharge directly to harbor or San Pedro Bay. The WRAP Model grid extends approximately 8 km (5 mi) beyond the Federal Breakwater into the ocean. The ocean extent to the model boundary was deemed to sufficient to negate any boundary effects in the area of interest, which is the harbor area inside of the breakwater.

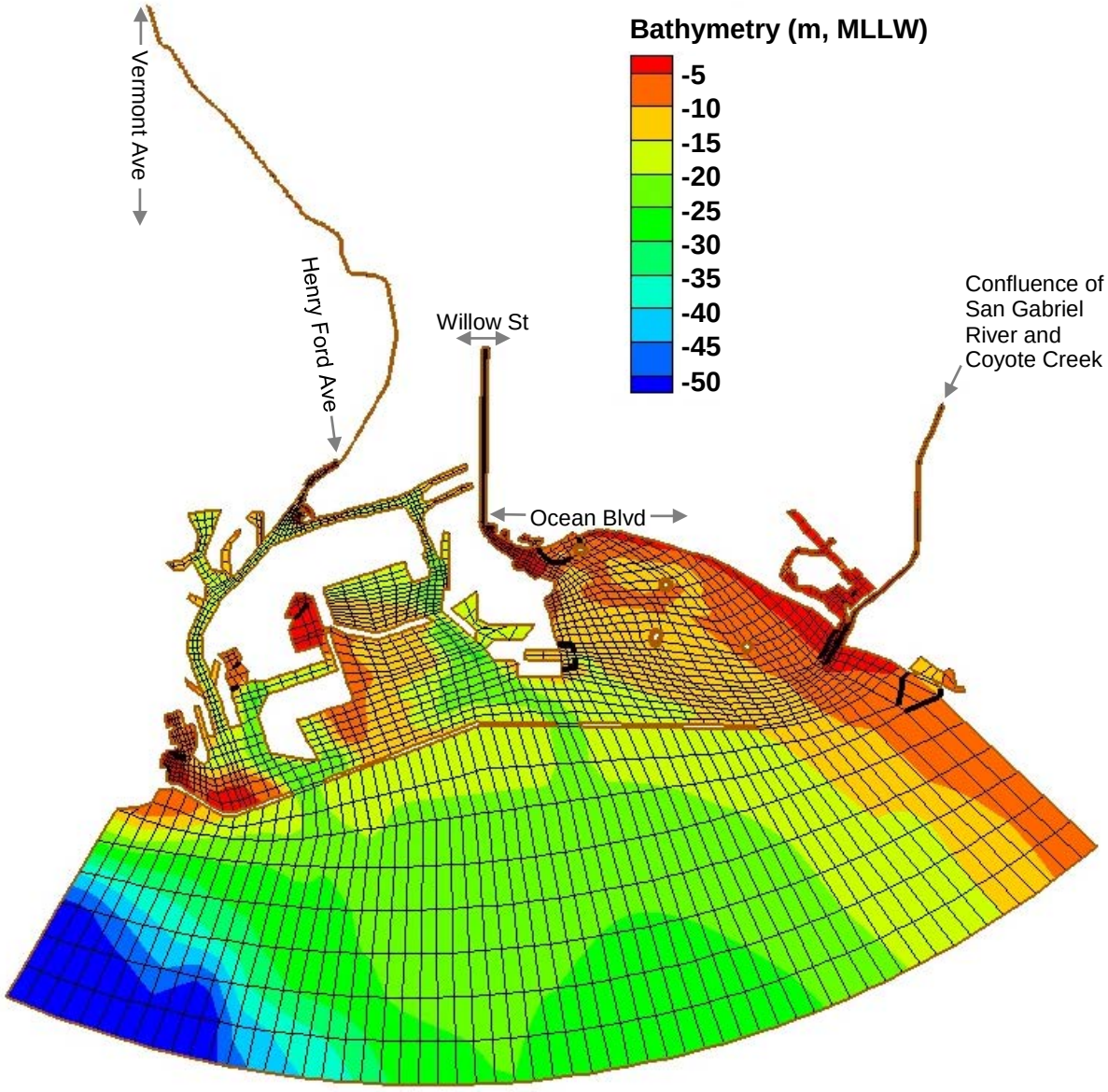

Figure 2.1 WRAP Model Grid and Bathymetry

The WRAP Model grid was designed as a curvilinear, orthogonal grid with a higher resolution of cells (i.e., small grid cells) in the estuarine areas and progressively larger cells towards the outer harbor and ocean areas. Generally, smaller grid cells improve model predictions but increase computation times. The grid cell size was optimized to balance grid resolution, model-predictions, and computation times; grid resolution was assessed for adequate performance during the initial DCEM development (Everest 2007). Typically, the smallest grid cells were specified along the river channels. For the DC, the channel was defined by three cells across with a cell size of approximately 11 by 60 m. The LAR was specified with five cells across and an average cell size of 32 by 100 m. The SGR contained two cells across with an average cell size of 46 m by 106 m. The largest cells were defined in the ocean area with a cell size of approximately 500 by 1,000 m. Grid refinements were made in the CS, Fish Harbor (FH), Cabrillo Marina, and Inner Cabrillo Beach to improve grid resolution, and therefore model predictions, in these TMDL receiving waterbodies. Vertically, the water column was defined by five uniform layers.

The greater harbor area also includes numerous breakwaters and jetties. The main harbor breakwater separating the LA/LB Harbor and ocean was modeled as a thin strip of land extending from Inner Cabrillo Beach into San Pedro Bay with gaps at the Angels and Queens Gates. The POLB West Basin breakwater, historically referred to as Navy Mole, was also modeled as land. Smaller breakwaters and jetties were simulated using the masking feature in EFDC, which blocks flow across cell faces. These breakwaters and jetties and include those at Cabrillo Marina, Inner Cabrillo Beach, FH, Seaplane Lagoon, Pier J, Golden Shore Wildlife Preserve, Long Beach Marina, Alamitos Bay/SGR, and Anaheim Bay.

Bathymetry data for the WRAP Model was generated from composited bathymetric surveys that account for the most recent major dredging projects, including the POLA Main Channel Deepening Project and POLB Main Channel Dredging Project. Bathymetry data were sourced primarily from National Oceanic and Atmospheric Administration (NOAA) nautical charts 18749 and 18751. The vast majority of the harbor and San Pedro Bay was recently surveyed by NOAA in 2013, as depicted in Figure 2.2. The NOAA 2013 survey was comprised of four data sets covering the LA/LB Harbor (NOAA 2013a), eastern San Pedro Bay (NOAA 2013b), the area offshore of the federal breakwater (NOAA 2013c), and the area downcoast of Anaheim Bay (NOAA 2013d). Areas not included in the NOAA 2013 survey were supplemented using other surveys. For the DC, bathymetry data were obtained from a March 2006 survey conducted by the POLA (POLA 2006). Bathymetry data within the POLA Seaplane Lagoon were sourced from a 2005 USACE and 2007 POLA survey (USACE 2005 and POLA 2007). A 2007 POLA survey was used for the Pier 400 submerged soil site (POLA 2007). Bathymetry data for the LARE were augmented using a 2008 USACE survey (USACE 2008). Bathymetry for the remaining areas not updated during the NOAA 2013 survey was based on the NOAA nautical chart 18749, covering San Pedro Bay (NOAA 2004a), and chart 18751 for Los Angeles and Long Beach Harbors (NOAA 2004b).

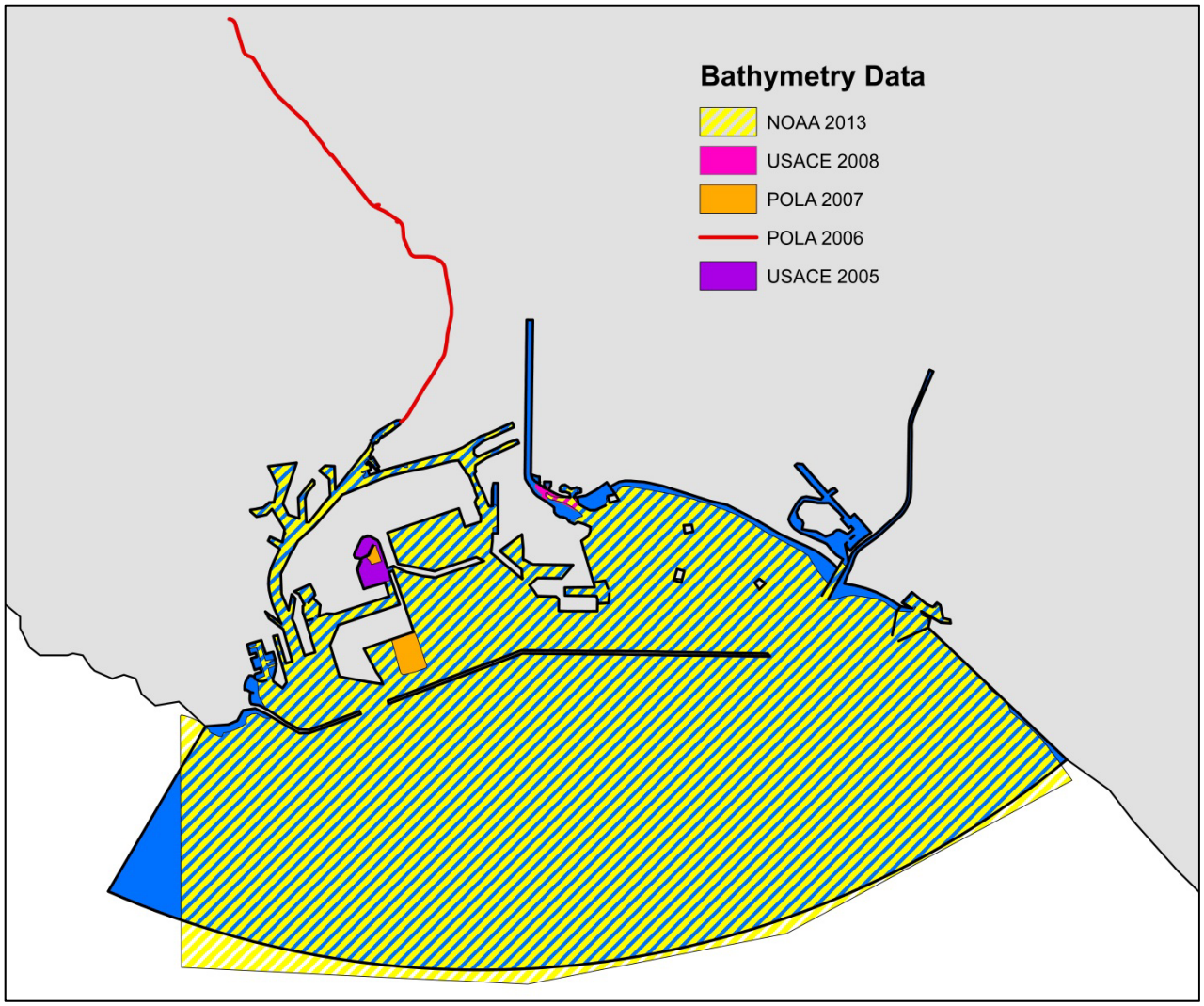

Figure 2.2 Bathymetry Data Sources

The harbor configuration and bathymetry were modified to account for recent and ongoing or planned projects with published environmental review documents, as illustrated in Figure 2.3. Fill, excavation, and dredge areas were determined based on environmental documents for the following projects:

- Berths 136-147 [TraPac] Container Terminal Project (POLA and USACE 2007)
- Berths 121-131 [Yang Ming] Container Terminal Redevelopment Project (USACE and POLA 2014)
- Al Larson Boat Shop Improvement Project [FH] (POLA 2012)
- Pier G Redevelopment Program (POLB 2000)
- Middle Harbor Redevelopment Project (USACE and POLB 2009)
- West Basin Deepening Project (USACE and POLB 2015)
- Pier S Marine Terminal and Back Channel Improvements Project (POLB and USACE 2011)

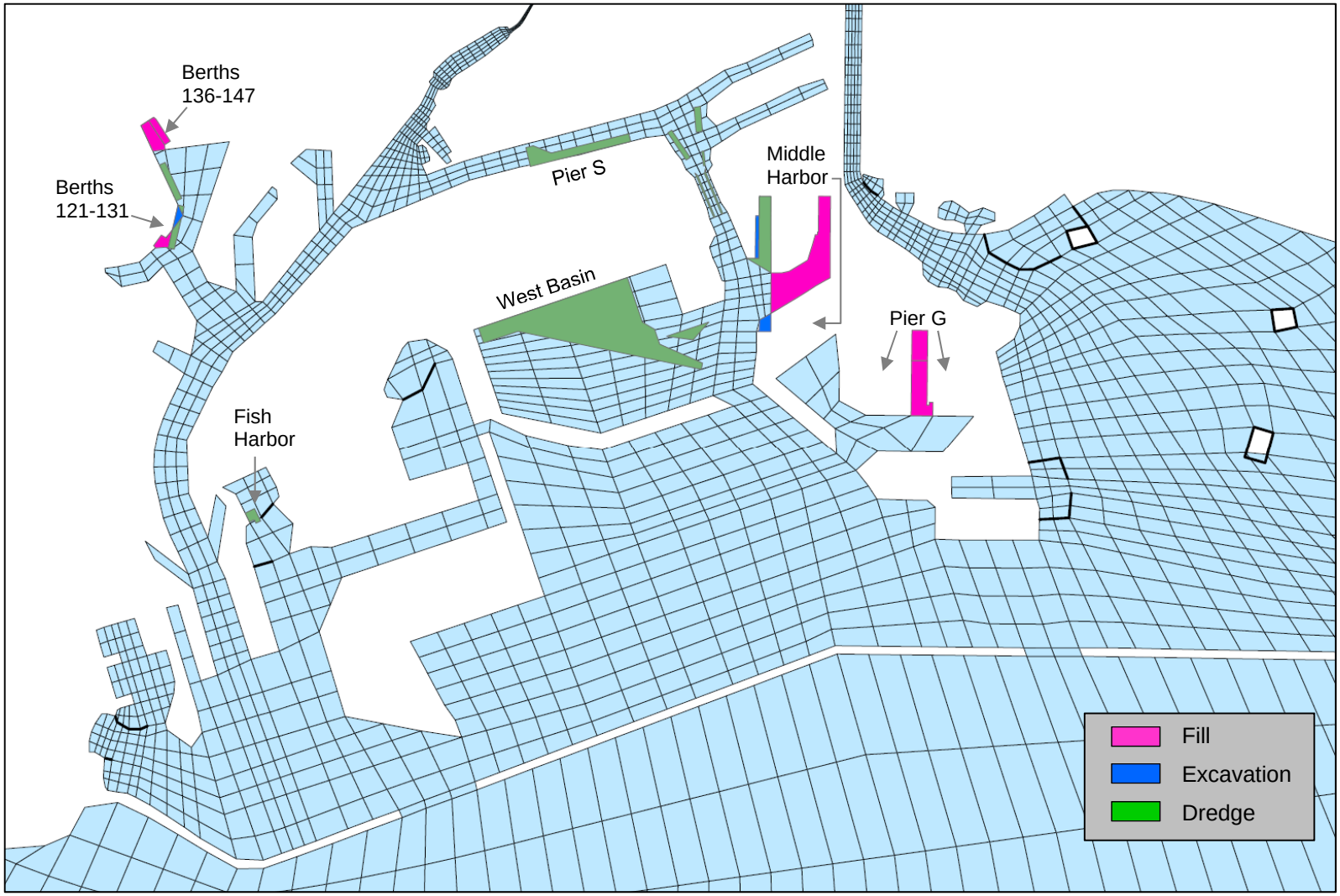

Figure 2.3 Baseline Harbor Configuration

2.5 BOUNDARY CONDITIONS

Hydrodynamics in the LA/LB Harbor and San Pedro Bay are driven by river flows, tide, and wind conditions. The WRAP Model boundary conditions for storm water inflows, tide, and wind boundary conditions are illustrated in Figure 2.4. Storm water inflows that discharge into the harbor were simulated with approximately 200 model inflows as indicated with orange circles in the figure. Model inflow locations were determined based on GIS data of storm drain and outfall locations. Details on watershed loadings, which describe the magnitude of the fresh water flow and corresponding sediment and organic chemical concentrations, are provided in Section 3. Tide and wind boundary conditions were specified using data from the NOAA National Ocean Service (NOS). Water levels and meteorological parameters are monitored as part of the Physical Oceanographic Real-Time System (PORTS®) for the LA/LB Harbor. The PORTS monitoring stations are listed in Table 2.1. Water levels and temperature are monitored at the NOAA LA Outer Harbor tide gage. Wind speed, wind gust, and wind direction are monitored at the other seven listed meteorological stations.

The water elevation boundary was specified based on the NOAA LA Outer Harbor tide gage. Tides are mixed, semi-diurnal with two daily highs and two daily lows. Tidal datums based on the latest National Tidal Datum Epoch (NTDE) from 1983 to 2001 are provided in Table 2.2. Water levels from the tide gage, located inside the breakwater at the end of Berth 60, were applied to the model ocean boundary outside of the harbor, as shown previously in Figure 2.4, without adjustments to tidal amplitude or phase. Comparison of the model-predicted water levels at the tide gage location with measured water levels, as shown in Figure 2.5, indicates that water levels from the tide gage can be applied directly at the model ocean boundary.

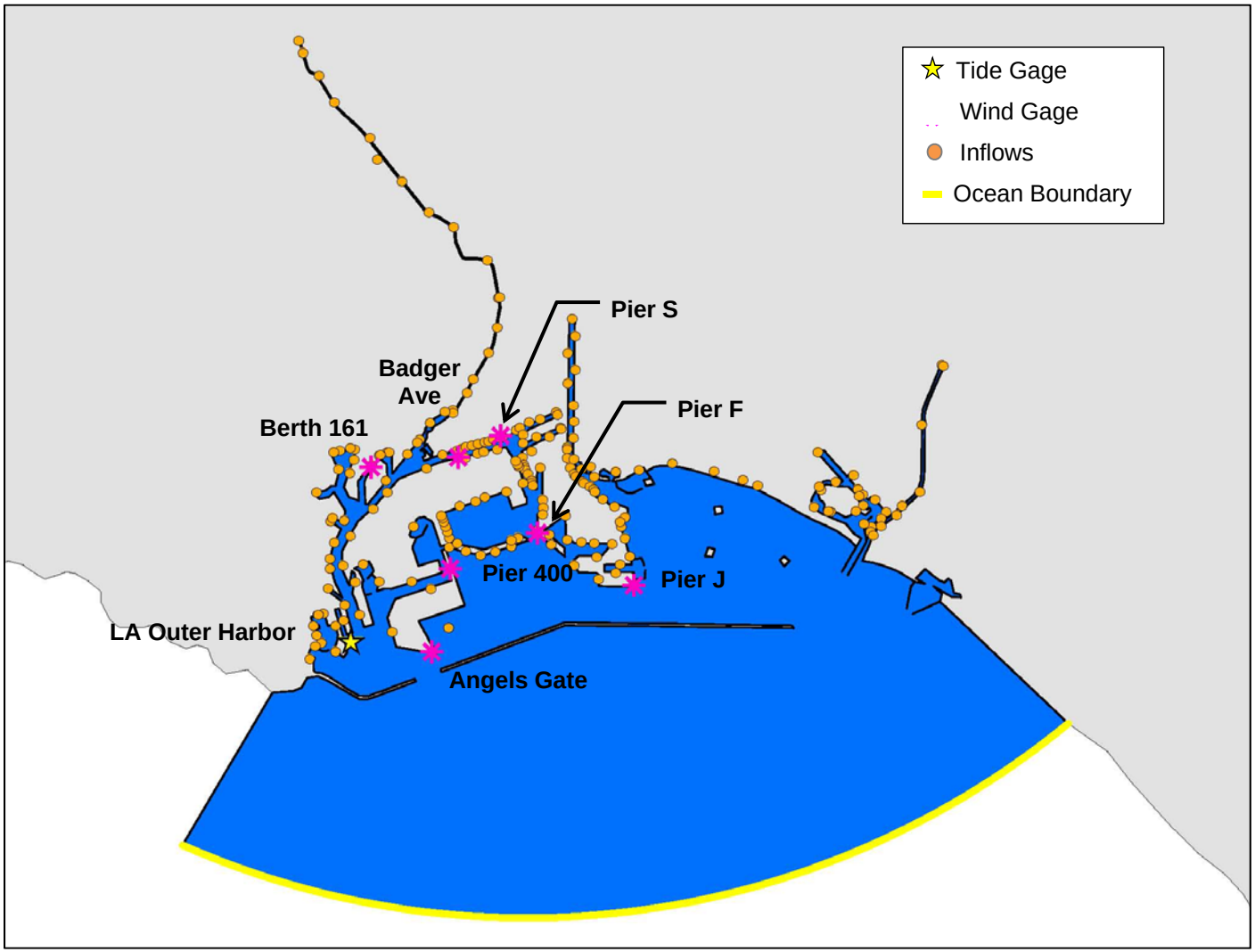

Figure 2.4 WRAP Model Boundary Conditions

Table 2.1 NOAA PORTS® Station Summary

STATION	ID	LATITUDE	LONGITUDE	DATA MONITORED
Angels Gate	9410647	33° 42.9' N	118° 14.8' W	Wind speed, gusts, direction, air temperature, air pressure
Badger Avenue Bridge	9410691	33° 46.0' N	118° 14.4' W	Wind speed, gusts, direction
Berth 161	9410690	33° 45.8' N	118° 15.9' W	Wind speed, gusts, direction
LA Outer Harbor	9410660	33° 43.2' N	118° 16.4' W	Water level, temperature, air pressure
Pier 400	9410666	33° 44.1' N	118° 14.5' W	Wind speed, gusts, direction
Pier F	9410670	33° 44.8' N	118° 12.9' W	Wind speed, gusts, direction, air temperature, air pressure
Pier J	9410665	33° 44.0' N	118° 11.1' W	Wind speed, gusts, direction
Pier S	9410692	33° 46.1' N	118° 13.5' W	Wind speed, gusts, direction

Table 2.2 Tidal Datums for LA Outer Harbor

TIDAL DATUM	ELEVATION (M, MLLW)
Highest Observed Water Level (01/10/05)	2.414
Mean Higher High Water (MHHW)	1.674
Mean High Water (MHW)	1.449
Mean Sea Level (MSL)	0.861
Mean Low Water (MLW)	0.287
North American Vertical Datum – 1988 (NAVD88)	0.062
Mean Lower Low Water (MLLW)	0.000
Lowest Observed Water Level (12/17/33)	-0.832

Source: NOAA 2011
Tidal Epoch 1983 – 2001

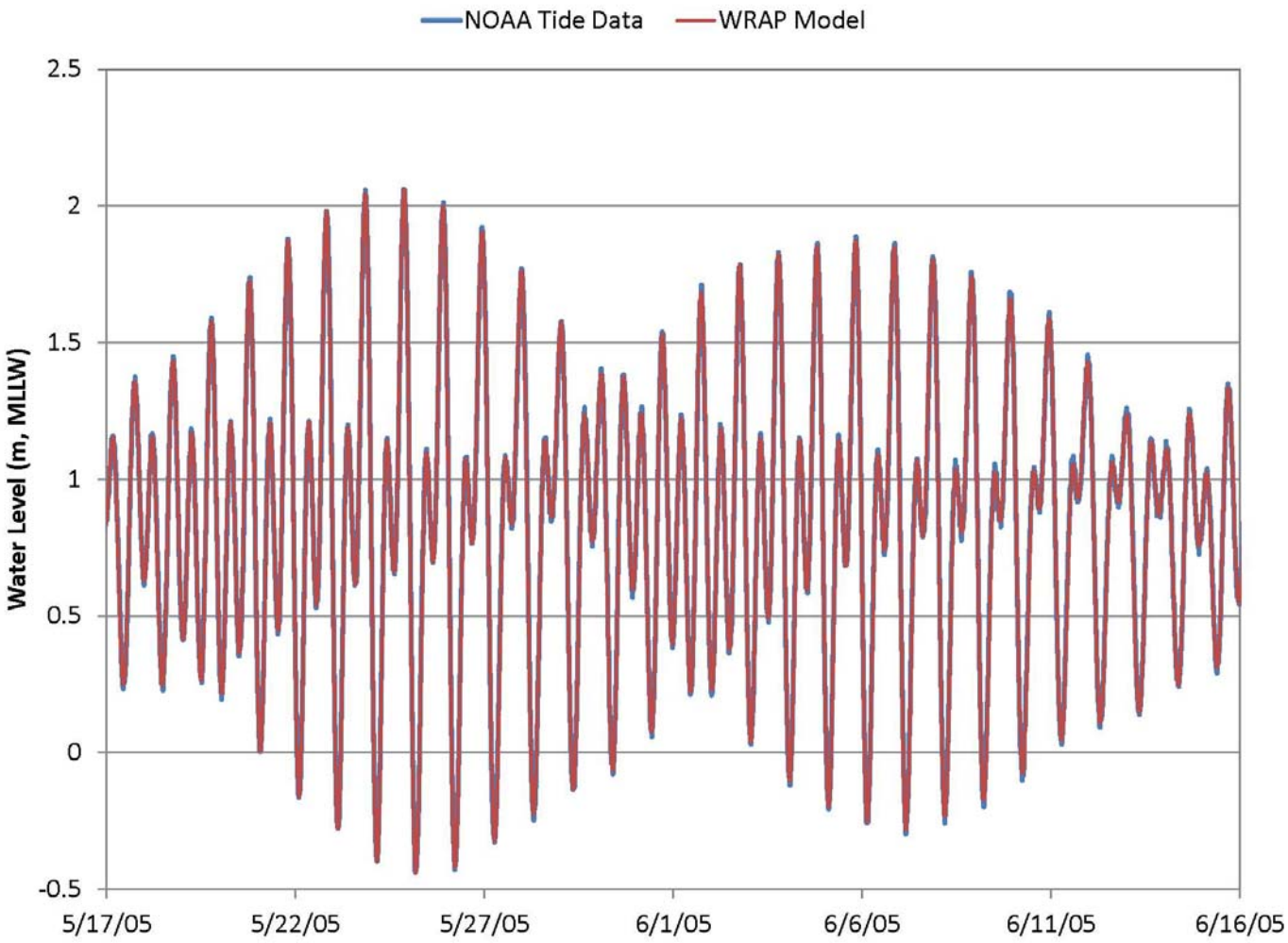

Figure 2.5 Comparison of Measured and Model-Predicted Water Levels at NOAA LA Outer Harbor

Spatially and temporally varying wind conditions were specified using data from the seven NOAA meteorological stations. During the initial development of the DCEM, spatially varying wind conditions were found to be important to the overall harbor circulation pattern. Velocity data indicates that the dominant wind flow direction is westward along the Cerritos Channel and southwestward (ebb-dominant) along the POLA Main Channel (or Main Ship Channel [MSC]). The dominant wind directions in the harbor are mainly from the south-southwest and contribute to the circulation pattern observed in the field data. The prior DCEM demonstrated that spatially varying wind conditions impact harbor velocities and result in a better comparison with field data (Everest 2007). The spatially varying wind conditions were applied in the model domain based on an inverse distance weighting of the meteorological stations. Wind boundary conditions were specified using 6-minute interval wind speed and direction. However, periodic gaps in the data routinely occur and/or data may not be available for months due to instrument maintenance or other malfunctions. For example, no wind data are available from June through October 2008 and May 2012 through December 2012. Gaps in the wind data that are greater than three hours were filled using wind data from the same station during a different year.

EFDC has the capability to simulate wave-induced currents, but was not utilized for the WRAP Model. Effects of waves are not important for the LA/LB Harbor since the harbor is protected by the federal breakwater resulting in relatively small waves. In addition, water depths in the harbor area are deep, ranging from about 15 to 25 m. Hence waves have insignificant effect on the hydrodynamics of the harbor, which is mainly driven by tidal and fluvial inputs. Wave-induced radiation stress may only have minor effects on the currents along the shoreline of Eastern San Pedro Bay.

3. WATERSHED LOADINGS

3.1 OVERVIEW

Watershed loadings are required for the model calibrations and long-term TMDL management scenario simulations. Thus, flows, sediment, and organic chemical concentrations for the nearly 200 storm water discharges (shown in Figure 2.4) were defined from 2002 through 2015. Several approaches were evaluated to estimate watershed loadings including previous estimates used for the Harbor Toxics TMDL, watershed models, and analytical methods. Given the time and budget constraints, an approach using analytical methods to estimate watershed loadings was developed and approved by the HTWG. Generally, the approach included the following three steps: (i) measured data were used when available to define the storm water flows and scaling factors used to estimate other flows, (ii) sediment concentrations from each of the four watersheds were estimated using dry weather, first flush and wet weather TSS concentrations, and (iii) organic chemical concentrations from each watershed were estimated based on correlation between organic chemical and TSS concentrations.

3.2 WATERSHED DESCRIPTION

The LA/LB Harbor and San Pedro Bay receive storm water discharges from four major watersheds – the Los Angeles River (LAR) Watershed, San Gabriel River (SGR) Watershed, Dominguez Channel (DC) Watershed, and Nearshore Watershed, as shown in Figure 3.1. The watershed delineations were compiled from GIS data of watershed drainage areas. Drainage areas for the LAR and SGR Watersheds were obtained from the National Hydrography Dataset Plus (NHDPlus), a geo-spatial, hydrologic framework database that contains watershed drainage areas based on stream networks and watershed topography. The NHDPlus database is a part of the Better Assessment Science Integrating Point and Nonpoint Sources (BASINS) developed by EPA (EPA 2015). Drainage areas for the DC and Nearshore Watersheds were based on the Loading Simulation Program in C++ (LSPC) watershed models developed for the Harbor Toxics TMDL (EPA and RWQCB 2011b). Subwatersheds within the DC and Nearshore Watersheds were refined based on GIS data of drainage areas based on storm drains provided by POLA and POLB. GIS data obtained from the POLA included storm drain drainage areas covering POLA and City of Los Angeles in the DC and Nearshore Watersheds (POLA 2010b). Drainage areas for the POLB covered portions of the Nearshore Watershed that discharge into the LA/LB Harbor, LARE, and San Pedro Bay (POLB 2013a). Nearshore drainage areas for the LARE, Alamitos Bay, and San Pedro Bay were obtained from the City of Long Beach (POLB 2013b). GIS data of the four

major watersheds were then combined to delineate the drainage areas for the LA/LB Harbor and greater San Pedro Bay.

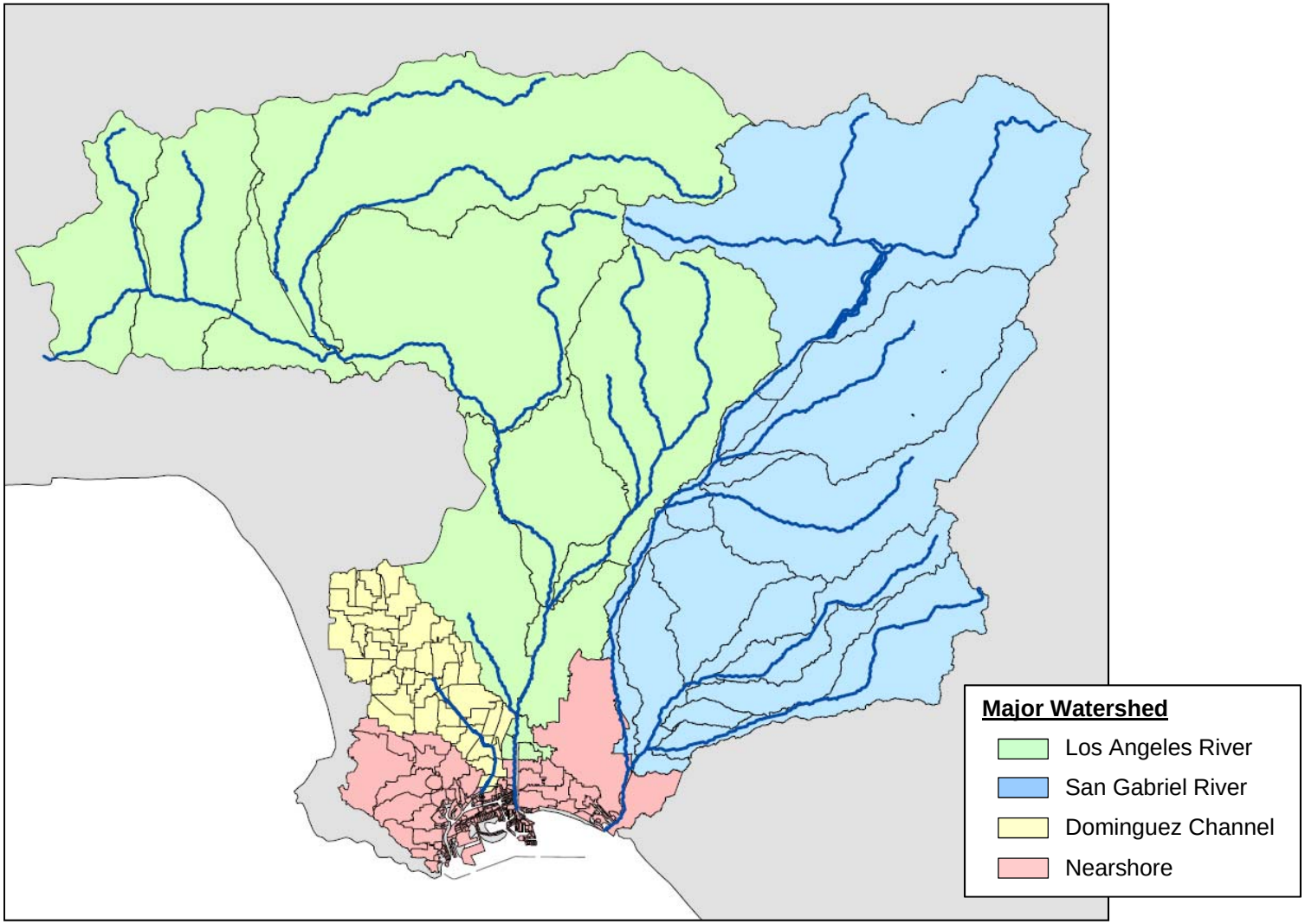

Figure 3.1 Major Watersheds for LA/LB and Greater San Pedro Bay

The LAR and SGR Watersheds comprise 90% of the entire LA/LB Harbor and greater San Pedro Bay drainage area. The DC Watershed, which includes the drainage area along the DC Estuary, covers approximately 4% of the entire drainage area. The remaining area is grouped into the Nearshore Watershed, which includes drainages areas of the Ports, LARE, San Pedro Bay, Alamitos Bay, and SGRE. The drainage areas of the four major watersheds are summarized in Table 3.1.

Table 3.1 Major Watersheds of LA/LB Harbor and Greater San Pedro Bay

WATERSHED	DRAINAGE AREA (KM^2)	PERCENT OF TOTAL AREA
Los Angeles River (LAR)	2,185	51%
San Gabriel River (SGR)	1,687	39%
Dominguez Channel (DC)	184	4%
Nearshore	255	6%
Total	4,310	100%

The LAR Watershed is the largest watershed making up 51% of the greater harbor drainage area. The upper portion of the watershed originates in the mountain ranges within the Angeles National Forest, which accounts for roughly 40% of the watershed. The rest of the watershed is predominantly composed of urban land uses. Major tributaries include the Pacoima Wash, Tujunga Wash, Arroyo Seco, Rio Hondo, and Compton Creek. The upper watershed contains several flood control dams including the Hansen, Pacoima, and Sepulveda Dams (RWQCB 2007).

The SGR Watershed is the second largest watershed making up 39% of the greater harbor drainage area. The watershed is about half vacant land and half urban land uses. In the upper watershed, the SGR extends from the San Gabriel Mountains through the Santa Fe Dam, joins Walnut and San Jose Creeks, and then runs to the Whittier Narrows Reservoir and Dam (LACDPW 2006 and RWQCB 2007). The Whittier Narrows Dam is a flood control structure constructed and operated by the USACE. In order to provide flood protection along the SGR, excessive flood waters from the upper SGR are diverted to the LAR via the Rio Hondo during wet weather, while dry weather flows, which are primarily from three water reclamation plants, are discharged to the lower SGR (USACE 1957 and USACE 2012). Hence, as illustrated in Figure 3.2, the upper SGR watershed is hydraulically connected to the LAR Watershed. The lower SGR continues from the Whittier Narrows Dam and confluences with CC just before reaching tidal influence south of Willow Street. The lower SGR includes several spreading grounds and two water reclamation plants.

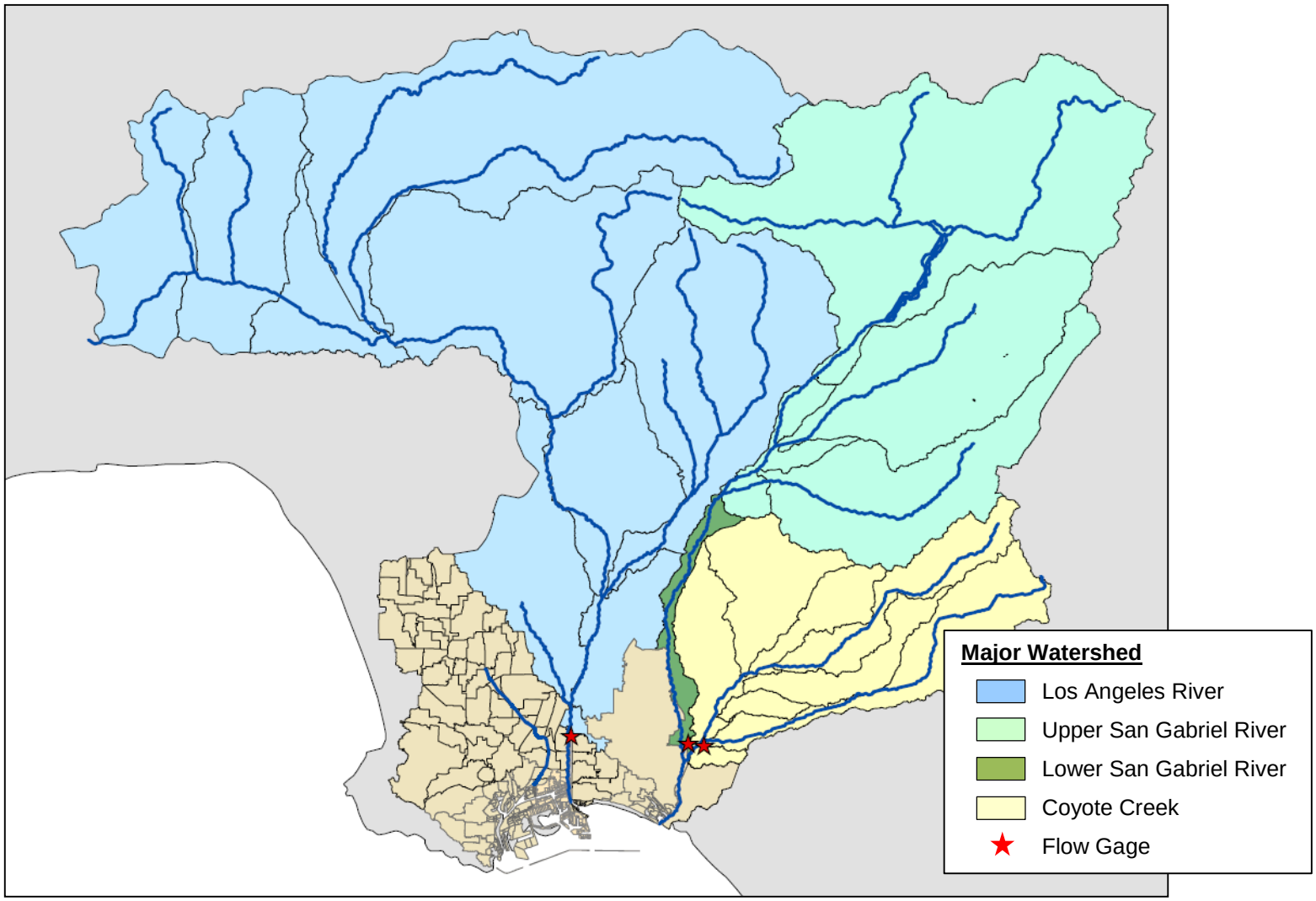

Figure 3.2 Los Angeles River and San Gabriel River Hydraulic Watersheds

The DC Watershed, as illustrated in Figure 3.3, consists of a fresh water portion and estuarine portion. The fresh water portion of the DC is a rectangular concrete channel that extends from 116th Street to Vermont Avenue. The drainage area above Vermont Avenue makes up about 56% of the DC Watershed. The entire DC Watershed is highly urbanized, and flows through the watershed are primarily routed through the storm drain system. The Montrose Superfund Site is located adjacent to the DC Estuary and discharges into the DC via the Torrance Lateral. This Superfund site is located on the property of a former dichlorodiphenyltrichloroethane (DDT) manufacturing plant that operated from 1947 to 1982 (LACDPW 2004). In 1985, the majority of the property was capped with asphalt to minimize transport of DDT via wind or storm water. Several cleanup actions have been conducted to remove contaminated soils from the surrounding area, along storm water channels (e.g. Kenwood Drain, Torrance Lateral, and DC), and within an adjacent sanitary sewer line (EPA 2016).

The Nearshore Watershed, as illustrated in Figure 3.3, encompasses the drainage areas that directly discharge to the LA/LB Harbor, LARE, San Pedro Bay, Alamitos Bay, and the SGRE. The drainage areas within the Nearshore Watershed along with the other major watersheds are summarized in Table 3.2. The drainage area for the LA/LB Harbor accounts for 50% of the Nearshore Watershed. The harbor drainage area includes Machado Lake, which is a waterbody with impairments due to polychlorinated biphenyls (PCBs) and DDT that are addressed in a separate TMDL and not the Harbor Toxics TMDL. Machado Lake is located in the Ken Malloy Harbor Regional Park and includes an open water lake and seasonal wetland area separated by a low earthen dam. Machado Lake is hydraulically connected to the harbor and discharges into the POLA West Basin. Overflows from Machado Lake fill the wetland area, where water levels increase before overtopping the outlet structure and discharging to the harbor (City of Los Angeles 2009). Flows monitored at the outlet structure indicate discharge to the harbor occurs during most of the wet season; this is discussed further in Section 3.3.1. The LARE drainage area extends along the tidally influenced portion of the LAR below Willow Street. The drainage area for San Pedro is a relatively small area along the shoreline. The drainage area for Alamitos Bay accounts for approximately 32% of the Nearshore Watershed and empties into San Pedro Bay. This area corresponds to the Los Cerritos Channel and Alamitos Bay Watershed Management Area (RWQCB 2007). The SGRE drainage area extends along the SGR below Spring Street, which flows into San Pedro Bay adjacent to the entrance of Alamitos Bay.

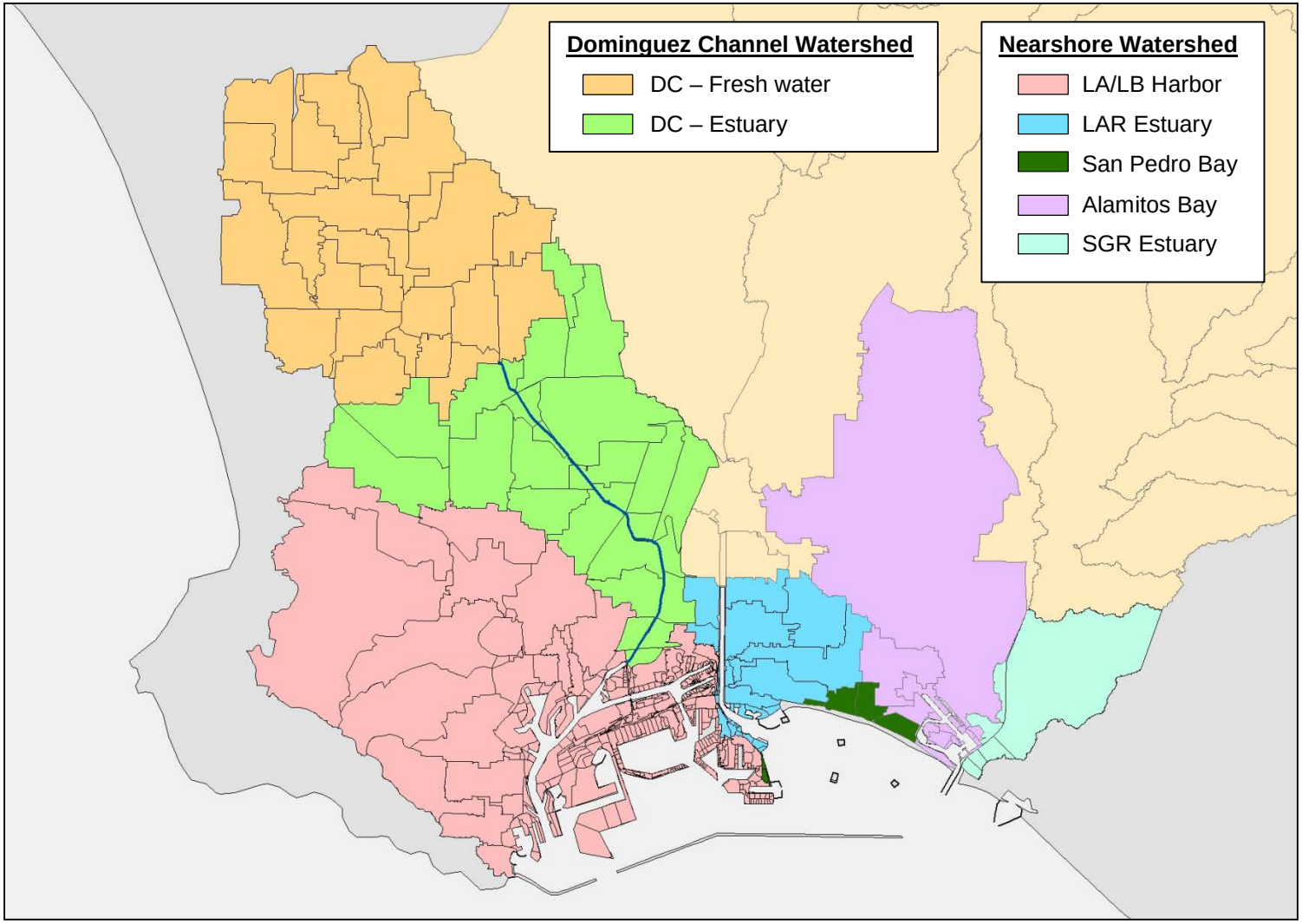

Figure 3.3 Dominguez Channel and Nearshore Watersheds

Table 3.2 Watershed Drainage Areas

WATERSHED	DRAINAGE AREA (KM^2)	SUBWATERSHED	DRAINAGE AREA (KM^2)
Los Angeles River (LAR)	2,185	Wardlow Rd	2,179
		Willow St	6.11
San Gabriel River (SGR)	1,687	Whittier Narrows	1,144
		Lower SGR	35.3
		Coyote Creek (CC)	507
Dominguez Channel (DC)	184	Artesia	91.2
		Vermont	12.6
		DC Estuary	81.0
Nearshore	255	Machado Lake	64.1
		Harbor	63.6
		LARE	23.1
		San Pedro Bay	2.86
		Alamitos Bay	81.5
		SGRE	20.1

3.3 FLOWS

Rainfall patterns in southern California generally have two distinct climatic periods. A relatively dry period occurs from late April to mid-October with little to no rainfall. The wet period between mid-October and late April typically accounts for 85 to 90% of the annual rainfall. Annual precipitation is approximately 12 inches per year in coastal areas and generally increases inland towards mountain areas. About 8 inches of rainfall occurs in February (LACDPW 2005). During the dry season, perennial flows occur from storm drains (dry weather flows) mostly from wastewater reclamation plant effluent and urban land uses (illicit storm water connections, excess irrigation, and other residential or commercial practices). These dry weather flows are substantially less than wet weather flows generated by rainfall (EPA and RWQCB 2011b). Wet weather flows are highly variable and generally coincide with rainfall events that last from a couple hours to several days (LACDPW 2005).

Flows from the major rivers were specified from measured flows monitored by Los Angeles County Department of Public Works (LACDPW). There are four flow gages, all located upstream of tidal influence that monitor the fresh water portions of the LAR, SGR, CC, and DC. The monitored drainage areas account for 92% of the total greater harbor watershed, as illustrated in Figure 3.4. The LACDPW Water Resources Division operates flow gages at the LAR below Wardlow Road (F319-R), SGR above Spring Street (F42B-R), and CC below Spring Street (F354-R) (LACDPW 2012b). Monitored flows of the LAR account for flow diversions from the SGR Watershed. The SGR and CC flow gages monitor flows from the upper and lower SGR watersheds. Flows from the DC are periodically monitored by the LACDPW Watershed Management Division. The DC flow gage (S28) is located at Artesia Boulevard (LACDPW 2013b). Figure 3.5 compares measured flows at the LACDPW gages from 2003 to 2005 as examples. As shown in the upper panel, the LAR has the largest flows. Flows from the SGR and CC are provided in the middle panel. Flow data for the SGR (green line) indicates relatively very low wet weather flows from the SGR because of the diversion of wet weather flow to the LAR as mentioned earlier. Flow data for the DC are shown in the bottom panel and include gaps in the data since flows are not continuously monitored.

The availability of flow data between 1994 and 2015 are summarized in Figure 3.6, which illustrates the timeline of available flow data. In the figure, the blue bars indicate the time frames of flow data. The darker blue indicates continuous flow data, while the lighter blue indicates flow data with periodic gaps. Available flow data for the LAR, SGR, and CC consisted of flow measurements at 15-min intervals (LACDPW 2010a, LACDPW 2013a, and LACDPW 2015). For the DC, periodic flow measurements were taken to trigger automated samplers (LACDPW 2010b, LACDPW 2012a, and LACDPW 2015). Additional flow data were collected from Machado Lake and 22nd Street (Cabrillo Marina) for a limited duration in 2008 – 2011 (POLA 2010a). For the major rivers (i.e., monitored locations), analytical methods were developed to fill gaps in the flow data, as discussed in Section 3.3.1. Flow data from Ballona Creek, which is located outside the greater harbor watershed, was also obtained for filling data gaps (LACDPW 2013a and LACDPW 2015). Separate methods were developed to estimate flows from unmonitored drainage areas based on scaling factors, as summarized in Section 3.3.2.

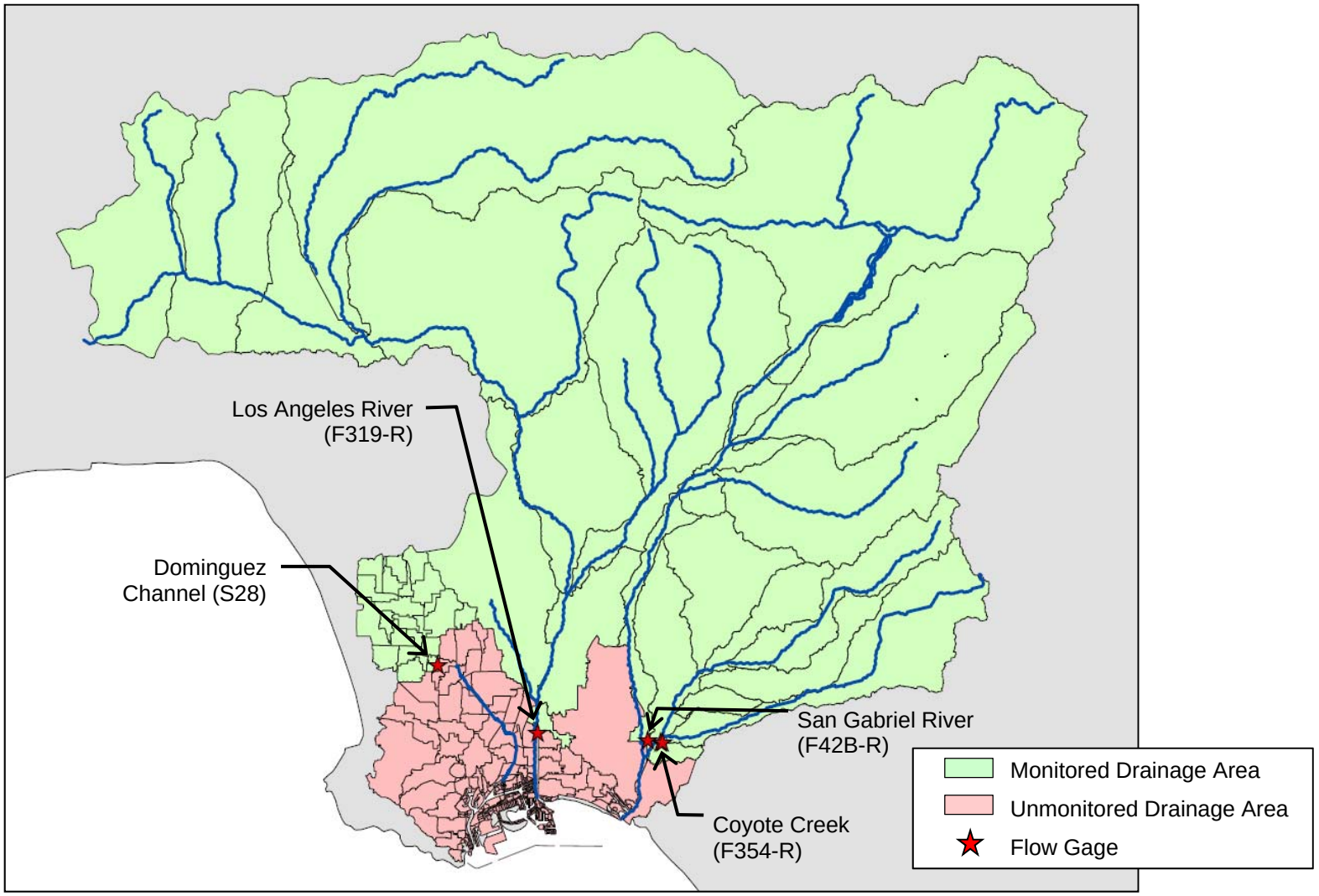

Figure 3.4 Flow Monitored Drainage Areas

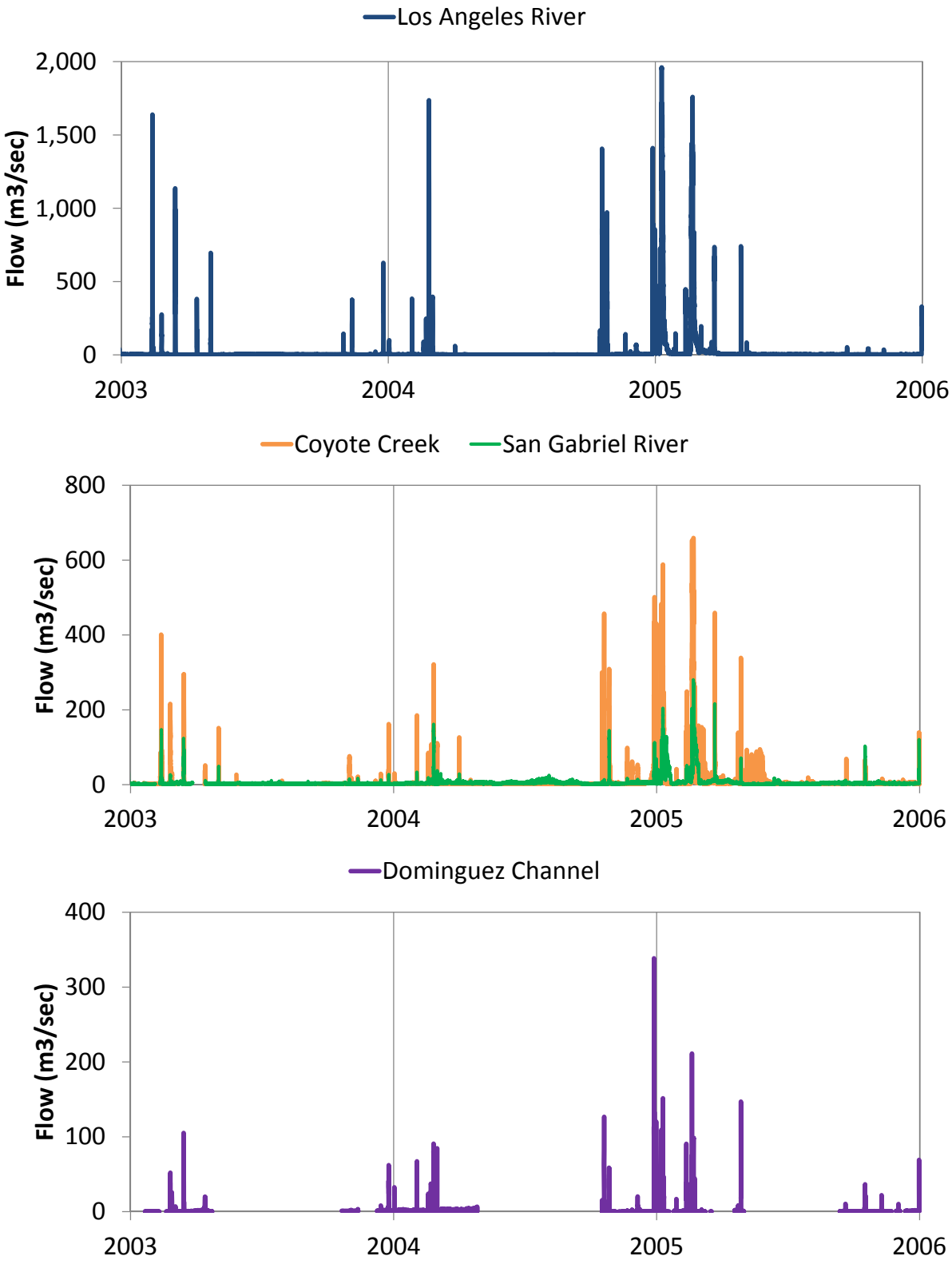

Figure 3.5 Monitored Flows 2003 - 2005

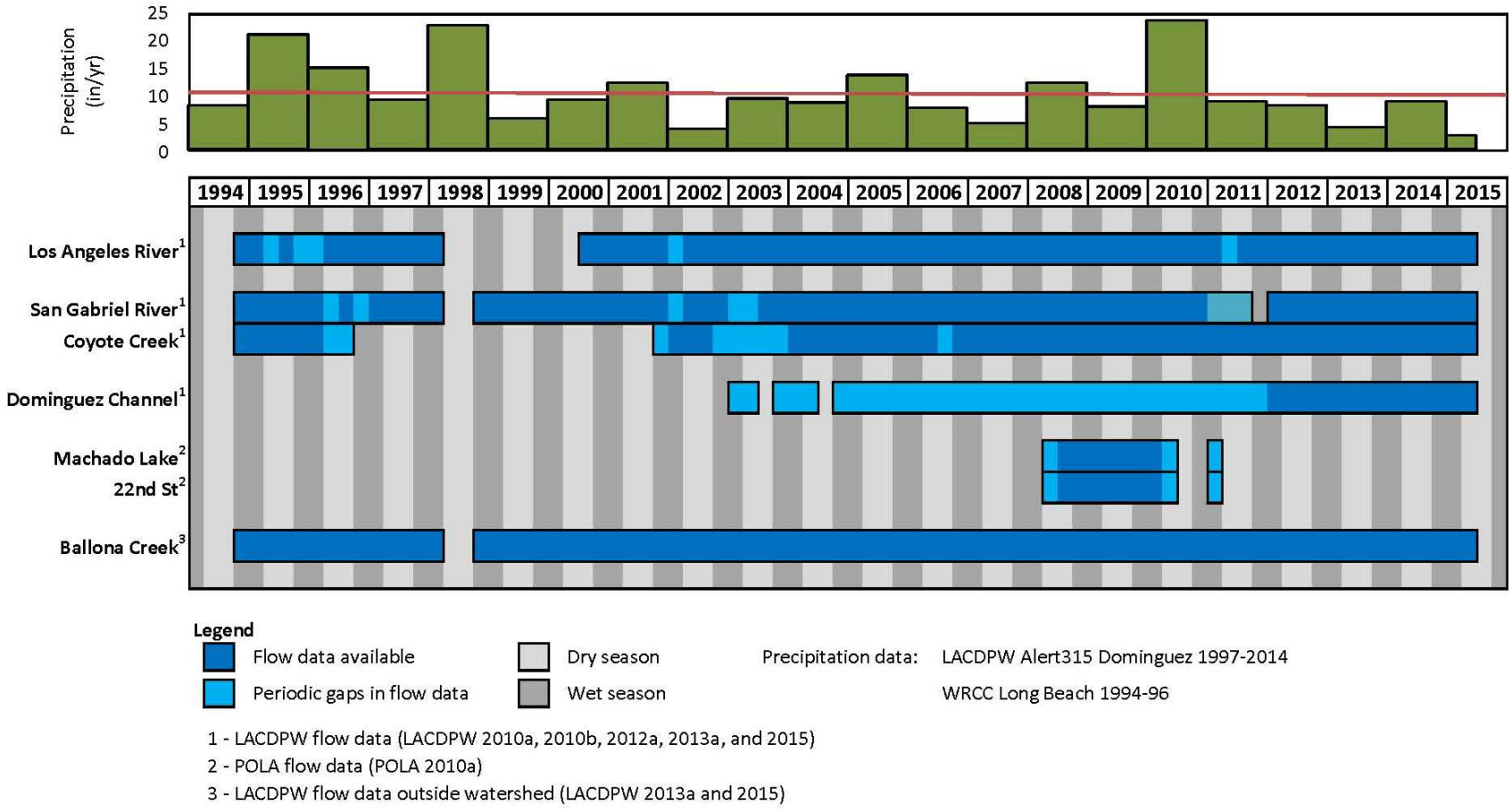

Figure 3.6 Flow Data Timeline

3.3.1 Monitored Locations

For monitored locations, gaps in flow data required estimates for dry and wet weather flows. Gaps for dry weather flows were estimated based on the average of monitored dry weather flows. Wet weather flow data gaps were estimated by scaling flow data from another gage with similar flow characteristics. Figure 3.7 compares flows during a significant rain event in December 2004 to illustrate differences in wet weather flow characteristics from each watershed. Flows from the LAR showed a relatively sharp rise in flow followed by a slower decline. The flows from CC were similar to the LAR, while flows from the SGR showed significantly reduced peaks due to the flow diversion to the LAR. Flows at the DC indicated differing flow characteristics, a relatively sharp rise and decline in flows, and an overall shorter duration for wet weather flows--relative to the flow durations at other locations--attributed to the smaller drainage area at DC. Due to the different flow characteristics of the DC, flow data from Ballona Creek (BC) were also evaluated to fill flow data gaps. The flow characteristics for BC were similar to the DC with a sharper rise and fall in flows than at the LAR or CC.

Scaling factors were determined from volume rating curves correlating two gages, as shown in Figure 3.8. The volume rating curves were generated from measured flow volumes during wet weather conditions. Flow volumes were computed from flow data. Durations of wet weather conditions were judged by increases in flow from typical base flows (dry weather flows) or prevailing pre-storm flows.

Flow characteristics, especially the timing and duration of flows, are the most similar between the LAR and CC. Hence, flow data from CC was used to fill the LAR data gaps. The volume rating curve between the LAR and CC based on data between 2003 and 2012 show a strong correlation (R^2=0.89). Conversely, flow data from LAR was used to fill the CC data gaps.

Flow characteristics for the SGR differ from the other watersheds because of flow diversion to LAR occurring during wet weather periods. Because of the flow diversion of storm flows, the dry weather or base flow typically accounts for 20 to 50 percent of total flows during wet weather conditions. It was found that the SGR flows are best correlated with the BC flow data instead of the nearby LAR. As shown in Figure 3.8, the volume rating curve generated from the wet weather flow volume of the SGR (i.e., excludes base flow) and flow volume of BC from data in 1996 and 1997 has a strong correlation (R^2=0.89).

Flow data for the DC contains periodic data gaps from 2003 to 2014 and no data are available prior to 2003. The DC flow data gaps were estimated based on the BC flow data. As shown in Figure 3.8, the volume rating curve between DC and BC based on flow data between 2003 and 2012 has a strong correlation (R^2=0.91).

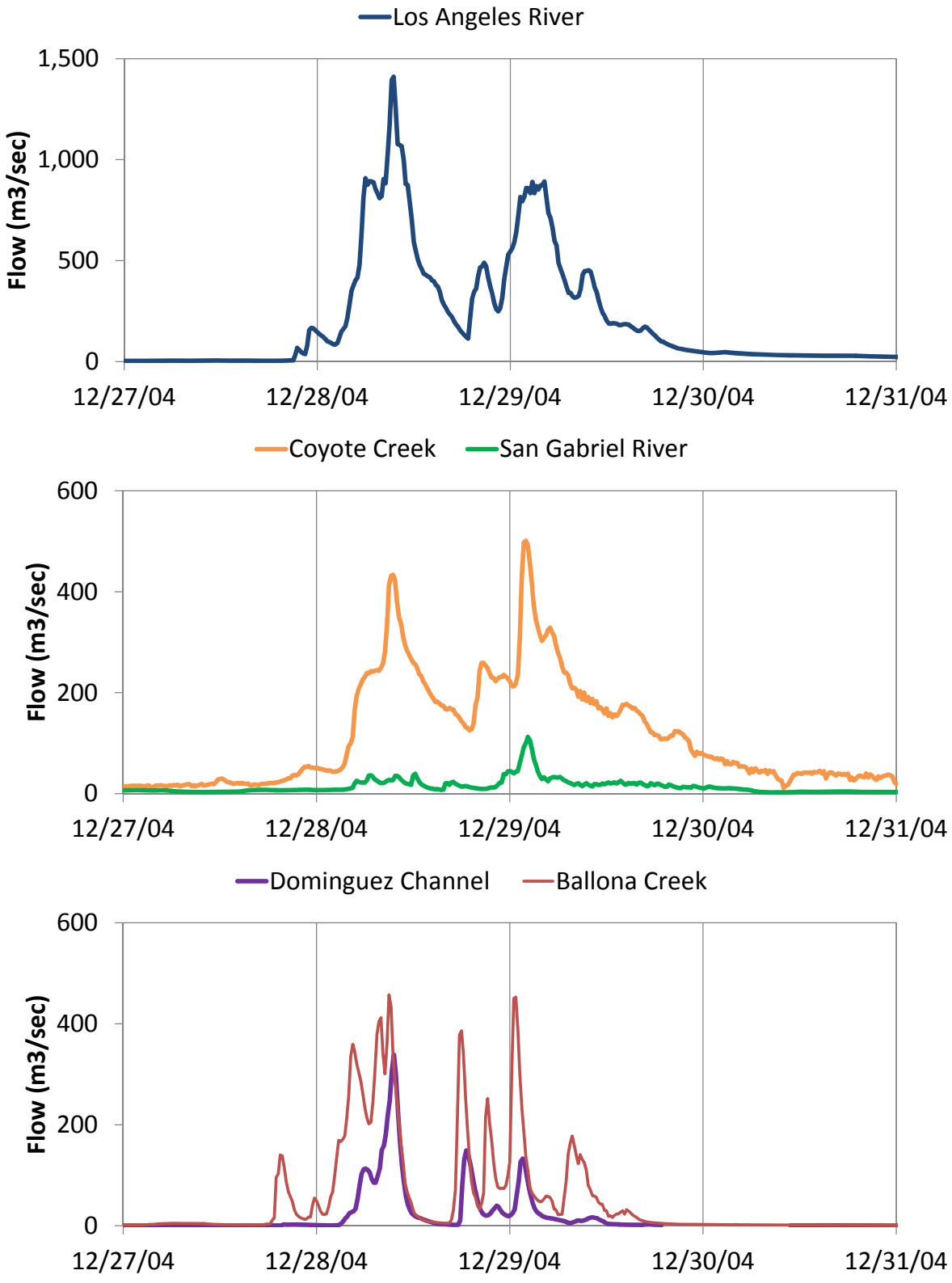

Figure 3.7 Comparisons of Wet Weather Flows

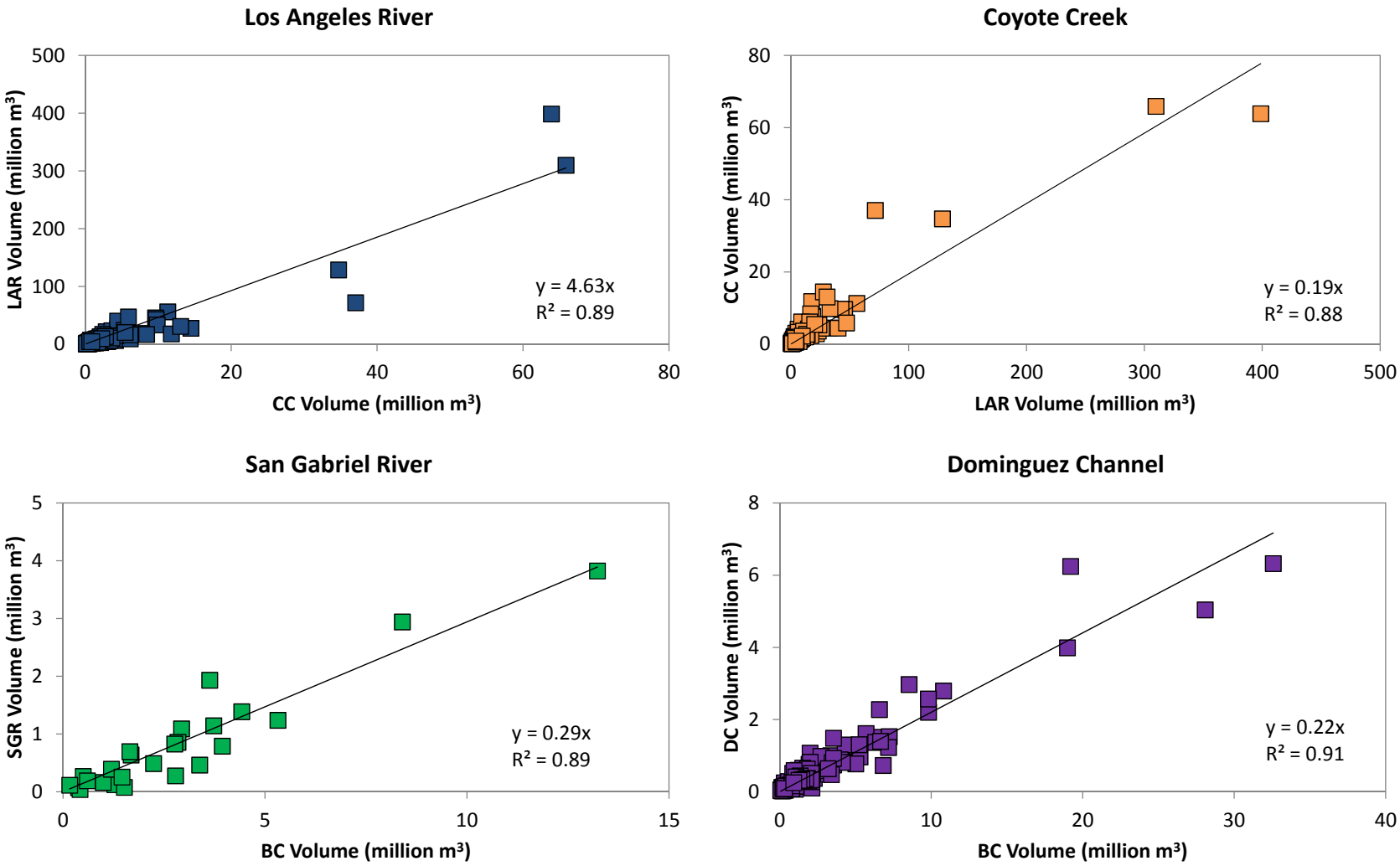

Figure 3.8 Volume Rating Curves between Flow Gages

As previously discussed, flows from Machado Lake are regulated by several structures that retard flows from directly discharging into the harbor. Flow into the harbor only occurs when the Machado Lake is full; hence, the first few storms during each wet season and/or small storm events may not result in discharge to the harbor. As illustrated in Figure 3.9, in general, when flows occur, the flood hydrographs for Machado Lake tend to have a longer duration compared to other nearby watersheds such as the DC Watershed. Given the unique flow characteristics for Machado Lake, the best correlation for estimating flows from Machado Lake was found to be flow data from the SGR. The flow diversion of the SGR results in the closest match to flow characteristics of Machado Lake, as illustrated in Figure 3.9. A volume rating curve, excluding base flows, was generated based on the Machado Lake flow volumes and SGR wet weather volumes between 2008 and 2011. Comparison of the Machado Lake and SGR volumes shows a strong correlation (R^2=0.86).

The volume rating curves were used to determine the scale factors to fill in flow data gaps. These scaling factors are summarized in Table 3.3. The flow data used to fill the data gaps were scaled to estimate the missing flows. For example, flow data from CC was multiplied by a scale factor of 4.63 to estimate the missing flows for the LAR.

Table 3.3 Scaling Factors for Flow Data Gaps

FLOW LOCATION	DATA FOR GAPS	SCALE FACTOR	CORRELATION (R^2)
Los Angeles River (LAR)	Coyote Creek (CC)	4.63	0.89
Coyote Creek (CC)	Los Angeles River (LAR)	0.19	0.88
San Gabriel River (SGR)	Ballona Creek (BC)	0.29	0.89
Dominguez Channel (DC)	Ballona Creek (BC)	0.22	0.91
Machado Lake	San Gabriel River (SGR)	0.58	0.86

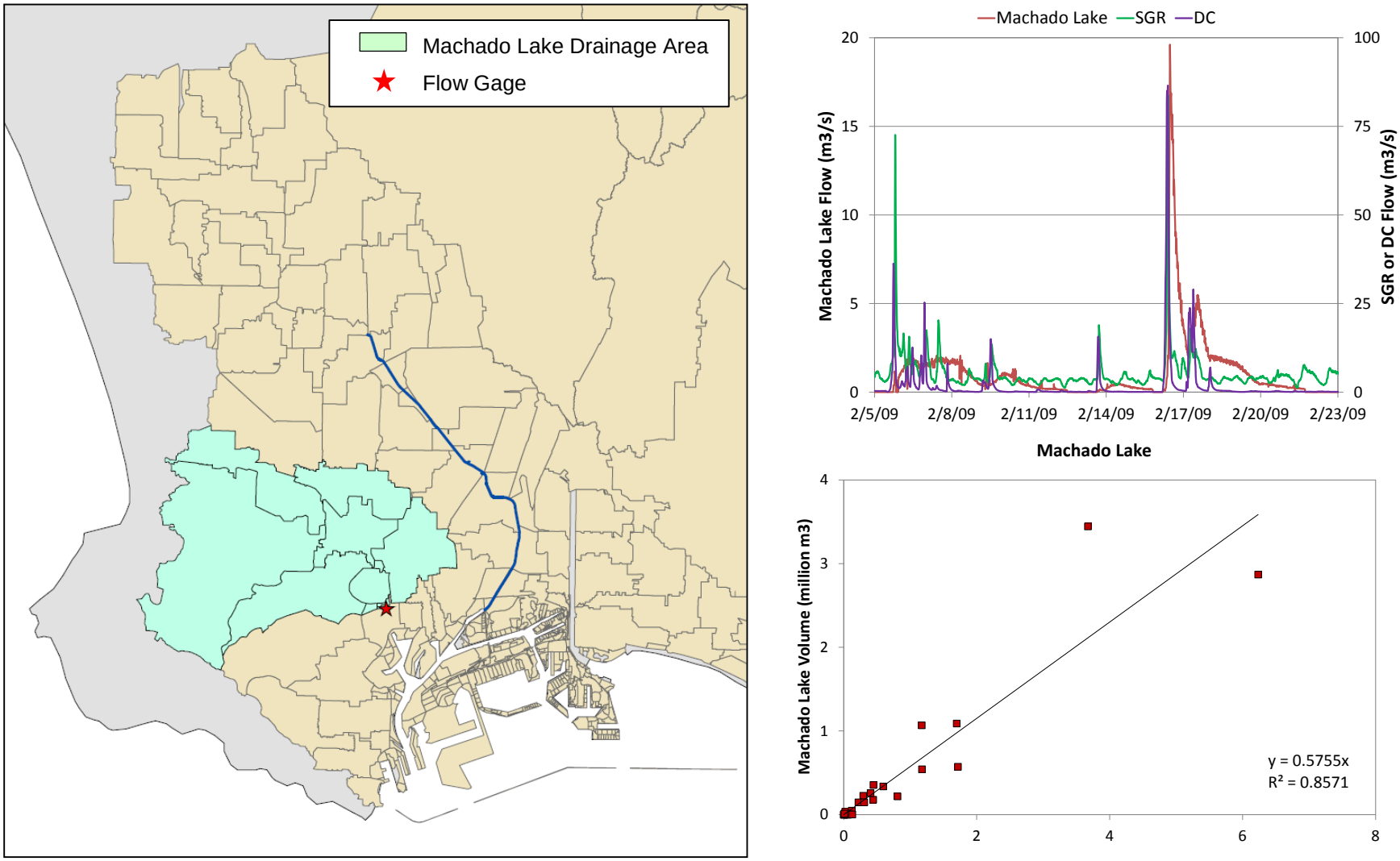

Figure 3.9 Machado Lake Flow Characteristics and Volume Rating Curve

3.3.2 Unmonitored Locations

Approximately 8% of the greater harbor watershed is not regularly monitored, as previously illustrated in Figure 3.4. This includes the drainage areas for the DC Estuary and the entire Nearshore Watershed.

Dry weather flows from the unmonitored drainage areas were estimated based on the size of their drainage areas. A correlation between urban dry weather flows and drainage area size was previously developed based on flow data from the LAR, SGR, BC Watersheds (Stein and Ackerman 2007). This dry weather flow correlation was also used during the DCEM development and for the Harbor Toxics TMDL.

For wet weather flows from unmonitored drainage areas, analytical methods were developed based on drainage area sizes. For the DC Estuary, wet weather flows were estimated by scaling the DC flows based on drainage area size. Individual scaling factors were determined for each storm water discharge along the channel. This includes the drainage area between the monitoring location at Artesia Boulevard and the model input location at Vermont Avenue. The scaling factor was calculated as the ratio of the storm water drainage area to the drainage area above Vermont Avenue. The same method was used for all Nearshore Watershed drainage areas except Machado Lake.

3.3.3 Summary

Continuous time series of flows for the four major rivers and nearly 200 storm drains were estimated between 2002 and June 2015. Measured data were used when available to define the storm water flows from the four major rivers – LAR, SGR, CC, and DC, which accounts for approximately 92% of total drainage area of the greater harbor waters. Volume rating curves were used to estimate flows for periods without flow data. Flows from unmonitored drainage areas mostly for the DC Estuary and Nearshore Watersheds were estimated by scaling flows from DC based on the drainage area sizes.

To summarize the flows that discharge into the greater harbor waters, the time series of flows (15-minute interval) were used to calculate the total volume of water (dry and wet weather flows) from each of the four major watersheds. The annual water volumes from 2002 to 2014 for the four major watersheds are summarized in Table 3.4. In general, the annual storm water volumes correspond to drainage area sizes. On average, the LAR Watershed accounts for 53% of the total storm water volume, followed by the SGR Watershed with 32%. This roughly corresponds to the 51% and 39% of the drainage areas for the LAR and SGR Watersheds, respectively (previously shown in Table 3.1). The DC and Nearshore Watersheds account for 5% and 10% of the total storm water volume, respectively. By year, the largest discharge occurred in 2005. The distribution between dry and wet weather volumes by watershed is illustrated in Figure 3.10.

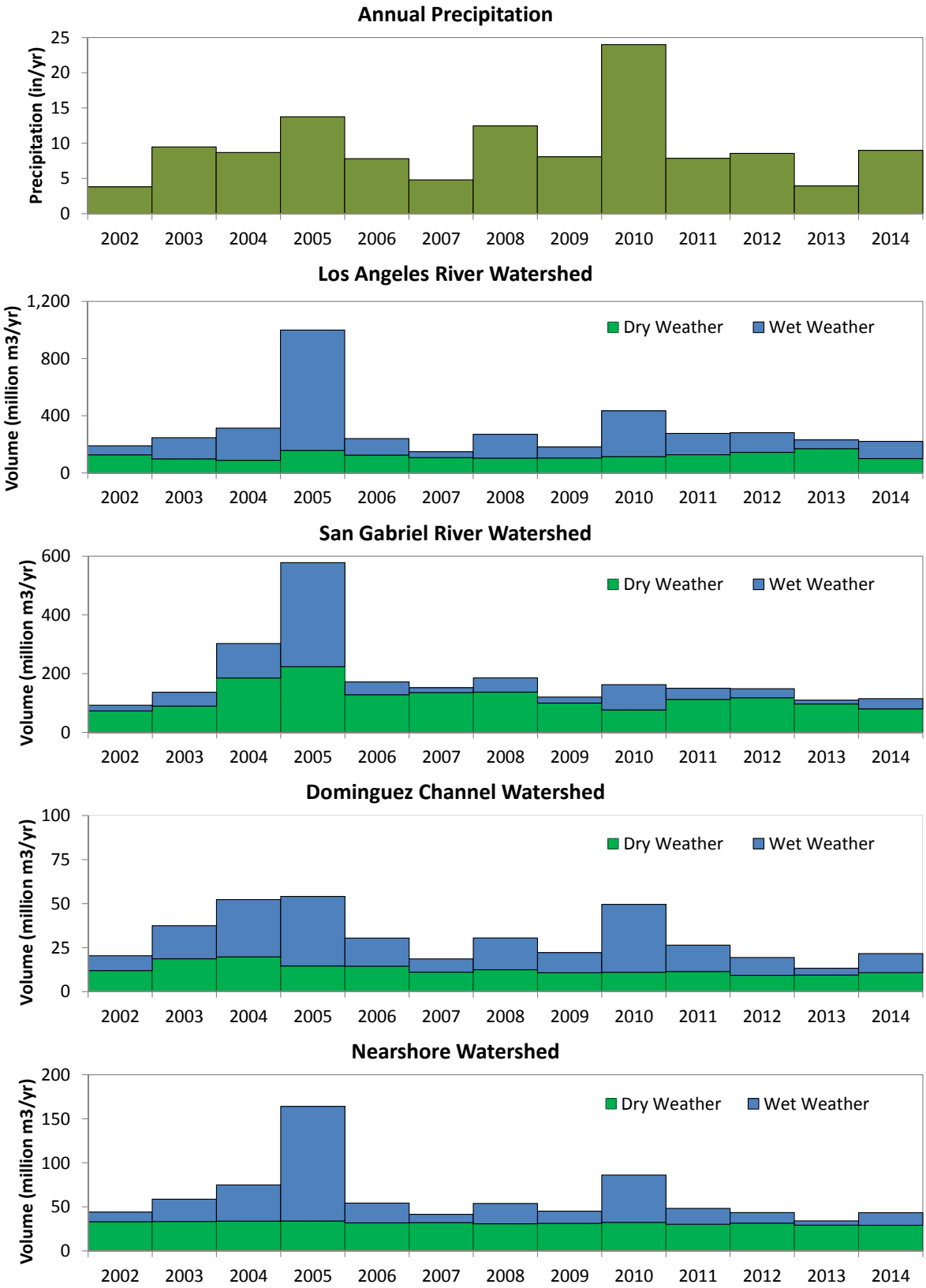

Figure 3.10 Dry and Wet Weather Storm Water Volumes by Watershed

Table 3.4 Annual Storm Water Volumes by Watershed

YEAR	PRECIPITATION (IN/YR)	ANNUAL STORM WATER VOLUME (MILLION M^3/YR)			
		LAR	SGR	DC	NEARSHORE
2002	3.82	190.0	92.6	20.4	44.2
2003	9.47	246.6	136.8	37.5	58.8
2004	8.68	313.8	302.6	52.3	75.0
2005	13.75	1,000	578.0	54.1	164.1
2006	7.81	240.9	171.7	30.5	54.4
2007	4.79	149.0	152.1	18.6	41.6
2008	12.47	270.6	185.8	30.5	53.9
2009	8.07	182.0	120.4	22.2	45.2
2010	24.00	434.4	162.4	49.6	86.2
2011	7.85	276.9	150.2	26.4	48.3
2012	8.55	282.3	148.9	19.4	43.7
2013	3.94	232.0	110.0	13.3	34.2
2014	8.99	221.4	114.8	21.6	43.4
Average	9.40	310.8 (53%)	186.6 (32%)	30.5 (5%)	61.0 (10%)

Dry weather volumes are mostly from wastewater reclamation plant effluent and urban land uses. The highest dry weather volumes are discharged from the SGR Watershed, which includes five wastewater reclamation plants. The Nearshore Watershed also contains one wastewater reclamation plant. In general, dry weather flows are relatively constant by year, while wet weather flows are more variable. Wet weather flows tend to dominate during years with above average rainfall (e.g., 2005 and 2010), while dry weather flows are greater during drier years such as 2002, 2007, and 2013. The percentage of storm water volumes during wet weather conditions are summarized by watershed in Table 3.5. The percentage of storm water volume during wet weather conditions varies year-to-year depending on the hydrologic conditions. For the LAR Watershed, wet weather flows account for 61% of the total storm water volume on average. In comparison, wet weather flows account for 36% of the total storm water volume for the SGR Watershed. Overall, 52% of the total storm water discharged into the greater harbor waters occur during wet weather conditions.

Table 3.5 Percentage of Wet Weather Storm Water Volumes by Watershed

YEAR	PRECIPITATION (IN/YR)	LAR	SGR	DC	NEARSHORE
2002	3.82	33%	21%	42%	25%
2003	9.47	60%	35%	50%	43%
2004	8.68	72%	39%	62%	55%
2005	13.75	84%	61%	73%	79%
2006	7.81	48%	25%	53%	41%
2007	4.79	28%	11%	40%	23%
2008	12.47	62%	26%	59%	43%
2009	8.07	43%	17%	51%	31%
2010	24.00	74%	53%	78%	62%
2011	7.85	54%	25%	57%	37%
2012	8.55	49%	21%	52%	28%
2013	3.94	27%	12%	29%	14%
2014	8.99	55%	30%	50%	33%
Average	9.40	61%	36%	58%	48%

3.4 SEDIMENT LOADINGS

Concurrent flow and TSS data were evaluated to identify potential relationships that could be used to estimate sediment watershed loadings. TSS data were available from ongoing monitoring programs and prior studies, as summarized in Table 3.6. Nearly all TSS data were from ongoing monitoring programs that periodically measure TSS as part of the National Pollutant Discharge Elimination System (NPDES) monitoring requirements. LACDPW measures TSS at three mass emission stations at the LAR, CC, and DC. These locations are monitored during several dry and wet events each year. The City of Long Beach also monitors three locations in the Nearshore Watershed that discharges to Alamitos Bay. The POLB monitors 21 storm drain outfalls in the harbor during a minimum of one dry and two wet events each wet season. Other TSS data also available were from prior studies that monitored individual wet weather events at several locations primarily in the Nearshore and DC Watersheds. In some cases, the prior studies included TSS measurements at the LACDPW mass emission stations. Locations where TSS data were collected under these programs are shown in Figure 3.11. In the figure, the TSS data locations are shown by drainage area.

Most of the TSS data were collected as composite samples during dry or wet weather events, and only a few samples were collected as grab samples. In general, composite TSS measurements followed sampling protocols used by LACDPW (LACDPW 2013b). Composite samples were collected using an automated sampler, which combines a series of discrete samples (aliquots) of specific volume collected at a specific interval over a sampling period. For dry weather, composite samples were commonly collected as time-weighted composites over a 24-hour period. Wet weather composite samples were typically collected as flow-weighted composites in which discrete samples are collected at flow-paced intervals. In the laboratory, discrete samples were then mixed in proportion to the measured flow rates in order to obtain a flow-weighted composite. Ideally, the wet weather composite samples would be conducted over the duration of an individual storm event so that the TSS measurement is representative of the entire wet weather event. Automated samplers can be triggered to collect discrete samples when a predetermined water level or pre-storm flow is exceeded. However, due to highly variable rainfall characteristics, wet weather composites may cover only a portion of or extend beyond, before, or after wet weather flows.

Table 3.6 Storm Water TSS Data Summary

WATERSHED	LOCATION	MONITORING PROGRAMS
Los Angeles River (LAR)	LAR	LACDPW NPDES monitoring 1995-2013 – Composite samples for multiple events per year (LACDPW 2013b) Storm Water Study – 1 dry and 2 wet events (AMEC Foster Wheeler 2015b)
San Gabriel River (SGR)	Coyote Creek (CC)	LACDPW NPDES monitoring 1995-2013 – Composite samples for multiple events per year (LACDPW 2013b)
Dominguez Channel (DC)	DC	LACDPW NPDES monitoring 1995-2013 – Composite samples for multiple events per year (LACDPW 2013b) Wet event 2/27/06 – 10 grab samples (Everest 2007) Storm Water Study – 1 dry and 2 wet events (AMEC Foster Wheeler 2015b)
	Del Amo Lateral	Wet event 2/27/06 – 10 grab samples (Everest 2007) LACDPW tributary monitoring 2008-2011 – composite samples for 9 dry and 16 wet events (LACDPW 2011)
	Torrance Lateral	Wet event 2/24/03 – 11 grab samples (POLA 2005) Wet event 2/27/06, 10 grab samples (Everest 2007) LACDPW tributary monitoring 2008-2011 – composite samples for 9 dry and 16 wet events (LACDPW 2011) Wet event 12/12/14 – Composite sample (AMEC Foster Wheeler 2015b)
Nearshore	Machado Lake	Wet event 3/6/01, single grab sample (City of Los Angeles 2002) Wet event 3/20/11 – 3 grab samples (POLA 2010a) Wet event 12/12/14 – Grab sample (AMEC Foster Wheeler 2015b)
	Port Land Uses	Wet event 2/24/03 – 2 locations, 11 grab samples (POLA 2005) POLB NPS monitoring 2006-10 – 21 locations, 3 dry events, 120 wet events (POLB 2010) Storm Water Study – Pier A, 2 wet events (AMEC Foster Wheeler 2015b)
	Other	Wet event 3/17/02 – Maritime Museum, 8 samples (POLA 2005) City of Long Beach NPDES monitoring 2002-07 – 3 locations, 10 dry events, 17 wet events (City of Long Beach 2007) Watershed monitoring – dry event 9/14/08 at 3 locations, wet event 4/1/10 at 1 location, wet event 2/26/11 at 1 location, wet event 3/20/11 at 2 locations (POLA 2010a)

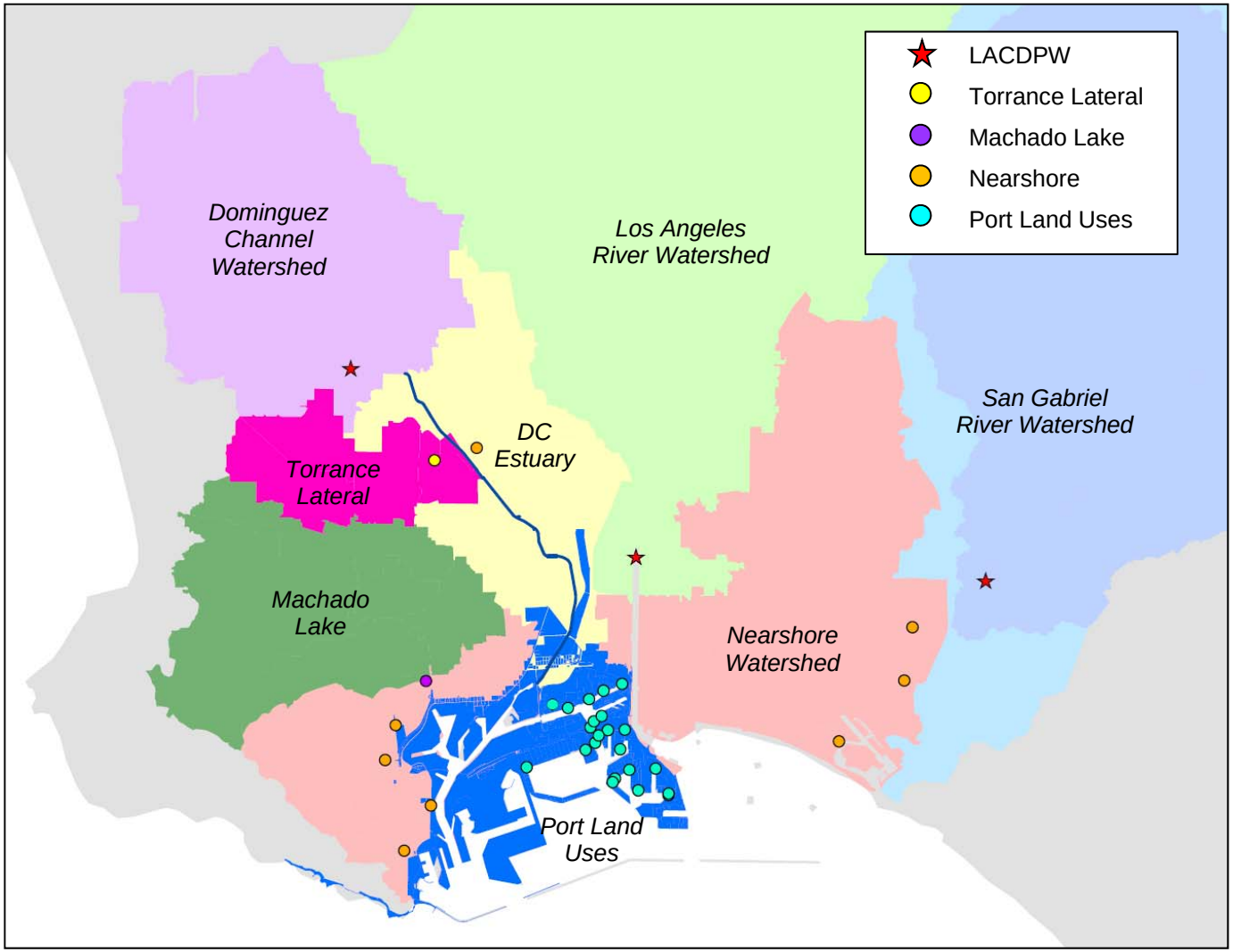

Figure 3.11 Storm Water TSS Data Locations

3.4.1 Sediment Concentrations

TSS data for the LAR, CC, and DC comprise the most comprehensive dataset and were used to develop the analytical method for estimating sediment loadings. An attempt was first made to develop sediment rating curves between storm water flow and TSS, but a very poor correlation was found to exist between flow and TSS for most of the data. Hence, instead of using a rating curve, an analytical method was developed to estimate sediment loading using seasonal, average TSS concentrations to represent dry, first flush, and wet weather conditions. For the seasonal average TSS concentrations, dry weather refers to TSS concentrations during non-wet weather conditions (i.e., perennial base flows that occur year round). Wet weather conditions represent flows generated by rainfall, while the first flush refers to the single rain event that occurs at the beginning of the wet season, which starts in October. Since the TSS data were primarily collected as composite samples, the wet weather and first flush seasonal average concentrations account for both the base flow and rainfall flows.

The seasonal average TSS concentrations for the LAR, CC, and DC are provided in Figure 3.12. In the figure, the TSS data are plotted against the average flow during the TSS sampling period, which shows the poor correlation between flow and TSS; the average flow was not used in determining the seasonal average TSS concentrations. Measured dry and wet weather TSS data, as previously discussed in Section 3.4, are shown by the blue and green diamond symbols, respectively. TSS data from first flush events are indicated by the yellow circles. The first flush event was defined as the first major rain event of the wet season, which typically occurs in October. However, the first major rain event, which is judged based on the flow magnitude, may occur as early as September or as late as December. The seasonal average TSS concentrations are indicated by the blue, red, and green lines corresponding to the dry, first flush, and wet weather conditions. TSS data for the LAR from 1995 to 2014 were used and show a wide range in concentrations. As expected, the wet weather TSS concentrations were about an order of magnitude higher than those for the dry weather conditions; TSS concentrations during the first flush events were higher still. TSS data for CC ranged from 1995 to 2013. Seasonal variations in the average TSS concentrations are similar to those in the LAR. For the DC, TSS data were available from 2003 to 2014. The TSS concentrations covered nearly the same range as the LAR and CC, but corresponded with lower flows. Similarly, distinct average TSS concentrations were observed for dry, first flush, and wet weather conditions.

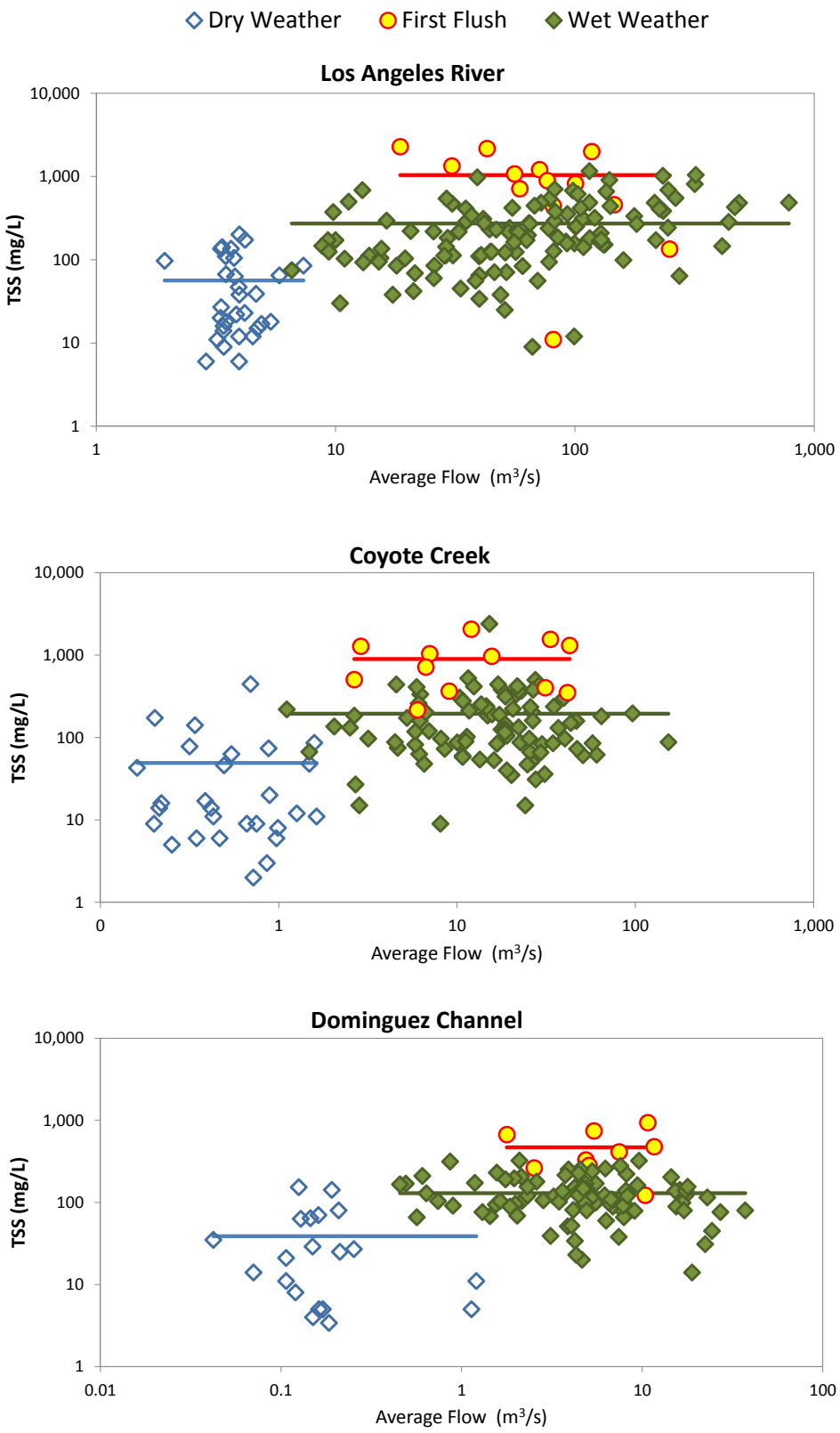

Figure 3.12 Seasonal Average TSS Concentrations for Los Angeles River, Coyote Creek, and Dominguez Channel

Seasonal TSS concentrations were also determined for the Torrance Lateral, port land uses, and Machado Lake, as shown in Figure 3.13. For the Torrance Lateral, TSS data were available from several studies conducted between 2003 and 2014. Although the available TSS data were limited, the data still show seasonal variations in average TSS concentrations. TSS data for port land uses were available from the POLB NPDES monitoring and several studies conducted from 2003 to 2015. The dry weather TSS data were limited to only three measurements since dry weather flows do not always occur from port land uses. First flush TSS data were only available for one event at 13 locations. Most of the TSS data for port land uses were for wet weather conditions. In general, TSS concentrations for port land uses are relatively low compared to other storm drains. For Machado Lake, a TSS concentration was determined for only wet weather conditions since no discharge occurs during dry weather conditions. TSS data were only available from prior studies of wet weather events in 2001, 2011, and 2014.

The seasonal average TSS concentrations are summarized in Table 3.7. The LAR TSS estimates were applied to the LAR flow from the fresh water portion of the watershed. The CC TSS estimates were used for both the SGR and CC loadings. The DC TSS estimates were used to estimate sediment loadings for the DC, including the DC Estuary and the Nearshore Watershed. TSS estimates for the Torrance Lateral and Machado Lake were applied to the individual discharges. The port land uses TSS estimates were used for all port drainage areas.

Table 3.7 Seasonal Average TSS Concentrations

LOCATION	AVERAGE TSS CONCENTRATION (MG/L)		
	DRY WEATHER	FIRST FLUSH	WET WEATHER
Los Angeles River (LAR)	56	1,040	273
Coyote Creek (CC)	49	897	195
Dominguez Channel (DC)	39	470	130
Torrance Lateral	38	658	194
Port Land Uses	16	99	90
Machado Lake	--	--	16

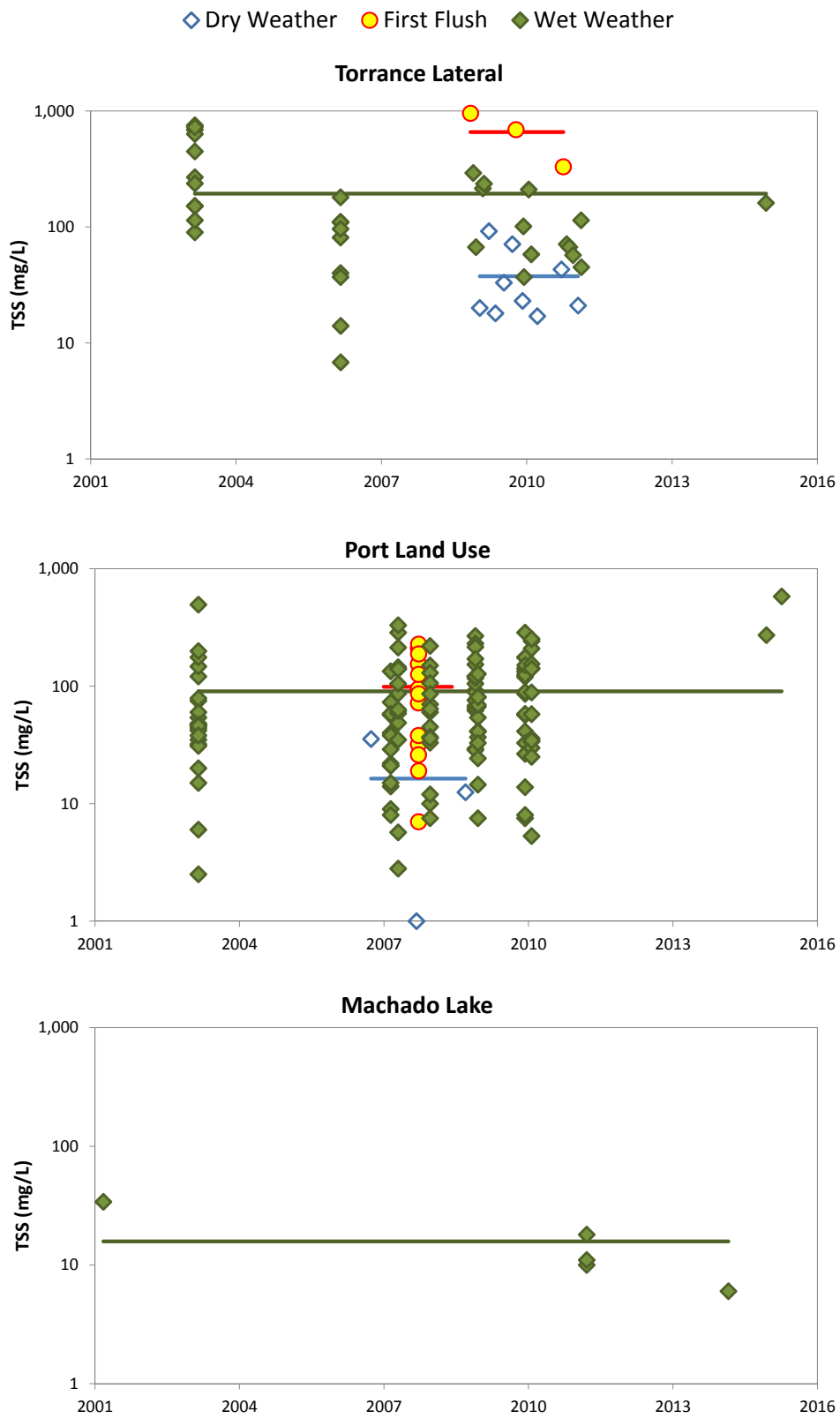

Figure 3.13 Seasonal Average TSS Concentrations for Torrance Lateral, Port Land Use, and Machado Lake

3.4.2 Summary

Storm water sediment concentrations were estimated using seasonal average TSS concentrations. This method was selected since the data did not support a TSS and flow discharge rating curve. The sediment loadings that discharge into the greater harbor waters were calculated based on the time series of flows and seasonal average TSS concentrations. Examples of the sediment loadings for the LAR, SGR, CC, DC, and Machado Lake are shown in Figure 3.14. In the figure, the sediment loading rates are shown for December 2004 through February 2005. The sediment loading rates correspond to the flows since the TSS concentrations were estimated from constant concentrations.

The annual sediment loadings from 2002 to 2014 are summarized by watershed in Table 3.8. The sediment loadings generally correspond to the annual precipitation with the highest sediment loadings for 2005 and 2010. On average, the LAR Watershed contributes 70% of the total sediment loading to the greater harbor waters, followed by 22% from the SGR Watershed. The DC and Nearshore Watersheds each contribute 4% of the total sediment loading.

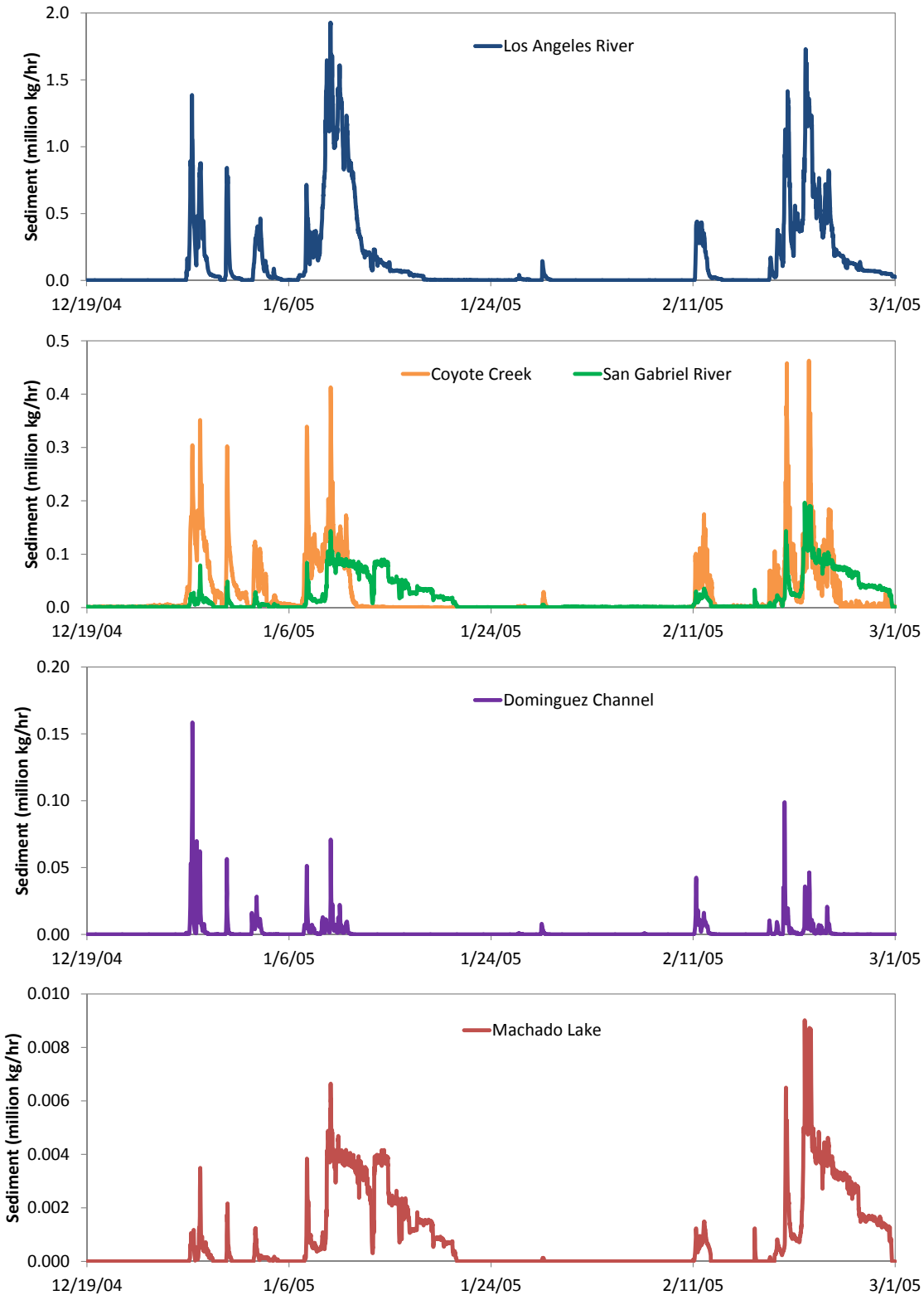

Figure 3.14 Comparisons of Sediment Loadings

Table 3.8 Annual Sediment Loadings by Watershed

Year	Precipitation (in/yr)	Annual Sediment Loading (million kg/yr)			
		LAR	SGR	DC	Nearshore
2002	3.82	36.6	10.3	2.42	2.31
2003	9.47	47.6	14.3	3.55	3.22
2004	8.68	69.7	34.5	5.38	4.92
2005	13.75	239.9	81.2	6.13	7.10
2006	7.81	41.3	15.5	2.87	2.74
2007	4.79	24.2	12.3	2.13	2.07
2008	12.47	62.6	19.8	2.98	2.90
2009	8.07	35.1	9.4	2.61	2.48
2010	24.00	95.3	21.2	6.17	5.99
2011	7.85	61.0	15.2	2.98	2.83
2012	8.55	48.5	12.2	1.78	1.85
2013	3.94	28.9	7.9	1.02	1.12
2014	8.99	42.3	11.4	2.55	2.48
Average	9.40	64.1 (70%)	20.4 (22%)	3.27 (4%)	3.23 (4%)

The distribution between dry and wet weather sediment loadings by watershed is illustrated in Figure 3.15. Unlike storm water flows, sediment loadings were predominantly estimated from wet weather events for all four watersheds. The percentage of sediment loading during wet weather conditions are summarized for each watershed in Table 3.9. Wet weather sediment loadings made up approximately 91% of the total sediment loading for the LAR Watershed and 71% for the SGR Watershed. For the DC and Nearshore Watersheds, wet weather sediment loadings accounted for 85% and 84% of the total sediment loads, respectively. Overall, 85% of the total sediment loading occurs during wet weather conditions.

Table 3.9 Percentage of Wet Weather Sediment Loadings by Watershed

YEAR	PRECIPITATION (IN/YR)	LAR	SGR	DC	NEARSHORE
2002	3.82	81%	65%	81%	78%
2003	9.47	88%	69%	80%	84%
2004	8.68	93%	74%	86%	90%
2005	13.75	96%	86%	91%	83%
2006	7.81	83%	59%	81%	82%
2007	4.79	75%	46%	80%	75%
2008	12.47	91%	66%	84%	82%
2009	8.07	83%	48%	84%	79%
2010	24.00	93%	82%	83%	92%
2011	7.85	88%	64%	85%	82%
2012	8.55	83%	53%	80%	73%
2013	3.94	67%	40%	65%	55%
2014	8.99	87%	66%	84%	80%
Average	9.40	89%	71%	85%	84%

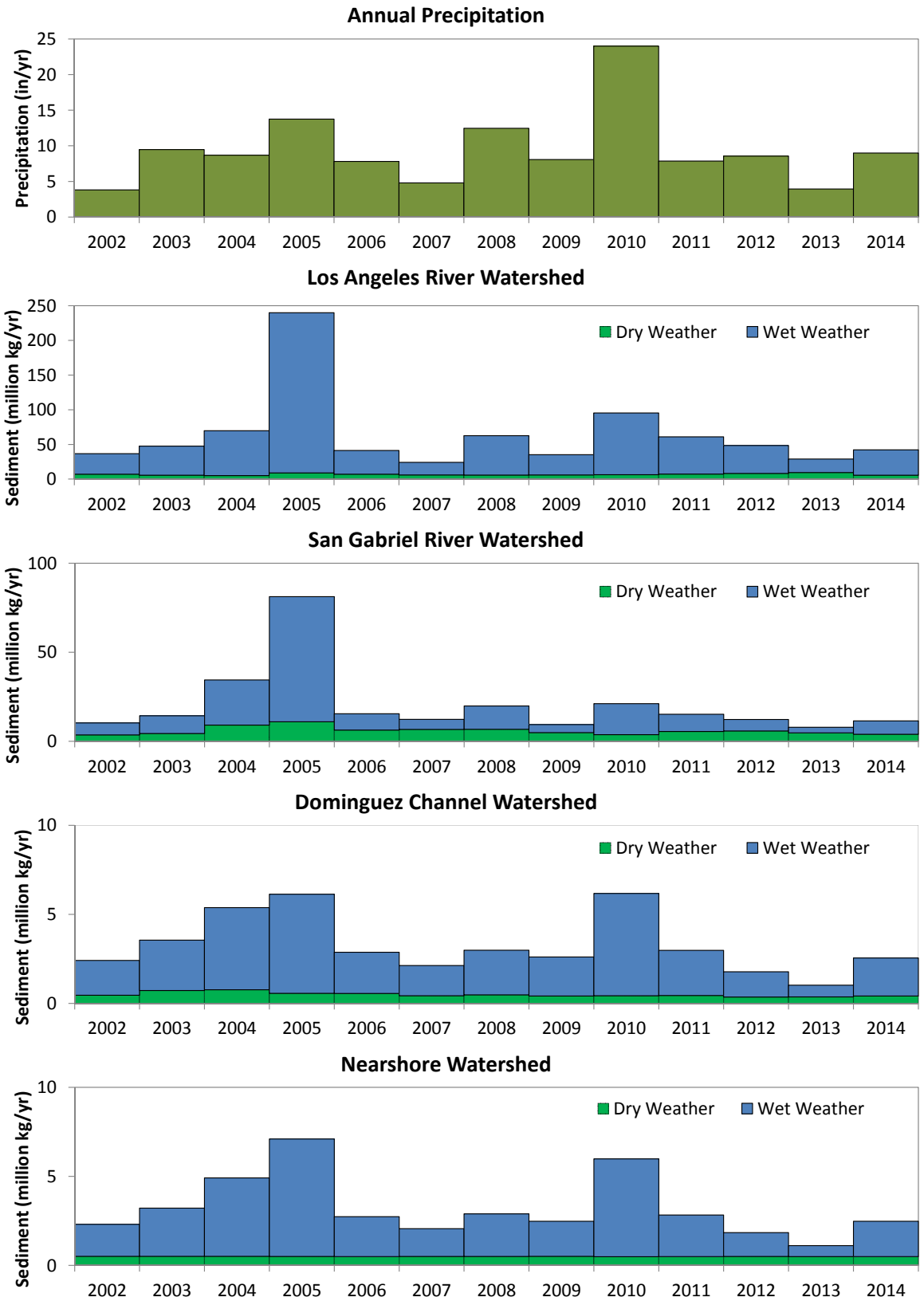

Figure 3.15 Dry and Wet Weather Sediment Loadings by Watershed

3.5 ORGANIC CHEMICAL LOADINGS

Nearly all prior storm water data for TPCB and TDDX have been below detection limits. Additional storm water data were required in order to generate estimates of organic chemical watershed loadings. Hence, a special study was conducted to provide data for estimating organic chemical loadings. The Storm Water Monitoring Study (Storm Water Study) was conducted to measure TPCB and TDDX concentrations at selected storm water locations at LAR, DC, Machado Lake, Torrance Lateral, and Pier A (AMEC Foster Wheeler 2015b). These monitoring locations are shown in Figure 3.16. The LAR and DC monitoring locations were selected to coincide with the LACDPW flow and water quality monitoring stations. Machado Lake and Torrance Lateral were selected to augment existing TDDX data.

The Pier A monitoring location in the POLB was selected to represent port land uses. The Storm Water Study consisted of monitoring one dry and three wet weather events, as summarized in Table 3.10. Dry Event 1 was conducted in February 18 – 19, 2014 with samples collected at the LAR and DC. Wet Event 1 occurred on February 27, 2014 with samples collected at the LAR, DC, and Machado Lake. For Wet Event 2, four locations were sampled on December 12 – 13, 2014. A third wet event was conducted to collect additional data at Pier A on April 7, 2015. Organic chemical data from the Storm Water Study as well as available data from prior studies were used establish correlations with suspended sediment concentrations that can be used estimate TPCB and TDDX watershed loadings.

Table 3.10 Storm Water Study Event Summary

LOCATION	DATE	DESCRIPTION
Dry Event 1	February 18 – 19, 2014	Composite samples at LAR and DC
Wet Event 1	February 27, 2014	Rainfall: 0.47 inch Composite samples at LAR and DC Grab sample at Machado Lake
Wet Event 2	December 12 – 13, 2014	Rainfall: 1.04 inch Composite samples at LAR, DC, Torrance Lateral, and Pier A TSS grab samples at LAR and DC
Wet Event 3	April 7, 2015	Rainfall: 0.27 inch Composite sample at Pier A

Figure 3.16 Storm Water Organic Data Locations

3.5.1 TPCB

Organic chemical concentrations in storm water were estimated through their relationships with suspended sediment concentrations. For TPCB, data from the Storm Water Study (one dry event and three wet events) were used to correlate organic chemicals and TSS concentrations. These data are shown in the upper left panel of Figure 3.17. A dry weather estimate was made based on the average of the dry weather data, as shown in the upper right panel of Figure 3.17. For wet weather, a rating curve was developed as shown in the lower left panel of the figure. The TPCB and TSS concentrations collected at four locations shows a very strong correlation (R^2=0.996). The correlation between TPCB and TSS reflects the tendency for organics to be associated with fine-grained sediment. This TPCB rating curve was used to estimate TPCB concentrations based on the estimated sediment concentrations, as illustrated by the gray dashed lines on the figure. It can be seen that the wet weather sediment concentrations are within the measured TSS range of the data. However, the first flush sediment concentrations are higher than the measured TSS data and the rating curve needed to be extrapolated, as shown by the red dashed line. A separate estimate was used for port land uses, as shown in the lower right panel. The average TPCB concentration measured at Pier A was used for the TPCB wet weather concentrations from port land uses.

The estimated storm water TPCB concentrations based on the corresponding sediment concentrations are summarized in Table 3.11. Dry weather TPCB concentrations were applied to all storm water discharges. The first flush and wet weather concentrations were estimated based on the wet weather TPCB rating curve (bottom left panel of Figure 3.17) and estimated sediment concentrations (Table 3.7). TPCB concentrations for the port land uses were applied as a constant concentration based on the average of the data.

Table 3.11 Storm Water TPCB Concentrations

LOCATION	DRY WEATHER (NG/L)	FIRST FLUSH (NG/L)	WET WEATHER (NG/L)
Los Angeles River (LAR)	2.27	287	68.1
Coyote Creek (CC)	2.27	245	47.4
Dominguez Channel (DC)	2.27	122	30.6
Torrance Lateral	2.27	176	47.1
Port Land Uses	2.27	32.4	32.4
Machado Lake	--	--	3.21

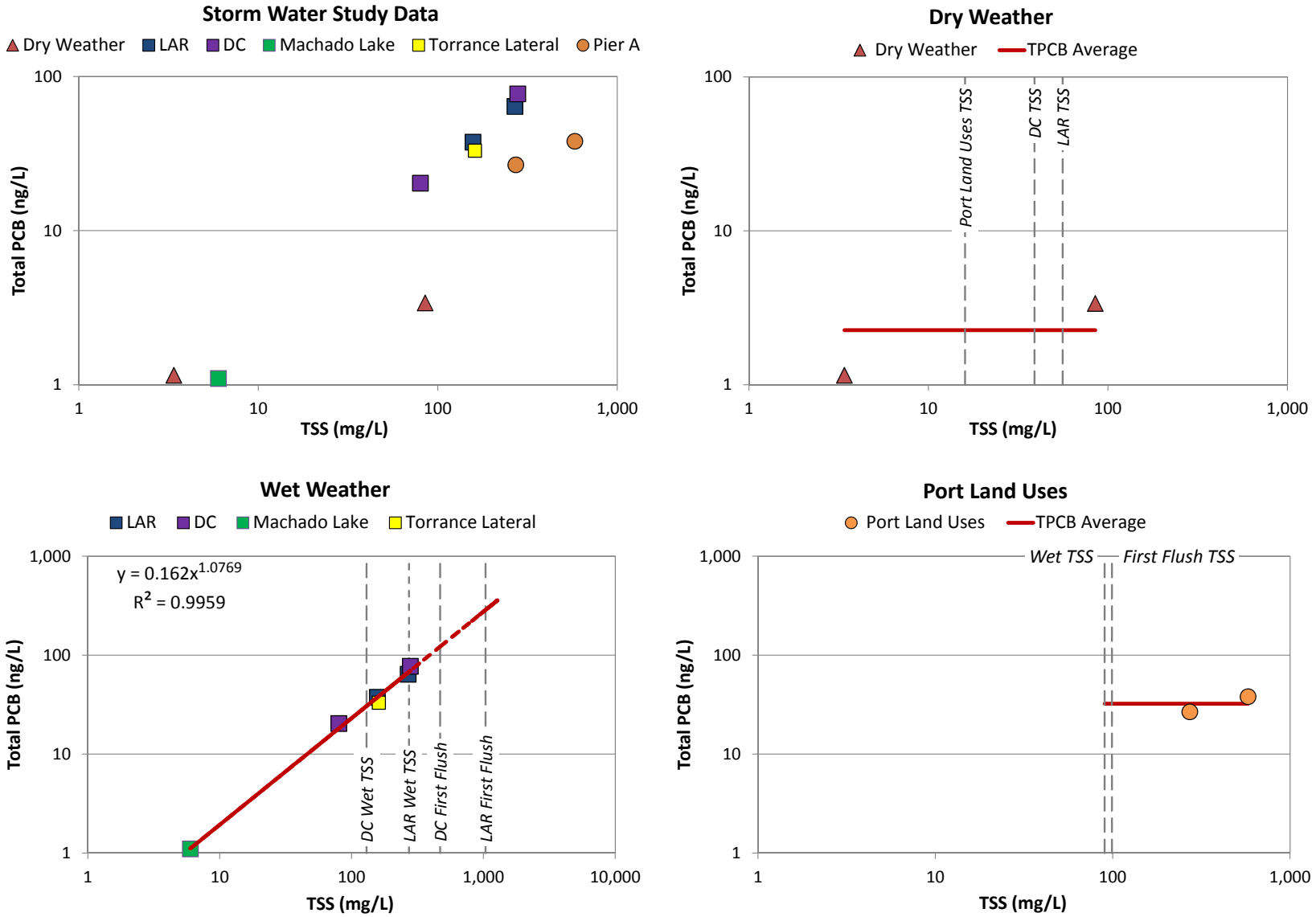

Figure 3.17 TPCB Storm Water Estimates

TPCB loadings that discharge into the greater harbor waters were calculated based on the time series of flows and estimate storm water TPCB concentrations. Examples of the TPCB loadings for the LAR, SGR, CC, DC, and Machado Lake are shown in Figure 3.18. In the figure, the TPCB loading rates are shown for December 2004 through February 2005, which show that the TPCB loading rates correspond to the flows.

The annual TPCB loadings for each of the four watersheds, determined based on the estimated flows and TPCB concentrations from 2002 to 2014, are summarized in Table 3.12. The TPCB loadings were computed based on estimated storm water flows and TPCB concentrations. On average, the LAR Watershed contributes about 74% of the total TPCB loading to the greater harbor waters, followed by 19% from the SGR Watershed. The DC and Nearshore Watersheds each contribute nearly 4% of the total TPCB loading.

Table 3.12 Annual TPCB Loadings by Watershed

YEAR	PRECIPITATION (IN/YR)	ANNUAL TPCB LOADING (KG/YR)			
		LAR	SGR	DC	NEARSHORE
2002	3.82	8.09	1.92	0.52	0.53
2003	9.47	10.78	2.65	0.72	0.75
2004	8.68	16.47	6.69	1.15	1.17
2005	13.75	58.02	17.62	1.36	1.65
2006	7.81	8.93	2.56	0.59	0.63
2007	4.79	5.03	1.77	0.45	0.47
2008	12.47	14.81	3.64	0.63	0.66
2009	8.07	7.83	1.34	0.57	0.57
2010	24.00	22.50	4.43	1.41	1.44
2011	7.85	14.21	2.71	0.65	0.66
2012	8.55	10.51	1.85	0.36	0.41
2013	3.94	5.32	1.00	0.18	0.22
2014	8.99	9.50	2.04	0.55	0.57
Average	9.40	14.77 (73.5%)	3.86 (19.2%)	0.70 (3.5%)	0.75 (3.7%)

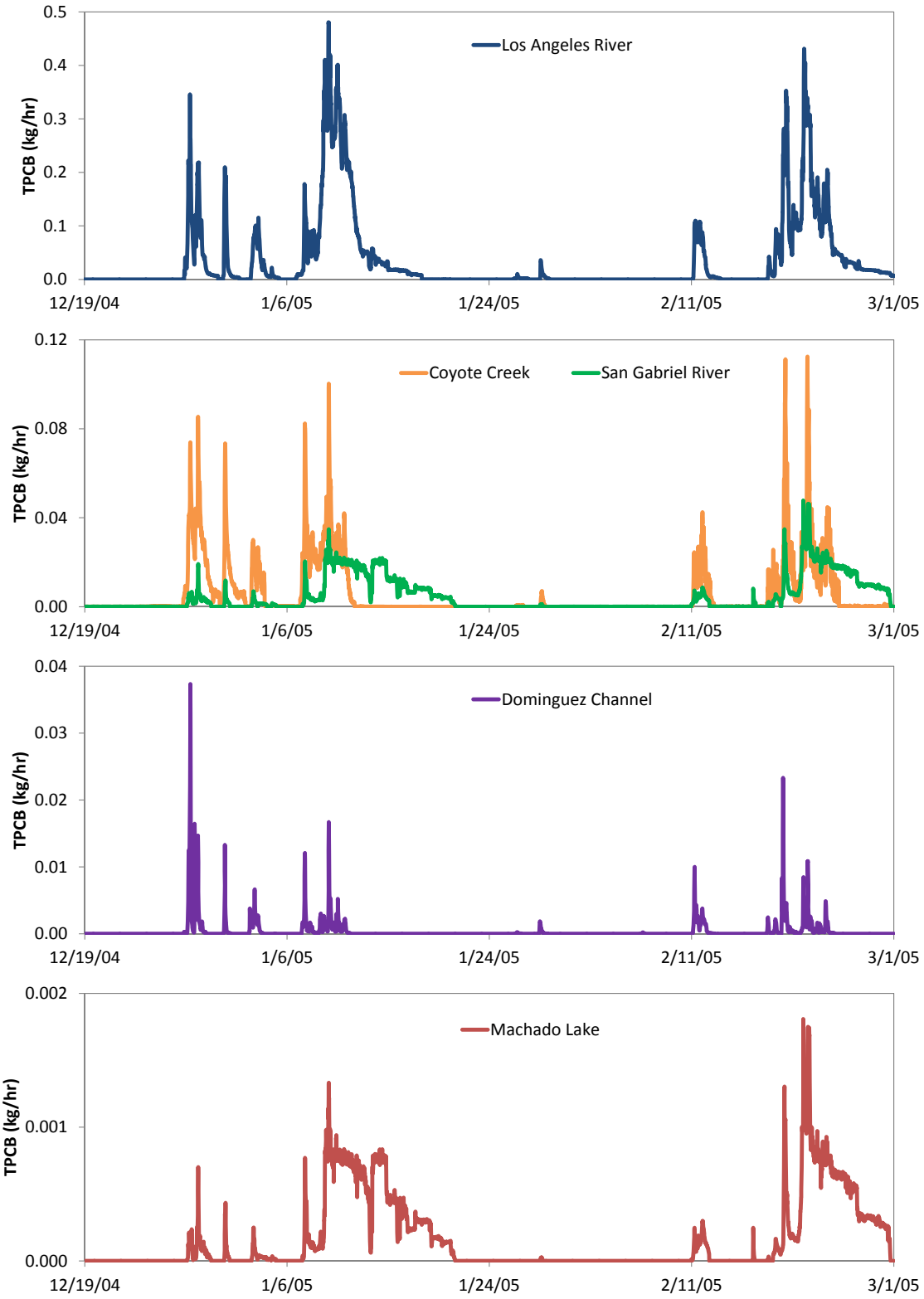

Figure 3.18 Comparisons of TPCB Loadings

The dry and wet weather TPCB loadings for each watershed are shown in Figure 3.19. Similar to sediment loadings, TPCB loadings were mostly from wet weather conditions. The percentage of TPCB loading from wet weather conditions for each watershed is summarized in Table 3.13. For the LAR Watershed, wet weather TPCB loadings made up approximately 98% of the TPCB loading. In the SGR Watershed, 93% of the TPCB loading was estimated from wet weather conditions. For the DC and Nearshore Watersheds, wet weather sediment loadings accounted for 96% and 90% of the TPCB loads, respectively. Overall, 97% of the TPCB loading occurs during wet weather conditions.

Table 3.13 Percentage of Wet Weather TPCB Loadings by Watershed

YEAR	PRECIPITATION (IN/YR)	LAR	SGR	DC	NEARSHORE
2002	3.82	96%	91%	95%	86%
2003	9.47	98%	92%	94%	90%
2004	8.68	99%	94%	96%	93%
2005	13.75	99%	97%	98%	95%
2006	7.81	97%	88%	94%	88%
2007	4.79	95%	83%	94%	85%
2008	12.47	98%	91%	95%	89%
2009	8.07	97%	83%	96%	88%
2010	24.00	99%	96%	98%	95%
2011	7.85	98%	91%	96%	89%
2012	8.55	97%	85%	94%	82%
2013	3.94	93%	78%	88%	70%
2014	8.99	98%	91%	96%	88%
Average	9.40	98%	93%	96%	90%

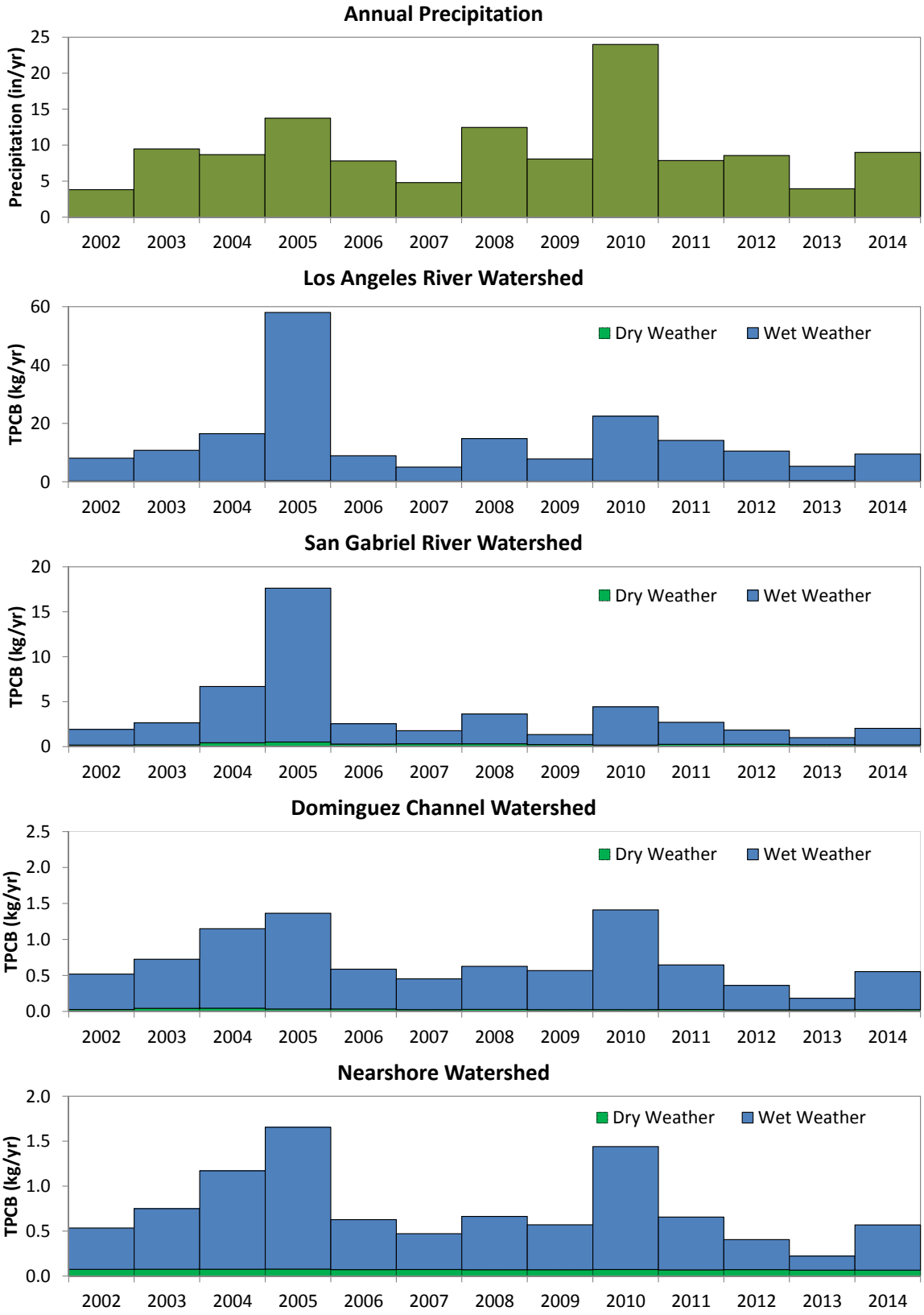

Figure 3.19 Dry and Wet Weather TPCB Loadings by Watershed

3.5.2 TDDX

For TDDX, data from the Storm Water Study were supplemented with data collected from prior studies to develop correlations between organic chemicals and TSS concentrations. These data are shown in the upper left panel of Figure 3.20. The prior studies included two locations within the Nearshore Watershed and two studies for the Torrance Lateral. Based on the data, TDDX concentrations for the Torrance Lateral are an order of magnitude higher than TDDX concentrations at other locations; hence, a separate rating curve was used for the Torrance Lateral, as provided in the middle left panel on Figure 3.20. Similarly, TDDX concentrations collected at Pier A to represent port land uses are an order of magnitude lower than those at other locations; hence, the average TDDX concentration from Pier A (lower left panel of Figure 3.20) was used to represent wet weather concentration for port land uses.

Only two data points are available for TDDX during dry weather; hence the average of the two data points was used to estimate the dry weather TDDX concentrations (upper right panel of Figure 3.20). A rating curve for wet weather TDDX concentrations was developed using data from LAR, DC, Machado Lake, and the Nearshore Watershed, as shown in the middle right panel of the figure. The storm water showed a very strong correlation between TDDX and TSS concentrations (R^2=0.95). The correlation between TDDX and TSS reflects the tendency for organics to be associated with fine-grained sediment. Except for the first flush sediment concentrations, the sediment concentrations are within the TSS range of the rating curve. The rating curve was extrapolated for the first flush sediment concentrations, as shown by the red dashed line.

The storm water TDDX concentrations corresponding to the estimated TSS concentrations are summarized in Table 3.14. A constant concentration was used to estimate the dry weather TDDX concentration for all storm water discharges. The wet weather TDDX rating curve was used to estimate the first flush and wet weather concentrations for the LAR, CC, DC, and Machado Lake discharges. The rating curve for the Torrance Lateral was used to estimate storm water TDDX concentrations from the Torrance Lateral, which are significantly higher than other storm water concentrations. The estimates for the port land uses were based on the average TDDX data from Pier A.

Based on the estimated flows and TDDX concentrations, the TDDX loadings that discharge into the greater harbor waters were calculated. Examples of the TDDX loadings for December 2004 through February 2005 are shown in Figure 3.21 for the LAR, SGR, CC, DC, and Machado Lake. Similar to sediment, the TDDX loading rates correspond to the flows.

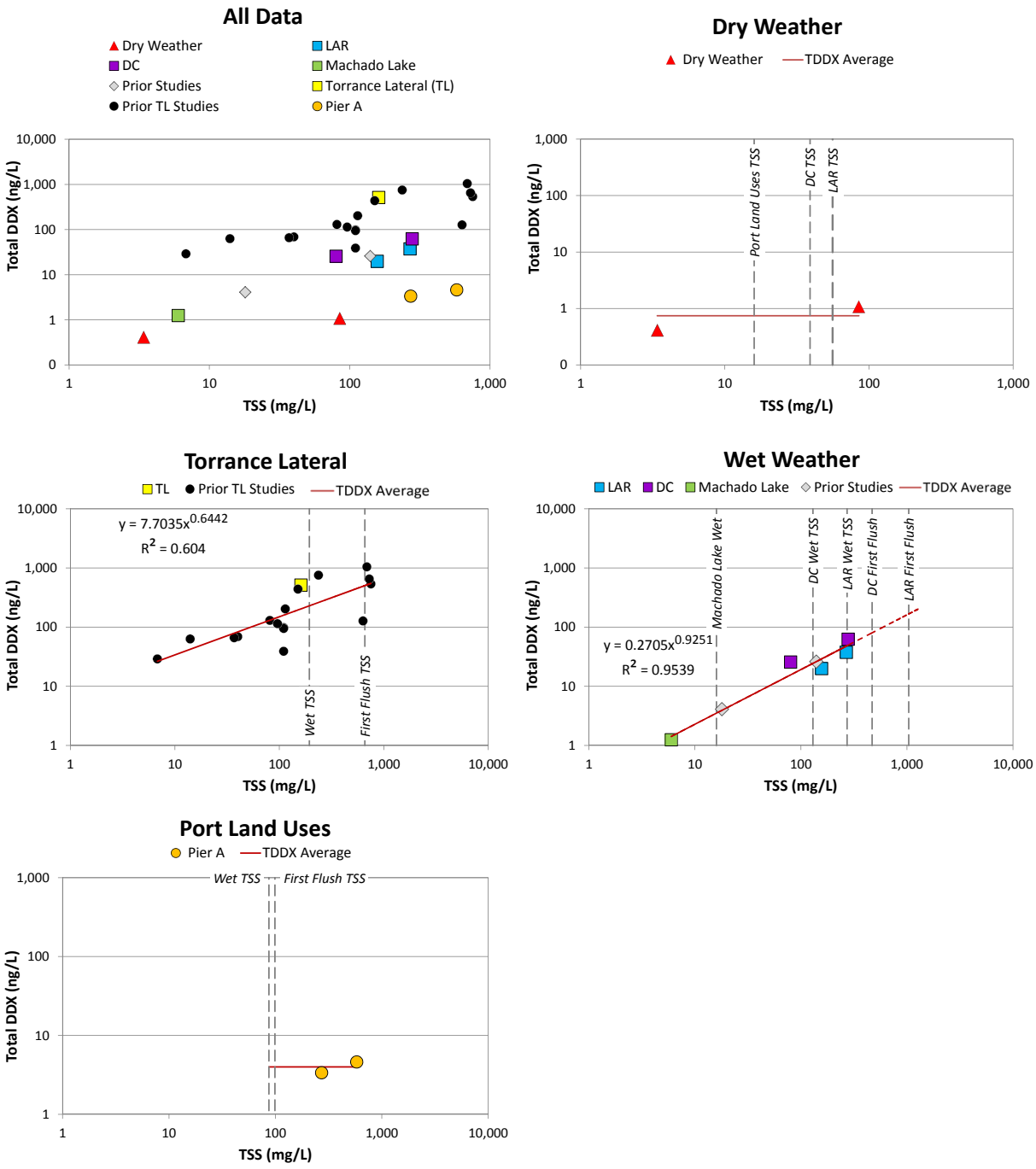

Figure 3.20 TDDX Storm Water Estimates

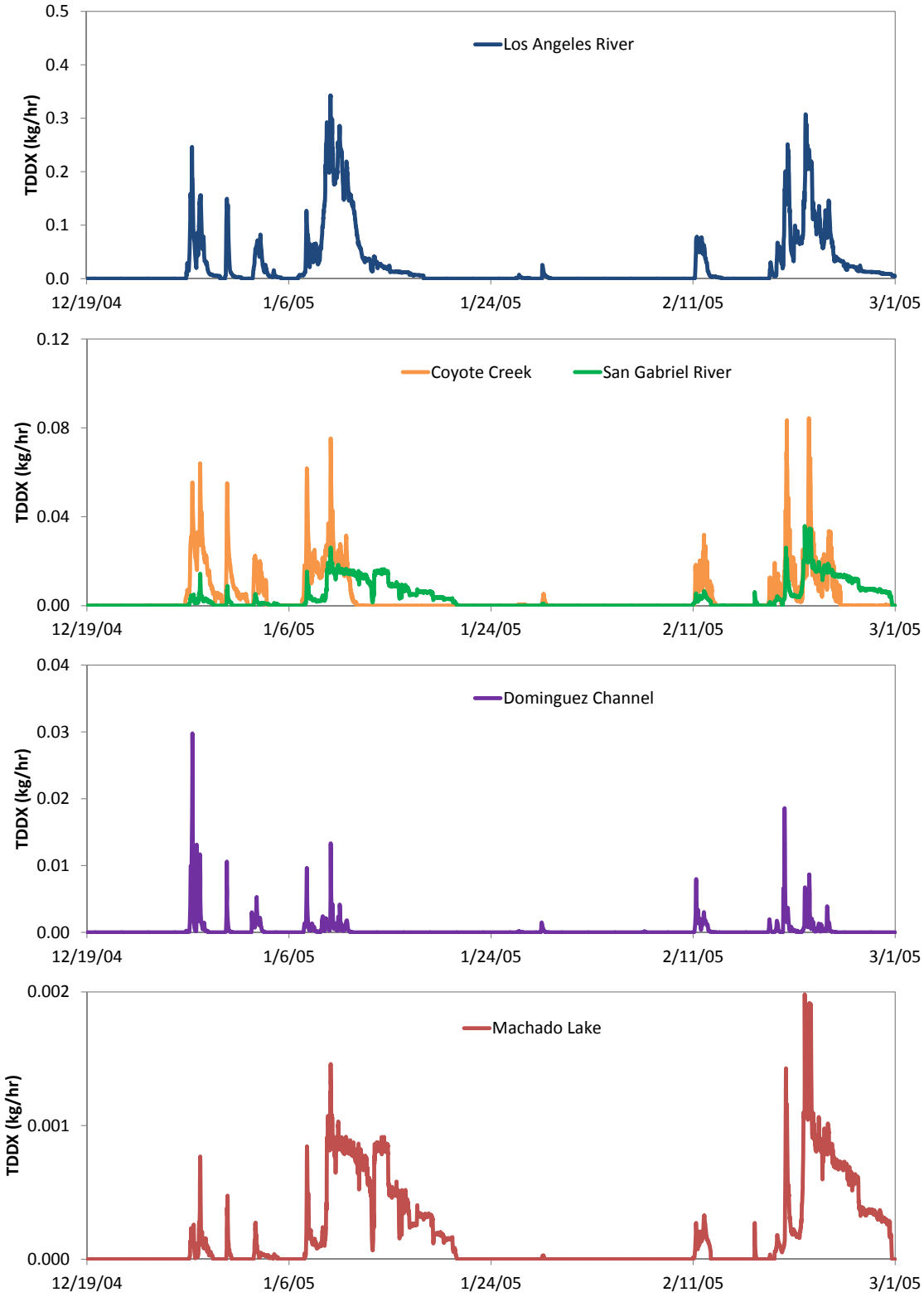

Figure 3.21 Comparisons of TDDX Loadings

Table 3.14 Storm Water TDDX Concentrations

LOCATION	DRY WEATHER (NG/L)	FIRST FLUSH (NG/L)	WET WEATHER (NG/L)
Los Angeles River (LAR)	0.744	167	48.5
Coyote Creek (CC)	0.744	146	35.5
Dominguez Channel (DC)	0.744	80.2	24.4
Torrance Lateral	0.744	497	227
Port Land Uses	0.744	3.98	3.98
Machado Lake	--	--	3.52

The resulting annual TDDX loadings that were computed based on estimated storm water flows and TDDX concentrations are provided in Table 3.15. The highest loadings are from the LAR Watershed, which accounts for about 71% of the total loading. Approximately 19% of the total loading is from the SGR Watershed. The DC Watershed TDDX loadings (7%) are twice as much as the Nearshore Watershed (3.5%) due to the higher loading from the Torrance Lateral.

Table 3.15 Annual TDDX Loadings by Watershed

YEAR	LAR (KG/YR)	SGR (KG/YR)	DC (KG/YR)	NEARSHORE (KG/YR)
2002	5.06	1.21	0.63	0.33
2003	7.52	1.86	1.04	0.49
2004	11.50	4.70	1.72	0.79
2005	41.16	12.94	2.07	1.23
2006	6.13	1.76	0.86	0.41
2007	3.16	1.07	0.55	0.29
2008	9.91	2.40	0.94	0.44
2009	5.09	0.88	0.74	0.36
2010	15.86	3.22	2.09	0.98
2011	9.37	1.80	0.89	0.42
2012	7.22	1.25	0.53	0.26
2013	3.53	0.63	0.24	0.13
2014	6.52	1.41	0.72	0.36
Average	10.16 (70.7%)	2.70 (18.8%)	1.00 (7.0%)	0.50 (3.5%)

The distribution of dry and wet weather TDDX loadings by watershed is shown in Figure 3.22. The TDDX loadings were predominantly estimated from wet weather events. The percentage of TDDX loading from wet weather conditions are summarized for each watershed in Table 3.16.

Table 3.16 Percentage of Wet Weather TDDX Loadings by Watershed

YEAR	PRECIPITATION (IN/YR)	LAR	SGR	DC	NEARSHORE
2002	3.82	98%	95%	99%	92%
2003	9.47	99%	96%	99%	95%
2004	8.68	99%	97%	99%	97%
2005	13.75	100%	99%	99%	98%
2006	7.81	98%	94%	99%	94%
2007	4.79	97%	90%	98%	92%
2008	12.47	99%	96%	99%	95%
2009	8.07	99%	91%	99%	93%
2010	24.00	99%	98%	100%	98%
2011	7.85	99%	95%	99%	95%
2012	8.55	98%	93%	99%	91%
2013	3.94	96%	88%	97%	83%
2014	8.99	99%	96%	99%	94%
Average	9.40	99%	97%	99%	95%

For the LAR Watershed, wet weather TDDX loadings made up 99% of the TDDX loadings. In the SGR Watershed, 97% of the loadings were estimated from wet weather conditions. Wet weather loadings accounted for 99% of the loadings from the DC Watershed and 95% of the Nearshore Watershed. Overall, 98% of the TDDX loading occurs during wet weather conditions.

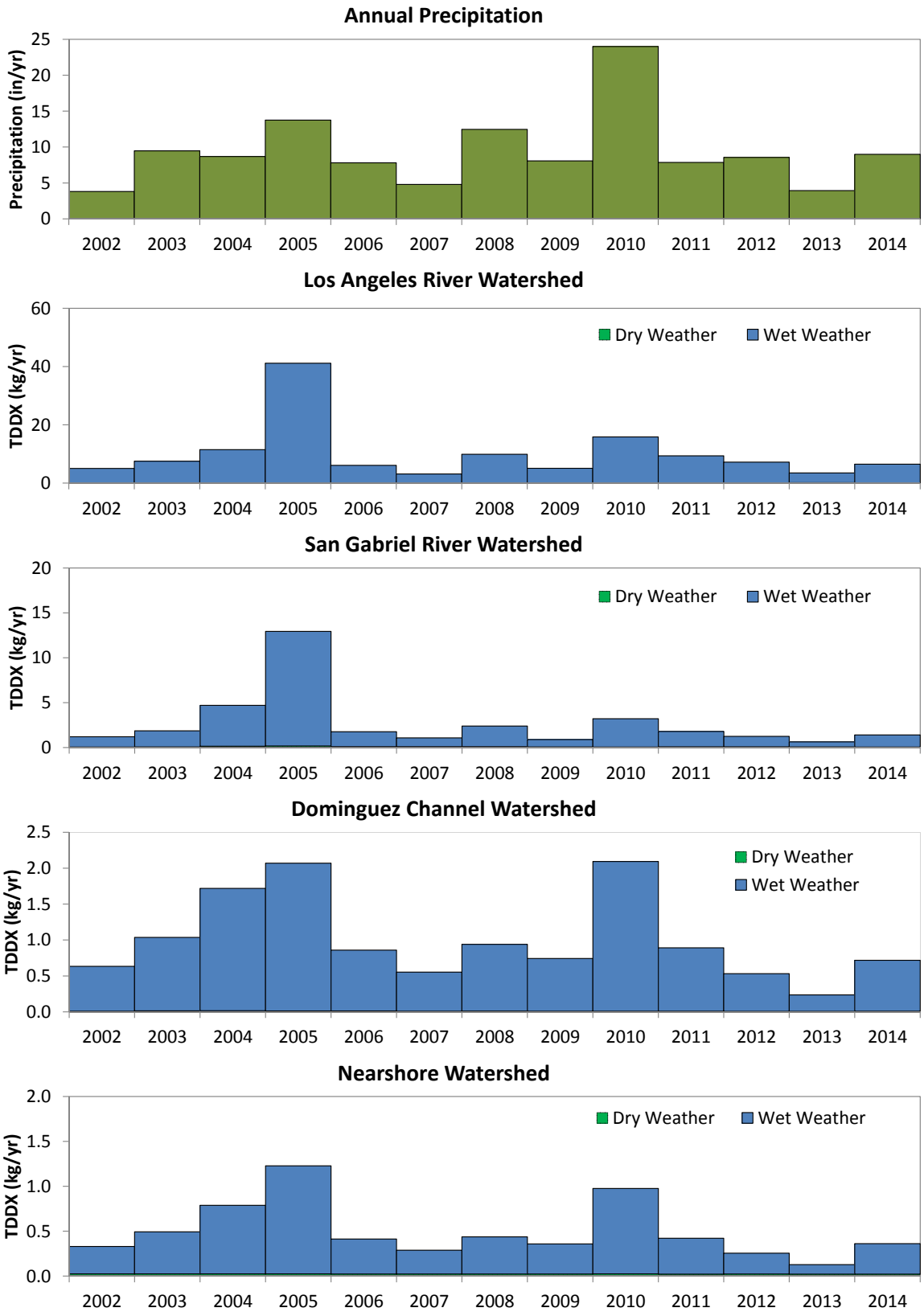

Figure 3.22 Dry and Wet Weather TDDX Loadings by Watershed

3.6 WATERSHED LOADING SUMMARY

Watershed loadings between 2002 and June 2015 were estimated for storm drains that discharge into the greater harbor waters, which include four major rivers (LAR, SGR, CC, and DC) and nearly 200 storm drains. Analytical methods were developed to estimate flows, sediment, and organic chemical concentrations. Continuous time series of flows were estimated for the four major rivers based on measured data, which accounts for approximately 92% of total drainage area of the greater harbor waters. Volume rating curves were used to estimate flows for periods without flow data. Flows from unmonitored drainage areas - mostly for the DC Estuary and Nearshore Watersheds, were estimated by scaling the DC flows based on the drainage areas. Sediment loadings were estimated based on seasonal, average TSS concentrations to represent dry, first flush, and wet weather conditions. For organic chemical concentrations, rating curves based on TSS concentrations were developed to estimate wet weather organic chemical concentrations. TSS rating curves showed a very strong correlations with TPCB (R^2=0.996) and TDDX (R^2=0.95). A separate rating curve was established to estimate TDDX loadings for the Torrance Lateral. Due to limited data, dry weather organic chemical concentrations were specified based on the average of the data, as well as organic chemical concentrations for port land uses.

The annual watershed loadings from 2002 to 2014 are graphically presented in Figure 3.23. In the figure, the top panel shows the annual precipitation illustrating the variation in wet weather conditions. The corresponding annual storm water loadings for flow volume, sediment, TPCB, and TDDX are shown in the subsequent panels that indicate the distribution between dry and wet weather loadings. The flow volume loadings show that about half of the annual volume is from wet weather loadings. However, nearly all the sediment and organic chemical loadings occur from wet weather flows. The annual average watershed loadings are summarized in Table 3.17. Overall, 52% of the total storm water discharged into the greater harbor waters occur during wet weather conditions and contributes 85% of the total sediment loading, 97% of the TPCB loading, and 98% of the TDDX loading.

Table 3.17 Average Annual Watershed Loadings

WATERSHED LOADING	AVERAGE ANNUAL LOADING	PERCENTAGE FROM WET WEATHER
Volume (million m^3/yr)	589	52%
Sediment (million kg/yr)	91	85%
TPCB (kg/yr)	20	97%
TDDX (kg/yr)	14	98%

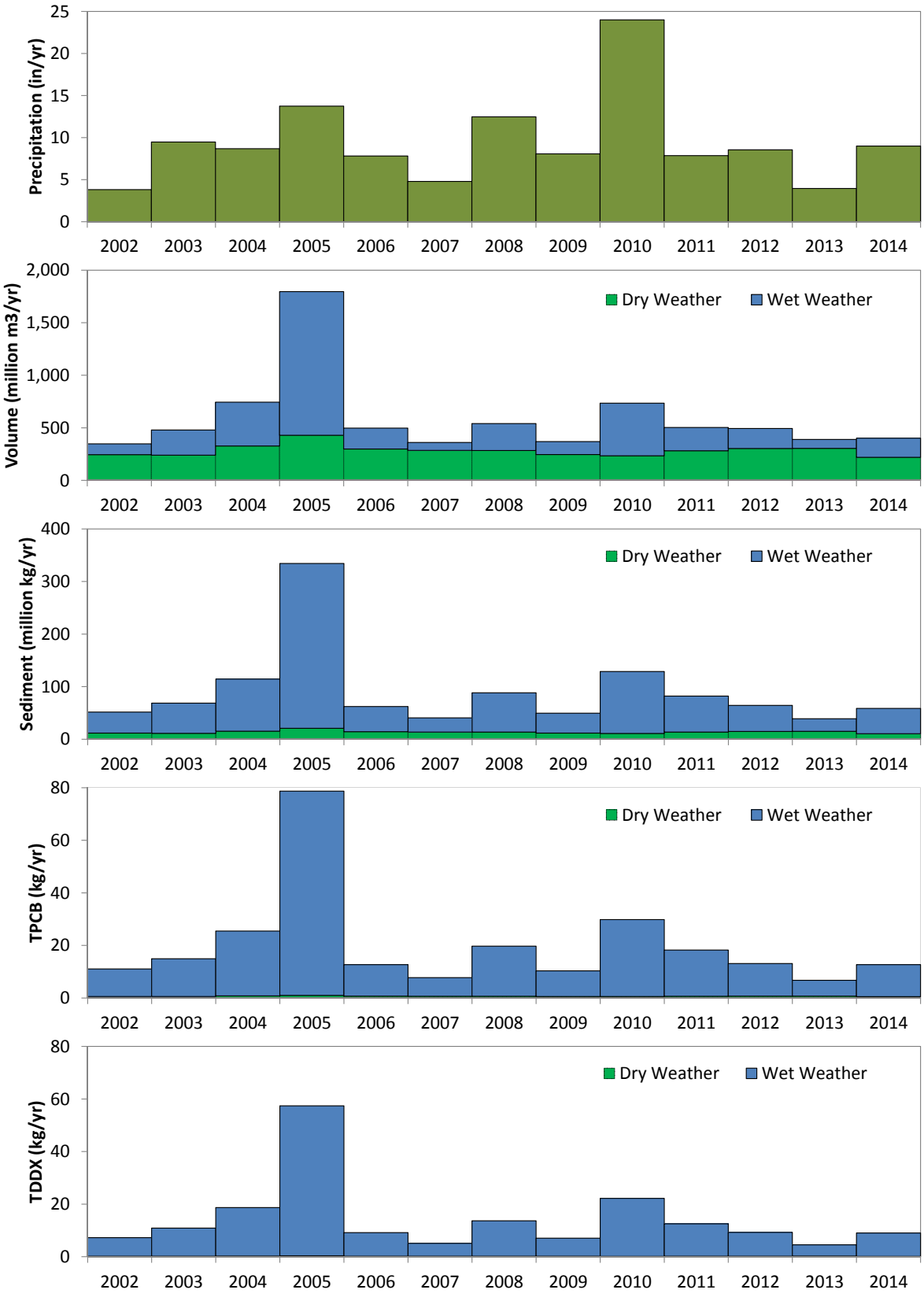

Figure 3.23 Annual Watershed Loadings 2002 - 2014

4. WRAP MODEL CALIBRATION OVERVIEW

4.1 MODEL CALIBRATION APPROACH

In total, the WRAP Model simulates four distinct yet interacting processes: hydrodynamics, mixing, sediment transport, and organic chemical transport. Hydrodynamic processes describe circulation in the harbor, which consequently affects mixing and sediment transport. In turn, sediment transport controls organic chemical transport, since the organic chemicals of interest are largely bound to sediment. Calibration of the WRAP Model is complex, since altering model variables may improve the representation of one process, but negatively impact another process since the hydrodynamic, sediment transport, and chemical fate components are dynamically linked.

As described in Section 2.1, extensive calibration efforts of hydrodynamic, mixing, and sediment transport took place during the development of the DCEM, which was later expanded to become the earlier version of the WRAP Model. Hence, the WRAP Model development, documented in this report, was limited to verifying that the calibrated model parameters for hydrodynamic, mixing and sediment transport for the DCEM and earlier version of the WRAP Model are still applicable after updating the model grid and harbor configuration to represent the baseline condition described in Section 2.3. For this study, model development focused on the calibration of organic chemicals using storm water and water column organic concentrations collected under two separate special studies.

Overall, the WRAP Model validation and calibration procedure can be summarized in the following steps.

1) Validation of the updated hydrodynamic and mixing variables. Hydrodynamic variables were validated by comparing simulated water velocity and elevations to observed water velocity and elevations. Mixing, or the overall harbor circulation, was validated by comparing model-predicted and measured salinity. Also, results of a dye release study were compared to model simulations of the dye release. Details are provided in Sections 5 and 6.

2) Validation of the updated sediment transport variables. Sediment transport was primarily validated by comparing results of a sediment tracer study to simulations of the tracer study. Also, estimated erosion/deposition rates in the CS and LARE were compared to simulated erosion/deposition rates. Details are provided in Section 7.

3) Calibration of the organic chemical parameters. Organic model parameters and boundary conditions were systematically altered to match measurements of organic chemical concentrations in the LA/LB Harbor. Details are provided in Section 8.

4.2 MODEL CALIBRATION DATA

The WRAP Model was calibrated to accurately simulate the complex hydrodynamic and transport conditions in the greater harbor waters. A comprehensive set of hydrodynamic (water level, velocity), mixing (dye, salinity), sediment transport (sediment tracer, deposition/erosion), and organic chemical data, as illustrated in Figure 4.1, were utilized in the WRAP Model calibration. The data included measurements from prior studies and new special studies designed to augment existing data. Data for the model calibration were selected to provide an overall spatial coverage of the greater harbor waters and seasonal variations (dry and wet weather conditions). The types of calibration data available varied by location, but the culmination of the different data types and locations supports the WRAP Model capabilities. Details on the data used for WRAP Model calibrations are provided in Sections 5 to 8.

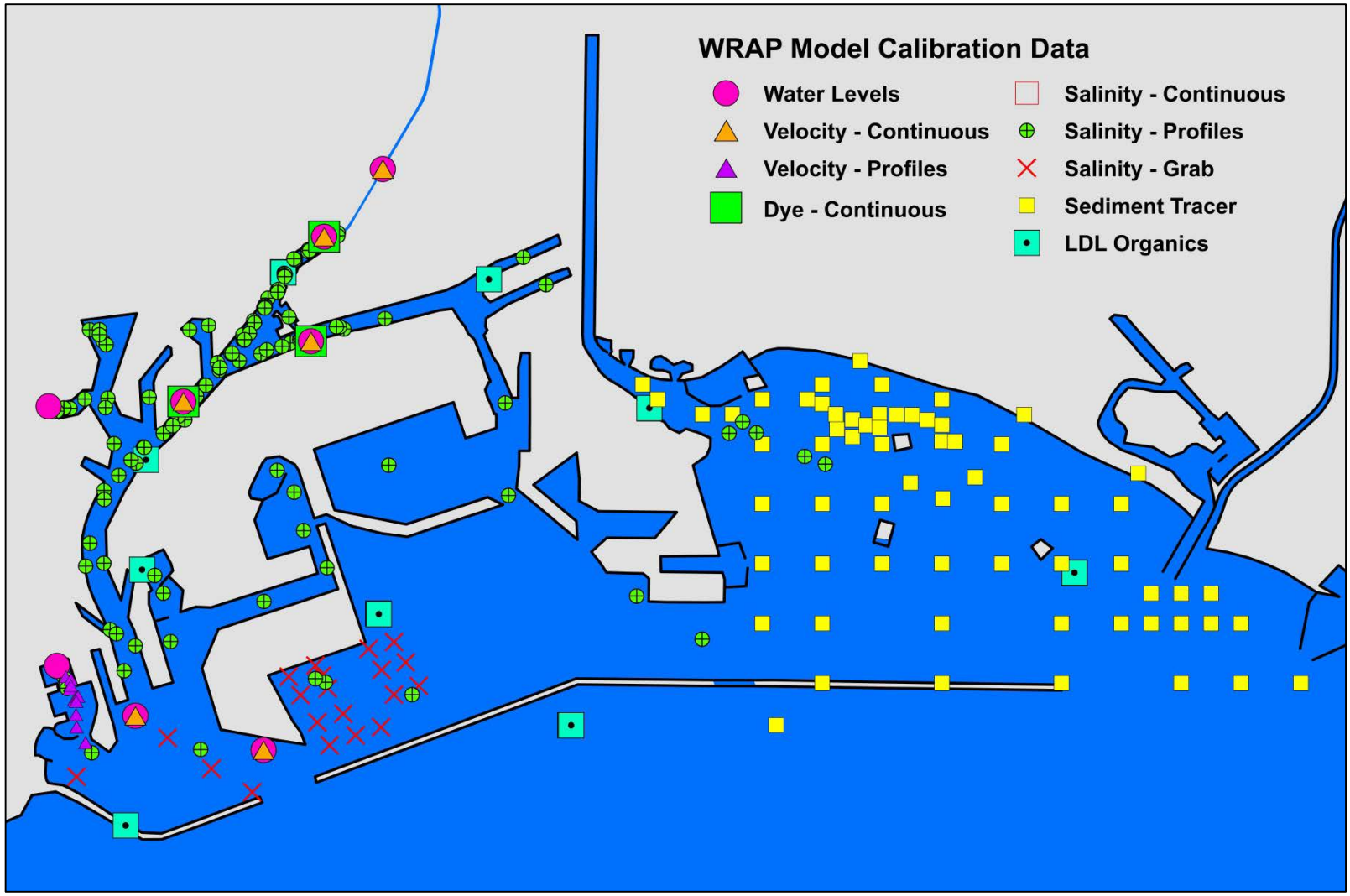

Figure 4.1 WRAP Model Calibration Data Overview

5. HYDRODYNAMICS

5.1 MODEL PARAMETERS

As mentioned in Section 4, hydrodynamic model parameters were originally calibrated as part of the DCEM development (Everest 2007), and later verified to still be applicable for the WRAP Model (Everest 2009) when the DCEM was updated to improve model resolution for the LA/LB Harbor and East San Pedro Bay. The model parameters were selected to represent the best overall fit to the field data and included water levels, velocities, salinity, and dye measurements. The calibrated hydrodynamic model parameters are summarized in Table 5.1. A spatially varying roughness height was specified as 0.02 m for the harbor and ocean areas with a higher roughness height of 0.03 m along the river channels. The horizontal eddy diffusivity was found to have insignificant effect on hydrodynamic components. The vertical viscosity and diffusivity parameters were calibrated based on velocity and salinity comparisons. These same model parameters were validated for this study to verify that the updated WRAP Model for this study can still accurately simulate the hydrodynamics for the harbor.

Table 5.1 WRAP Model Hydrodynamic Model Parameters

MODEL PARAMETER	UNITS	VALUE
Roughness Height	m	0.02 – 0.03
Horizontal Diffusivity	m^2/sec	1.0E-6
Maximum Vertical Eddy Viscosity	m^2/sec	2.0E-3
Maximum Vertical Eddy Diffusivity	m^2/sec	1.0E-4

5.2 HYDRODYNAMIC CALIBRATION DATA

The WRAP Model hydrodynamic validation was conducted by comparing model-predicted water levels and velocities to measurements from studies conducted by the POLA to characterize hydrodynamic conditions throughout the harbor, as summarized in Table 5.2. Water levels and velocities were measured using acoustic Doppler current profilers (ADCP). Long term water levels and velocities were monitored at one location along the DC and three locations in the inner harbor as part of the DC Estuary Model Study (DCEMS) calibration (Everest 2007). New hydrodynamic data have been collected since the previous DCEM and

WRAP Model calibrations. These data were used to validate the WRAP Model at other locations in the harbor. These additional data include:

- ADCP data collected in the POLA outer harbor over a three-month period in 2010 to assess harbor-wide circulation patterns
- ADCP measurements in the West Basin and Cabrillo Marina collected for the POLA Receiving Water Study
- Velocity profile collected in Cabrillo Marina as part of a special study to evaluate innovative technologies for collecting *in situ* measurements during dredging operations (AMEC 2009)

Locations of the water level and velocity data used for the WRAP Model hydrodynamic calibration are provided in Figure 5.1.

The processing of ADCP data for model comparisons included adjustments from magnetic to true north, averaging vertical bin data for five even layers, conversion to along-channel velocities, and filtering to remove high frequency noise. The ADCP data filtering was conducted using a fast Fourier transform (FFT) technique developed during the previous DCEM calibration (Everest 2007).

Table 5.2 Hydrodynamic Calibration Data Summary

STUDY	DURATION	DESCRIPTION
DCEMS	2/26/05 – 3/16/06	One year field program to collect hydrodynamic and water quality data at four locations: DC at S. Pacific Drive, Berth 200G, Berth 206, and Berth 173
POLA ADCP	1/7/10 – 4/8/10	Collect supplemental ADCP data in the outer harbor area
POLA RW	2/23/09 – 3/10/09	Field data collection program to monitor storm water and receiving water in West Basin
	1/12/11 – 3/14/11	Field data collection program to monitor storm water and receiving water in Cabrillo Marina
Cabrillo Marina Dredging	5/27/09 – 6/12/09	Evaluation of innovative technologies for monitoring suspended sediment during dredging operations that included ADCP profiles in Cabrillo Marina

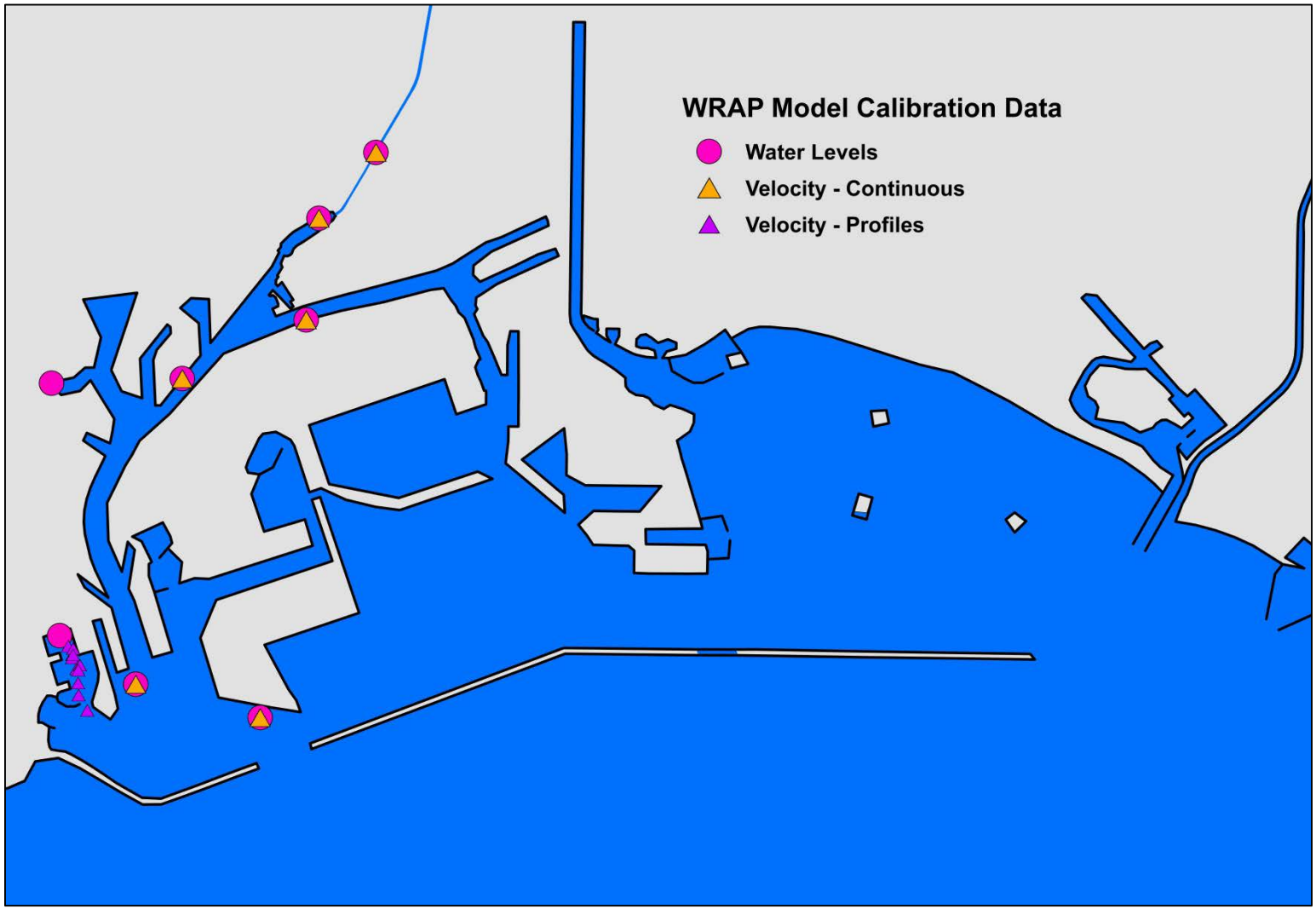

Figure 5.1 Hydrodynamic Calibration Data Locations

5.3 CALIBRATION RESULTS

5.3.1 Water Levels

WRAP Model-predicted water levels were compared with measured water levels at various locations within the harbor; examples for DC Estuary are provided in Figures 5.2a – 5.2c. The selected time frames shown correspond to the DCEMS dry weather calibration, dry weather verification, and wet weather calibration periods, respectively, and cover a wide range in tidal ranges (i.e., spring, neap, and mean tide ranges). Water levels are compared at four locations, with one location at the downstream portion of the DC and three locations within the inner harbor. Comparison of water levels at other locations in the Harbor is shown in Figure 5.3. The time frames vary depending on where the data were collected. Water levels are compared in the POLA MSC, POLA outer harbor (Pier 400), POLA West Basin, and Cabrillo Marina. As shown in the figures, the WRAP Model water levels match well with the measured water levels.

5.3.2 Velocities

The WRAP Model calibration of velocities included velocity time series and snapshots of vertical profiles at several locations within the harbor. Velocity time series comparisons for the DCEMS locations are provided in Figures 5.4a – 5.4c, for the DCEMS dry weather calibration (May – June 2005), dry weather verification (August – September, 2005), and wet weather calibration (February to March, 2006) periods, respectively. The along-channel velocities are shown in these figures. The inset next to each panel indicates the along-channel velocity direction; the yellow arrow is the positive velocity direction while the orange arrow indicates the negative velocity direction. At S. Pacific Drive and Berth 200G, velocities show a relatively balanced flow (positive and negative velocity). However, velocities at Berth 206 and Berth 173 show an ebb-dominant flow as indicated by the primarily negative velocities in a westward direction. In general, the model-predicted velocity time series agrees well with the field data and show similar trends in dominant velocity direction and magnitude. The velocity distributions of measured and modeled velocities were also evaluated using a histogram of the velocity. The measured and modeled velocity distributions are compared in Figures 5.5a – 5.5c. Similar to the velocity time series comparisons, the histograms show a relatively balanced flow for S. Pacific Drive and Berth 200G and an ebb-dominant flow at Berths 206 and 173. Overall, the WRAP Model velocities are comparable with the measured velocities.

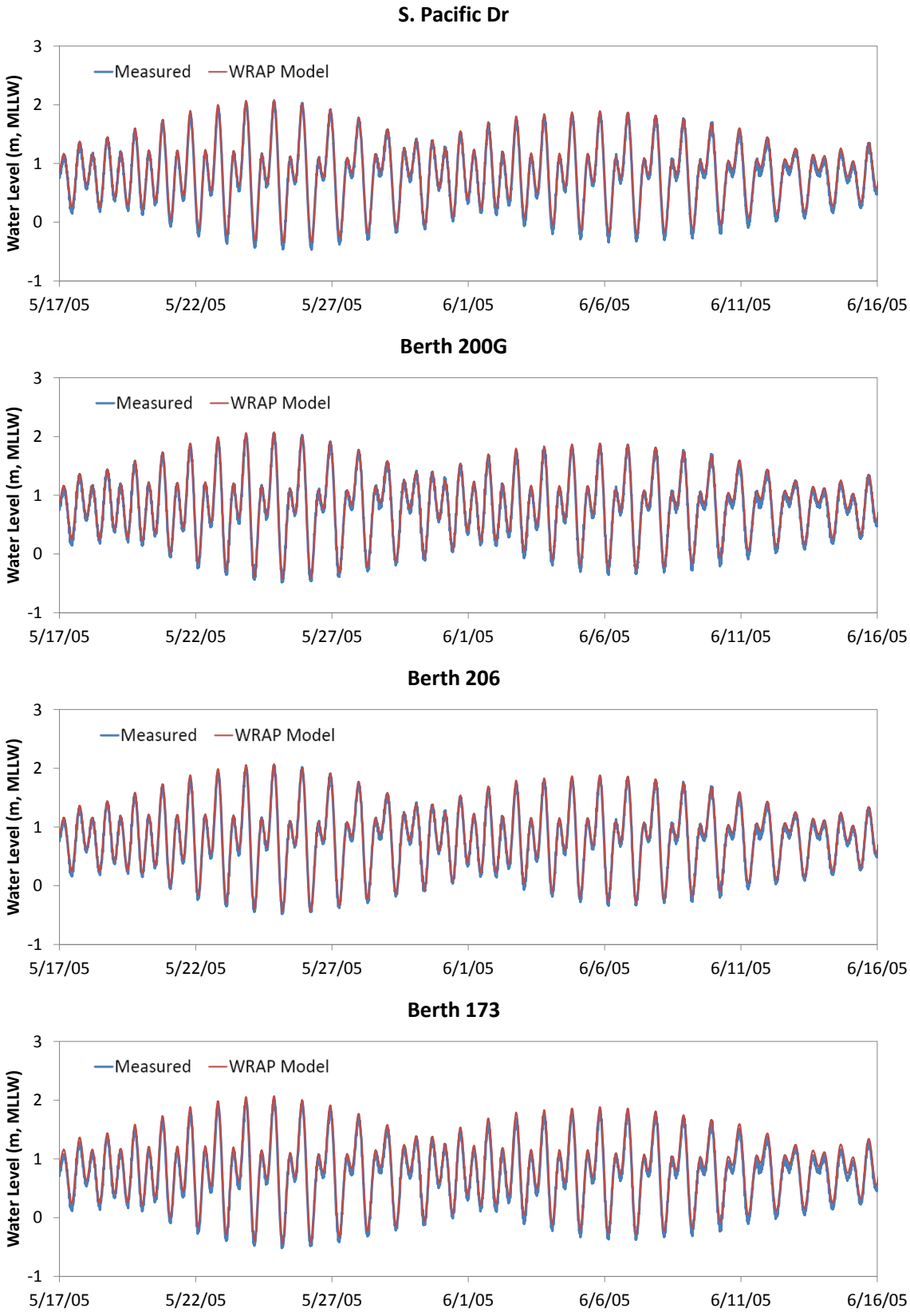

Figure 5.2a Water Level Comparisons in Dominguez Channel Estuary May-Jun 2005

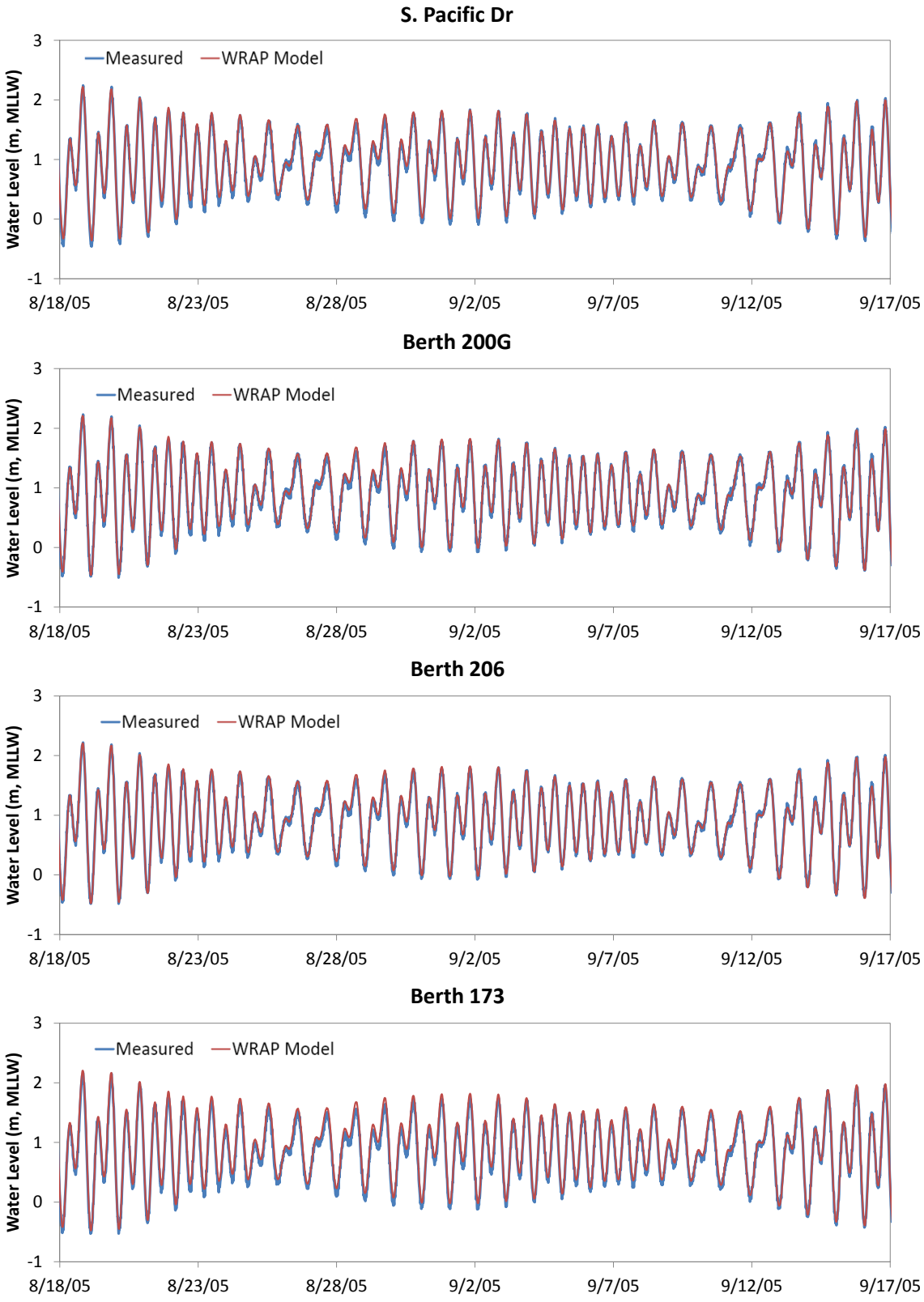

Figure 5.2b Water Level Comparisons in Dominguez Channel Estuary Aug-Sep 2005

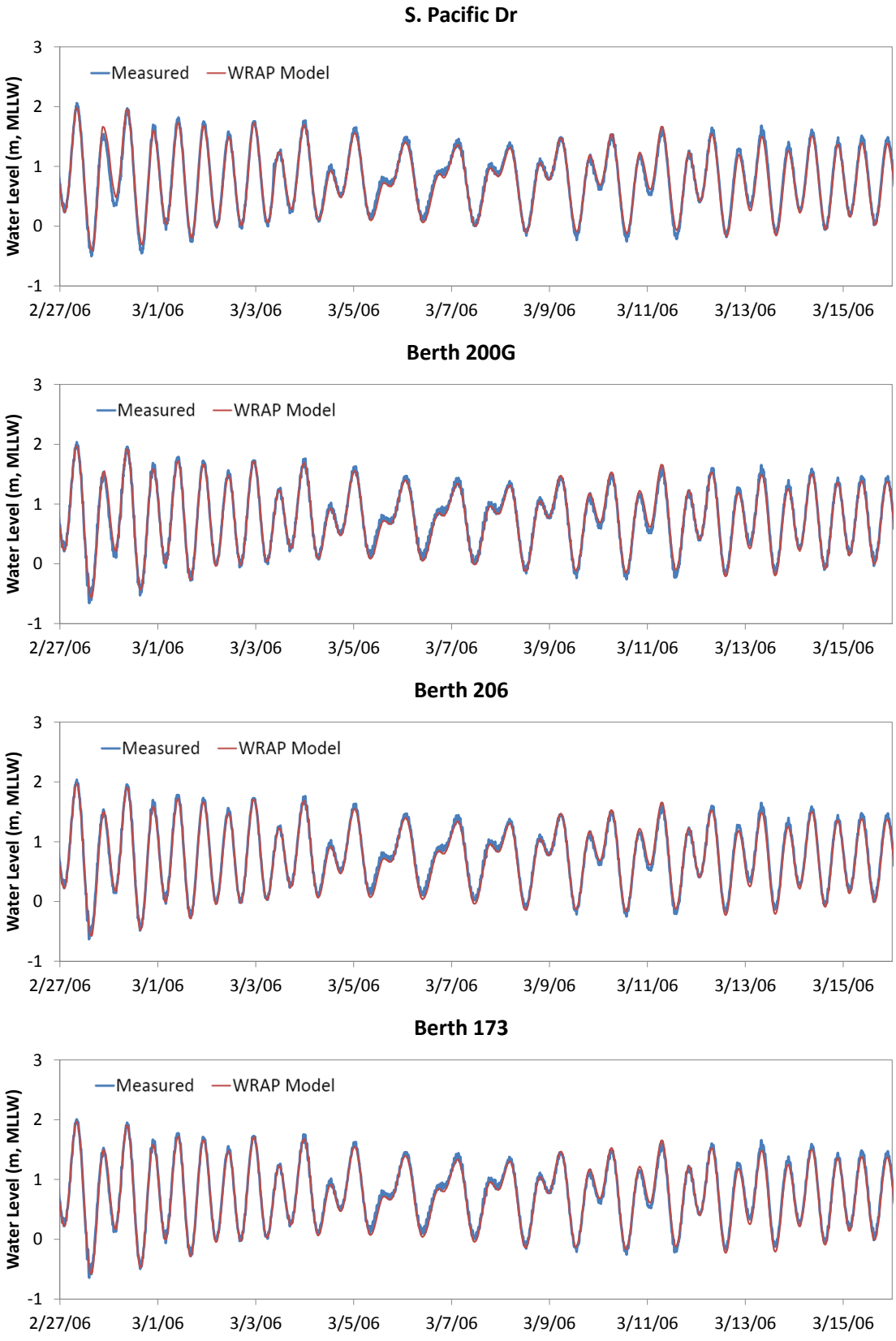

Figure 5.2c Water Level Comparisons in Dominguez Channel Estuary Feb-Mar 2006

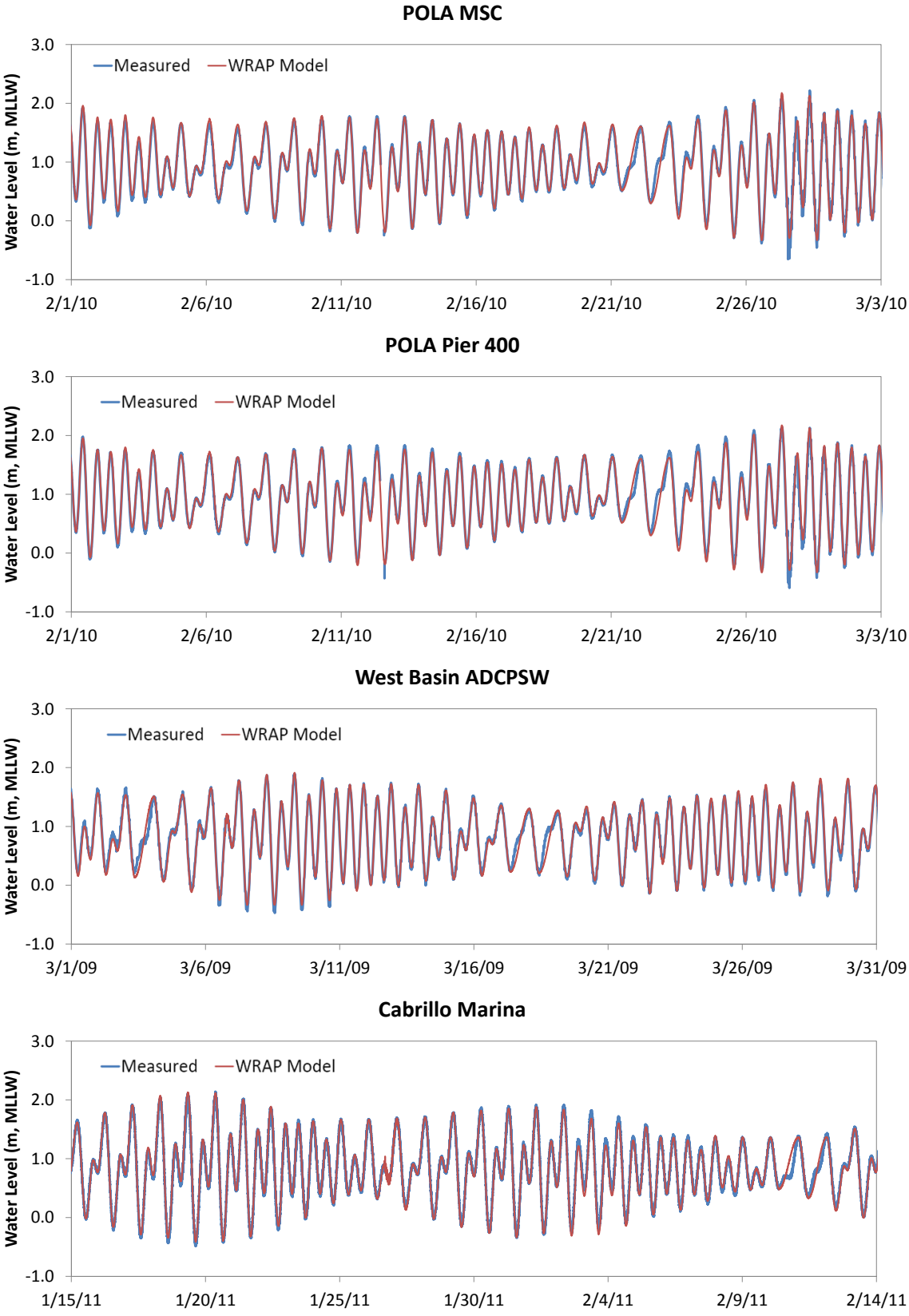

Figure 5.3 Water Level Comparisons in LA/LB Harbor

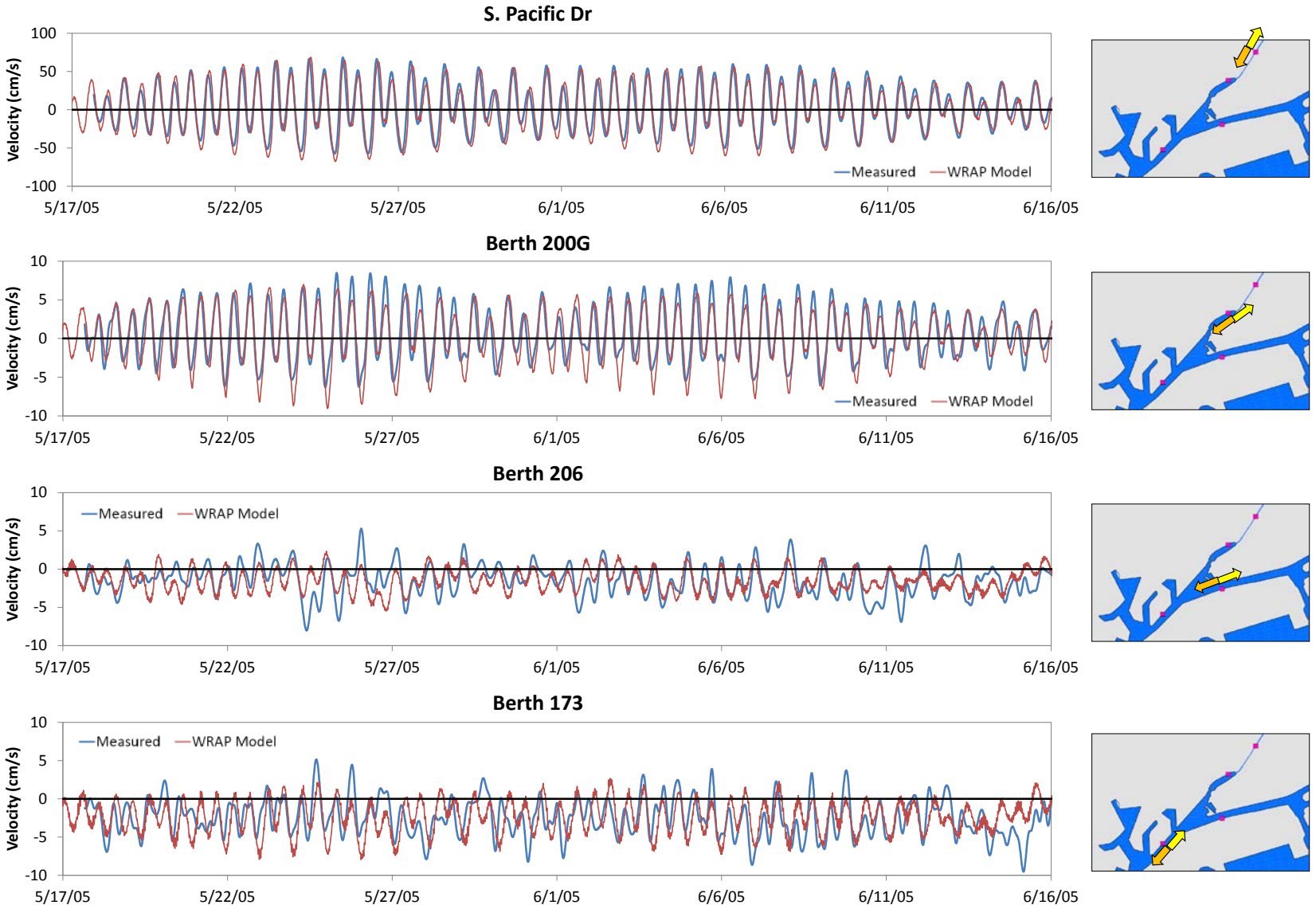

Figure 5.4a Velocity Comparisons in Dominguez Channel Estuary May - June 2005

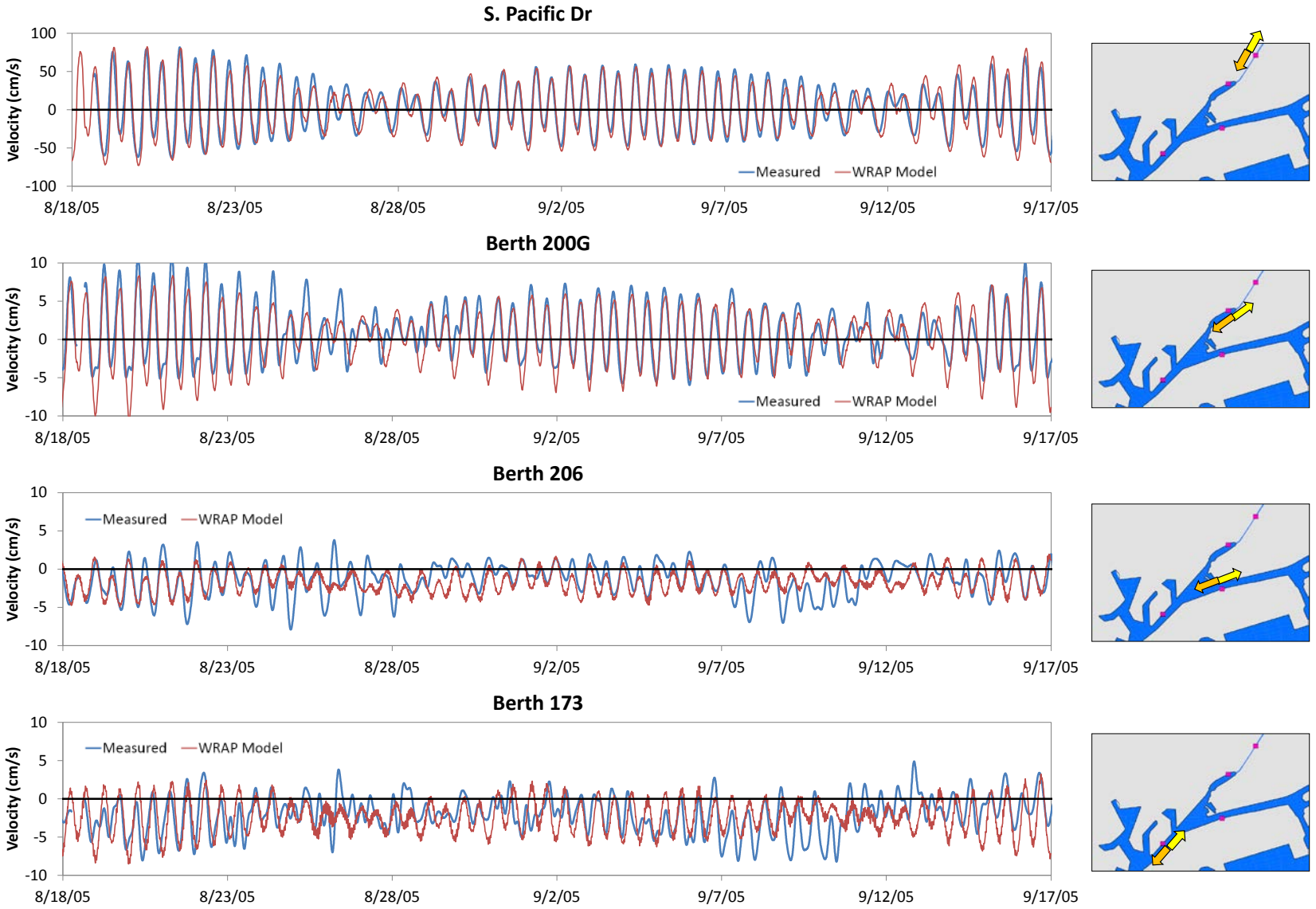

Figure 5.4b Velocity Comparisons in Dominguez Channel Estuary August - September 2005

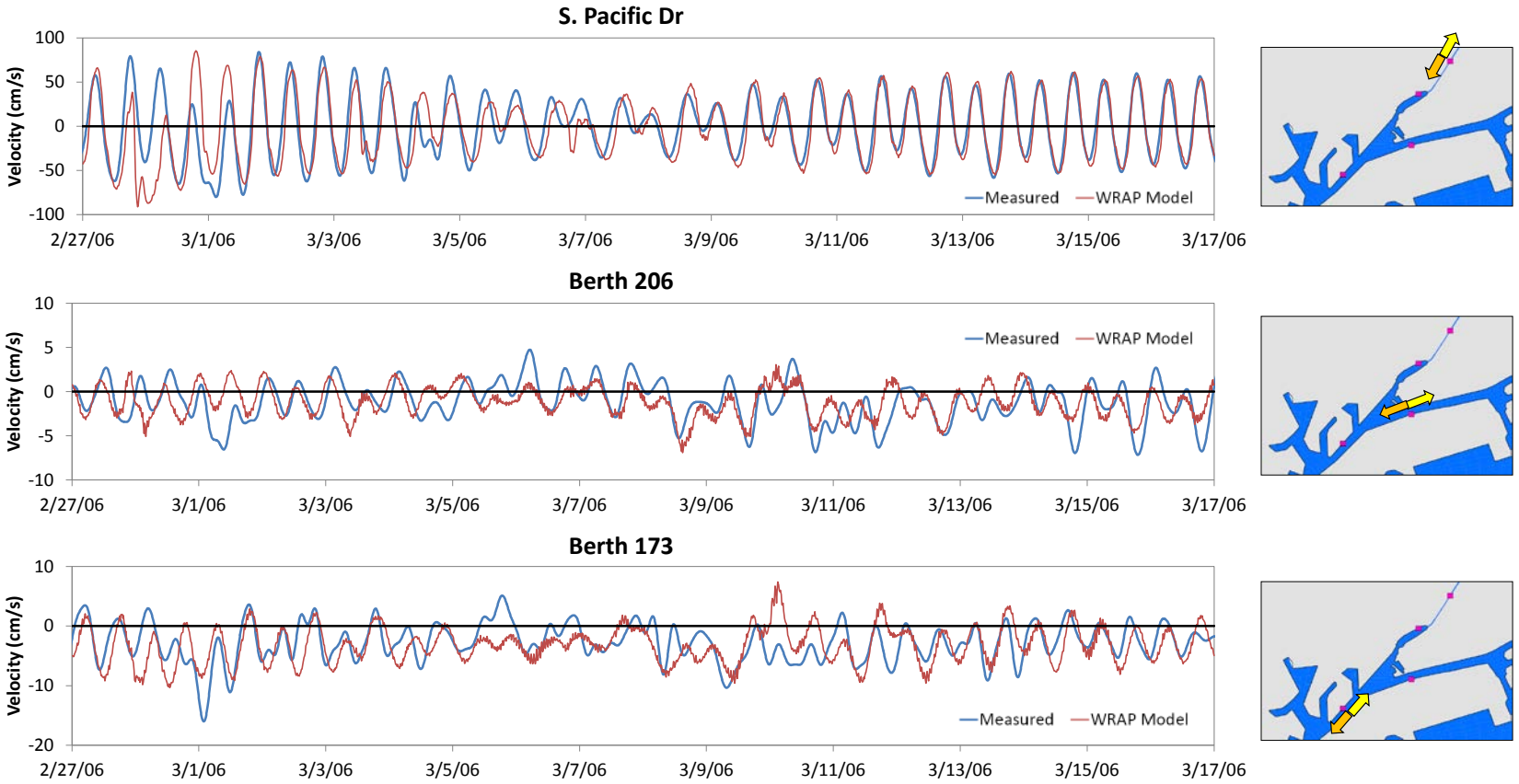

Figure 5.4c Velocity Comparisons in Dominguez Channel Estuary February - March 2006

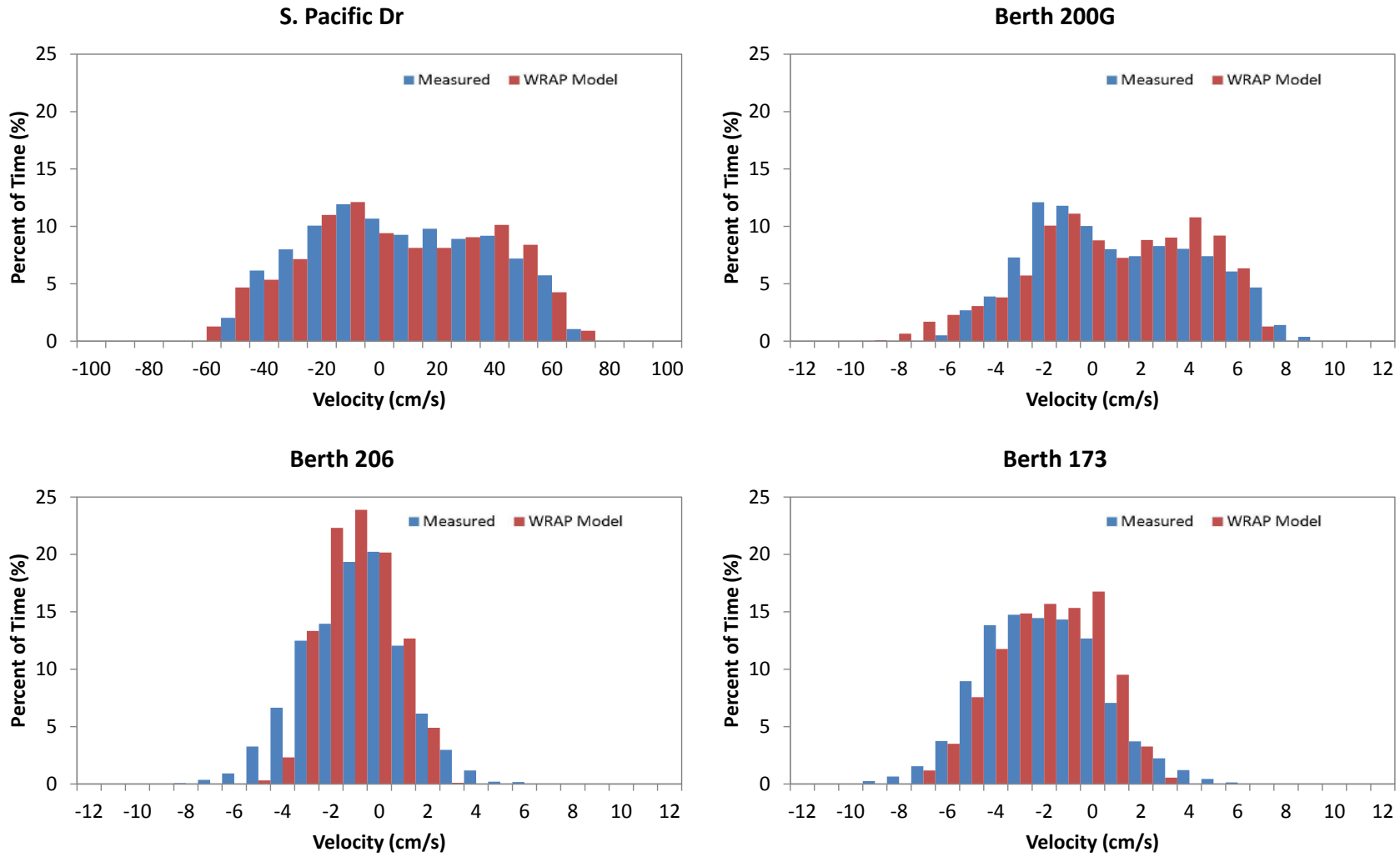

Figure 5.5a Velocity Distribution Comparisons in Dominguez Channel Estuary May - June 2005

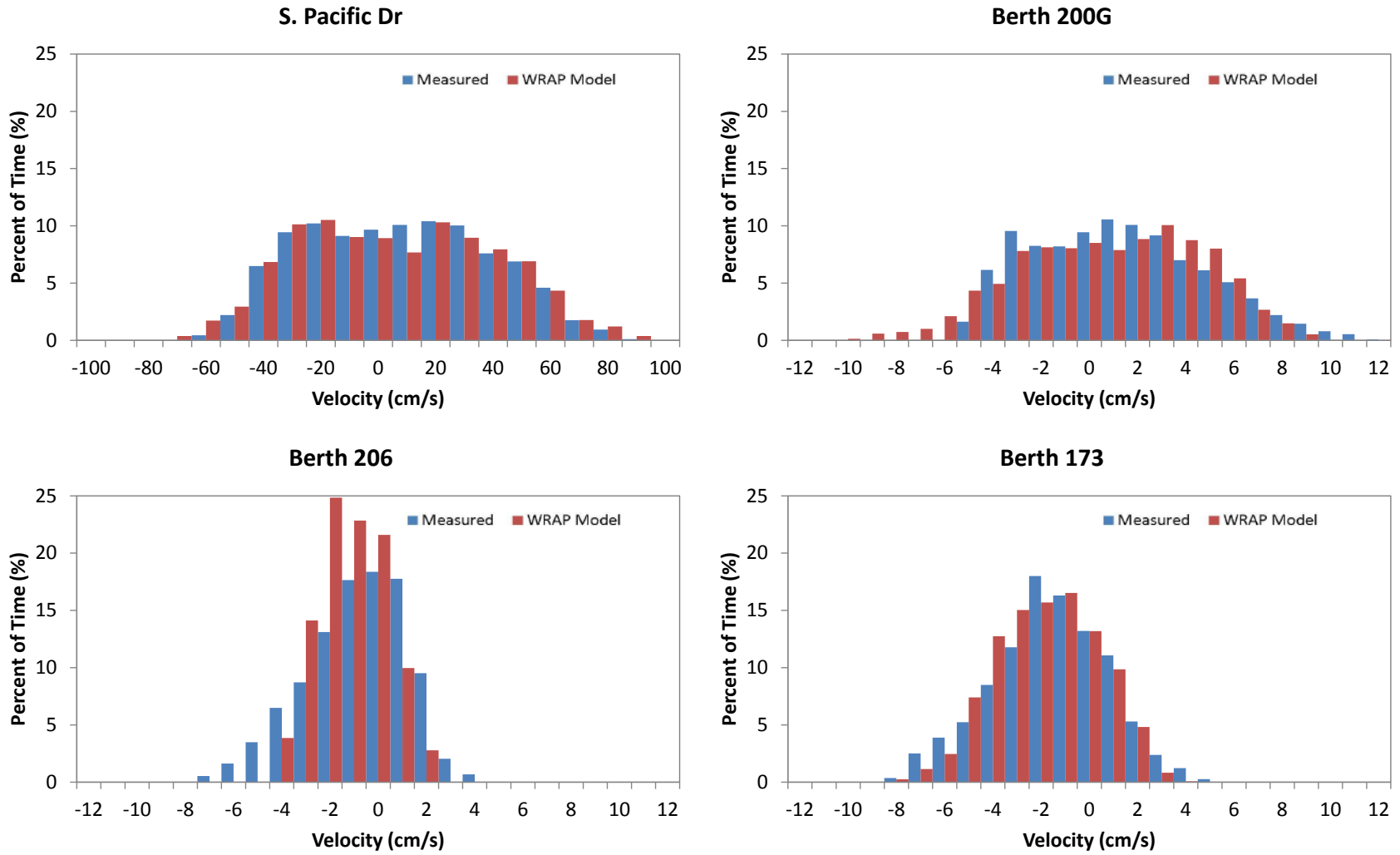

Figure 5.5b Velocity Distribution Comparisons in Dominguez Channel Estuary August - September 2005

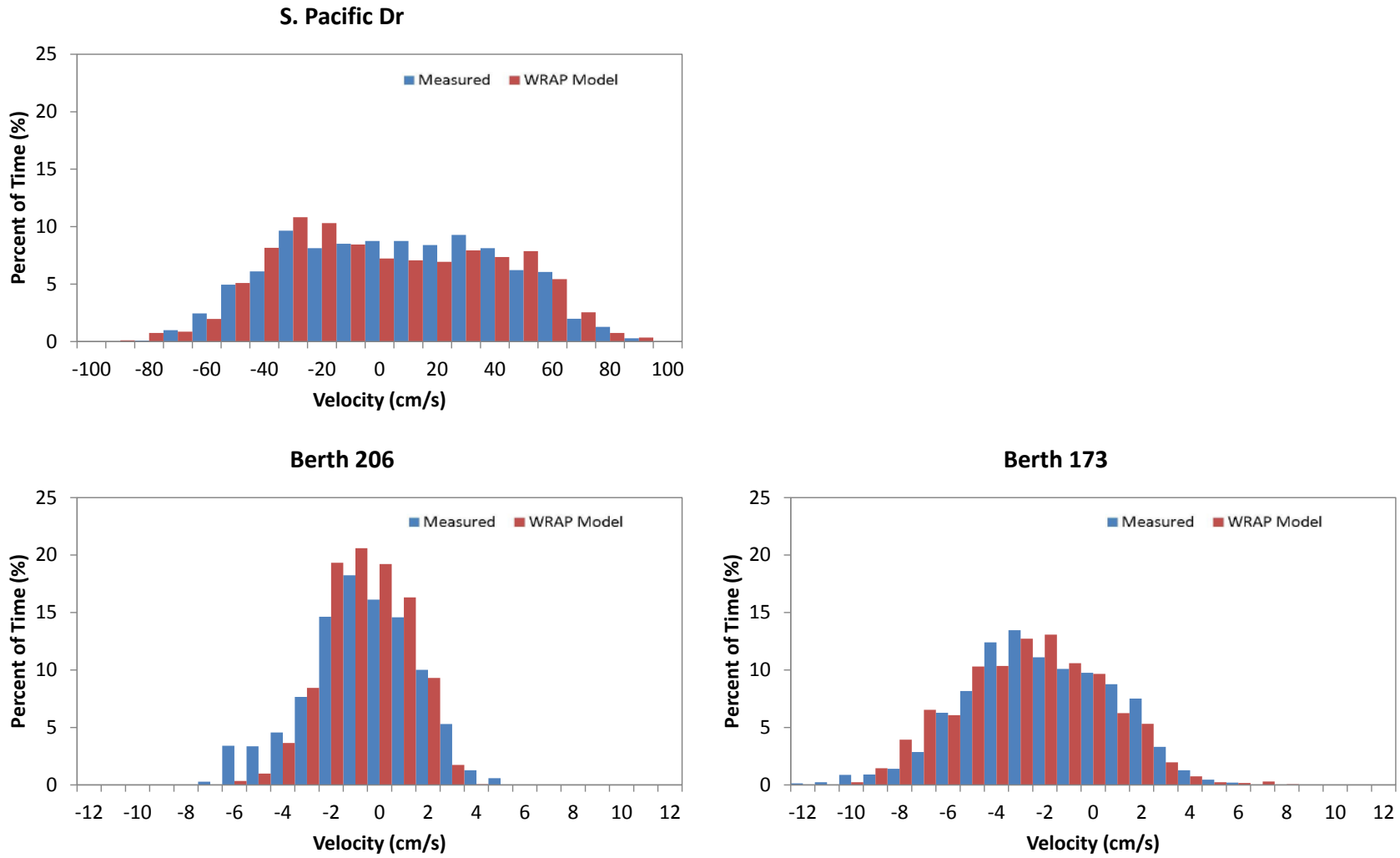

Figure 5.5c Velocity Distribution Comparisons in Dominguez Channel Estuary February - March 2006

New data have been collected since the original DCEM and WRAP Model calibrations and were used to validate the WRAP Model at other locations in the harbor. Velocities were monitored at two locations in the POLA outer harbor in January to April 2010. Velocity time series and profile comparisons at the POLA MSC are provided in Figure 5.6. In the figure, velocity time series comparisons are shown at three water depths corresponding to the surface, middle, and bottom water layers. The data location and velocity directions are indicated in the upper inset picture. The yellow arrow indicates the positive velocity direction, which points into the harbor channel. The orange arrow shows the negative velocity direction as moving out of the harbor channel. The time frame includes two wet weather events indicated by the shaded gray areas.

In general, the WRAP Model-predicted velocities show a similar magnitude and direction as the field data throughout the water column. Higher velocities are found in the surface layer and decrease with water depth, illustrating the vertical velocity gradient. In the surface layer, the dominant flow direction is out of the MSC as indicated by the predominantly negative velocities. The wet weather flows are obvious as shown by the increase in velocity magnitude in the negative direction. Velocities in the middle layer are smaller in magnitude compared to the surface layer, but the velocity direction shows a more balanced flow. The smallest velocities occur in the bottom layer. Velocities are primarily in the positive direction during both dry and wet weather conditions, indicating flows moving into the harbor.

Both the WRAP Model and field data show that the transport directions differ between the surface and bottom layers. To better illustrate the vertical velocity gradient, velocity profiles at the peak wet weather flow are also provided in Figure 5.6 for the two wet weather events. The velocity profiles show the flow moving out of the harbor channel at the surface, while transport at the bottom is in the opposite direction. The vertical velocity gradients also illustrate the complexity of 3D transport conditions that occur in the harbor. Histograms for the velocity distributions at the POLA MSC for the surface, middle, and bottom layers are compared in Figure 5.7.

Velocity time series at different water depths were also compared at Pier 400, as shown in Figure 5.8. The velocities indicate transport patterns into and out of the harbor that show some differences between the surface and bottom layer. The WRAP Model-predicted velocities are similar in magnitude and direction as the field data, which is also illustrated by the histograms of the velocity distributions shown in Figure 5.9. In general, the WRAP Model velocities are consistent with the measured velocities.

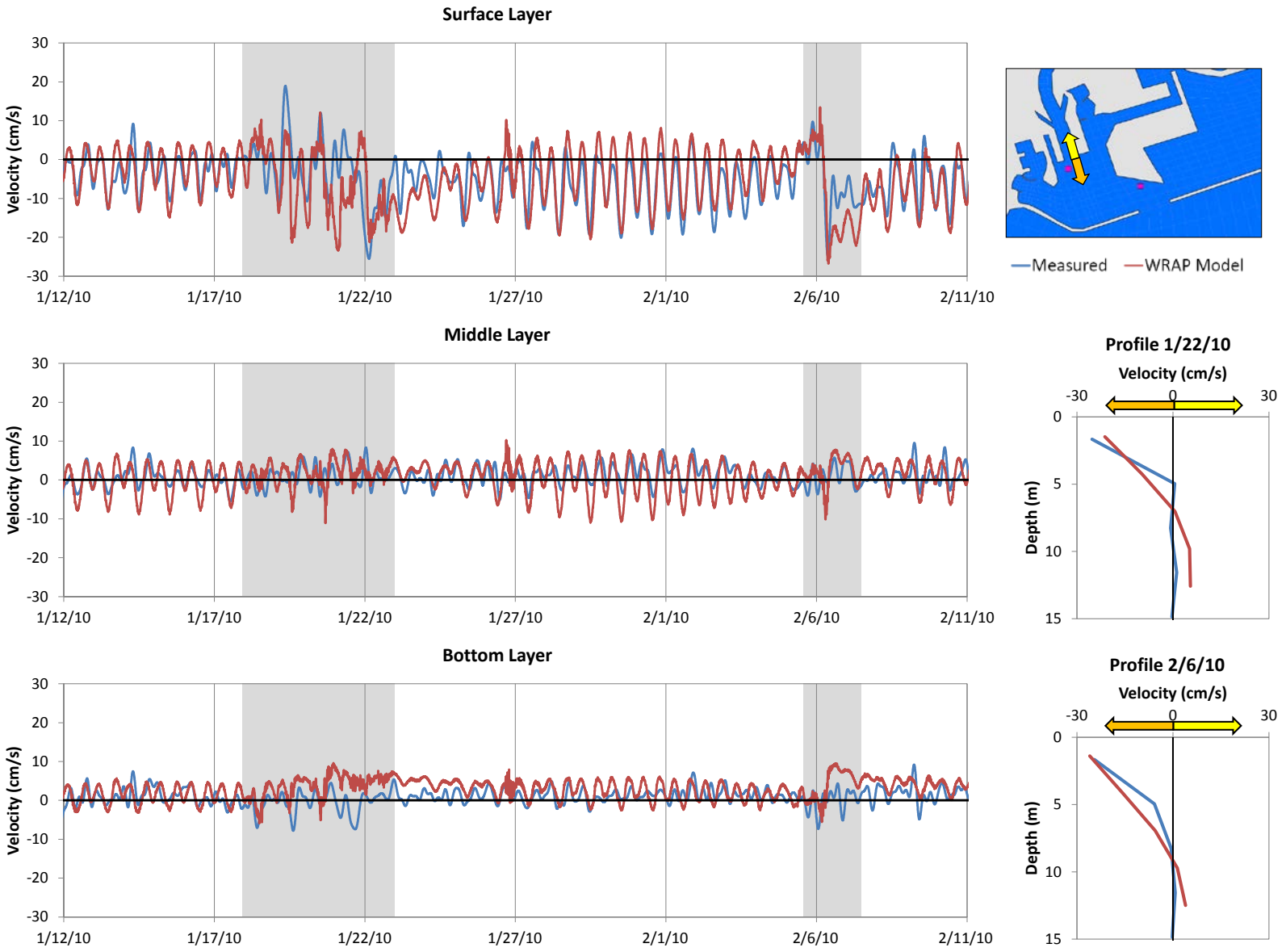

Figure 5.6 Velocity Comparisons at POLA Main Channel

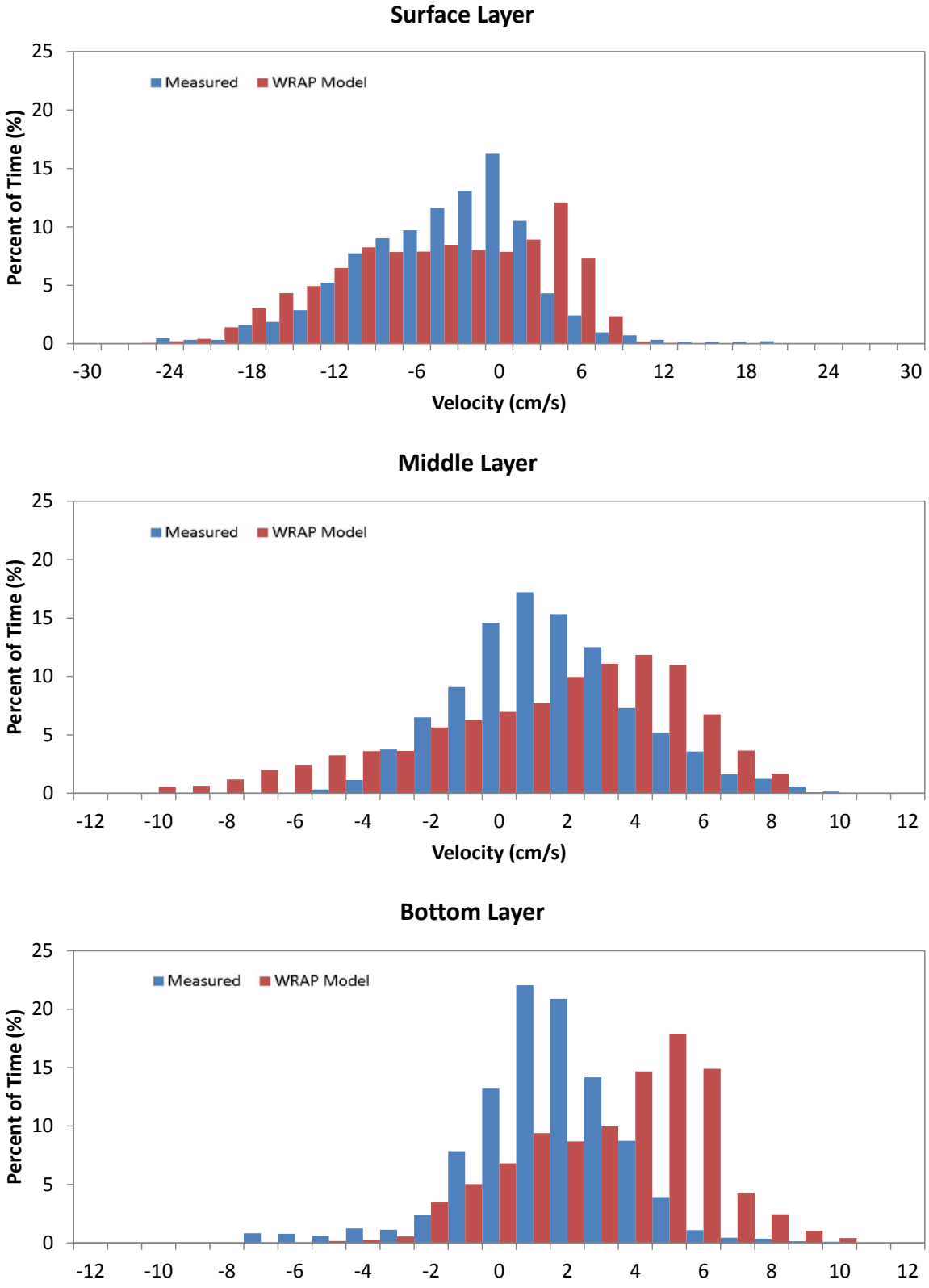

Figure 5.7 Velocity Distribution Comparisons at POLA Main Channel

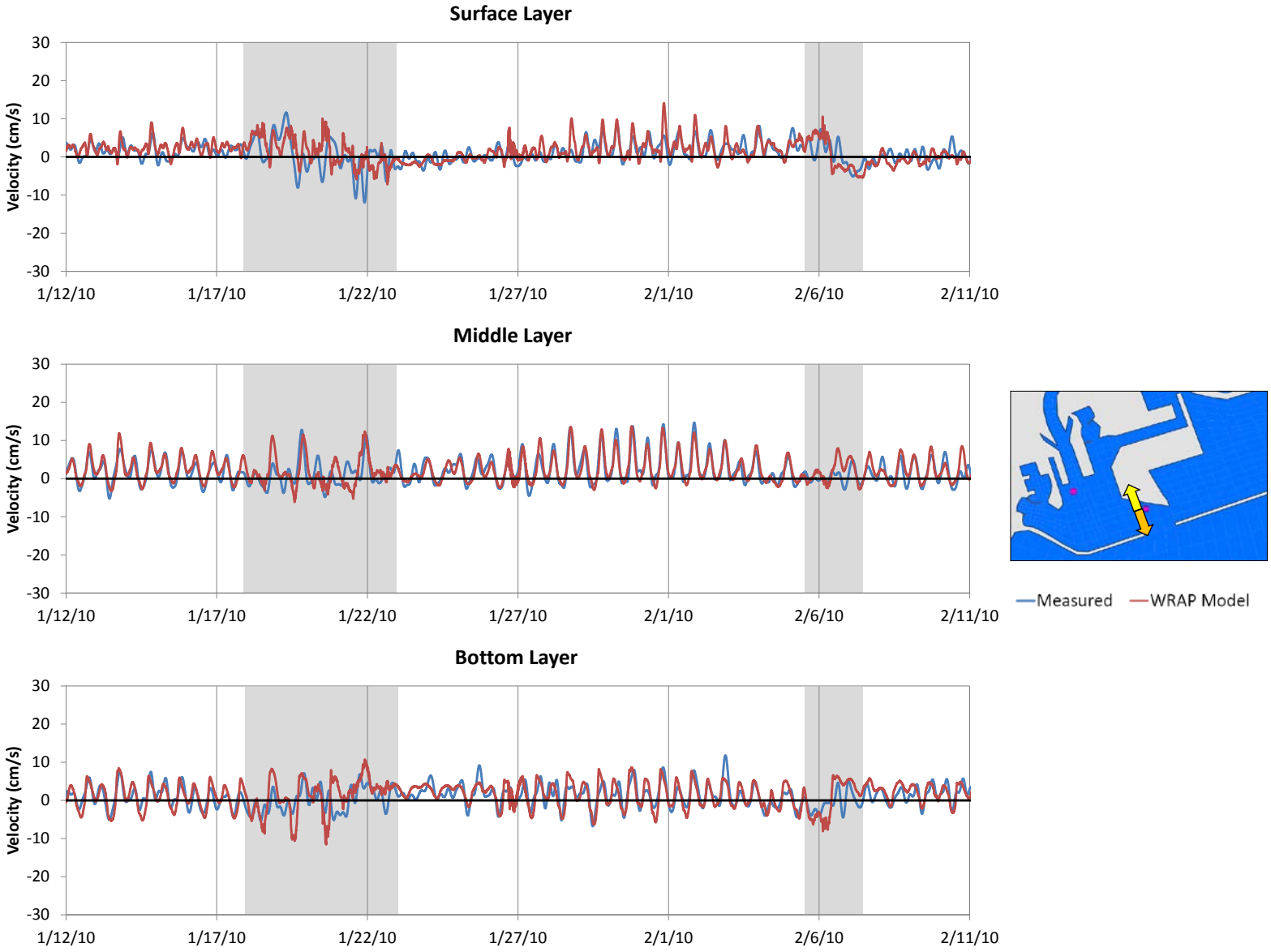

Figure 5.8 Velocity Comparisons at POLA Pier 400

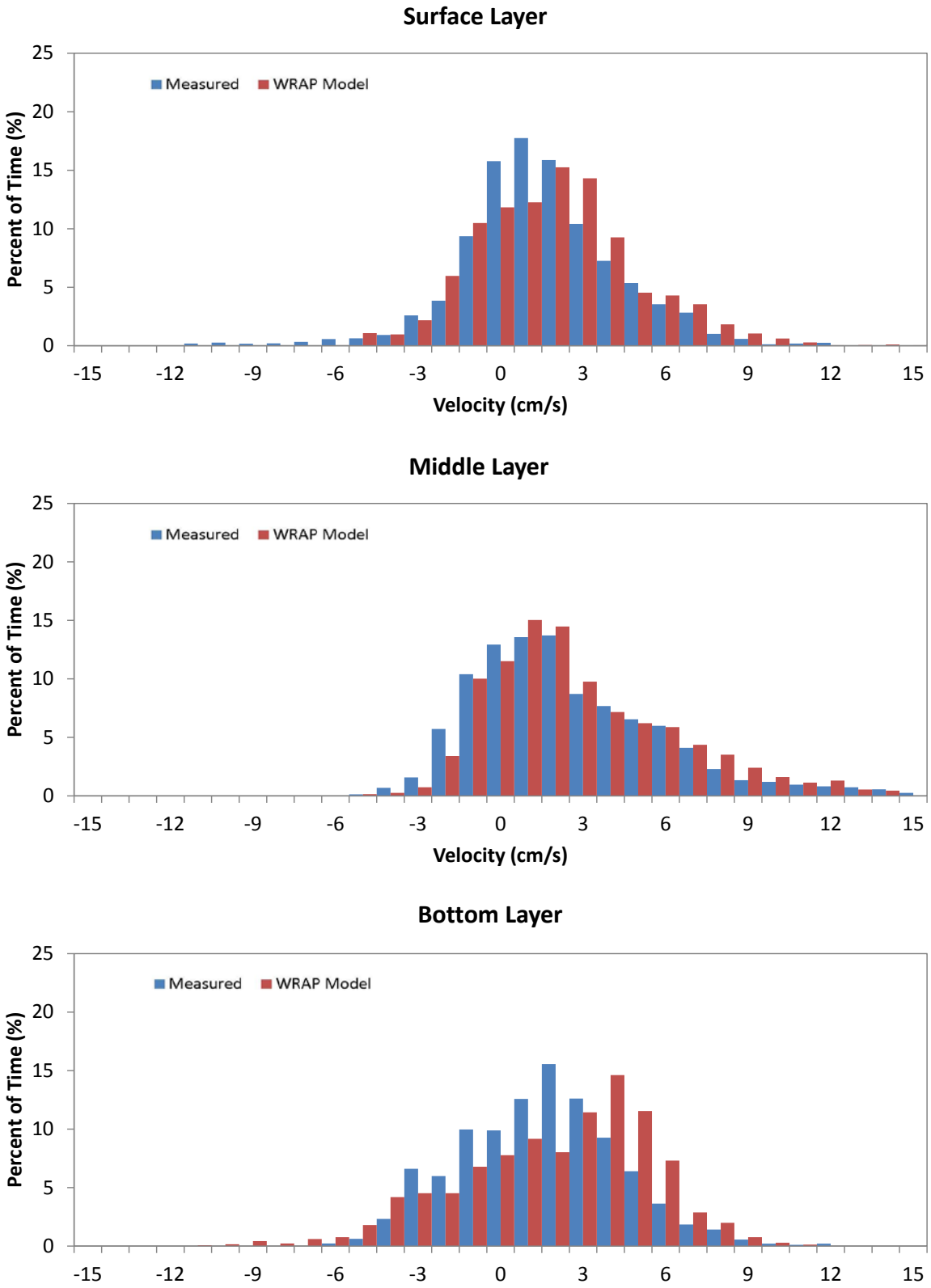

Figure 5.9 Velocity Distribution Comparisons at POLA Pier 400

Velocity profiles in Cabrillo Marina were compared with ADCP profile data. For each profile, ADCP measurements were taken over 5 to 15 minute durations at even increments throughout the water column. ADCP data were processed, filtered, and averaged over the measurement duration in order to obtain the velocity profiles. Review of the ADCP data revealed that the currents within Cabrillo Marina do not have a strong tidal oscillation, unlike the dominant flood and ebb tide currents observed in areas of the harbor. Hence, comparisons of the velocity profiles were made based on velocity vectors (east and north velocity) and magnitude. Velocity profile comparisons are provided in Figures 5.10a – 5.10c. In general, velocities within Cabrillo Marina are smaller than velocities at other harbor locations (i.e., MSCs). Velocity profiles taken on May 27 and 28, 2009 are shown in Figure 5.10a. Measurements were made at the same locations on different days. Velocity profiles taken on June 12, 2009 are shown in Figures 5.10b and 5.10c, and were made at multiple locations throughout the day. Overall, the WRAP Model showed velocities that are the same order of magnitude as the field data, but generally showed less vertical variation compared to the field data.

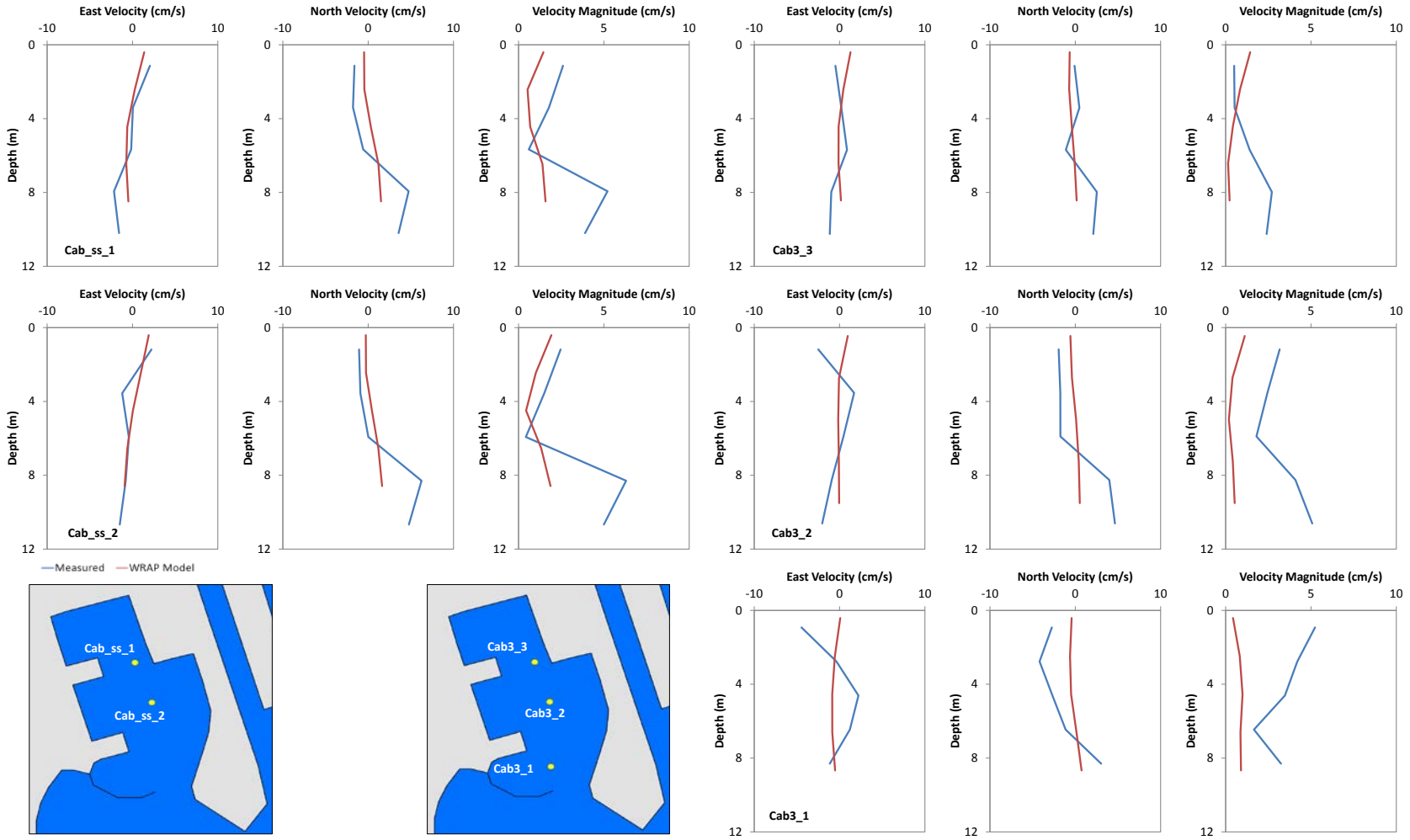

Figure 5.10a Velocity Profile Comparisons in Cabrillo Marina 5/27 and 5/28/09

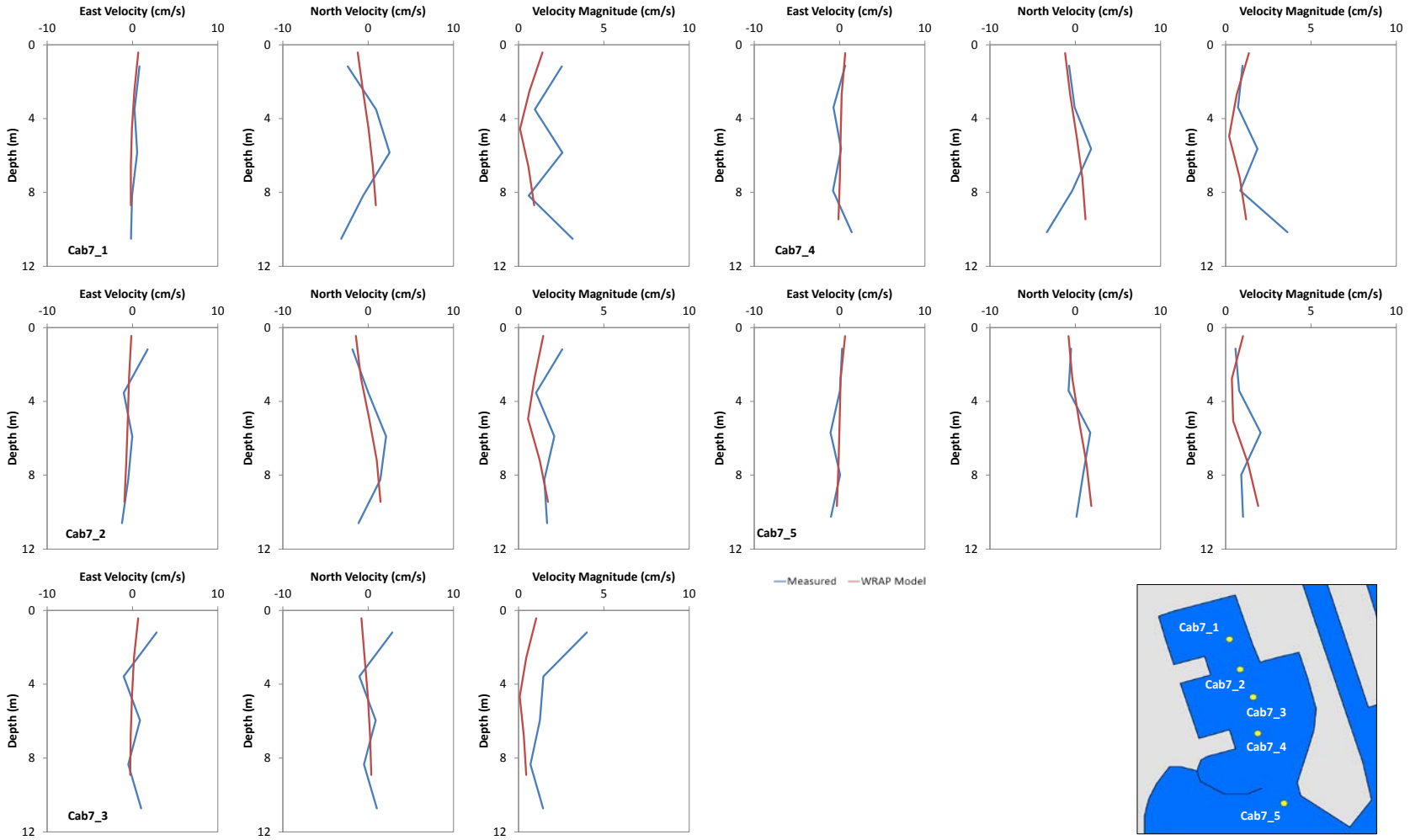

Figure 5.10b Velocity Profile Comparisons in Cabrillo Marina 6/12/09

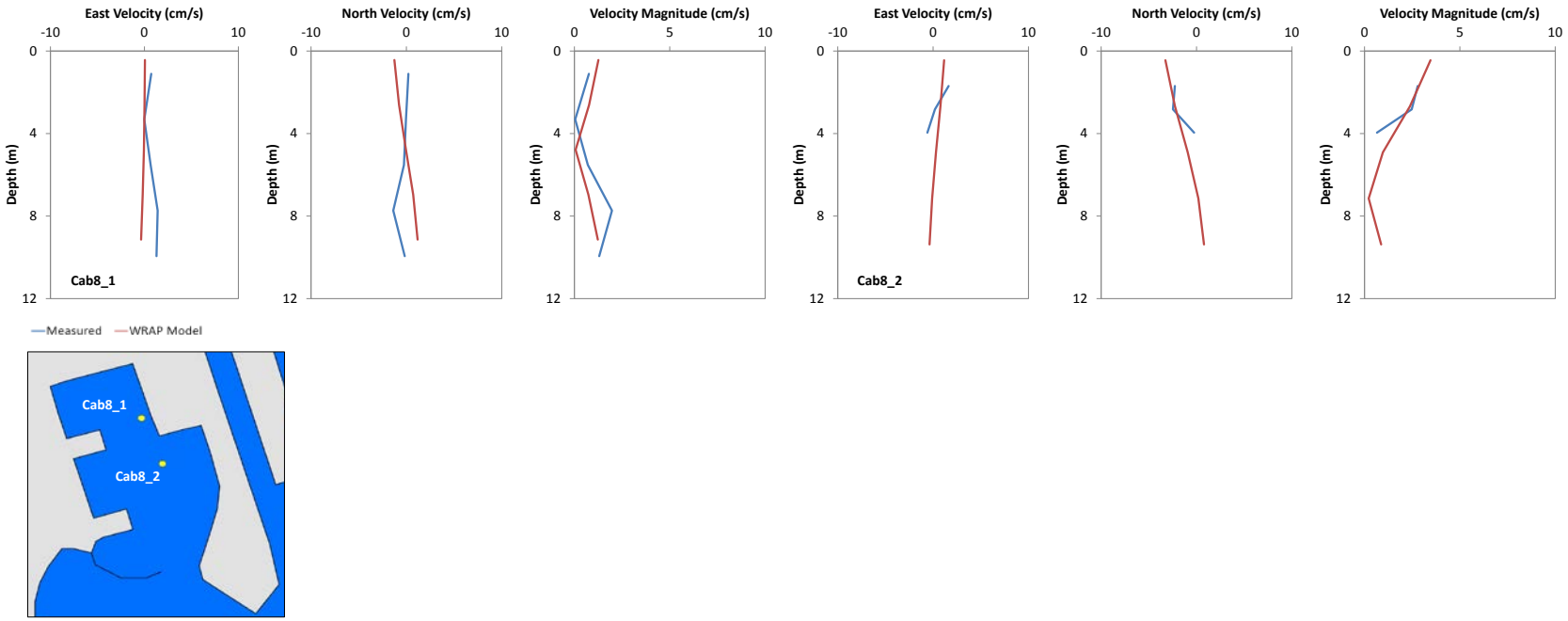

Figure 5.10c Velocity Profile Comparisons in Cabrillo Marina 6/12/09

6. MIXING AND TRANSPORT

6.1 INITIAL CONDITIONS

6.1.1 Temperature

Water temperatures in the LA/LB Harbor and greater San Pedro Bay are relatively consistent throughout the year. Monthly water temperatures at the NOAA LA Harbor gage are shown in Table 6.1. The water temperatures are monthly averages based on data from 2002 to 2012. Over a year, water temperatures range from 14.4 to 18.0°C with an average of 16.4°C. Seasonal fluctuations occur with warmer water temperatures during summer months and peak in September. Cooler water temperatures occur in early spring with the lowest temperatures in March and April. Annual average water temperatures between 2002 and 2012 ranged from 15.3 to 17.8°C.

Table 6.1 Average Monthly Water Temperatures at NOAA LA Harbor

MONTH	TEMPERATURE (°C)
January	15.0
February	15.2
March	14.7
April	14.4
May	16.0
June	17.5
July	17.9
August	17.6
September	18.0
October	17.8
November	17.0
December	15.7
Average	16.4

In general, vertical variations in water temperatures indicate warmer temperatures at the water surface that decrease with water depth. Thermal gradients (i.e., difference between surface and bottom water temperatures) typically occur during warmer summer months. During warmer months, thermal gradients can range from 3 to 6°C, whereas thermal gradients are typically between 0 to 2°C during cooler months (POLB and POLA 2002, POLA and POLB 2010, and POLB 2011).

Observed temperature gradients do not indicate significant thermocline gradients that would affect stratification or thermally induced currents, thus water temperature variation was not simulated. A constant water temperature of 16°C was specified. The average water temperature specified in the WRAP Model was based on multiple studies with data from multiple locations throughout the harbor (POLB and POLA 2002, Everest 2007, and Environ 2015c).

6.1.2 Salinity

The salinity initial and boundary conditions were originally specified during the DCEM development based on salinity vertical profile data from 2000 (Everest 2007). One sample location outside the breakwater, where seven measurements were taken between August and December 2000 (ACTA 2001), showed a uniform vertical profile of about 33.5 Practical Salinity Units (PSU). This was consistent with salinity data from the Harbor area taken in 2000 (POLB and POLA 2002). The ocean salinity was also verified based on recent salinity data from the TMDL Low Detection Limit Special Study (LDL Study) taken outside the breakwater (REF-01), which showed an average salinity of 33.45 PSU (Environ 2015c). The initial and ocean boundary salinity was specified as 33.5 PSU. The initial salinity concentration was uniformly specified horizontally and vertically as a constant concentration. A minimum spin-up period of 30 days was used to allow spatially varying salinity conditions to develop from storm water discharges (Everest 2007).

6.2 MIXING AND TRANSPORT CALIBRATION DATA

Mixing and transport calibration data consisted of dye and salinity data that were used to evaluate the WRAP Model capabilities to simulate storm water discharges and transport through the harbor. Evaluation of dye and salinity concentrations provides additional lines of evidence to support the overall WRAP Model calibration especially since availability of other types of data for model calibration (e.g., velocity, sediment, or organic chemicals) can be limited. Similar to sediment or organic chemicals, transport of dye and salinity are driven by the same physical processes of advection and dispersion from tidal hydrodynamics and storm water discharges.

A dye study provides data with which to evaluate mixing and transport conditions. As part of the DCEMS, a dry weather tracer study was conducted on May 17, 2005 to document dispersion and mixing characteristics of flows from the DC discharging into the CS and transporting into the harbor (Everest 2007). Rhodamine dye was released at the downstream end of the DC during an ebb tide, as shown in Figure 6.1. The photograph shows the dye moving toward the CS shortly after the release. Continuous dye concentrations were made at three harbor locations (Berth 200G, Berth 206, and Berth 173) using an *in situ* fluorometer.

Salinity levels in the LA/LB Harbor are normally constant with little variation through the water depth except during wet weather conditions when storm water discharges reduce surface salinities. Locations of salinity calibration data are shown in Figure 6.2. Salinity profiles are periodically measured by the POLA and POLB. Several POLA studies have collected salinity profiles in the harbor. Measurements in the POLB are part of NPDES permit monitoring requirements that monitors ambient receiving water conditions in proximity to 21 storm drains (POLB 2011). Additional salinity profiles were taken during the DCEMS, which included dry and wet weather profiles in the CS and inner harbor (Everest 2007). Surface and bottom depth salinities (grab samples) were also monitored several times as part of the Waste Discharge Requirements (WDRs) for the Terminal Island Water Reclamation Plant (TIWRP). Compilation of these salinity profiles, as shown in Figure 6.3, illustrates the spatial variation in salinity throughout the harbor. In the figure, over 200 salinity profiles were grouped by location (POLA, middle, and POLB) and region (inner, middle, and outer harbor). Salinity profiles during dry and wet weather are shown in green and orange, respectively. As illustrated by the green lines, salinity throughout the harbor is fairly uniform during dry weather. For wet weather, shown as the orange lines, the largest gradients in salinity occur in the POLA inner harbor areas, which directly receive storm water discharges. In addition, the western portion of the harbor (POLA side) has a larger drainage area compared to the eastern portion of the harbor (POLB side). The most uniform salinity profiles are observed in the POLB, but the timing of wet weather salinity profiles taken may not have captured minimum salinities. In general, the larger gradients are observed closest to storm water discharges, while smaller gradients occur in the outer harbor areas.

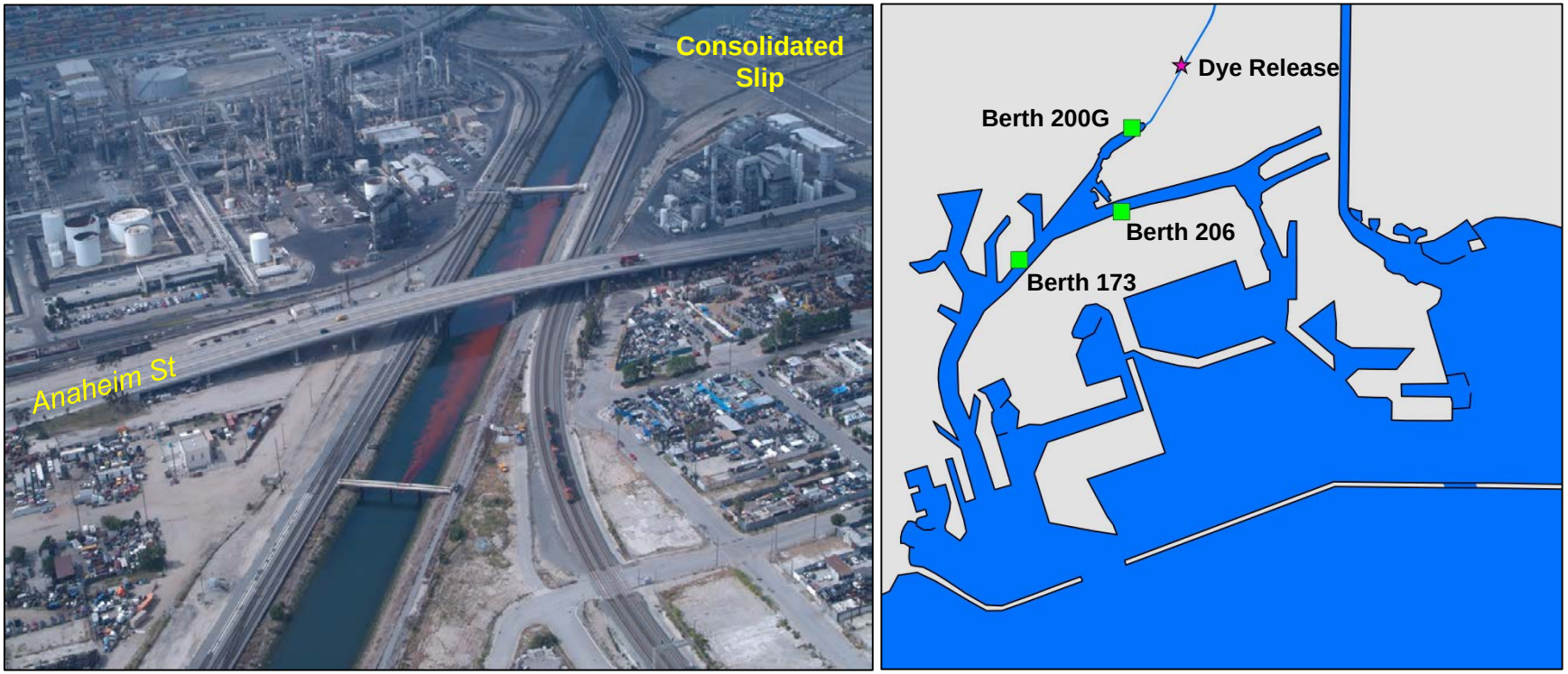

Figure 6.1 Dye Release and Monitoring Locations

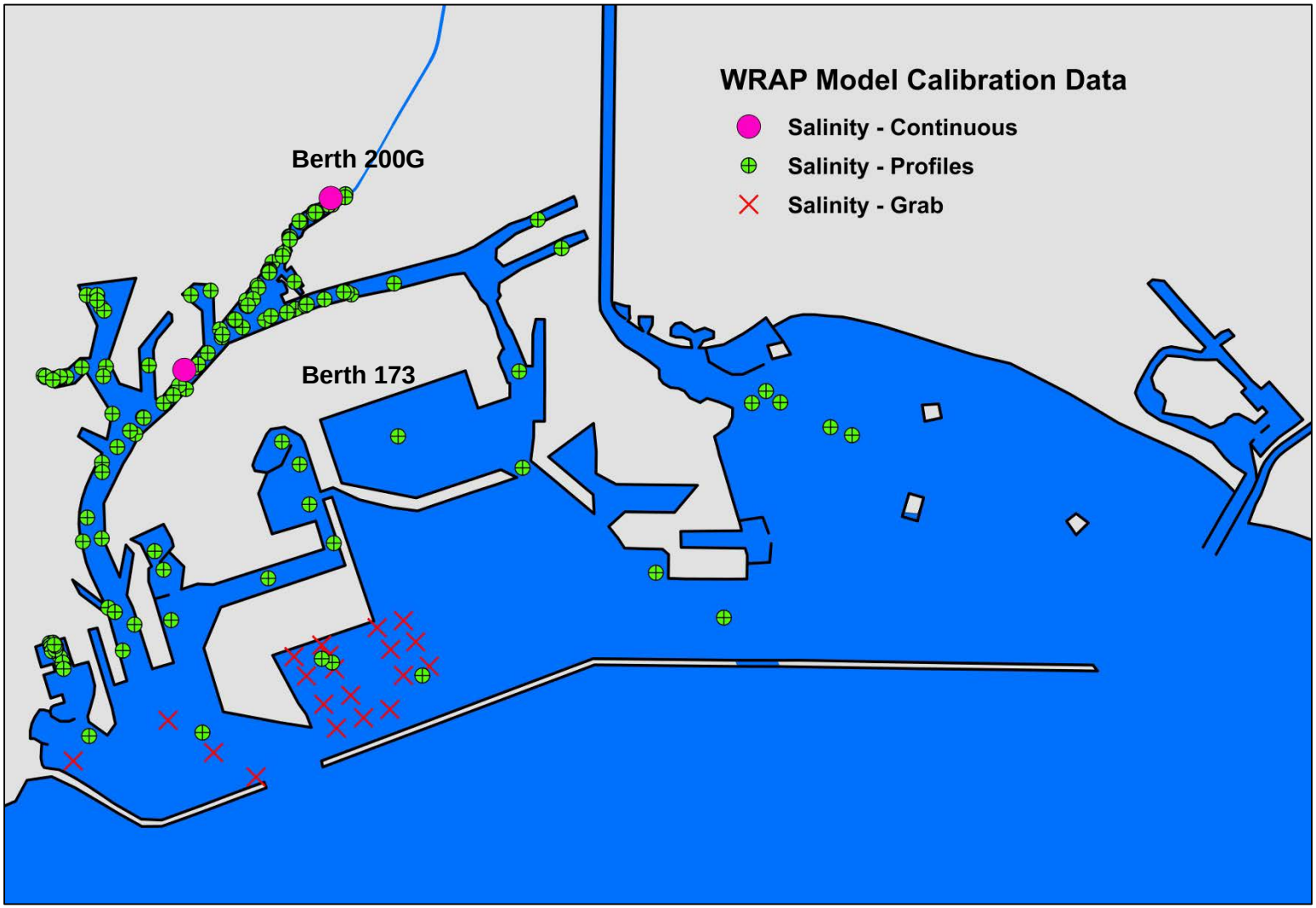

Figure 6.2 Salinity Calibration Data Locations

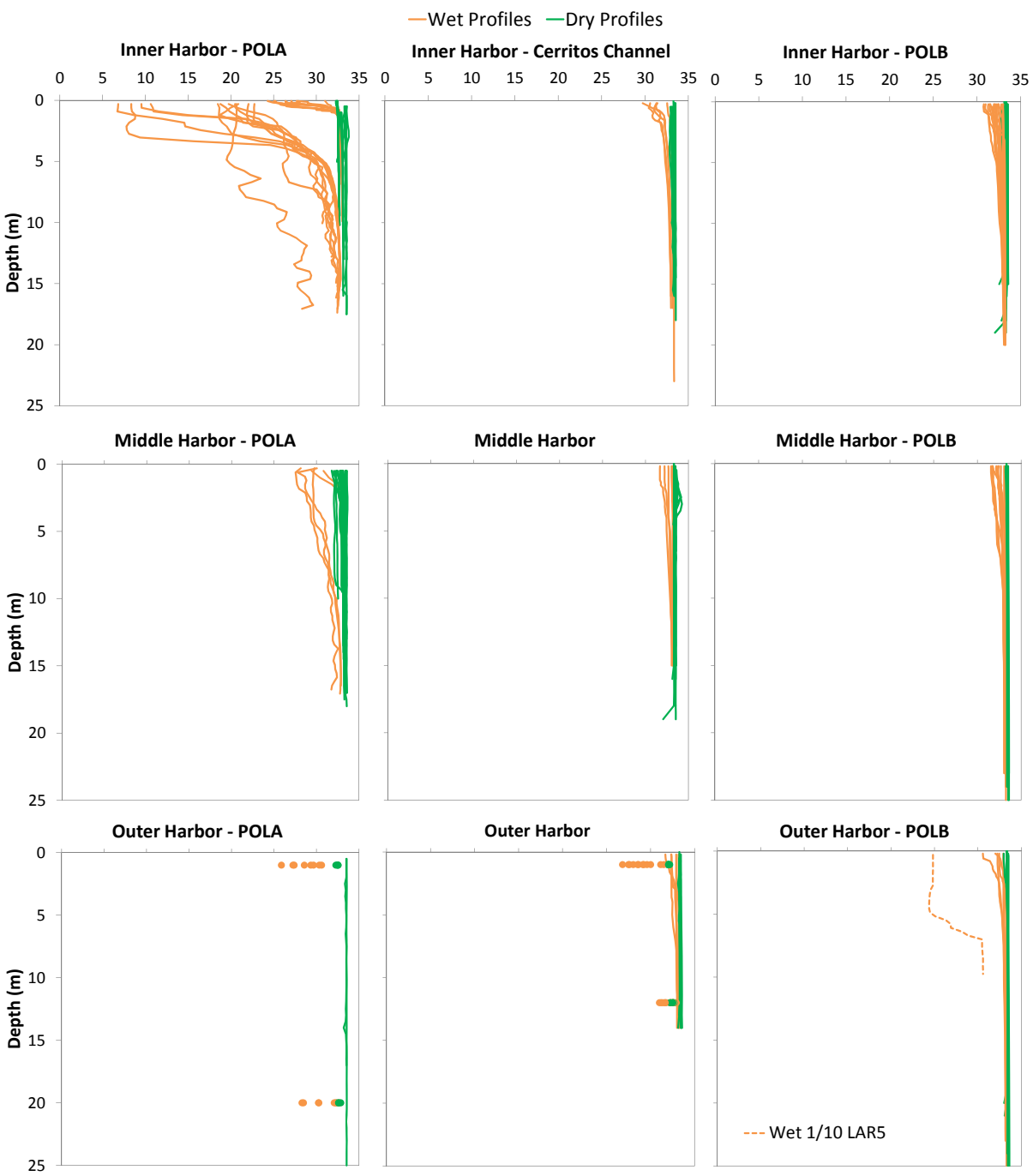

Figure 6.3 Spatial Variations in Harbor Salinity Profiles

6.3 CALIBRATION RESULTS

6.3.1 Dye

Time series plots of dye concentrations from the DCEMS dry weather dye study were compared at three harbor locations, as shown in Figure 6.4. Dye concentrations are shown in units of parts per billion (ppb). The highest dye concentrations were observed at Berth 200G in the CS, as shown in the top panel. The measured dye concentrations show a spike in concentrations corresponding to arrival of the dye at Berth 200G after being released at the DC, followed by a gradual decrease as the dye is dispersed. The WRAP Model-predicted dye concentration shows nearly the same peak dye concentration and gradual decrease over time as the measured concentrations. This indicates that the WRAP Model not only accurately simulated the arrival (timing and magnitude), but also the subsequent mixing and dilution over the next couple of days.

At the other two locations further into the harbor, dye concentrations were significantly less than that at Berth 200G, thus the dye concentration comparisons are shown with a different vertical scale. Measured dye concentrations at Berths 206 and 173 indicated a significant time lag for the dye to be transported from the CS and through the East Basin. In general, the WRAP Model-predicted dye concentrations at Berth 206 and Berth 173 compared well with the field data with similar concentrations of about 1 ppb.

6.3.2 Salinity

Mixing and transport characteristics using salinity data are best evaluated during wet weather conditions in which storm water discharges reduce salinity levels. Continuous salinity measurements made at Berths 200G and 173 during a rain event as part of the DCEMS wet weather monitoring were compared with model-estimated salinity (Figure 6.5) during the rain event on February 27-28, 2006 and during the subsequent two-week period as the salinity gradually returned to normal levels. In the upper panel, the salinity comparison at Berth 200G shows the WRAP Model is capable of simulating the storm water discharges both in timing and magnitude corresponding to the rain event. Following the rain event, salinity levels begin to increase back to normal due to tidal mixing. The measured salinity at Berth 173 shows that the response to storm water discharges at that location is less pronounced compared to the response at Berth 200G since Berth 173 is located further away from major discharges. The measured salinity shows a combination of effects due to tidal oscillations and storm water discharge with a general decrease due to the rain event, followed by a general increase back to normal levels. The WRAP Model-predicted salinity is shown for the model surface layer, which shows the same general trend. However, the model surface layer at Berth 173 is larger than the water depth at which salinity was measured, thus resulting in some differences. Differences in the model surface layer and measured surface salinity are discussed below based on the salinity profiles from the LARE.

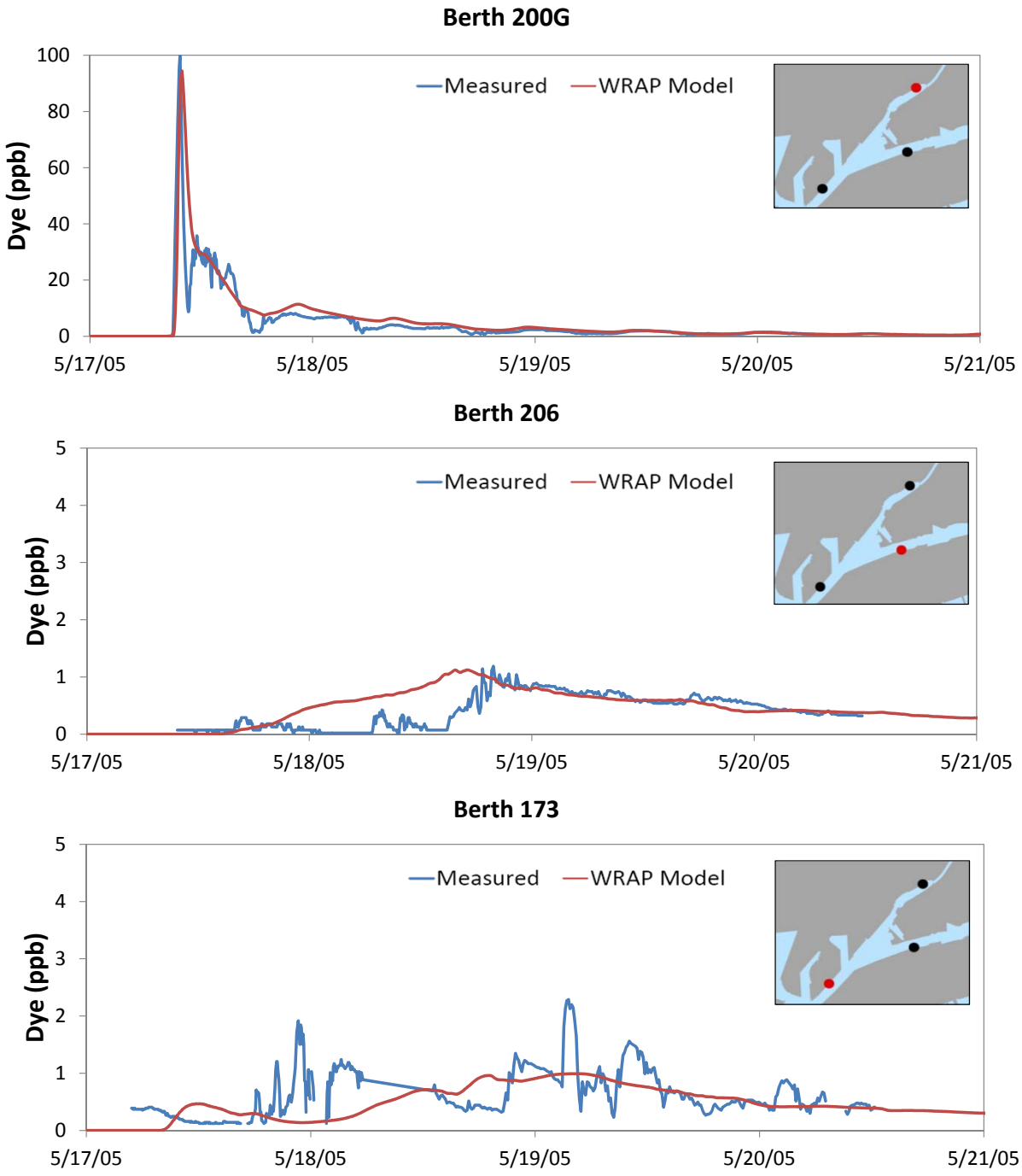

Figure 6.4 Dye Comparisons in Dominguez Channel Estuary

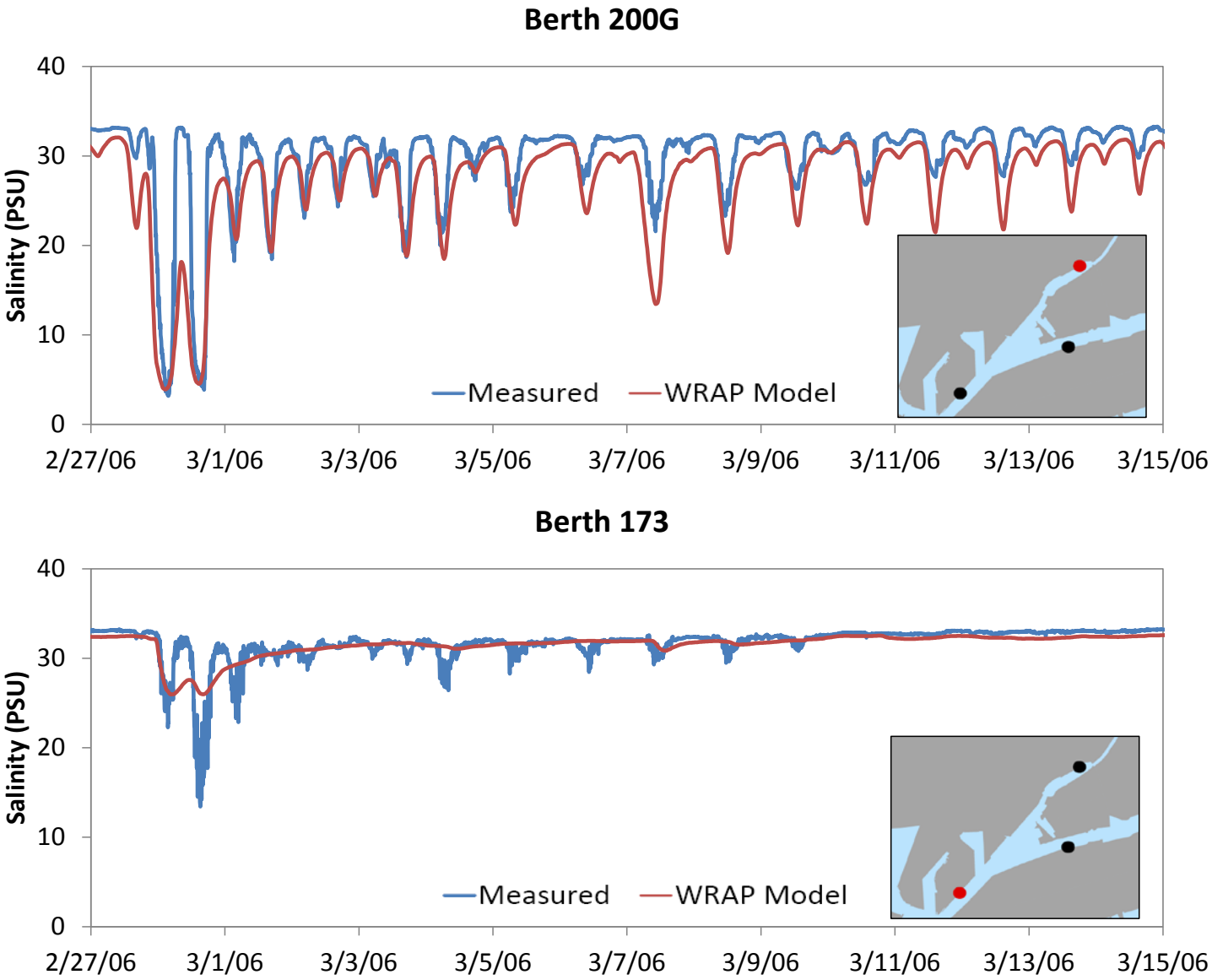

Figure 6.5 Salinity Comparisons in Dominguez Channel Estuary

Vertical salinity variations in the outer harbor were evaluated from surface and bottom water depth salinity data taken during dry and wet weather conditions as part of the TIWRP monitoring requirements. Salinities were compared for the period between December 2004 and March 2005, which includes two of the largest rain events in January and February 2005. Comparisons in surface and bottom salinity are provided in Figures 6.6a – 6.6e for 20 locations. For each location, the measured surface (blue square) and bottom (open circle) salinity (two dry and two wet events) are compared to the WRAP Model time series of surface (solid red line) and bottom (dotted red line) layer salinities. In general, the WRAP Model indicates salinity stratification similar to the measured salinities. There is essentially no difference in surface and bottom salinity during dry weather. During wet weather, the salinity stratification shows lower salinities at the surface.

Mixing and transport were also evaluated from salinity profiles near the LARE. Wet weather salinity profiles were compared just outside the LARE, as shown in Figure 6.7a. Four salinity profiles were taken during a POLA special study in January 2010. In January 2010, a series of five rain events occurred over a 6-day period, as illustrated by the LAR flow in the lower right inset of Figure 6.7a. Salinity profile measurements (indicated in the red) were made at the start of the fourth rain event on January 21, 2010. Hence, the measured salinities represent the storm water discharges and mixing of multiple consecutive events. For the salinity profile comparisons, the solid, blue line shows the measured salinity taken at a 0.3-m interval through the water column depth. However, the WRAP Model vertical resolution uses an interval measuring approximately 2-m that is based on five equally spaced layers. For a direct comparison, the measured salinity was averaged into five equally spaced depths, as indicated by the blue line with blue squares (each blue square represent an average measured salinity for one of the WRAP Model layer). The measured average salinity profile (with blue squares) can be compared directly with the WRAP Model salinity profile shown by the red line. Comparisons of the salinity profiles are ordered based on distance from the LARE with LAR3 being the farthest away. In general, the WRAP Model salinity profiles show a similar salinity gradient between the surface and bottom water depths as measured gradients. The measured average surface salinity ranged from 18 to 25 PSU, and is comparable to the WRAP Model surface salinity range of 17 to 24 PSU. Given the complexity of the hydrodynamics in the LARE area, the WRAP Model is shown to reasonably predict mixing and transport conditions based on the salinity profiles.

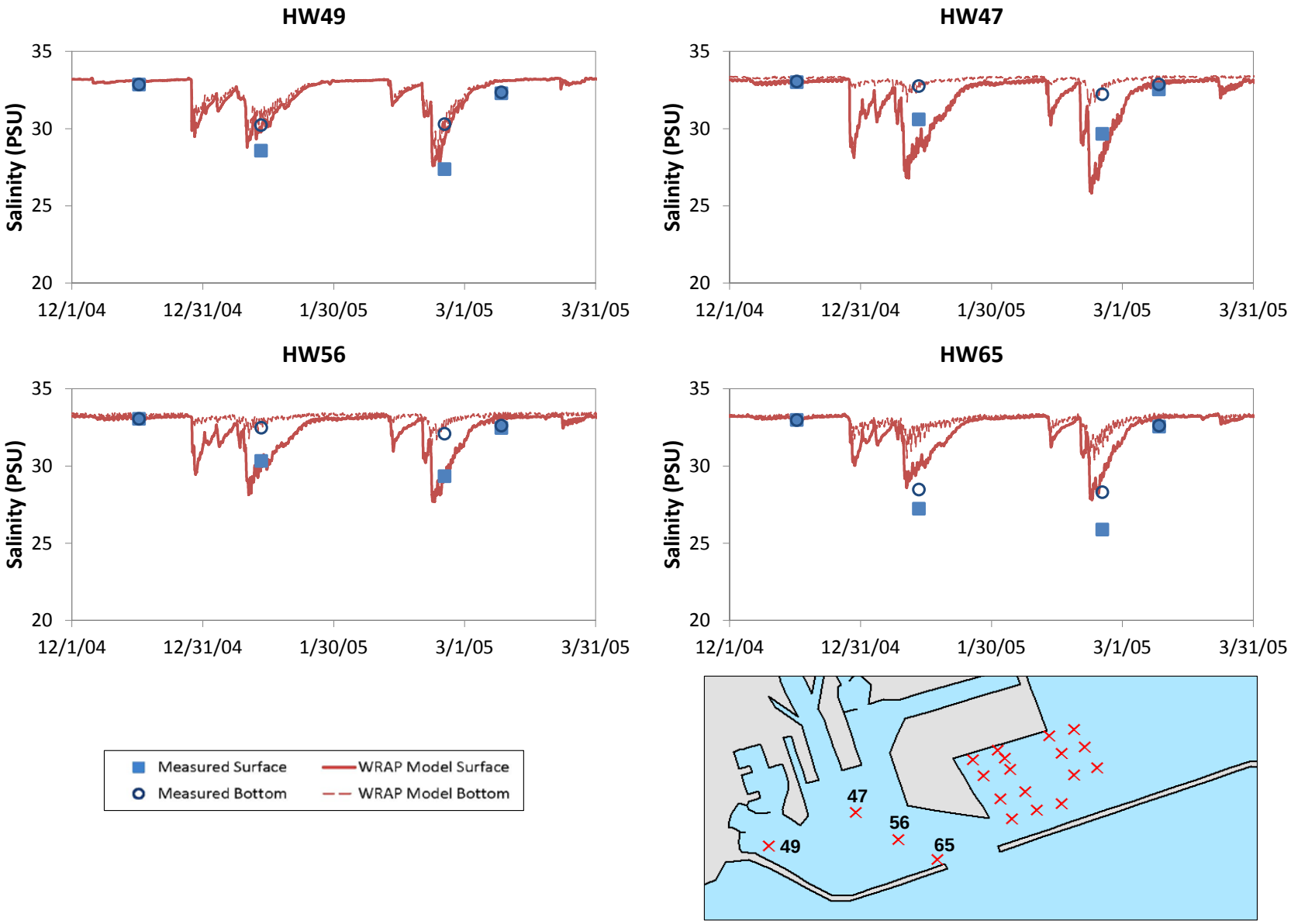

Figure 6.6a Salinity Comparisons in POLA Outer Harbor

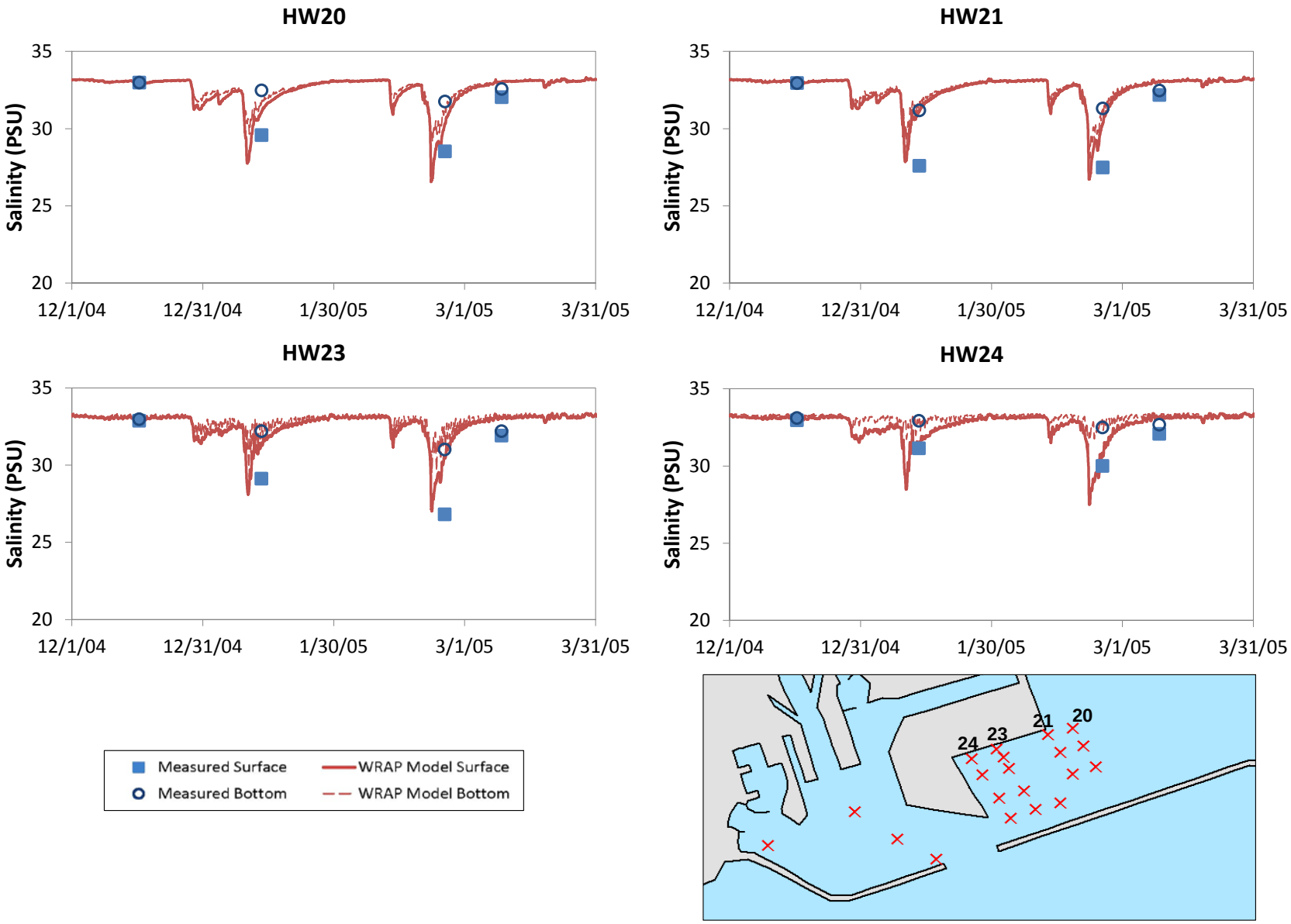

Figure 6.6b Salinity Comparisons in POLA Outer Harbor

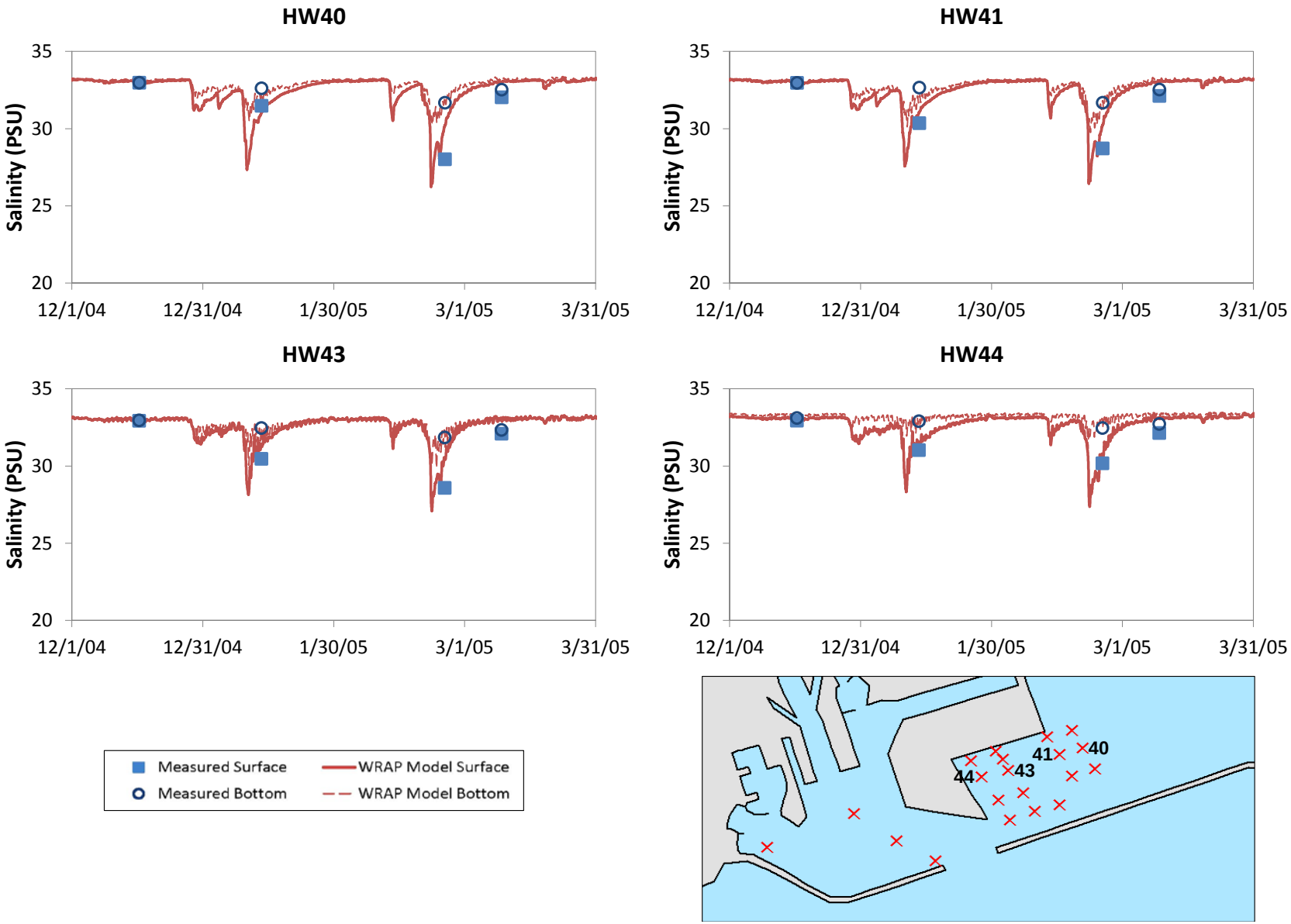

Figure 6.6c Salinity Comparisons in POLA Outer Harbor

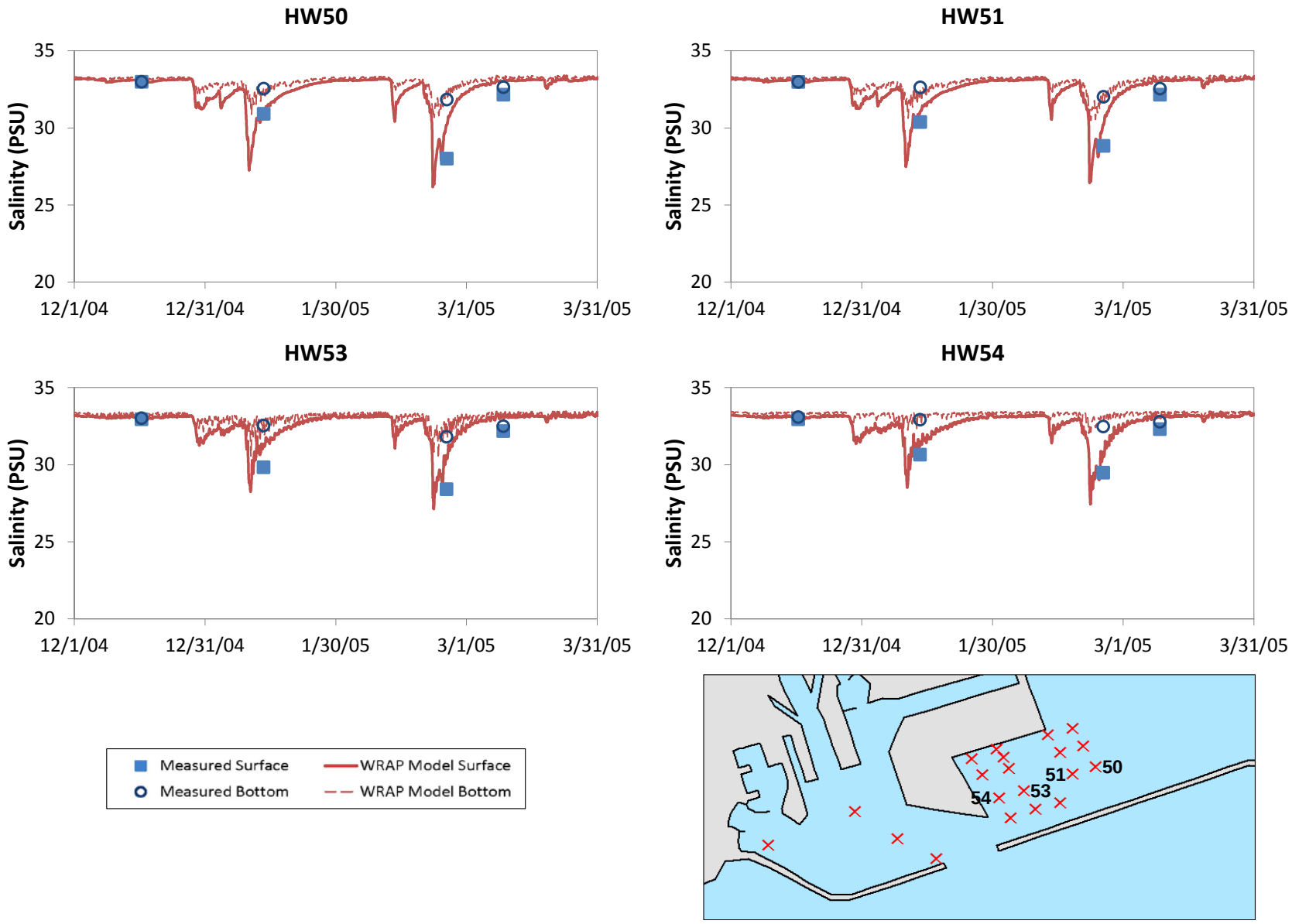

Figure 6.6d Salinity Comparisons in POLA Outer Harbor

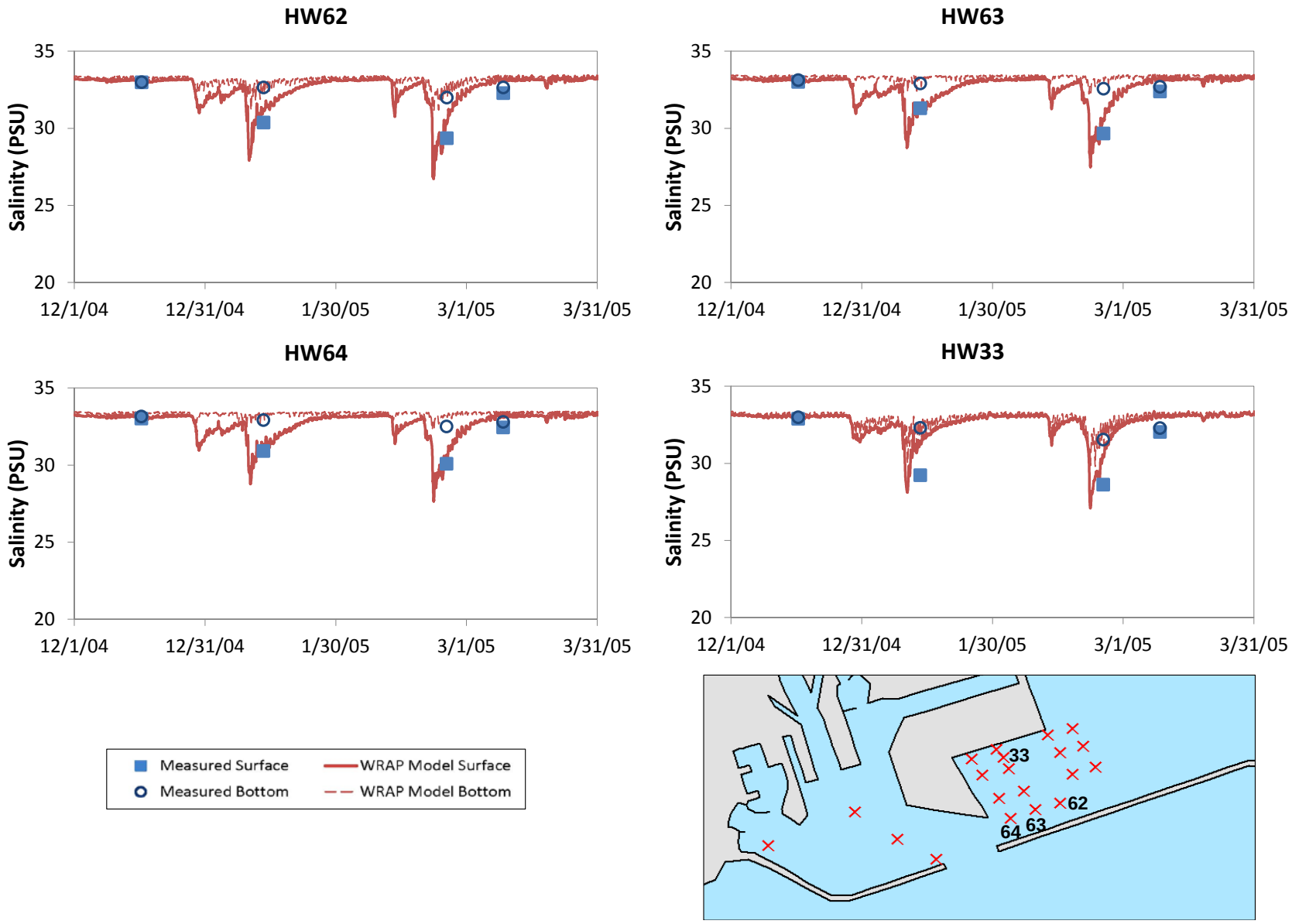

Figure 6.6e Salinity Comparisons in POLA Outer Harbor

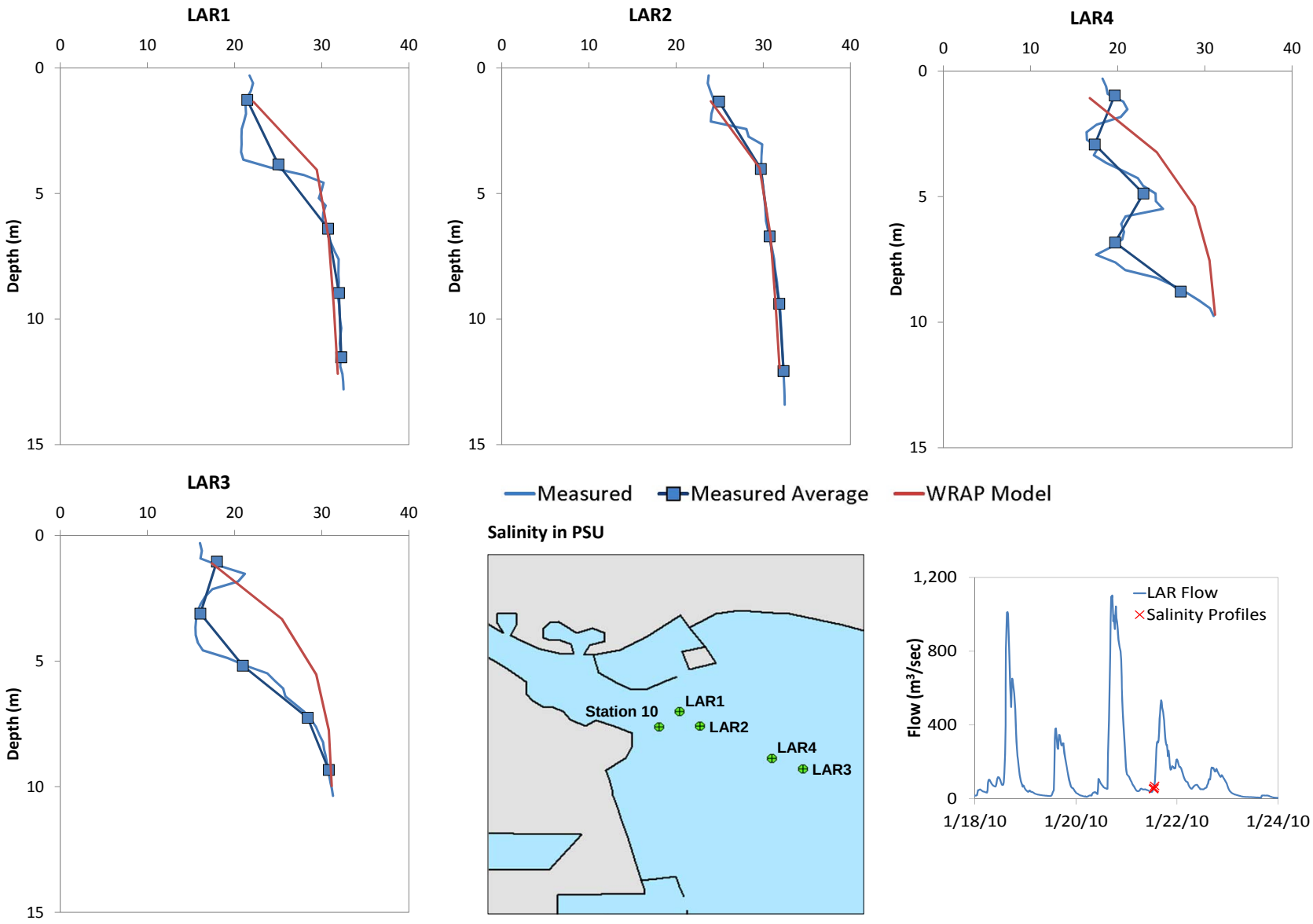

Figure 6.7a Salinity Profile Comparisons in Los Angeles River Estuary

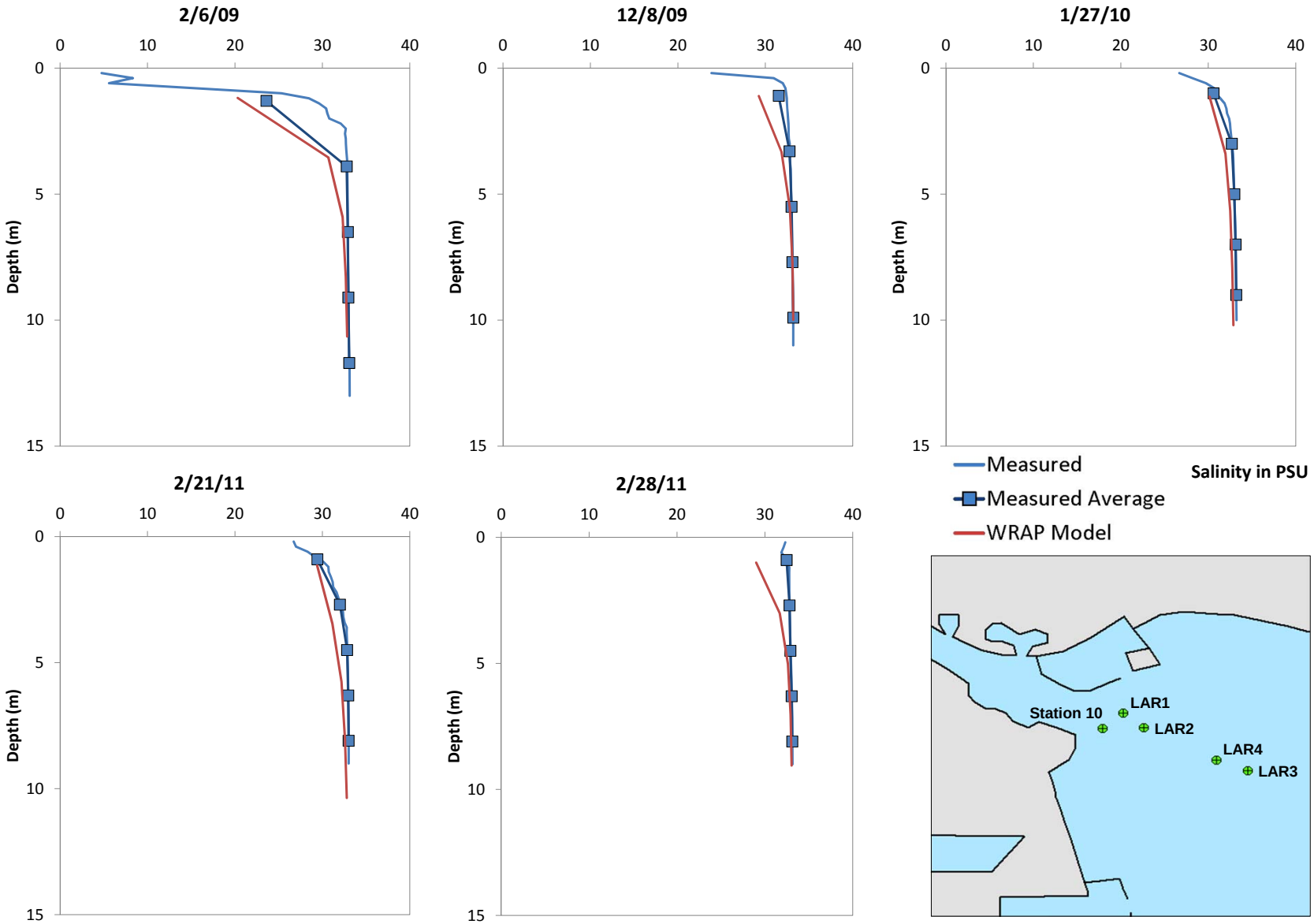

Figure 6.7b Salinity Profile Comparisons in Los Angeles River Estuary

Additional salinity profiles near the LARE were also available at one location (Station 10) during several wet weather events in 2009, 2010, and 2011 which are shown in Figure 6.7b. Single salinity profiles from each event were compared. Similar to Figure 6.7a, the measured salinity profiles are shown by the measured (blue line) and the measured average salinity (n=blue line with blue squares) profiles. Measured salinity profiles for the February 6, 2009 wet event best illustrate the difference in salinity profile based on the vertical resolution. The measured salinity profile based on a 0.2-m depth interval (solid blue line) illustrates the fresh water lens with a minimum salinity of about 5 PSU that increases to 30 PSU over 1.5 m; while the same measured salinity profile averaged over a 2.6-m depth interval (blue line with blue squares) results in a surface salinity of 23.6 PSU. The WRAP Model salinity profile (red line) compares well with the measured average salinity profile (blue line with blue squares) based on both salinity magnitude and depth. The remaining salinity profiles indicated smaller salinity gradients. Overall, the WRAP Model salinity profiles near the LARE show reasonable predictions of the salinity gradients.

Salinity profile comparisons in the CS as presented in Figure 6.8 were from the DCEMS wet weather calibration period. Comparisons are shown for wet weather profiles taken in the CS and East Basin, which occurred at the start of the rain event prior to the peak storm water discharges. In general, the measured salinity profiles show a greater salinity gradient inside the CS nearest the DC and a smaller salinity gradient in the East Basin. The WRAP Model salinity profiles also show a larger salinity gradient in the CS compared to the East Basin. Differences between the measured and modeled salinity profiles may be attributed to the estimated storm water inflows, which may not accurately account for the timing of wet weather flows from smaller drainage areas.

Harbor-wide salinity patterns were evaluated based on the spatial variation previously presented in Figure 6.3. In Figure 6.9, the WRAP Model-predicted harbor-wide salinity patterns using over 200 salinity profiles are compared with the measured salinity pattern. In the figure, salinity profiles during dry and wet weather are shown in green and orange, respectively. As shown in the figure, the WRAP Model-predicted salinity profiles (shown in the right panels) show the same spatial variation as the measured salinity profiles (shown in the left panels). Dry weather salinity profiles are typically uniform in depth throughout the harbor. The largest salinity gradients occur in the POLA inner harbor areas corresponding to storm water discharges.

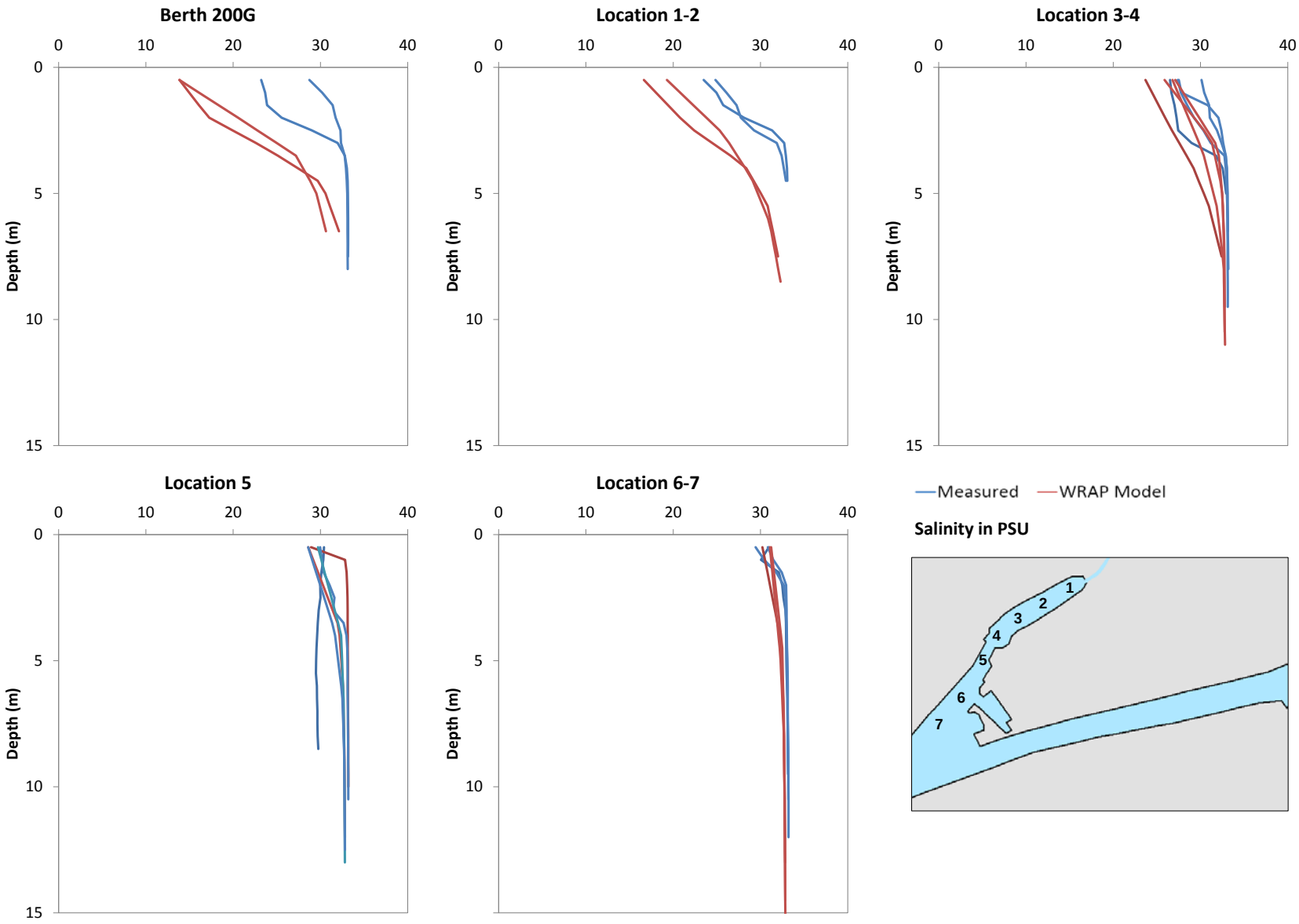

Figure 6.8 Salinity Profile Comparisons in Consolidated Slip

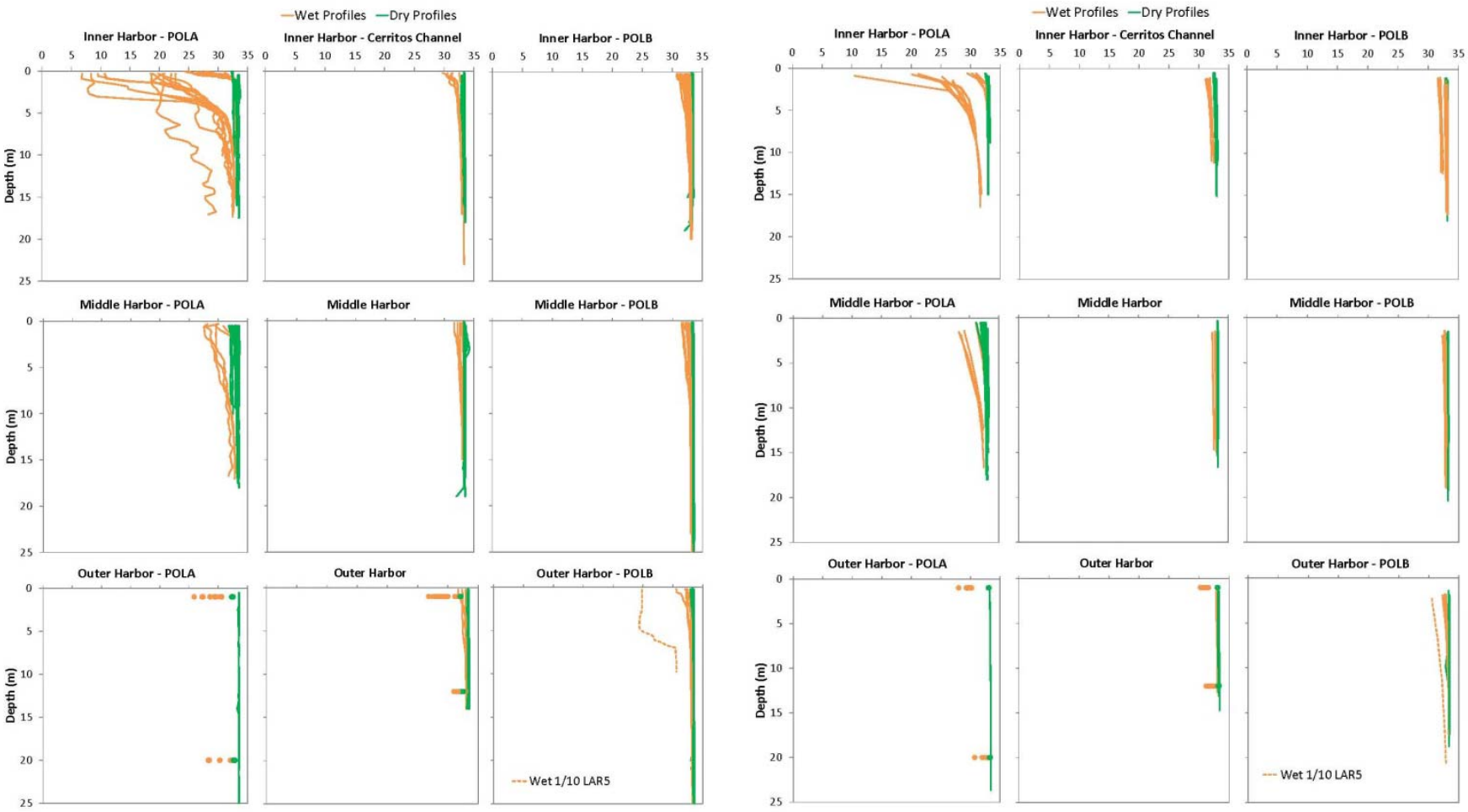

Measured Harbor Salinity Profiles ***WRAP Model Harbor Salinity Profiles***

Figure 6.9 Harbor Salinity Profile Comparisons

7. SEDIMENT TRANSPORT

7.1 MODEL SETUP AND PARAMETERS

The WRAP Model sediment bed properties were specified with a compilation of grain size, bulk density, and porosity sediment data. Data from multiple studies conducted in different years were required in order to provide sufficient spatial representation of the sediments. A listing of sediment data is provided in Table 7.1. The majority of the data utilized were collected after 2003. Older data from 1997 and 1998 were included to augment the spatial coverage of data. One sample from the Bay Protection and Toxic Cleanup Program (BPTCP) 1997 data was included to characterize sediment properties at Inner Cabrillo Beach. Southern California Bight (Bight) 1998 data were used to supplement data in San Pedro Bay and ocean area outside of the breakwater. A map of the sediment data is provided in Figure 7.1. Sediment properties for the WRAP Model were specified using Theissen polygons of the sediment data. The Theissen polygons of the sediment bed silt fraction (left legend) were based on the sediment grain size data (right legend). In general, the sediments in the greater harbor waters (inside the breakwater) are predominantly silts, while sediments outside the breakwater are mostly sands.

Table 7.1 Summary of Sediment Data

YEAR	STUDY	REFERENCE
2014	Surface Sediment Characterization and Polychaete Tissue Collection Program	Environ 2015b
2013	Berth 36 Cabrillo Yacht Club Maintenance Dredging Project	AMEC 2013
2011	POLA Dominguez Channel/Consolidated Slip Erosion Study	AMEC 2011
2010	Los Angeles River Estuary Maintenance Dredging	USACE 2010
2008	Bight 2008	SCCWRP 2012
2006	Characterization of Sediment Contaminant Flux to Support TMDL Implementation	Weston 2007
2003	Bight 2003	SCCWRP 2007
2003	Huntington Harbor and Anaheim Bay - SARWQCB	SWRCB 2005
1998	Bight 1998	SCCWRP 2003
1997	Bay Protection and Toxic Cleanup Program	SWRCB 2005

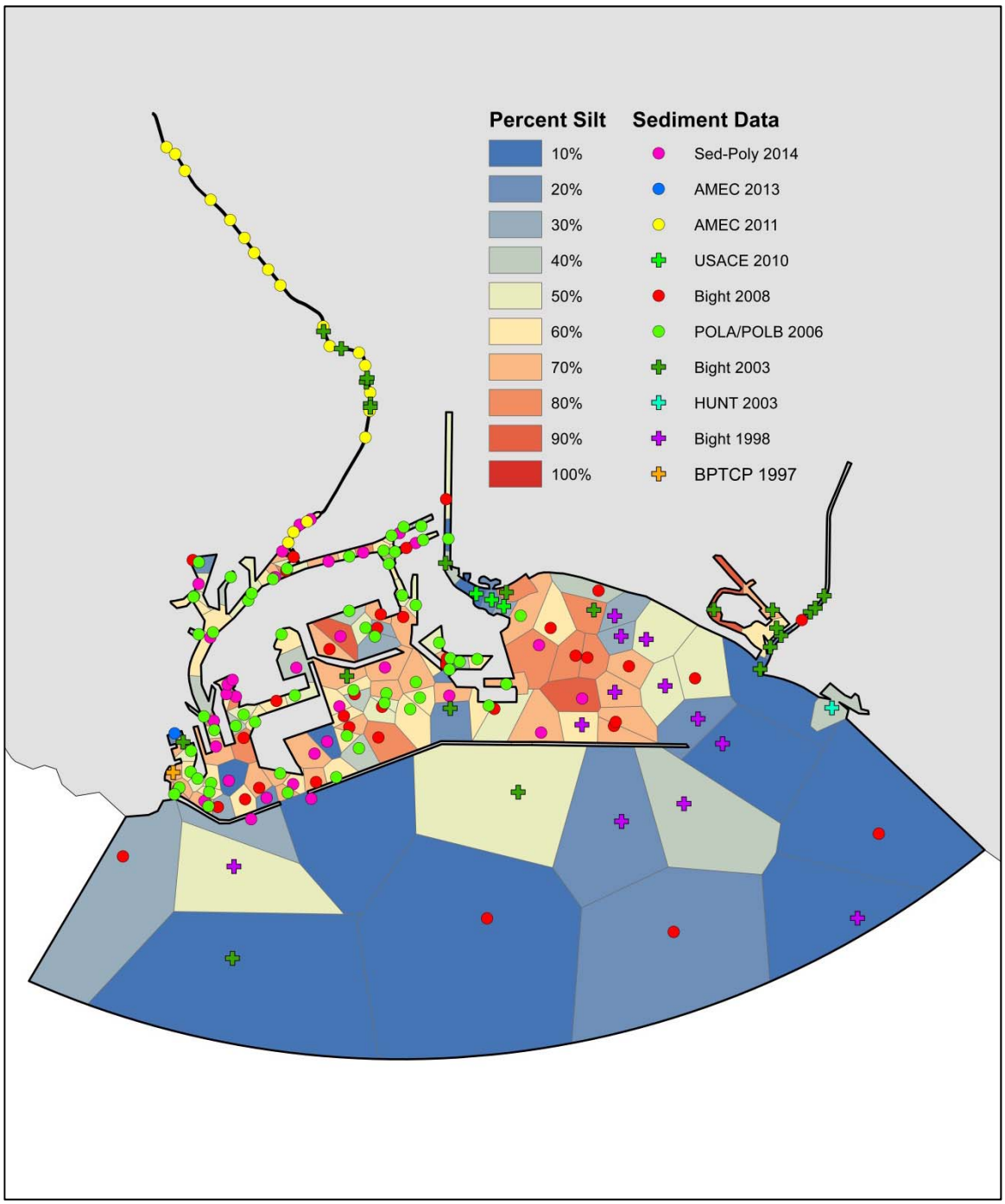

Figure 7.1 Sediment Grain Size Data

7.1.1 Sediment Bed

The sediment grain size data were used to characterize the sediments in the bed. Particle size distributions of sediments of the rivers, harbor, and ocean area are illustrated in Figure 7.2. Particle size distributions for the DC, LAR, SGR, and ocean area outside of the breakwater are shown in the upper panel. In general, these sediments are predominantly sands. Particle size distributions in the harbor are shown in the lower panel. In general, the harbor areas are predominantly silts, while outside the breakwater sediments are predominantly sands. The sediment bed composition is illustrated in Figure 7.3, which shows the percent clay, silt, and sand.

The WRAP Model sediment bed was characterized with five sediment classes, as summarized in Table 7.2. The sediment type and minimum grain diameter was defined based on the Wentworth classification (USACE 2002). Based on the range in sediment sizes, five sediment classes were defined for the WRAP Model. One sediment class was specified for clay particles. Silt particles were specified using two sediment classes. Sands were also represented using two sediment classes. The settling velocity for each sediment class was calculated based on the representative diameter of the particle (Dietrich 1982). The settling velocities were calibrated during the prior WRAP Model development. Thus, for the cohesive sediment, the effect of flocculation was inherently considered.

The WRAP Model sediment bed was specified with four bed layers with spatially varying sediment properties. The sediment grain size data were used to determine the mass fraction for each of the five sediment classes along with the corresponding bulk density and porosity data. The sediment data were then applied to the WRAP Model based on Thiessen polygons of the sediment data. Selection of the bed layer heights were based on the needs of the Bioaccumulation Model. The bed layer heights were specified as 5 cm for each of the top two bed layers and 5.24 cm and 15.24 cm for the bottom two bed layers. The top two bed layers (10 cm) correspond to the bioactive surface layer (Anchor QEA 2014b). The surface layer of 5 cm was considered to be important for the organic sediment concentrations and the linkage of the WRAP Model to the Bioaccumulation Model is through the average organic concentrations of this top 5 cm surface layer. The third bed layer corresponds to the depth of the organic sediment data, and the lowest bed layer was specified to accommodate possible erosion at some isolated locations.

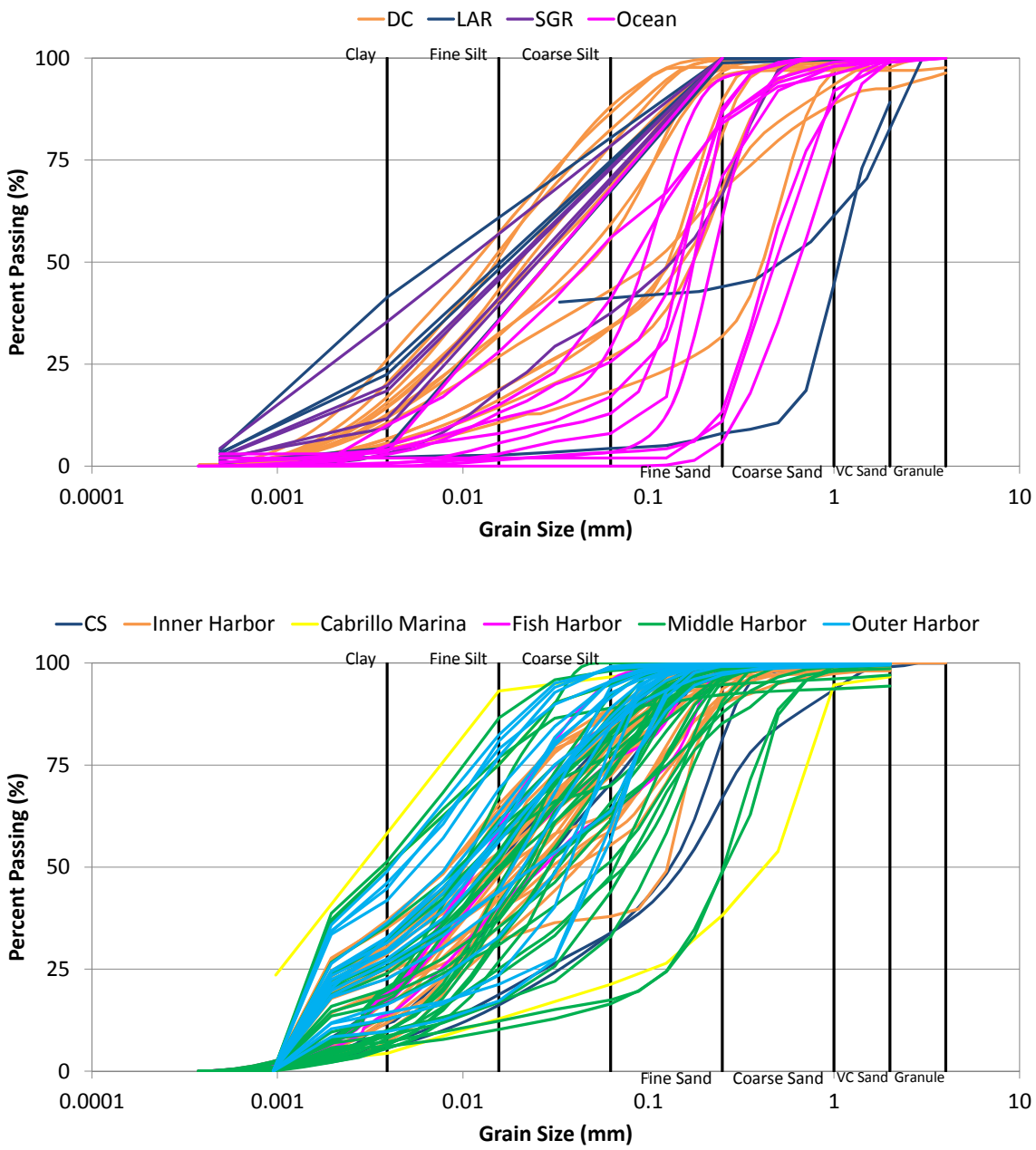

Figure 7.2 Sediment Grain Size Distributions

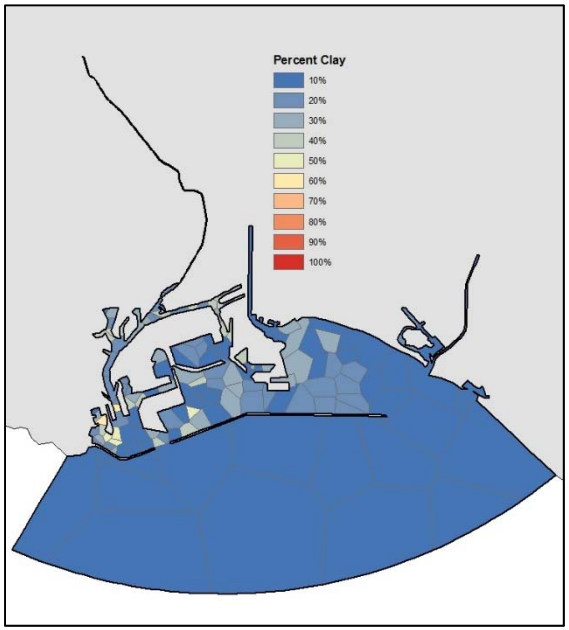

Percent Clay

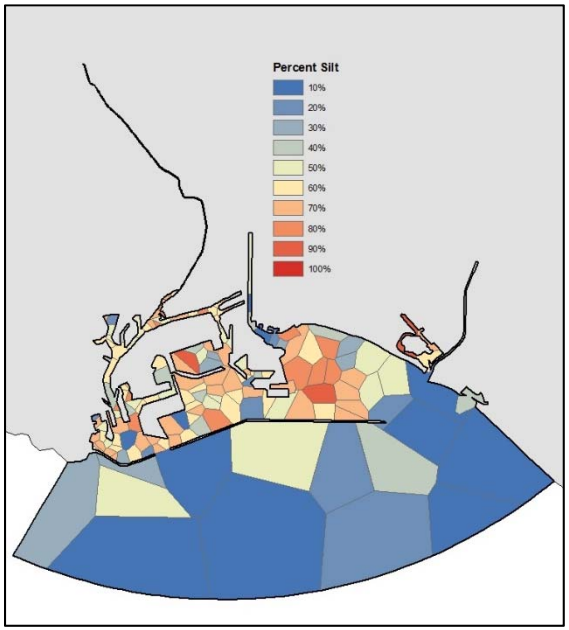

Percent Silt

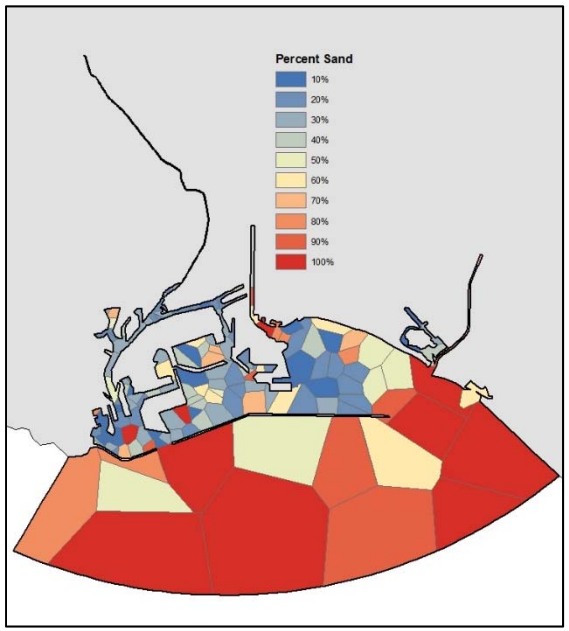

Percent Sand

Figure 7.3 Sediment Bed Composition

Table 7.2 WRAP Model Sediment Parameters

Sediment Type	Diameter (mm)	WRAP Model Sediment Class	Representative Diameter (mm)	Settling Velocity (cm/s)
Gravel	2.0 – 4.0	Coarse Sand	0.5	7.40
Very Coarse Sand	1.0 – 2.0			
Coarse Sand	0.5 – 1.0			
Medium Sand	0.25 – 0.50			
Fine Sand	0.125 – 0.25	Fine Sand	0.125	1.08
Very Fine Sand	0.0625 – 0.125			
Coarse Silt	0.0312 – 0.0625	Coarse Silt	0.0312	0.088
Medium Silt	0.0156 – 0.0312			
Fine Silt	0.0078 – 0.0156	Fine Silt	0.0078	0.0046
Very Fine Silt	0.0039 – 0.0078			
Clay	<0.0039	Clay	0.00242	0.00032

7.1.2 Storm Water

The grain size distribution of suspended sediments from the storm water discharges was measured during the Storm Water Study, as summarized in Table 7.3. These sediment compositions were based on composite samples taken with an automated sampler near the sediment bed. Overall, the sediment composition indicated that storm water sediment is primarily composed of sands and silts with a relatively small percentage of clay. This differs from the assumption used for the Harbor Toxics TMDL, which assumed a composition of primarily silts and clay. In addition, the composite samples also indicated a relatively high percentage of sands, especially for the dry weather event which resulted in 62% sands. Since composite samples are collected near the bottom, it was theorized that the method of sampling used may bias the resulting grain size distribution data. Hence, a supplemental monitoring program was conducted during Wet Event 2 to investigate the grain size distributions from the middle of the water column. The supplemental monitoring was designed to compare particle size distributions between mid-water column grab samples and the flow-weighted composite samples.

Table 7.3 Storm Water Study Composite Sample Sediment Composition

LOCATION	EVENT	SAND (%)	SILT (%)	CLAY (%)
LAR	Dry Event 1	62	36	2
	Wet Event 1	42	55	4
	Wet Event 2	32	63	4
DC	Wet Event 1	26	68	6
	Wet Event 2	36	59	4
Harbor Toxics TMDL*		5	55	40

**Modeling assumption (EPA and RWQCB 2011b)*

During the Wet Event 2 monitoring, supplemental TSS data (grab samples) were collected from two water depths at the LAR and DC monitoring sites. Specialized, proprietary samplers were developed to enable collection of simultaneous grab samples at the mid-water depth and the bottom water depth corresponding to the composite sampling depth (AMEC Foster Wheeler 2015b). Multiple grab samples were collected at each site over the course of the wet weather event, as illustrated in Figure 7.4. At the LAR monitoring site, six grab samples were collected during the peak wet weather flows. Five grab samples were collected following the peak wet weather flows at the DC monitoring site. Particle size distributions from the grab and composite samples are compared in Figure 7.5. In the figure, particle size distributions based on the composite samples are indicated by the red lines. Composite samples for the LAR were taken from one dry and two wet events, while composite samples for the DC were taken during two wet events. The grab sample particle size distributions are shown by the blue and orange lines for the mid-water and near bottom samples, respectively. The grab sample particle size distributions consistently show higher amounts of silts and lower amounts of sand compared to the composite samples, illustrating that the composite samples overestimate the coarser sediment portion of the storm water sediments. Hence, the grab sample particle size distribution data were analyzed to determine the storm water sediment composition since the grab samples provided a better representation of overall storm water characteristics.

The most representative sediment distribution for characterizing storm water discharges was selected by comparing those of mid- and bottom-water depth samples. The sediment compositions of the mid-water and near bottom depth grab samples are summarized in Tables 7.4 and 7.5 for the LAR and DC, respectively. For the LAR, the mid-water and near bottom samples had similar sediment compositions with identical average compositions of sand, silt, and clay fractions. This indicates that sediment compositions are essentially uniform throughout the water column during higher wet weather flows at this location. The DC samples were obtained following the peak wet weather flows, and the near bottom samples indicate a higher percentage of sand compared to the mid-water samples. Both the LAR and DC mid-water samples showed a similar sediment composition, thus the mid-water samples were used to determine the sediment distribution for storm water discharges, as summarized in Table 7.6. The storm water sediment composition was determined based on the average of the LAR and DC mid-water grab samples. All storm water sediment discharges were composed of 3% coarse sand, 14% fine sand, 46% coarse silt, 29% fine silt, and 8% clay.

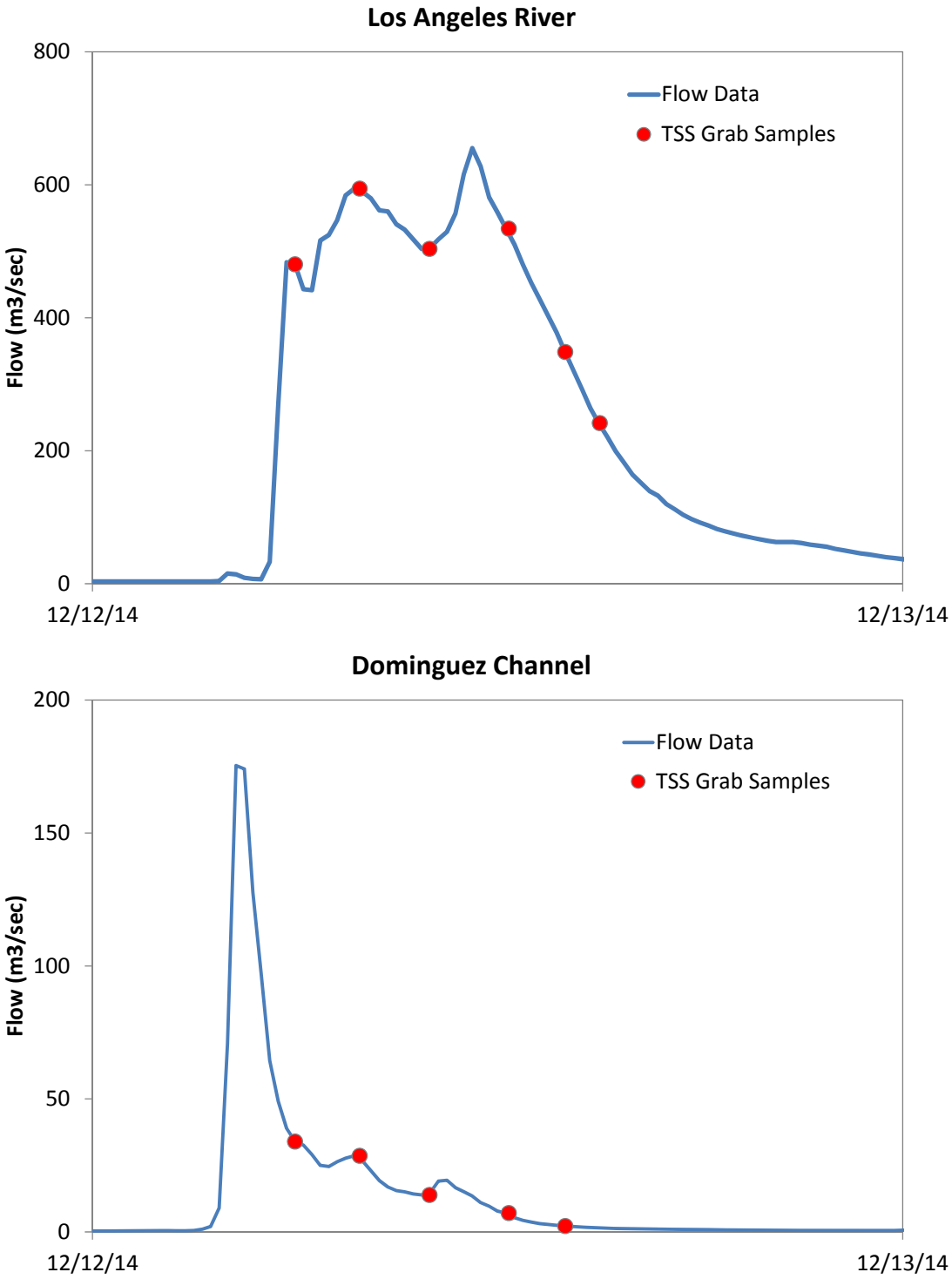

Figure 7.4 Storm Water Study Supplemental TSS Sampling

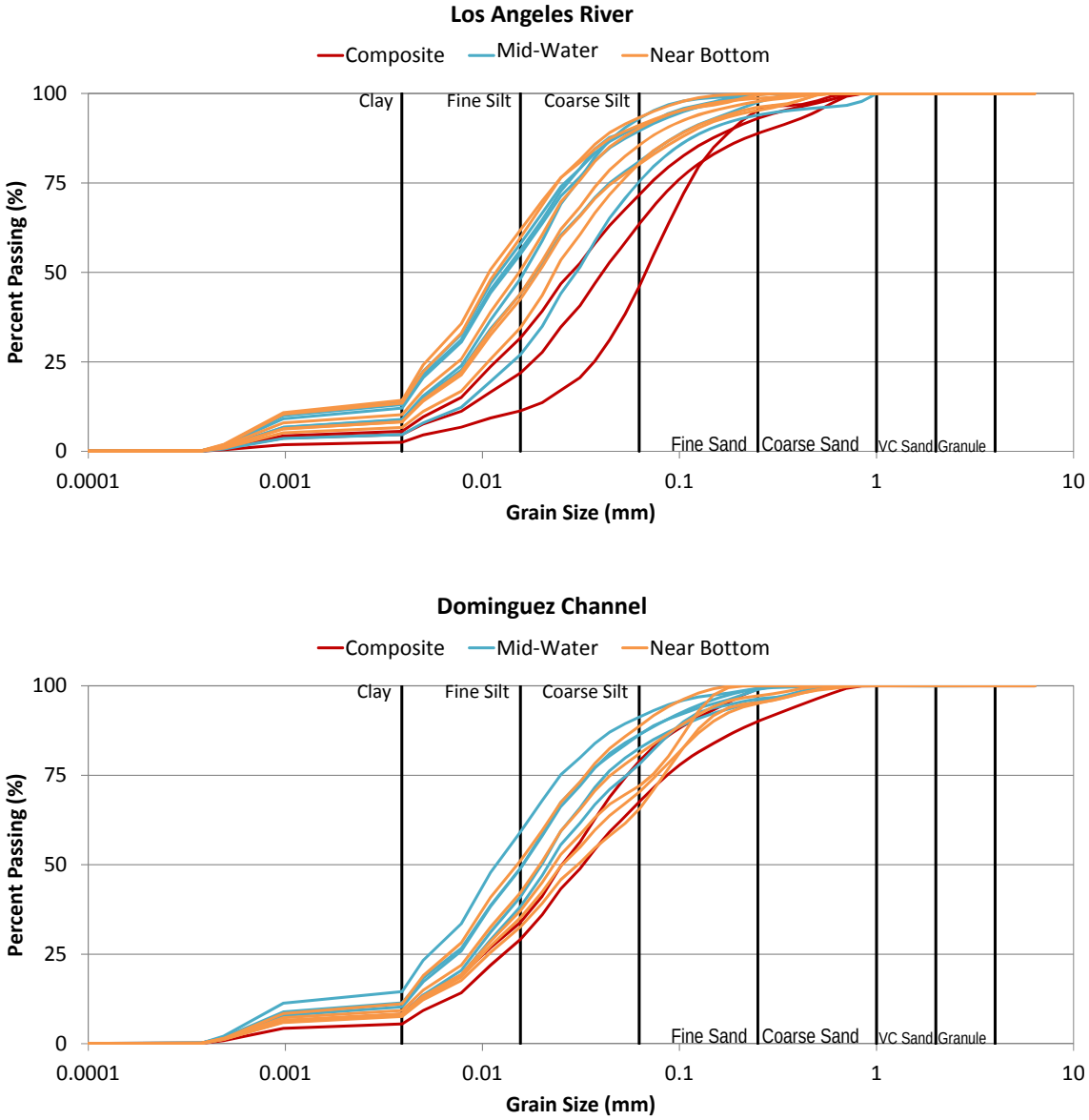

Figure 7.5 Storm Water Particle Size Distributions

Table 7.4 Los Angeles River Grab Sample Sediment Compositions

DEPTH	SAMPLE	SAND (%)	SILT (%)	CLAY (%)
Mid-Water	1	29	67	4
	2	10	84	7
	3	22	72	7
	4	13	78	9
	5	11	79	10
	6	11	78	11
	Average	16	76	8
Near Bottom	1	24	71	5
	2	18	76	6
	3	22	71	6
	4	12	80	8
	5	10	79	11
	6	9	81	10
	Average	16	76	8

Table 7.5 Dominguez Channel Grab Sample Sediment Compositions

DEPTH	SAMPLE	SAND (%)	SILT (%)	CLAY (%)
Mid-Water	1	16	76	8
	2	25	68	6
	3	17	75	9
	4	20	73	6
	5	11	78	11
	Average	18	74	8
Near Bottom	1	33	61	6
	2	38	56	6
	3	30	63	7
	4	22	71	7
	5	14	77	8
	Average	28	66	7

Table 7.6 Storm Water Sediment Composition

SEDIMENT CLASS	LAR*	DC*	STORM WATER
Coarse Sand	2%	3%	3%
Fine Sand	14%	15%	14%
Coarse Silt	46%	46%	46%
Fine Silt	30%	29%	29%
Clay	8%	8%	8%

**Average of mid-water grab samples*

7.2 SEDIMENT TRANSPORT CALIBRATION DATA

The sediment transport validation involved evaluating sediment transport and sediment loading estimates. Sediment transport data used for the WRAP Model calibration are summarized in Table 7.7. Data from a sediment tracer study was used to evaluate sediment transport from the LAR and subsequent deposition in San Pedro Bay. The sediment tracer data offers a unique dataset for model calibration and assessment of sediment properties (e.g., settling velocity). Estimation of sediment loadings is an important component in simulating sediment transport. Bathymetry survey data and dredge records were utilized to estimate sedimentation rates in the CS and LARE. The sedimentation rates were used to evaluate sediment loading estimates from the DC and LAR.

Table 7.7 Sediment Transport Data Summary

DATA TYPE	LOCATION	DESCRIPTION
Sediment Tracer	LARE and San Pedro Bay	USACE sediment tracer study to quantify LAR sediment deposition pattern
Bathymetry Surveys	Consolidated Slip (CS)	Bathymetry surveys taken in portion of CS: 1995, 1998, 2005, 2007, 2010, 2013
Dredge Record	LARE	Dredge records from 1990 – 2001 for federal navigation channel

7.2.1 USACE Sediment Tracer Study

The USACE LAR tracer release study was conducted between January and May 2008 (Everest 2010). The tracer release occurred on January 5, 2008 at the lower end of the LAR at the Anaheim Bridge, as illustrated in Figure 7.6. A total of 300-kg of tracer was mixed with water and then pumped through a discharge line to the release point, located approximately one-third of the way across the bridge. The discharge line was suspended above the river water surface to avoid becoming snagged by floating debris. The tracer release occurred from 6:36 am to 8:00 am. The timing of the tracer release with LAR flow is shown in the lower right panel of the figure. The sediment tracer, which comes in powder form, was designed to mimic sediments from the LAR. Hence, tests were conducted to verify that the tracer properties were similar in terms of particle size, density, and settling velocity. The grain size distribution of the sediment tracer is illustrated in Figure 7.7. The sediment tracer was represented by four sediment classes – fine sand, coarse silt, fine silt, and clay, as summarized in Table 7.8. The fifth sediment class for coarse sand was not simulated since the tracer did not contain coarse sands. The sediment composition of the tracer was similar to the estimated storm water sediment composition.

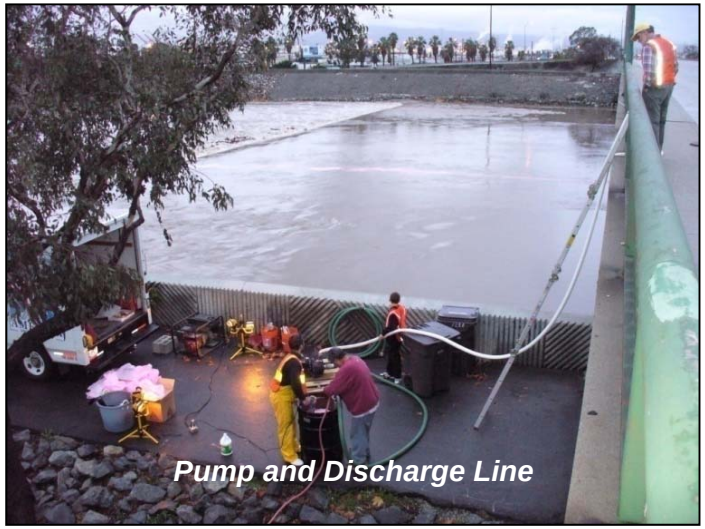

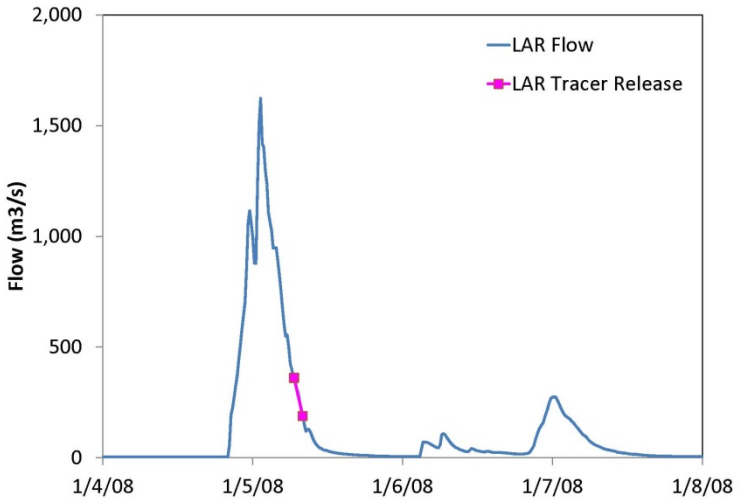

Figure 7.6 Los Angeles River Tracer Release

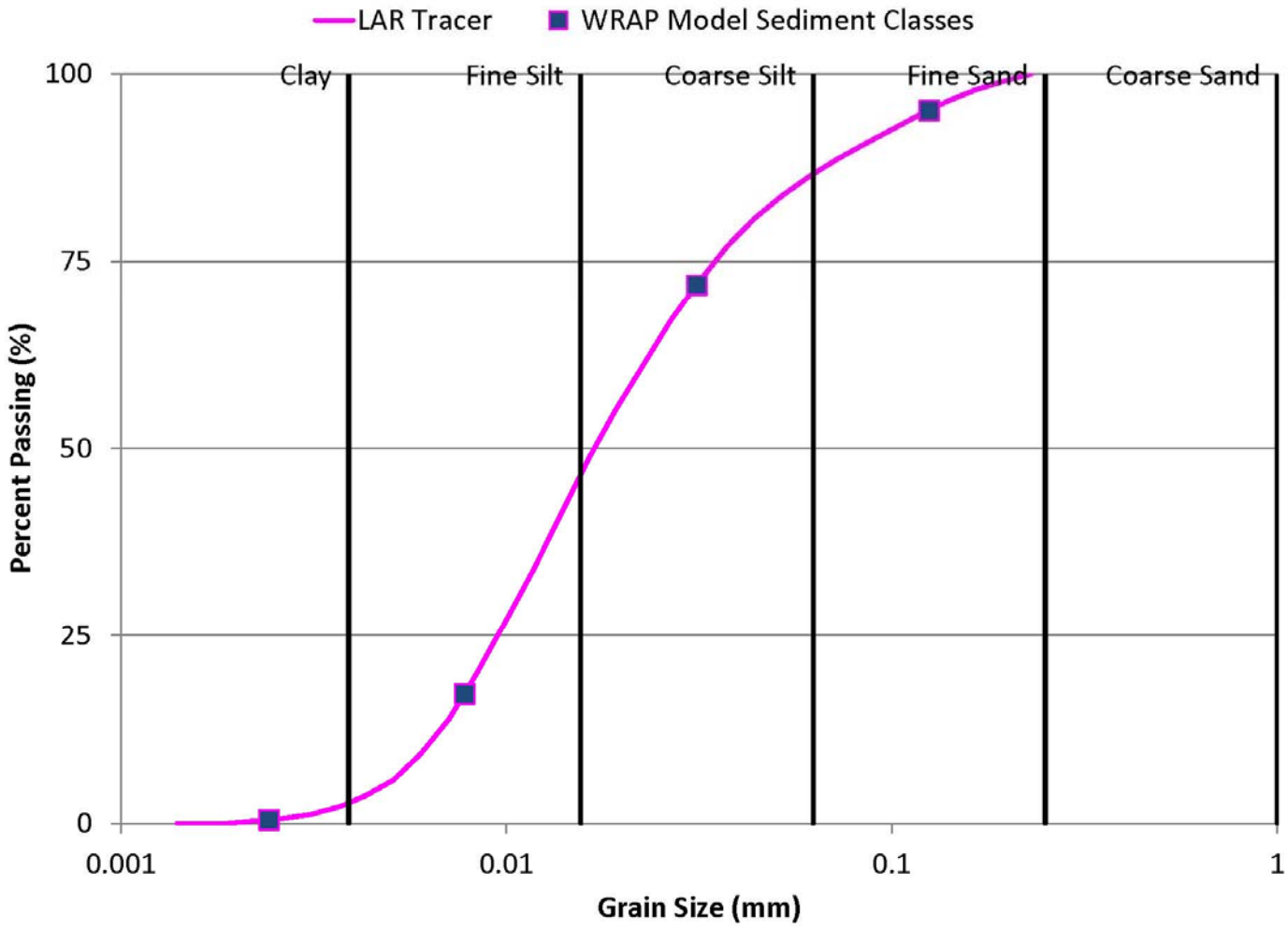

Figure 7.7 Los Angeles River Tracer Sediment Grain Size Distribution

Table 7.8 LAR Tracer Sediment Composition

SEDIMENT CLASS	LAR TRACER	STORM WATER
Coarse Sand	0%	3%
Fine Sand	14%	14%
Coarse Silt	45%	46%
Fine Silt	39%	29%
Clay	2%	8%

Transport of the tracer was tracked by sediment sampling at 65 locations throughout San Pedro Bay, as shown in Figure 7.8. The purpose of the USACE tracer study was to evaluate the transport and deposition of LAR sediments into the North Energy Island Borrow Pit (NEIBP) and the South Energy Island Borrow Pit (SEIBP); hence, the sampling locations were designed to focus on the deposition within the NEIBP and the SEIBP. Fifteen locations were sampled in the NEIBP and three locations in the SEIBP. Seven sampling events (Batch A – G) were conducted over a 5-month period following the tracer release. Two of the sampling events (Batch E and F) were partial sampling events with only 15 samples collected in the NEIBP. Sediment samples were collected using an Ekman grab sampler with an electric winch and davit. Dates of the sampling and rain events are summarized in Table 7.9. The first sampling event (Batch A) was conducted about a week following the tracer release and two rain events. Three moderate rain events occurred between Batch A and B sampling events. Several smaller rain events occurred during the remainder of the sampling period.

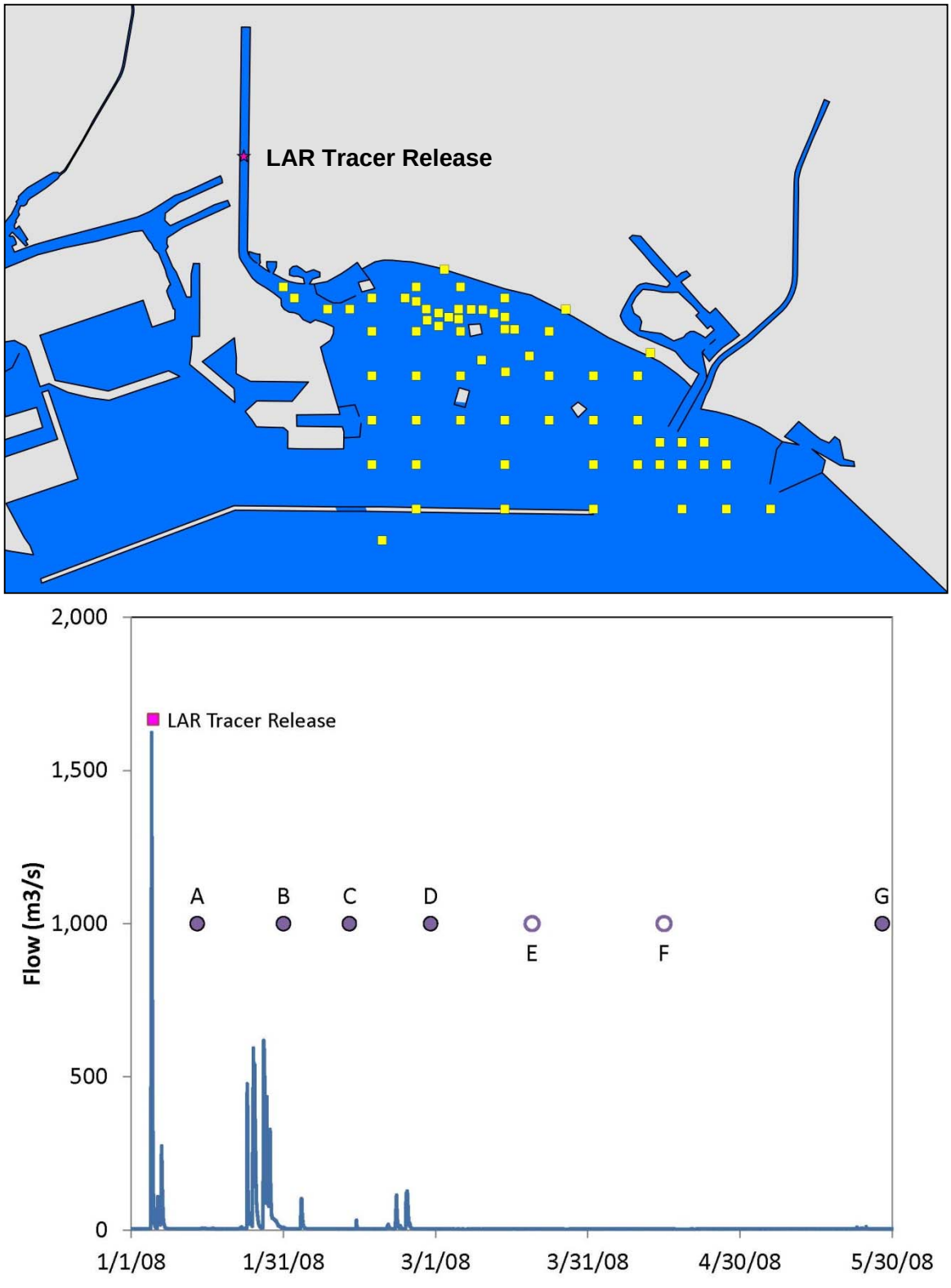

Figure 7.8 Tracer Sampling Locations

Table 7.9 Tracer Sampling and Rain Events

EVENT	DATE	DETAILS
LAR Tracer Release	1/5	LAR peak flow 1,624 m^3/s
Rain Event	1/6	LAR peak flow 109 m^3/s
Rain Event	1/7	LAR peak flow 269 m^3/s
Batch A	1/14 – 1/15	Full sampling event
Rain Event	1/23	LAR peak flow 477 m^3/s
Rain Event	1/25	LAR peak flow 594 m^3/s
Rain Event	1/27 – 1/30	LAR peak flow 619 m^3/s
Batch B	1/31	Full sampling event
Rain Event	2/3	LAR peak flow 103 m^3/s
Batch C	2/13 – 2/14	Full sampling event
Rain Event	2/14	LAR peak flow 32 m^3/s
Rain Event	2/20	LAR peak flow 18 m^3/s
Rain Event	2/22	LAR peak flow 114 m^3/s
Rain Event	2/24	LAR peak flow 128 m^3/s
Batch D	2/29	Full sampling event
Batch E	3/20	Partial sampling event (15)
Batch F	4/15	Partial sampling event (15)
Rain Event	5/23	LAR peak flow 9 m^3/s
Rain Event	5/25	LAR peak flow 11 m^3/s
Batch G	5/28	Full sampling event

The tracer sampling was conducted to quantify the tracer sediment transport from the LAR and subsequent deposition within San Pedro Bay over time. Following each sampling event, the tracer sediment samples were packaged and shipped for specialized testing using fluorescence microscopy to quantify the sediment tracer concentrations within each sample. The tracer sample concentrations were converted to percentages of the total tracer mass that were deposited in different regions of San Pedro Bay. The tracer mass budget provides sediment transport information that can be used for validating the WRAP Model.

The tracer mass budget was determined by extrapolating the sample tracer concentrations to the entire San Pedro Bay sediment bed. Voronoi polygons encompassing each sampling location were constructed as depicted in Figure 7.9, to extrapolate the tracer data. Assuming each sample was representative of the tracer concentration within each polygon, the total mass of tracer deposited within each polygon was calculated. This method of translating point data (i.e., tracer data) to data over a larger area is similar to the method commonly used to convert point rainfall measurements into total rainfall over an area. This method can lead to significant errors, particularly when samples are far apart, though the results between sampling events can be compared to generalize the sediment deposition pattern since the sample locations are consistent for all sampling events.

The sediment deposition pattern was determined for five regions – LARE, NEIBP, SEIBP, SGRE, and San Pedro Bay, as shown previously in Figure 7.9. The percent deposition of the sediment tracer in each region is summarized in Table 7.10. The percent deposition is calculated as the ratio of the mass deposited in each region to the total tracer mass released. Between Batch A and C, about 50% to 60% of the tracer was accounted for within the total sampling area, with 20% to 30% of the tracer being depositing in the LARE. Given the small quantity of tracer and large sampling area, the tracer mass budget resulted in a reasonable estimate of the sediment deposition pattern. The majority of the unaccounted-for tracer amount was likely deposited along the LAR upstream of the sampling area. The sediment deposition within the LARE indicated an initial sediment deposition of 23% following the tracer release at Batch A. Three consecutive large rain events then transported additional tracer into the LARE sampling area resulting in an increase in deposition from 23% to 28% between Batches A and B. Following Batch B, there were smaller rain events and only minor changes in the sediment deposition pattern. The mass budget for Batch D and Batch G resulted in an over-estimation in the tracer deposition and required adjustments in the percent deposition (i.e., the total deposition exceeded 100%). The percent deposition in each region was normalized such that 100% of the tracer was captured in Batch D, which is shown in Table 7.10. It is likely that the sediment deposition estimates from Batch D onward are less reliable. Hence, for the WRAP Model sediment transport calibration, only results from Batch A, B and C were used to evaluate the model.

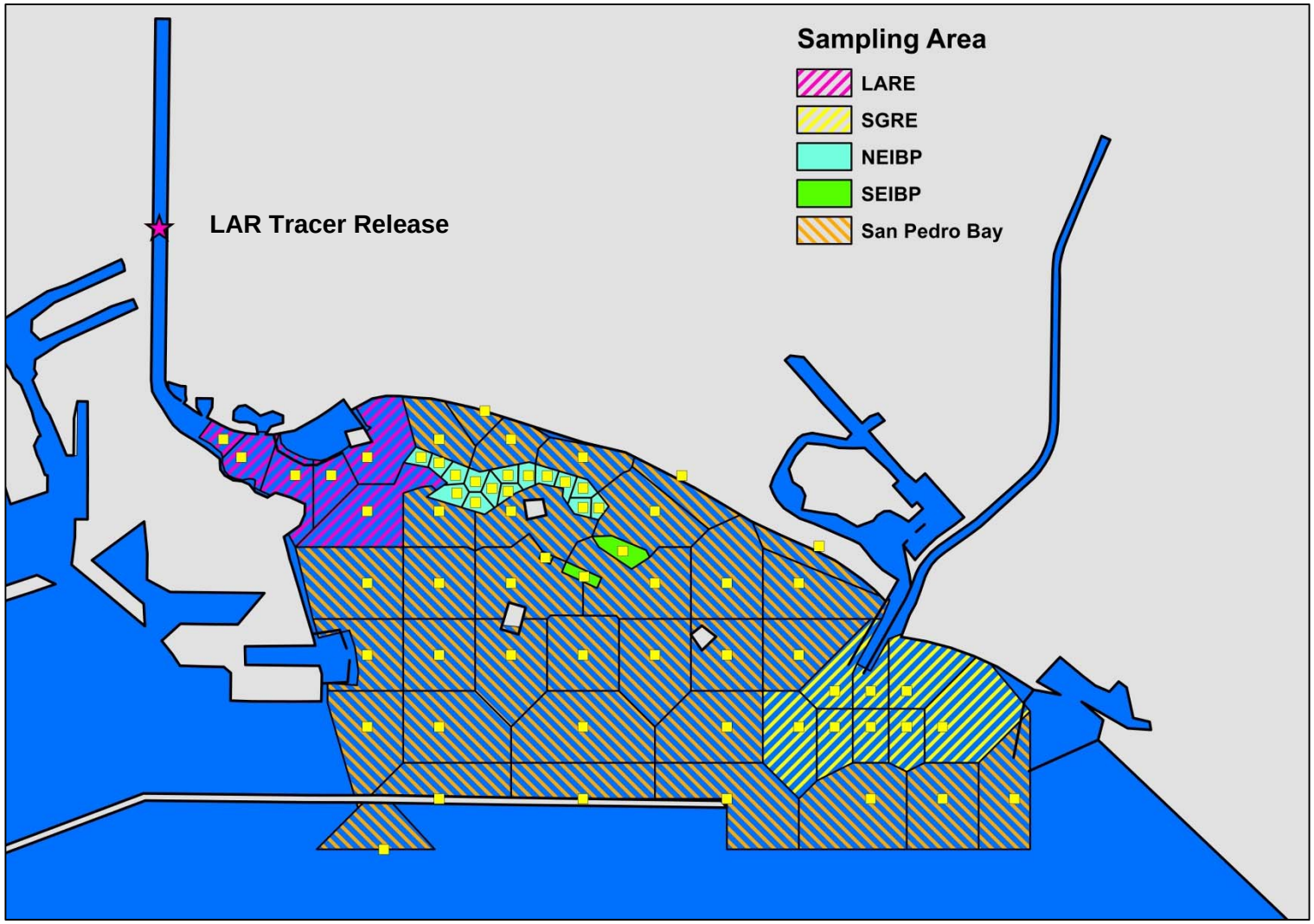

Figure 7.9 Tracer Field Data Analysis

Table 7.10 LAR Sediment Tracer Field Data Analysis

REGION	BATCH A	BATCH B	BATCH C	BATCH D	BATCH E	BATCH F	BATCH G
LARE	23%	28%	21%	33%*	--	--	24%*
NEIBP	3%	2%	4%	3%*	3%	4%	4%*
SEIBP	1%	0%	1%	1%*	--	--	0%*
SGRE	0%	3%	0%	0%*	--	--	0%*
San Pedro Bay	29%	22%	26%	63%*	--	--	37%*
Total Sampling Area	55%	56%	53%	100%*	--	--	66%*

** Mass budget adjusted*

7.2.2 Consolidated Slip Bathymetry Data

The CS is an active small-craft marina with docks along both sides including Leeward Bay Marina at the northern end and Island Yacht Anchorage along the southern edge. Bathymetry data in the CS were analyzed to estimate an average sedimentation rate. The POLA has periodically surveyed portions of the CS in 1995, 1998, 2005, 2007, and 2010. Surveys were based on soundings along 15.24-m (50-ft) spaced transects at 1.524-m (5-ft) intervals along each transect, which were used to estimate bathymetry contours. The most recent survey in the CS was conducted by NOAA in September 2013. This NOAA survey was based on a 2-meter (6.5-ft) grid in the lower portion of the CS. The spatial extent of each survey varied as shown in Figure 7.10. The 1998 survey was the only survey to cover the entire CS. The 1995 survey covered the central area of the CS between the docks. Surveys in 2005 and 2010 were conducted along a portion of the northern edge, whereas the 2007 survey covered the southern edge. The 2013 survey covered most of the CS below Leeward Bay Marina.

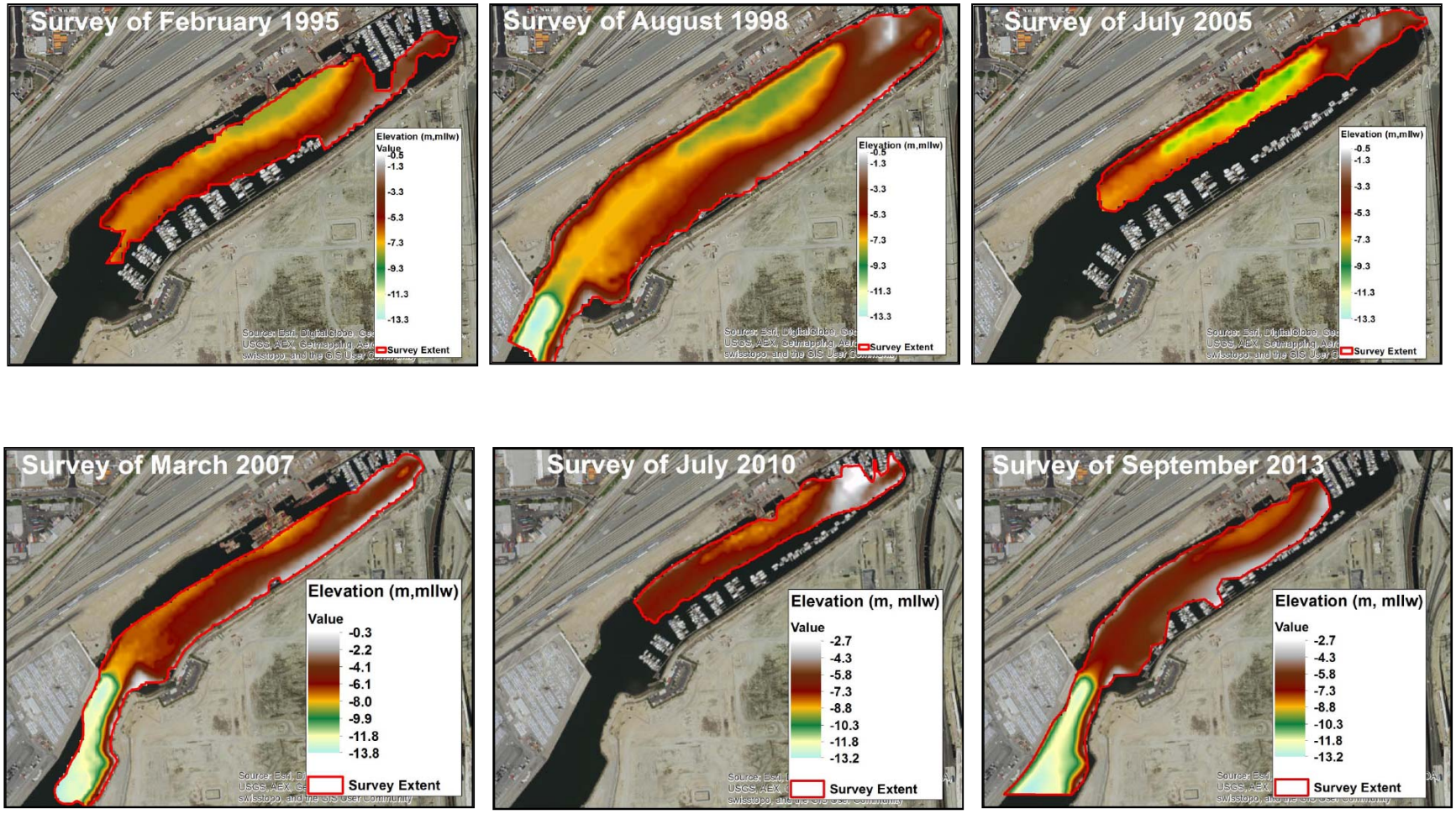

Figure 7.10 Consolidated Slip Bathymetry Data

The varying spatial extents and limited resolution of the data limited the ability to estimate sedimentation rates between surveys. In addition, the CS is an active marina that can result in localized changes in bathymetry due to boat movements or other activities such as trawling. Estimated sedimentation rates between bathymetry surveys ranged widely, from 6 to 73 mm/yr, as shown in Table 7.11. The overlapping areas between surveys are shown in Figure 7.11. Bathymetry data with the greatest overlapping spatial coverage were from between 1995 and 1998 and between 1998 and 2013, with sedimentation rates of 41 and 28 mm/yr, respectively. An average sedimentation rate of 35 mm/yr was determined from these sedimentation rates, which also represent the change from Year 1995 to 2103. An order of magnitude comparison of sedimentation rates was used to validate the sediment loadings used in the WRAP Model.

Table 7.11 Consolidated Slip Bathymetry Data Sedimentation Rates

SURVEY DATES	OVERLAP	ESTIMATED SEDIMENTATION RATE (MM/YR)
1995 – 1998	Center between docks	41*
1998 – 2005	Northern edge	43
2005 – 2010	Northern edge	6
2007 – 2010	Channel enter	73
2010 – 2013	Northern edge	38
1998 – 2013	Below Leeward Bay Marina	28*

** Used to estimate average sedimentation rate*

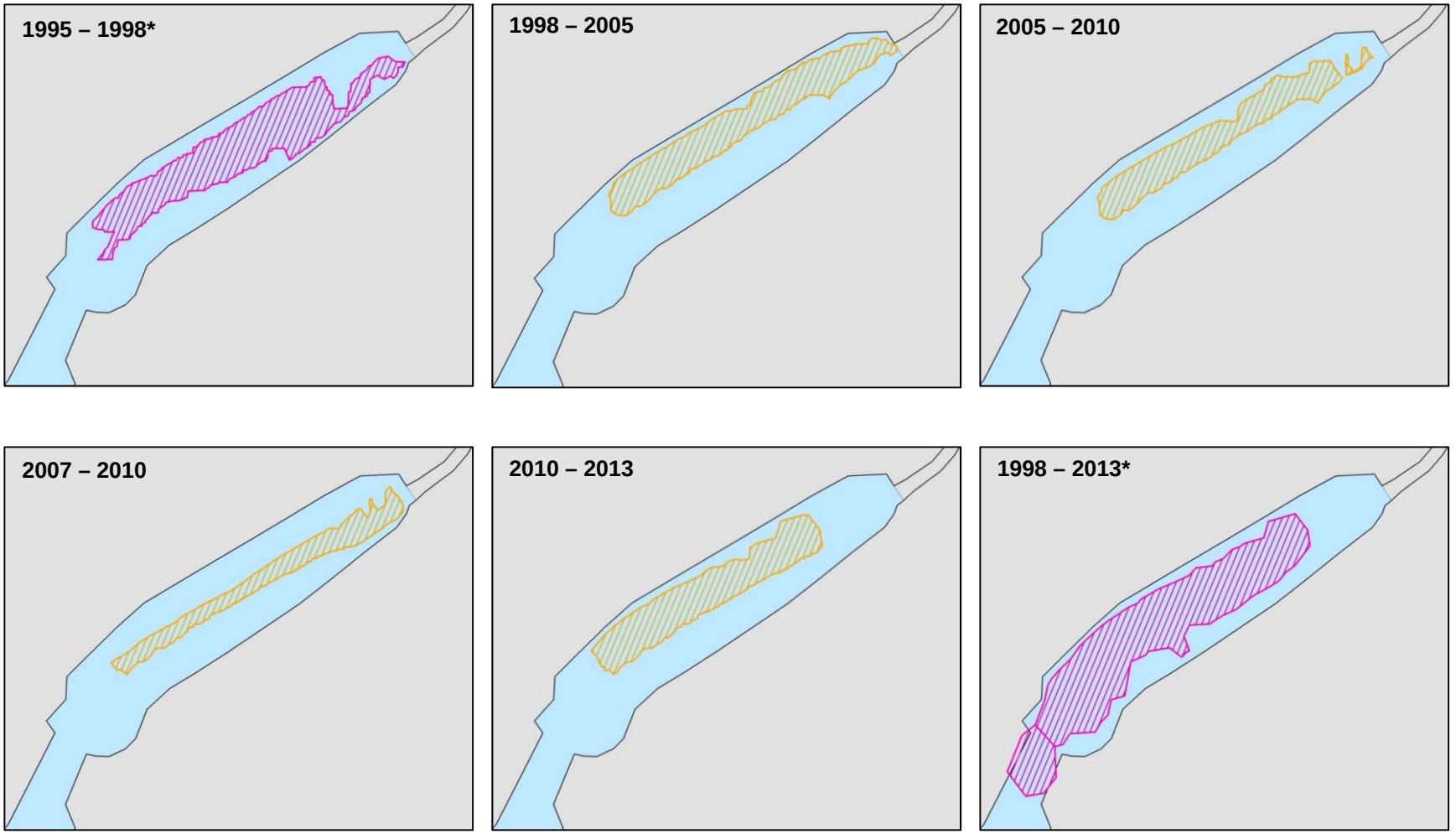

**Used to estimate average sedimentation rate*

Figure 7.11 Consolidated Slip Bathymetry Data Overlap

7.2.3 LAR Estuary Dredge Records

The USACE routinely dredges the federal navigation channel within the LARE due to sediment accumulation that limits navigable access. Historically, shoaling in the LARE has created navigation hazards for recreational and commercial vessels using the waterways and marine facilities within the estuary including Queensway (Catalina) Landing, Golden Shore Boat Ramp, and Rainbow Harbor. Closures of facilities due to excessive shoaling typically occur following significant storm events. USACE conducts maintenance or emergency dredging within the federal navigation channel between Queensway Landing and San Pedro Bay approximately every two to five years.

Dredge records between 1990 and 2001 were assessed to estimate the sedimentation rate in the LARE (USACE 2004). The sedimentation rate was calculated based on the dredge volume divided by the number of years since the previous dredge event. The sedimentation rates based on the dredge records are summarized in Table 7.12. The sedimentation rates ranged from 5.7 to 48.9 million kg/yr, with the highest rate occurring in 1999 following one of the wettest years to occur in the past two decades. The average sedimentation rate based on the dredge record was estimated to be 29.7 million kg/yr, which provides an order of magnitude estimate of the sediment deposition in the LARE.

Table 7.12 Los Angeles River Estuary Sedimentation Rates from Dredge Record

YEAR	ESTIMATED SEDIMENTATION RATE (MILLION KG/YR)
1995	5.7
1997	24.2
1999	48.9
2001	40.0
Average	29.7

7.3 CALIBRATION RESULTS

7.3.1 LAR Sediment Tracer Study

The WRAP Model was used to simulate the LAR sediment tracer release and subsequent deposition in the LARE and San Pedro Bay. The sediment depositions were compared to the measured sediment deposition for Batch A, B, and C, as provided in Table 7.13. The sediment depositions were compared based on the five deposition regions – LARE, NEIBP,

SEIBP, SGRE, and San Pedro Bay. The WRAP Model deposition for Batch A (taken shortly after the release of the tracer) shows a much lower deposition (10% in LARE) than the field data (23% in LARE). However, by the time Batch B was taken, the WRAP Model predicted Batch B depositions in the LARE and San Pedro Bay would increase to levels comparable with the field data. The increase in deposition is attributed to subsequent transport of the initially deposited tracer at the release area to the downstream sampling areas during the time between Batch A and Batch B were taken. The WRAP Model Batch B total tracer deposition was 58% compared to the measured deposition of 56%. Minimal changes were observed for the WRAP Model sediment deposition from Batch B to Batch C. Overall, the WRAP Model sediment tracer deposition compares well with the measured tracer deposition, but differences occur in the short-term transport and deposition (e.g., Batch A). The "time lag" in sediment transport is attributed to the number of sediment classes used for the updated WRAP Model compared to the earlier version of the WRAP model and is discuss below.

Table 7.13 LAR Sediment Tracer Deposition Comparison

REGION	FIELD DATA			WRAP MODEL		
	A	B	C	A	B	C
LARE	23%	28%	21%	10%	39%	39%
NEIBP	3%	2%	4%	1%	2%	1%
SEIBP	1%	0%	1%	0%	0%	0%
SGRE	0%	3%	0%	1%	1%	1%
San Pedro Bay	29%	22%	26%	9%	16%	17%
Total Sampling Area	55%	56%	53%	22%	58%	58%

The updated WRAP Model sediment tracer was simulated with four sediment classes, but for the original USACE LAR tracer study, the same tracer simulation was previously conducted with 10 sediment classes (Everest 2010). A comparison of the tracer sediment classes is provided in Table 7.14, which summarizes the representative diameter and percent composition of each sediment class used to define the tracer.

Table 7.14 Comparison of Tracer Sediment Classes

WRAP Model			USACE LAR Tracer Study		
Sediment Class	Diameter (mm)	Composition	Sediment Class	Diameter (mm)	Composition
Coarse Sand	0.5	0%	Coarse Sand	N/A	0%
Fine Sand	0.125	14%	Fine Sand	0.1234	10%
Coarse Silt	0.0312	45%	Coarse Silt	0.0562	10%
				0.0349	10%
			Medium Silt	0.0253	10%
				0.0191	10%
Fine Silt	0.0078	39%	Fine Silt	0.0151	10%
				0.0121	10%
				0.0095	10%
			Very Fine Silt	0.0073	10%
			Clay	0.0048	10%
Clay	0.00242	2%			

NA – not applicable

To illustrate differences due to the number of sediment classes, comparison of the tracer deposition for the previous LAR tracer study and WRAP Model results is provided in Table 7.15. In the table, the percent deposition is shown for the release and sampling areas. The WRAP Model results indicates that most of the sediment initially deposited upstream of the sampling area (Batch A), as indicated by the deposition in the release area. The modeled deposition in the release area is about twice as much for the WRAP Model compared to the LAR Tracer Study, which is attributed to the differences in the number of sediment classes. Following the initial deposition at Batch A, subsequent flows between Batch A and B eroded and transported sediment from the release area to the LARE and San Pedro Bay. This is indicated by the WRAP Model reduction in deposition within the release area and increase in deposition within the sampling areas for Batch B. As expected, the LAR Tracer Study with 10 sediment classes is initially more accurate compared to the four sediment classes of the WRAP Model (Batch A), but are comparable over time by Batch B. Overall, the WRAP

Model compares well the field data and the number of sediment classes reasonably represents the sediment characteristics.

Table 7.15 LAR Sediment Tracer Deposition Sediment Class Comparison

REGION	LAR TRACER STUDY*			WRAP MODEL**		
	A	B	C	A	B	C
Release Area	34%	19%	19%	59%	16%	16%
LARE	27%	37%	37%	10%	39%	39%
NEIBP	2%	3%	3%	1%	2%	1%
SEIBP	0%	0%	0%	0%	0%	0%
SGRE	1%	1%	1%	1%	1%	1%
San Pedro Bay	12%	14%	14%	9%	16%	17%
Total Sampling Area	43%	55%	56%	22%	58%	58%

**LAR Tracer Study results based on 10 sediment classes (Everest 2010)*
***WRAP Model sediment tracer based on 4 sediment classes*

7.3.2 Consolidated Slip Sedimentation

The WRAP Model was used to simulate sedimentation in the CS between 2002 and 2005. This time frame corresponds to the four-year simulation period used for the Harbor Toxics TMDL development. In addition, the four-year period covered a wide range of hydrologic conditions including large storm events between December 2004 and February 2005. The annual precipitation, DC sediment loading, and WRAP Model sediment deposition rates from 2002 to 2005 are provided in Table 7.16. The sedimentation rates in the CS primarily reflect sediment deposition from the DC. The annual sedimentation rates ranged from 23 to 63 mm/yr. Comparison of annual precipitation and sedimentation rates within the CS show that the highest sedimentation rates do not correspond to the highest precipitation. Rather, during higher precipitation years such as 2005 (i.e., large storm events) sediment is transported out of the CS into the POLA East Basin. In general, the range in the WRAP Model sedimentation rates was consistent with the estimated CS bathymetry data range of between 6 and 73 mm/yr. The WRAP Model average sedimentation rate of 43 mm/yr compares well with the estimated average sediment deposition of 35 mm/yr from the bathymetry data, indicating that the estimated sediment loadings from the DC based on the analytical method described in Section 3.4 are reasonable.

Table 7.16 WRAP Model Consolidated Slip Sedimentation Rates

YEAR	ANNUAL PRECIPITATION (IN/YR)	DC SEDIMENT LOADING (MILLION KG/YR)	SEDIMENTATION RATE (MM/YR)
2002	3.82	2.42	38
2003	9.47	3.55	47
2004	8.68	5.38	63
2005	13.75	6.13	23
Average	8.93	4.37	43

7.3.3 LAR Estuary Sedimentation

The WRAP Model sedimentation in the LARE was evaluated based on the simulated sedimentation rates between 2003 and 2005. The average annual precipitation from 2003 to 2005 corresponds to the long term annual average precipitation of 10.8 in/yr. The annual precipitation, LAR sediment loading, and WRAP Model sedimentation rates are provided in Table 7.17. In general, the WRAP Model sedimentation rates correspond to the annual precipitation and LAR sediment loadings, with the highest sedimentation corresponding to the highest annual precipitation and LAR sediment loading. The WRAP Model annual sedimentation rate in the LARE was approximately 20.1 million kg/yr, which is the same order of magnitude as the estimated annual sediment rate of 29.7 million kg/yr based on the dredge record. The area with the highest sedimentation occurs along the waterway fronting the Golden Shore Boat Ramp, Queensway (Catalina) Landing, and Rainbow Harbor, where shoaling is common issue.

Table 7.17 WRAP Model LAR Estuary Sedimentation Rates

YEAR	ANNUAL PRECIPITATION (IN/YR)	LAR SEDIMENT LOADING (MILLION KG/YR)	SEDIMENTATION RATE (MILLION KG/YR)
2003	9.5	47.6	10.0
2004	8.7	69.7	19.8
2005	13.8	239.9	31.8
Average	10.7	119.1	20.1

Given that two separate time periods were used for the dredge record (1990–2001) and model simulation (2003 – 2005), an attempt was made to normalize the data by correlating the sedimentation rate and precipitation so that the measured data could be compared with the WRAP Model results. The sedimentation rates were plotted against annual precipitation, as shown in Figure 7.11. In Figure 7.12, the red line represents the correlation between sedimentation and precipitation based on the WRAP Model, while the correlation established based on dredged record is shown as the blue line. Since dredging typically occurs following wetter years, the dredge rate was plotted against the annual precipitation of the prior year, which shows a general correlation between annual precipitation and dredge rate. The WRAP Model sedimentation rate shows a similar correlation with annual precipitation as the dredge rate. In general, the WRAP Model sedimentation rate is consistent with the estimated sedimentation based on dredge records and indicates the estimated sediment loadings from the LAR are reasonable.

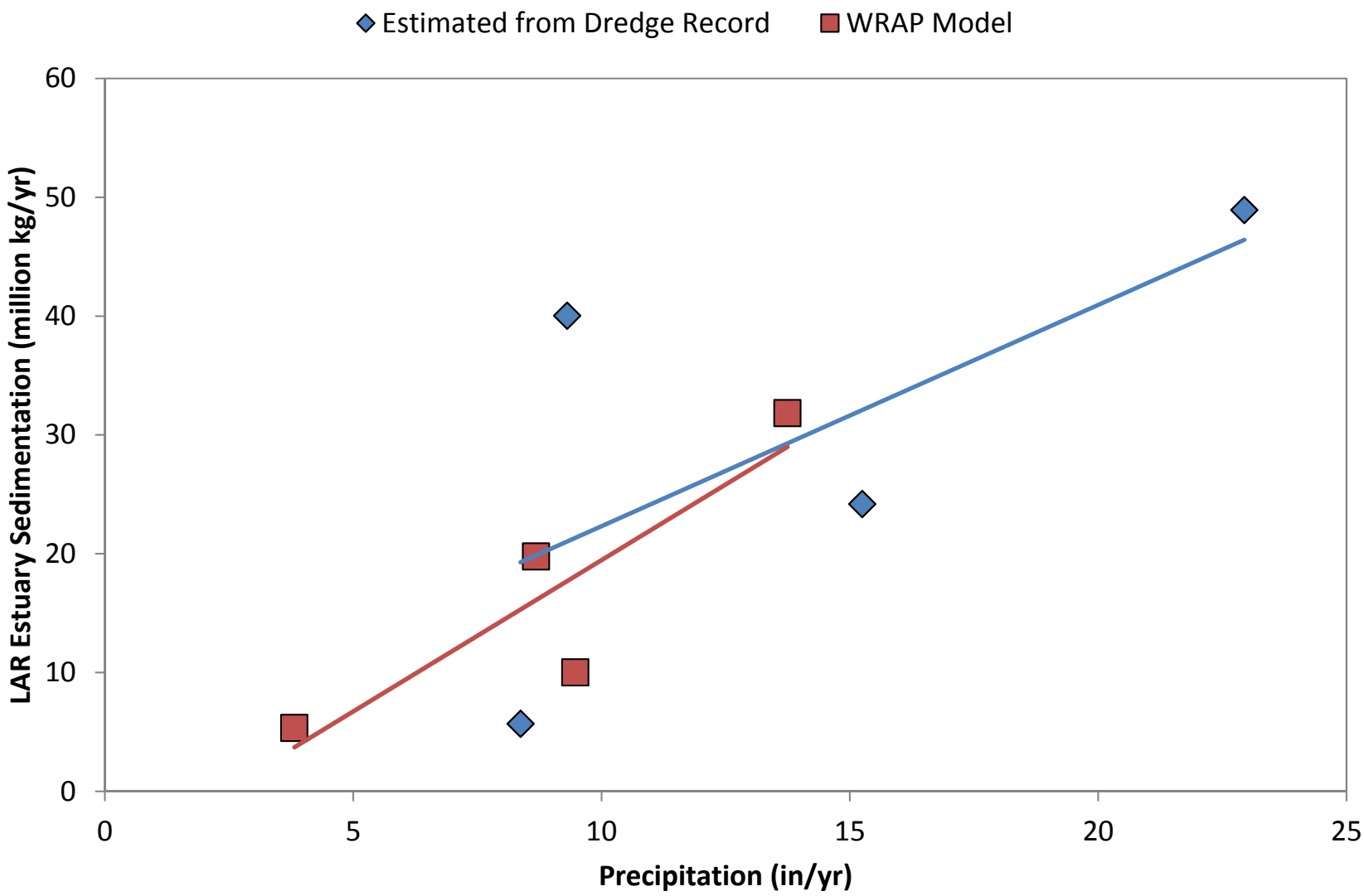

Figure 7.12 Comparisons of Los Angeles River Estuary Sedimentation Rates

8. ORGANIC CHEMICALS

The WRAP Model was developed to provide organic chemical (TPCB and TDDX) water column and sediment bed concentrations for linkage with a bioaccumulation model. Organic chemicals were simulated using three-phase partitioning for freely dissolved, DOC, and particulate phases. As mentioned earlier, the WRAP Model has been previously calibrated and validated for hydrodynamics, mixing and sediment transport, but not for organic transport. Hence, prior to calibrating the WRAP Model for organic transport, a series of quality control tests were conducted to verify that the model would be able to simulate the fundamental processes for organic transport. The quality control tests focused on assessing the sediment-water exchange of organics and the conservation of mass of organics in the water column and sediment bed. Details for these quality control tests are provided in Appendix D.

8.1 CONCEPTUAL SITE MODEL

A CSM for TPCB and TDDX within waters of greater LA/LB Harbor was initially developed to prioritize special studies for data collection and to guide modeling efforts (Anchor QEA 2014a). This conceptual framework was utilized for understanding and quantifying contaminant sources and sinks to harbor waters and provides an overall assessment of processes that control the transport of contaminants. The CSM evaluated the following processes that can affect contaminant transport:

- Wet and dry atmospheric deposition
- Gas exchange (volatilization)
- Watershed loadings
- Tidal exchange between the harbor and ocean
- Settling onto the sediment
- Sediment-water diffusion
- Groundwater advection
- Degradation within the water column

The CSM was used to identify the dominant sources and sinks contributing to TPCB and TDDX concentrations in the harbor. Wet and dry deposition, groundwater advection, and degradation within the water column were determined to be negligible and were not considered in the chemical fate modeling. Gas exchange was classified as a moderate sink, thus volatilization was incorporated into the WRAP Model as previously discussed in Section 2.2. Three dominant processes were identified from the CSM – watershed loadings, sediment-water diffusion, and tidal exchange. Watershed loadings were assessed as a

potentially moderate source and sediment-water diffusion as a significant source. Tidal exchange was determined to be a significant sink. The WRAP Model was developed to simulate the primary organic chemical processes identified in the CSM: volatilization, watershed loadings, tidal exchange, settling onto the sediment, and sediment-water diffusion. In addition, water column concentrations were identified as an influential component affecting all three processes. Thus, the WRAP Model organic chemical calibration focused on the calibration of water column concentrations and on accurately quantifying sediment bed concentrations and watershed loadings.

8.2 MODEL SETUP

8.2.1 Initial Sediment Bed

Organic chemical sediment data were evaluated and used to characterize current organic chemical concentrations in the sediment bed. A comprehensive sediment, fish tissue, and mussel tissue dataset was compiled to support the calibration of the WRAP Model and bioaccumulation model (Anchor QEA 2013a and 2014b). Sediment physical (e.g., grain size) and chemical (e.g., TPCB and TDDX) data compiled were from the LA/LB Harbor, Eastern San Pedro Bay, DC, or nearshore areas of the Bight taken between 1980 and 2012. The sediment database has since been augmented by more recent sediment data collected in 2013 and 2014. Specifically, the Bight 2013 Monitoring Program (AMEC Foster Wheeler 2015a) and two special studies conducted in 2014 by the Ports (Environ 2015a and 2015b). The sediment database was refined to ensure that data are sufficient to characterize current sediment conditions and that laboratory analytical methodologies allow for comparison between studies (Anchor QEA 2014b). Some of the sediment data were excluded for the following reasons:

- Sediment data collected prior to 2002 were excluded since the older samples may not be representative of current conditions, and because historical programs used different analytical methods, which are laboratory and method specific.
- PCB data analyzed with less than 40 congeners were excluded since data with fewer congeners may not be comparable to more recent measurements with 40 – 56 congeners. In general, data collected prior to 2003 were based on 25 or fewer congeners.
- Sediment samples from depths greater than 16 cm were excluded because the greater depths do not closely represent the bioactive surface layer (approximately 10 cm).
- Sediment data taken from areas that have been dredged were excluded since data are not representative of current conditions.
- Sediment data from former water areas were excluded. These data include such areas that have since been filled.

- Sediment data taken outside the geographic limits of the WRAP Model domain were excluded.

Organic chemical concentrations in the WRAP Model sediment bed were established using the sediment exposure concentrations developed for the bioaccumulation model (Anchor QEA 2016) to maintain consistency between models and ultimately the Linked Model. Sediment organic chemical concentrations were defined based on the sediment chemistry. Sediment bed TPCB and TDDX concentrations were specified based on sediment data between 2002 and 2014, as listed in Table 8.1. The selected sediment chemistry data by study are shown in Figure 8.1. The organic chemical concentrations were specified using Theissen polygons of the sediment chemistry data. The initial sediment bed TPCB and TDDX concentrations in the WRAP Model are shown in Figures 8.2 and 8.3, respectively.

Due to the large spatial extent of the LA/LB Harbor and San Pedro Bay, data from multiple studies conducted in different years were required to provide sufficient spatial coverage to define sediment organic chemical concentrations. Hence, the spatial distribution and collection date of data varied for each TMDL receiving waterbody. Sediment organic chemical concentrations along the DC were based on data collected in 2002, 2003 and 2011. In the CS, sediment chemistry data from 2002, 2003, 2008, 2011, 2012, 2013, and 2014 were used. For the 2002 data in the DC and CS, TPCB data were based on aroclors rather than congeners. Sediment organic chemical concentrations in FH were based on data collected in 2003, 2008, 2012, 2013, and 2014. In the southern portion of FH, multiple data sets were located within a model grid cell, in which case the average concentration was used. In Cabrillo Marina, sediment organic chemical concentrations were specified based on data taken in 2003, 2008, and 2013. Data from 2008, 2013, and 2014 were used for Inner Cabrillo Beach. In the LARE, data from 2003 and 2008 were used to define sediment organic chemical concentrations along the river channel. Organic chemical concentrations in the lower estuary were extrapolated (based on Thiessen polygons) from 2014 data taken adjacent to the estuary in San Pedro Bay.

In Alamitos Bay, the sediment concentration was specified based on the average concentration of the Bight 2003 data located inside Alamitos Bay. In the ocean outside of the breakwater, higher sediment concentrations were located to the west of Angeles Gate. Two polygons were created for the ocean outside of the breakwater. The sediment concentrations were specified based on the average of the data within each polygon.

Table 8.1 Summary of Sediment Organic Chemical Data

YEAR	STUDY	# OF DATA	REFERENCE
2014	Geochronology Core Study	10	Environ 2015a
2014	Surface Sediment Characterization and Polychaete Tissue Collection Program	33	Environ 2015b
2013	Bight 2013	28	AMEC Foster Wheeler 2015a
2012	POLA Fish Harbor	9	Anchor QEA 2012
2012	San Gabriel River Regional Monitoring Program	4	ABC 2014
2012	POLA SQO Phase II	12	Weston 2013
2011	POLA Dominguez Channel/ Consolidated Slip Erosion Study	19	AMEC 2011
2010	IR Site 7 Sediment Remediation	2	Anchor QEA 2011
2010	PV Shelf	3	LACSD 2013
2008	Bight 2008	39	SCCWRP 2012
2008	POLA Biobaseline 2008	26	SAIC 2010
2008	POLA WRAP	28	Weston 2008
2005	Environmental Monitoring and Assessment Program	3	EMAP 2008
2003	Bight 2003	41	SCCWRP 2007
2002	Consolidated Slip Restoration Project	39	AMEC 2003

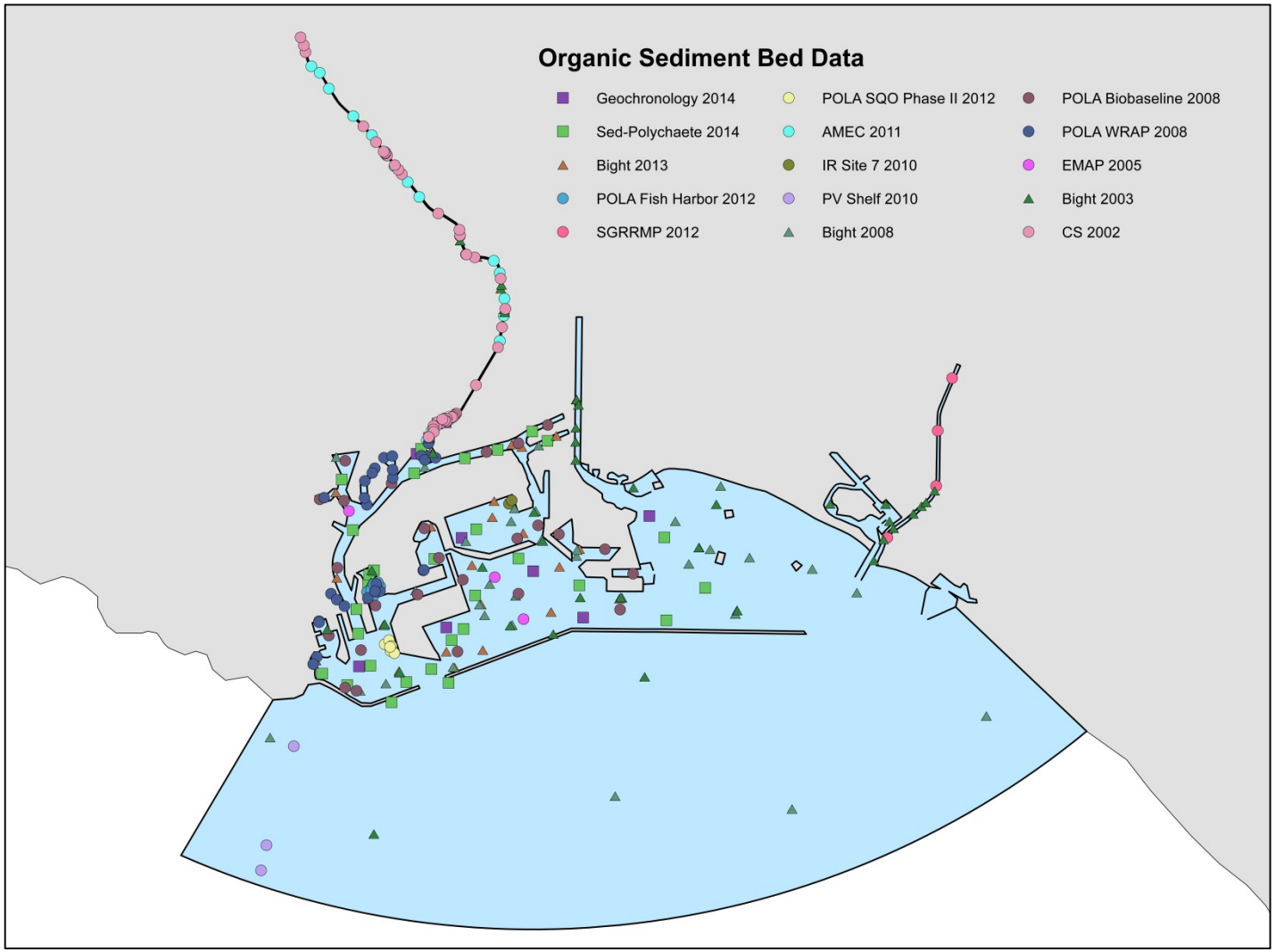

Figure 8.1 Sediment Chemistry Data Locations

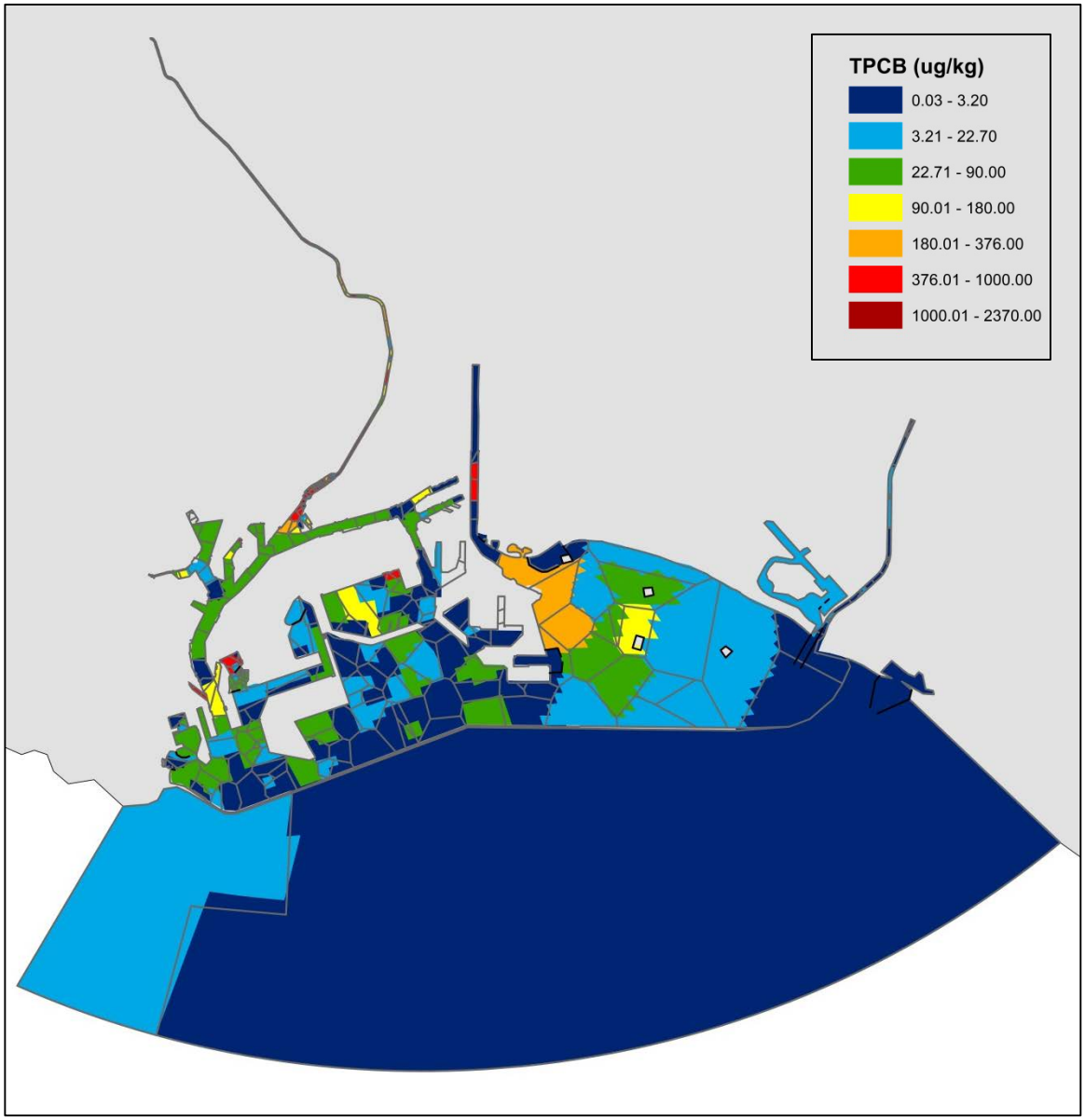

Figure 8.2 Sediment Bed Initial TPCB Concentrations

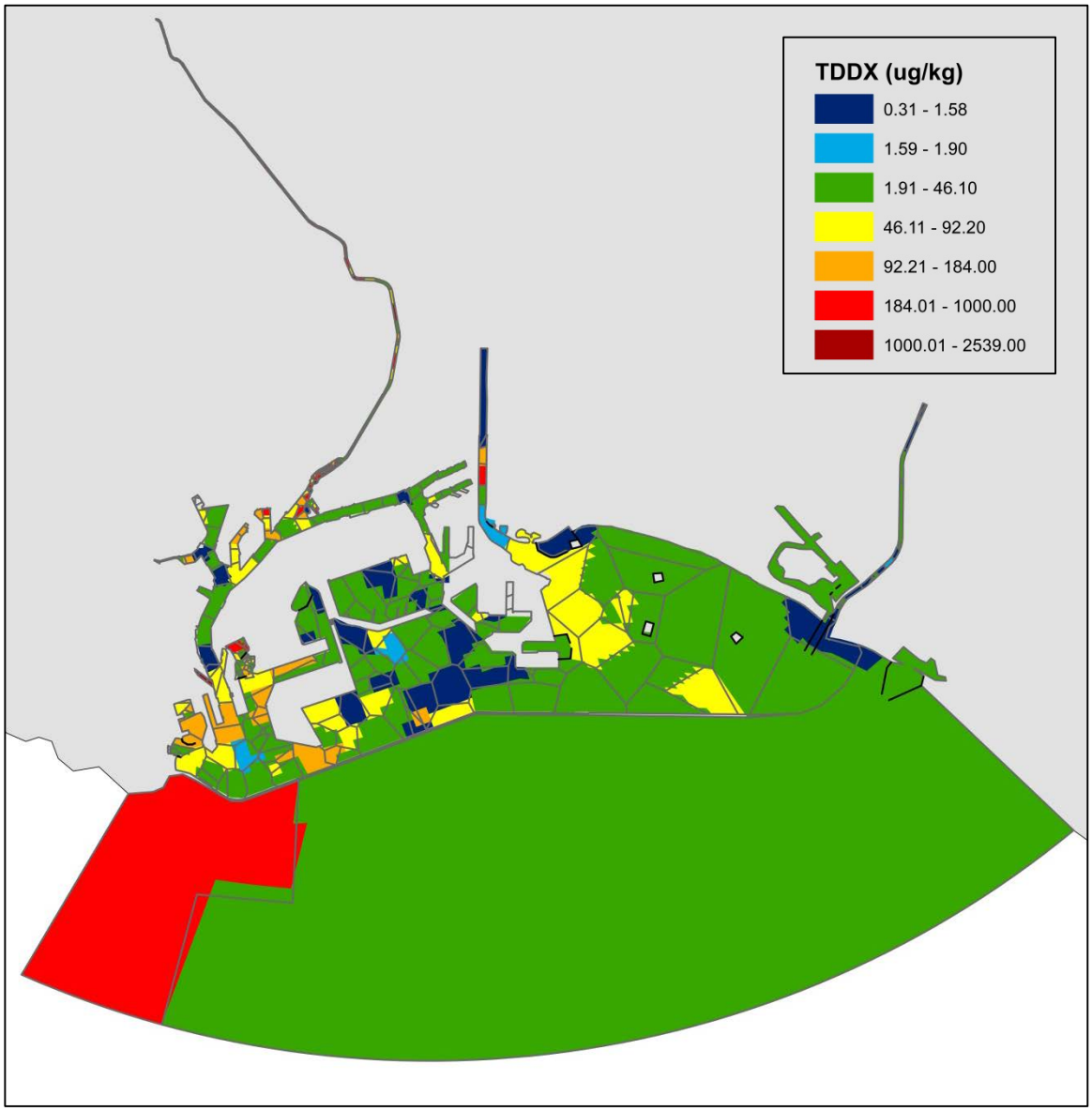

Figure 8.3 Sediment Bed Initial TDDX Concentrations

8.2.2 Watershed Loadings

Watershed loadings were estimated based on analytical methods previously discussed in Section 3.5. Storm water organic chemical concentrations were estimated based on correlations with sediment concentrations. Separate correlations were developed for the LAR, CC, DC (at Vermont), Machado Lake, port land uses, and Torrance Lateral. The WRAP Model organics calibration period was from January 2014 through June 2015, which was preceded by a two-year spin-up period. The watershed loadings during the calibration period are summarized in Table 8.2. The organic chemical watershed loadings during the calibration period were less than the average annual loading of 20.12 and 14.33 kg/yr for TPCB and TDDX, respectively. This reflects the lower than normal precipitation observed in southern California over the last four years.

Table 8.2 Organic Chemical Watershed Loadings

YEAR	TPCB (KG/YR)	TDDX (KG/YR)
2012	13.08	9.24
2013	6.69	4.50
2014	12.63	8.88
2015*	2.85	4.00

**Partial year from January through June 2015*

8.3 ORGANIC CALIBRATION DATA

Previous water quality studies within the harbor have demonstrated TPCB and TDDX concentrations typically below detection limits, and thus insufficient for model calibration. In order to provide sufficient data for the WRAP Model calibration, the LDL Study was conducted by the POLA and POLB to measure organic chemical concentrations throughout the harbor (Environ 2015c). The LDL Study was conducted in three phases, as summarized in Table 8.3. Phase 1 of the LDL Study consisted of sampling at five locations to evaluate data collection and laboratory methods needed to achieve sufficient detection limits. Three sampling methods were evaluated: grab samples, high volume samples, and solid-phase microextraction (SPME). Based on Phase 1 results, the SPME sampling method was selected for additional sampling throughout the harbor, since the SPME enabled the most detections compared to the other methods. For Phases 2 and 3, SPME measurements were made at nine locations along with TSS, DOC, and particulate organic carbon (POC) during instrument deployment and retrieval.

Table 8.3 LDL Study Sampling Summary

LDL STUDY	DURATION	SAMPLING DESCRIPTION
Phase 1	2/19/14 – 3/27/14	Grab samples at five locations High volume sampling at five locations SPME deployed at four locations* TSS and POC during retrieval
Phase 2	12/9/14 – 1/8/15	SPME deployed at nine locations TSS, DOC, and POC during deployment and retrieval
Phase 3	5/15/15 – 6/16/15	SPME deployed at nine locations TSS, DOC, and POC during deployment and retrieval

** SPME instrument at REF-01 loss during deployment*
SPME – Solid-phase microextraction
TSS – Total suspended solids
POC – Particulate organic carbon
DOC – Dissolved organic carbon

The LAR flow during the LDL Study is provided in Figure 8.4 to illustrate hydrologic conditions during the sampling phases. In the figure, the LAR flow data is indicated by the blue line. The other colored lines show the average LAR flow and duration of each phase. During Phase 1, a large rain event over a three-day period occurred about a week after the instruments were deployed, as indicated by the orange line. The Phase 2 sampling was preceded by two rain events about one week prior. Two additional large rain events occurred a few days after the start of Phase 2 (magenta line). During Phase 3, two smaller rain events occurred at the beginning of the sampling period, as shown by the green line.

LDL Study sampling locations are shown in Figure 8.5 and coordinates provided in Table 8.4. The Phase 1 mid-water sampling occurred at the CS, LARE, POLB outer harbor, and eastern San Pedro Bay. The reference site was located outside of the breakwater between Angels and Queens Gate. A SPME instrument was also deployed during Phase 1 at the reference site, but was lost during deployment. For Phases 2 and 3, SPME measurements were made at all nine locations at mid-water depths. Additional bottom-water samples were taken at three of the following locations: CS, POLB inner harbor, and POLB outer harbor.

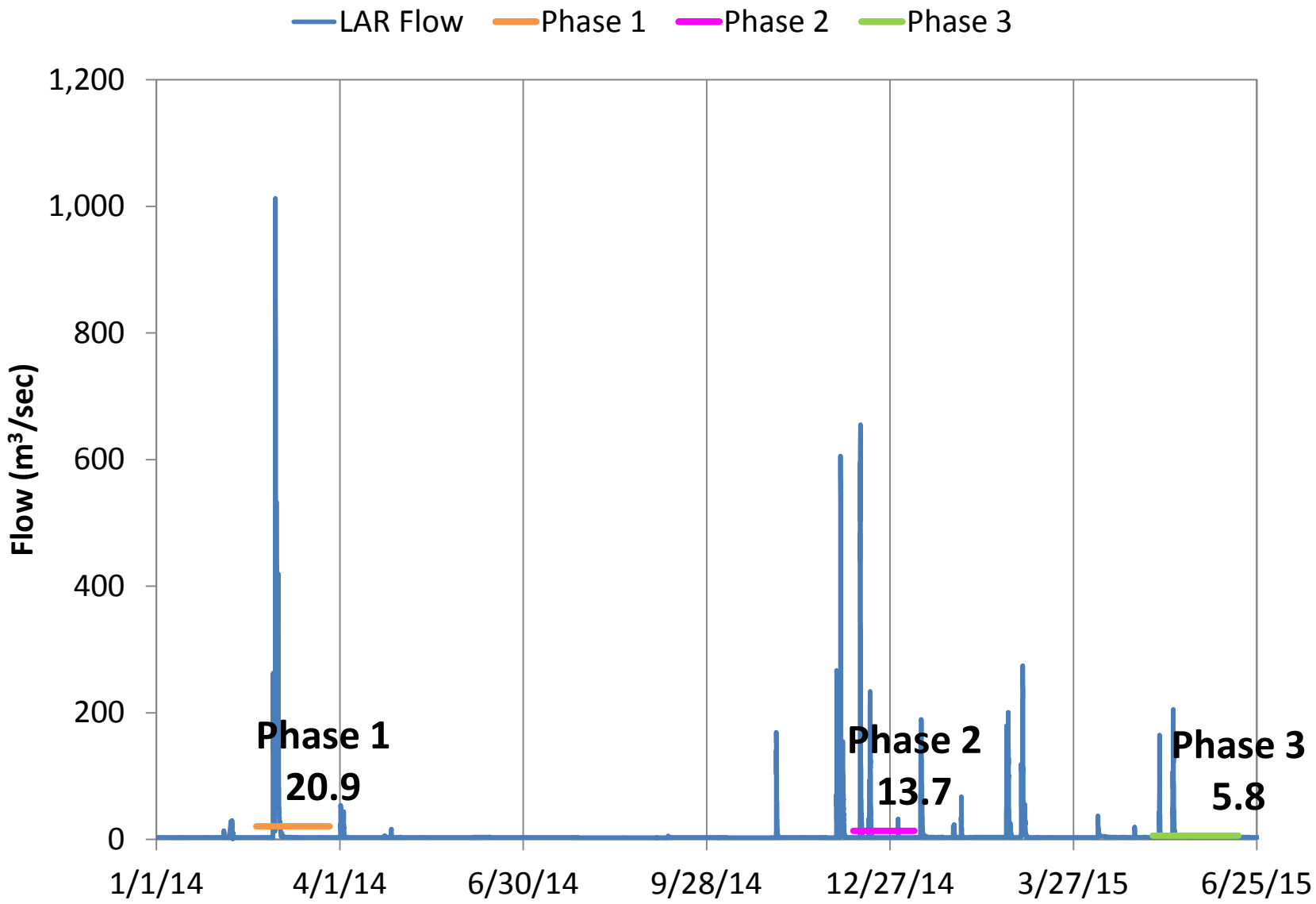

Figure 8.4 LAR Flow during the LDL Study

Figure 8.5 Low Detection Limit Special Study Sampling Locations

Table 8.4 LDL Study Sampling Locations

LOCATION	SAMPLE ID	LATITUDE	LONGITUDE
Cabrillo Pier (CP)	CP-01	33° 42.310' N	118° 16.258' W
Consolidated Slip (CS)	CS-01	33° 46.335' N	118° 14.976' W
Fish Harbor (FH)	FH-01	33° 44.165' N	118° 16.161' W
POLA Inner Harbor	IA-01	33° 45.390' N	118° 15.831' W
POLB Inner Harbor	IB-01	33° 46.301' N	118° 13.191' W
LARE	LARE-01	33° 45.378' N	118° 11.788' W
POLB Outer Harbor	OB-01	33° 43.865' N	118° 14.114' W
Reference Site	REF-01	33° 43.085' N	118° 12.426' W
San Pedro Bay	SP-01	33° 44.213' N	118° 8.090' W

Maps of the SPME results are provided in Figures 8.6 and 8.7 for TPCB and TDDX, respectively. In the figures, the freely dissolved concentration measurements are shown at each location. For locations with two sampling depths, the mid-water sample results are provided above the bottom-water sample results. In general, the SPME TPCB concentrations are highest in the inner harbor locations, and decrease closer to the ocean, with the lowest concentrations measured at the reference site. SPME TDDX concentrations were more consistent at all locations compared to TPCB. Overall, TPCB and TDDX concentrations were similar for all three sampling phases. In addition, mid- and bottom-water concentrations did not indicate significant vertical gradients in the water column.

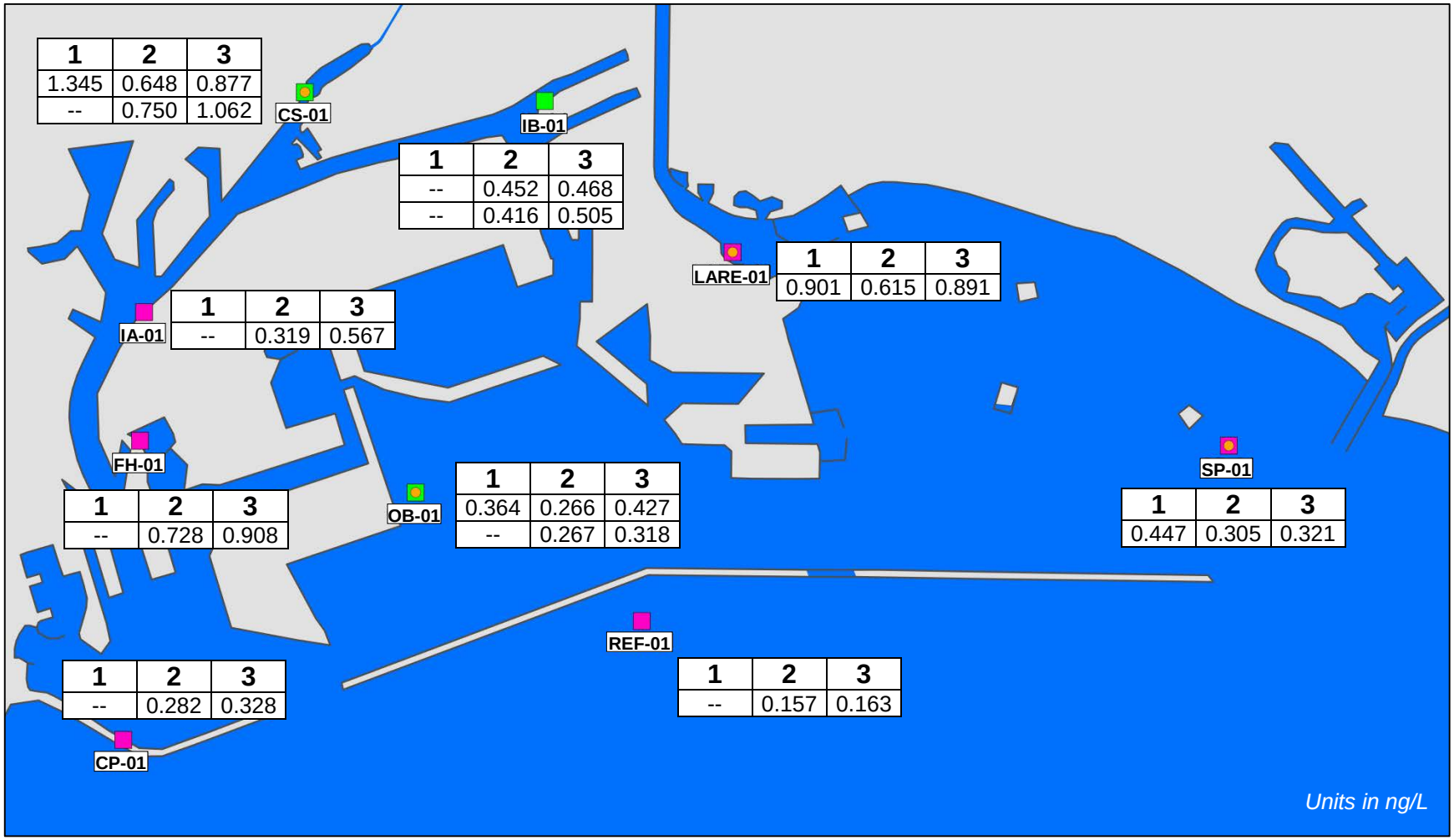

Figure 8.6 Low Detection Limit Special Study SPME TPCB

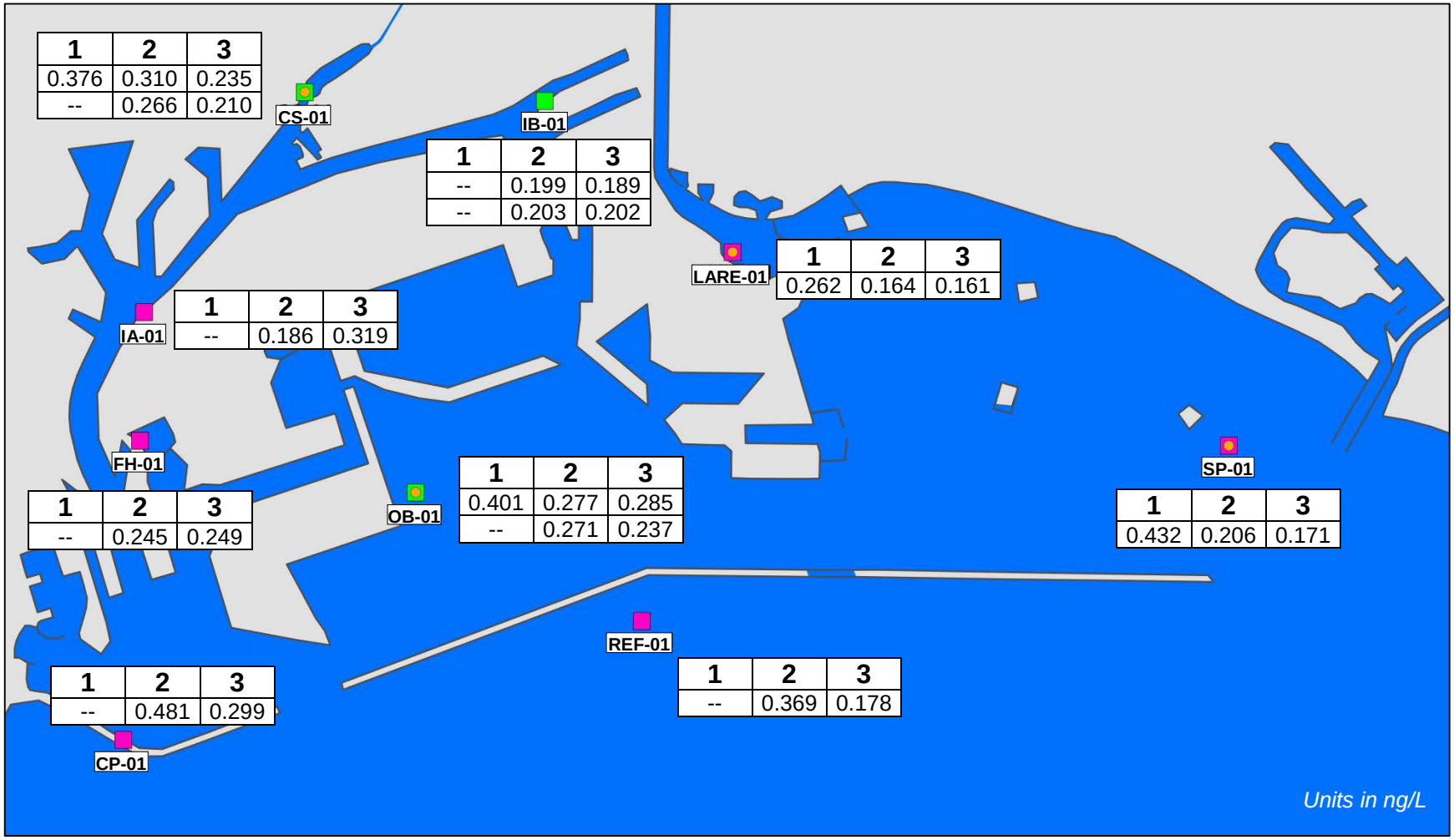

Figure 8.7 Low Detection Limit Special Study SPME TDDX

8.4 MODEL INPUT PARAMETERS

Organic chemicals (TPCB and TDDX) were simulated using a three-phase partitioning for freely dissolved, DOC-complexed, and particulate phases. EFDC uses a generalization of Chapra's (1997) formulation for sorption to DOC and POC. The linear equilibrium partitioning requires the three phases to sum to unity, as shown by Equation 8.1. The partitioning among the phases is controlled by the organic carbon partition coefficients, K_{poc} and K_{doc}, as defined by Equations 8.2 and 8.3, respectively. The fractions for the freely dissolved, DOC-complexed, and particulate phases are summarized by Equations 8.4, 8.5, and 8.6, respectively. Partitioning between the freely dissolved and DOC-complexed phases is dependent on the DOC partition coefficient (K_{doc}) and DOC concentration. The portion of chemical associated with the particulate phase is controlled by the particulate organic carbon partition coefficient (K_{poc}) and fraction of organic carbon of the suspended sediment.

$$f_d + f_{doc} + f_p = 1 \tag{8.1}$$

$$K_{poc} = \frac{C_p}{C_d * POC} \tag{8.2}$$

$$K_{doc} = \frac{C_{doc}}{C_d * DOC} \tag{8.3}$$

$$f_d = \frac{C_d}{C} = \frac{\emptyset}{\emptyset + f_{oc}K_{poc}m_s + K_{doc}m_{doc}} \tag{8.4}$$

$$f_{doc} = \frac{C_{doc}}{C} = \frac{K_{doc}m_{doc}}{\emptyset + f_{oc}K_{poc}m_s + K_{doc}m_{doc}} \tag{8.5}$$

$$f_p = \frac{C_p}{C} = \frac{f_{oc}K_{poc}m_s}{\emptyset + f_{oc}K_{poc}m_s + K_{doc}m_{doc}} \tag{8.6}$$

Where:

f_d = Fraction of freely dissolved contaminant
f_{doc} = Fraction of DOC-complexed contaminant
f_p = Fraction of particulate phase contaminant
K_{poc} = Particulate organic carbon partition coefficient
K_{doc} = Dissolved organic carbon partition coefficient
C = Total concentration of contaminant
C_d = Concentration of dissolved phase contaminant

C_{doc} = Concentration of DOC-phase contaminant
C_p = Concentration of particulate phase contaminant
POC = Concentration of particulate organic carbon
DOC = Concentration of dissolved organic carbon
$\emptyset$ = Volume fraction of water (1=for water column, porosity for sediment bed)
m_s = Concentration of sediment (suspended solids for water column, dry bulk density for bed)
m_{doc} = Concentration of dissolved organic carbon in water column or porewater

Additional model parameters were also specified for the sediment-water exchange and ocean boundary. Relevant model parameters are described below, and the calibration of model parameters is discussed in Section 8.6.

8.4.1 Organic Carbon Partition Coefficients

The organic carbon partition coefficients were determined from data collected during the LDL Study. As part of the Phase 1 sampling, three sampling methods were conducted to provide the three-phase concentrations, as summarized in Table 8.5. Grab samples were obtained to measure total (bulk) water concentrations. High volume sampling using solid phase extraction (SPE) were used to measure total dissolved (freely dissolved and DOC-complexed), particulate, and total concentrations. SPME fibers were used to measure the equilibrated freely dissolved concentrations. The SPME freely dissolved concentrations were determined for individual congeners, resulting in 173 PCB congeners and six DDX congeners. The total PCB and total DDX were then defined as the sum of all detectable congeners.

Table 8.5 LDL Study Phase 1 Sampling Method Summary

SAMPLING METHOD	FREELY DISSOLVED	DOC-COMPLEXED	PARTICULATE	TOTAL (BULK)
Grab	Estimated*	N/A	N/A	Measured
High Volume	Measured		Measured	Measured
SPME	Measured	Estimated*	Estimated*	Estimated*

** Estimated based on organic carbon partition coefficients and organic carbon*
N/A – not applicable

The particulate organic carbon partition coefficient (K_{poc}) was calculated using the SPME freely dissolved, high volume particulate, and POC data. The organic carbon partition coefficients computed for the four Phase 1 sampling locations as provided in Table 8.6. In

the table, the partition coefficients are shown as the Log K_{poc} value. For the model calibration, the average K_{poc} was used as the organic carbon partition coefficients, which fall within the expected range based on literature values.

Table 8.6 LDL Study Phase 1 Organic Carbon Partition Coefficients

LOCATION	TPCB LOG K_{POC} (L/KG)	TDDX LOG K_{POC} (L/KG)
CS-01	6.22	6.23
LARE-01	5.47	5.53
OB-01	6.28	6.47
SP-01	5.83	5.89
Average	6.06	6.16
Literature Values	5.67 – 7.80[a]	6.00 – 6.65[b]

a Source: USACE and EPA 2004; Range shown for tri, hexa, hepta, and octa congeners
b Source: EPA 1996 and USGS 2001; Range shown for DDD, DDE, or DDT

Determination of the DOC partition coefficient (K_{doc}) requires the DOC-complexed concentration, which was not directly measured and could not be estimated from other measured phase concentrations. Due to differences in sampling methods, the SPME freely dissolved concentrations were greater than the grab sample estimates of the total dissolved concentrations (bulk-particulate) and in some cases the measured bulk concentrations. Thus, an alternative method was used to calculate the DOC partition coefficients. Firstly, the K_{oc} coefficients were determined for individual congeners. The K_{oc} was calculated for congeners if the high volume particulate and SPME concentrations were detected and then averaged among sampling locations. A regression analysis of the Log K_{oc} and Log K_{ow} was then used to determine K_{oc} values for all congeners. Secondly, the K_{doc} coefficients was calculated for individual congeners if the grab sample bulk and SPME concentrations were detected and if the grab sample bulk was greater than the sum of the high volume particulate and SPME concentrations. The K_{doc} by congener was then averaged among sampling locations and regressed to determine K_{doc} values for all congeners. Thirdly, the K_{doc}/K_{oc} ratio of individual congeners were calculated and averaged among all congeners. The average ratio of the congeners was determined to be 0.35 and 0.33 for TPCB and TDDX, respectively. Finally, the K_{doc} was calculated as the average ratio times the K_{poc} (shown in Table 8.6). The Log K_{doc} partition coefficients were determined to be 5.61 and 5.68 L/kg for TPCB and TDDX, respectively.

8.4.2 Organic Carbon

DOC and POC concentrations in the water column and sediment bed are required for determining the three-phase equilibrium partitioning. Water column DOC and POC concentrations were defined based on data from the LDL Study. As mentioned previously, DOC and POC were measured at the time of the SPME deployment and retrieval. The average concentrations were determined at each sampling location, as summarized in Table 8.7, and applied to the appropriate region, as illustrated in the top panel of Figure 8.8. The reference site concentrations were applied to the ocean outside of the breakwater.

Table 8.7 Water Column Organic Carbon Concentrations

LOCATION	SAMPLE ID	DOC (MG/L)	POC (MG/L)
Cabrillo Pier (CP)	CP-01	1.0257	0.0892
Consolidated Slip (CS)	CS-01	1.1518	0.2613
Fish Harbor (FH)	FH-01	1.1012	0.3066
POLA Inner Harbor	IA-01	1.0587	0.1456
POLB Inner Harbor	IB-01	0.9358	0.3515
LARE	LARE-01	1.4841	0.4479
POLB Outer Harbor	OB-01	1.0839	0.2463
Reference Site	REF-01	1.0372	0.1718
San Pedro Bay	SP-01	1.1696	0.1956

For the sediment bed, the DOC concentrations were obtained from porewater data and the POC concentrations were specified as the fraction organic carbon (f_{oc}) from total organic carbon (TOC) data. Sediment bed organic carbon values for the harbor area were specified based on data from the 2014 sediment and polychaete study (Environ 2015b), which included both porewater DOC and TOC data. For the DC, the f_{oc} was determined based on data from the 2011 POLA DC/CS Study (AMEC 2011). The average of DOC and f_{oc} data within each region was used, as shown in the lower panel of Figure 8.8, and summarized in Table 8.8.

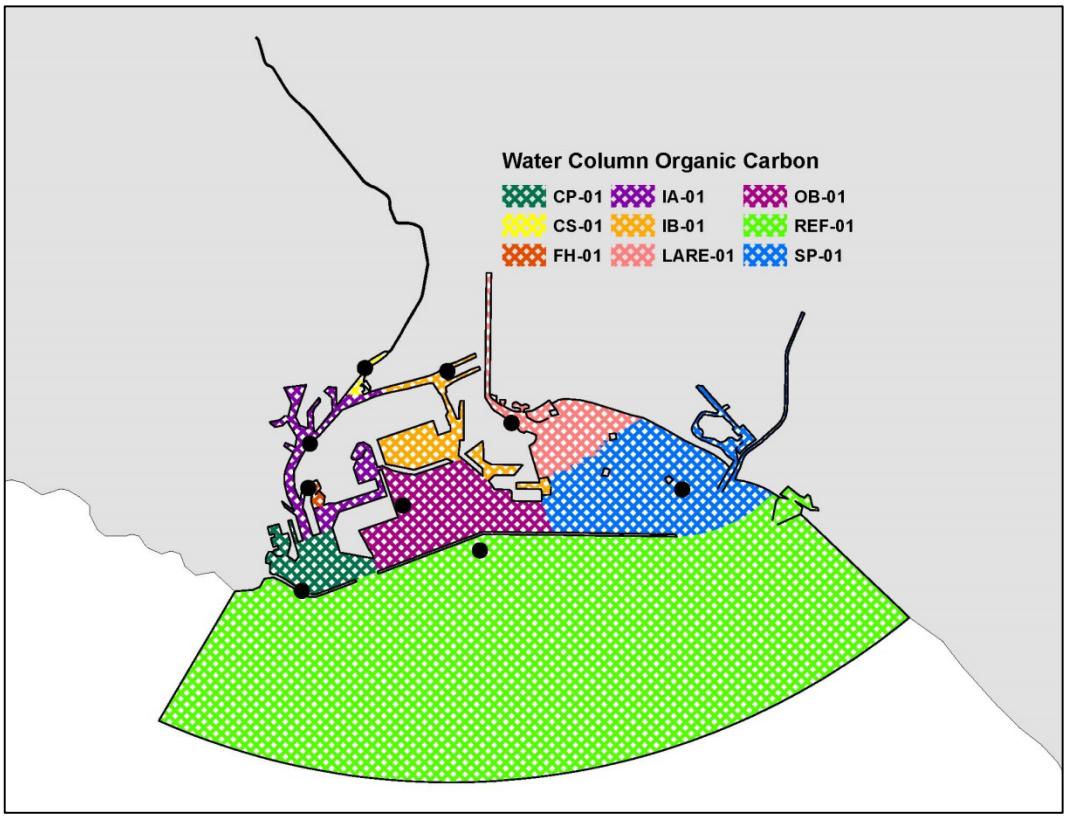

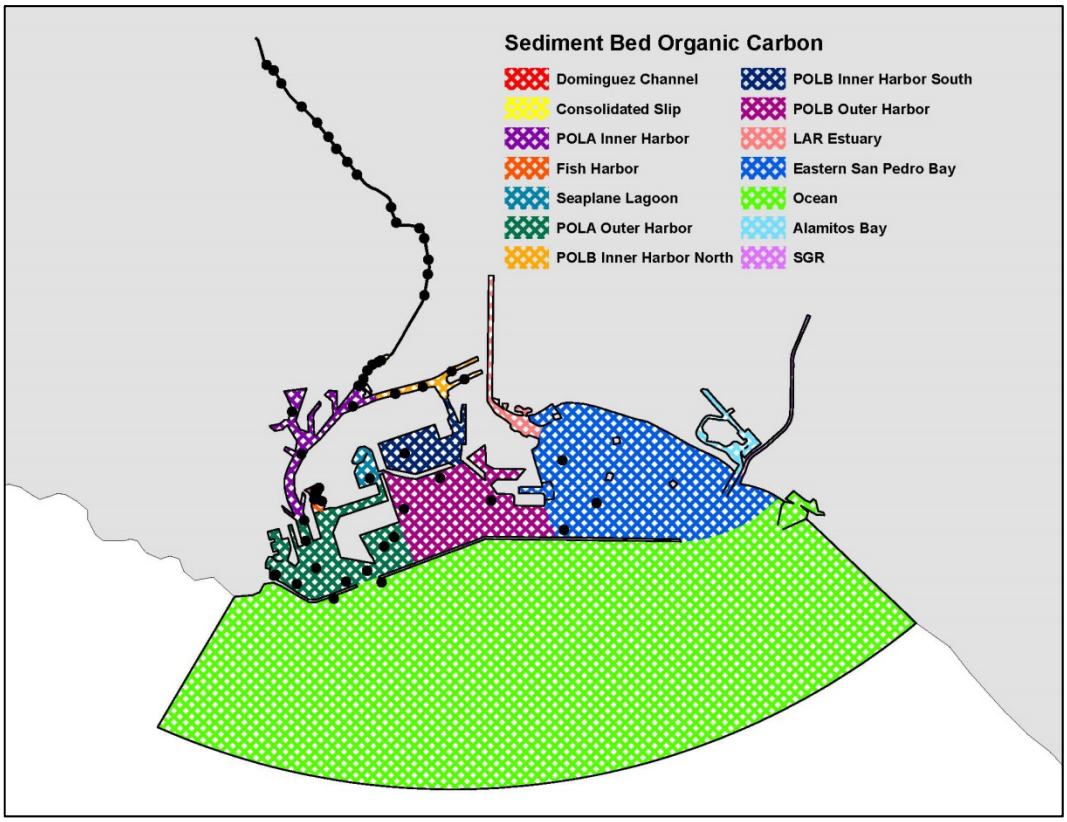

Figure 8.8 Regions for Organic Carbon Concentrations

Table 8.8 Sediment Bed Organic Carbon Concentrations

REGION	DOC (MG/L)	F_{oc} (%)
Dominguez Channel (DC)	5.11	2.88
Consolidated Slip (CS)	6.43	3.15
POLA Inner Harbor	5.96	1.82
Fish Harbor (FH)	4.01	2.00
Seaplane Lagoon	2.91	0.62
POLA Outer Harbor	3.47	1.34
POLB Inner Harbor North	7.68	1.43
POLB Inner Harbor South	4.53	0.64
POLB Outer Harbor	6.21	0.69
LARE	4.49	2.30
Eastern San Pedro Bay	3.74	1.57
Ocean	8.63	0.58
Alamitos Bay	3.74	1.57
San Gabriel River (SGR)	3.50	1.60

8.4.3 Suspended Sediment

The three-phase organic partitioning is dependent on suspended sediment concentrations. Hence, model-predicted sediment concentrations were compared to TSS measurements to ensure the WRAP Model can simulate reasonable suspended sediment concentrations. TSS measurements were collected as instantaneous grab samples. Measured TSS concentrations from the LDL Study ranged from non-detect (ND) to 12 mg/L, as summarized in Table 8.9. In general, measured TSS concentrations were relatively low with half of the measurements resulting in NDs (Minimum Detection Limit [MDL] 0.95 mg/L). For the TSS comparisons, predicted suspended sediment concentrations were verified as not being excessively high or low compared with TSS measurements.

Table 8.9 LDL Study Measured TSS

LOCATION	PHASE 1	PHASE 2		PHASE 3	
	RETRIEVAL	DEPLOYMENT	RETRIEVAL	DEPLOYMENT	RETRIEVAL
Cabrillo Pier (CP)	NS	5.4	ND	3.7	12
Consolidated Slip (CS)	ND	ND	ND	2.3	2.4
Fish Harbor (FH)	NS	ND	1.3	ND	4.0
POLA Inner Harbor	NS	ND	ND	3.3	3.3
POLB Inner Harbor	NS	1.8	ND	ND	ND
LARE	7.2	2.0	1.6	9.4	4.8
POLB Outer Harbor	1.2	ND	ND	ND	ND
Reference Site	ND	ND	ND	2.7	ND
San Pedro Bay	1.2	2.3	ND	2.7	ND

TSS units in mg/L
NS – Not Sampled, ND – Non-detect

TSS comparisons at the nine LDL Study locations are provided in Figures 8.9a – 8.9c. In these figures, measured TSS concentrations are indicated by the blue squares. For Phase 1, TSS measurements were conducted during instrument retrieval, whereas during Phase 2 and 3, TSS measurements were conducted during both deployment and retrieval of the instrument. The MDL was specified for all ND TSS concentrations. The WRAP Model-predicted mid-water daily-averaged suspended sediment concentrations are shown by the red line. TSS comparisons for the CS, LARE, and POLA Inner Harbor are shown in Figure 8.9a. As shown in this figure, the highest suspended sediment concentrations were observed at the LARE; hence, a different vertical scale has been used compared to the other locations. TSS comparisons for the POLB Inner Harbor, FH, and POLB Outer Harbor are provided in Figure 8.9b. Figure 8.9c contains the TSS comparisons for Cabrillo Pier (CP), San Pedro Bay, and the Reference Site. The WRAP Model results indicate spikes in suspended sediment concentrations that correspond to rain events. Higher spikes are observed at locations closest to large watershed loadings such as CS, LARE, and San Pedro Bay. Smaller suspended fluctuations occur at the POLA and POLB Inner Harbor locations. The lowest suspended concentrations occur at FH, POLB Outer Harbor, CP, and the reference site. Overall, the WRAP Model predicts reasonable suspended sediment concentrations compared to the TSS measurements.

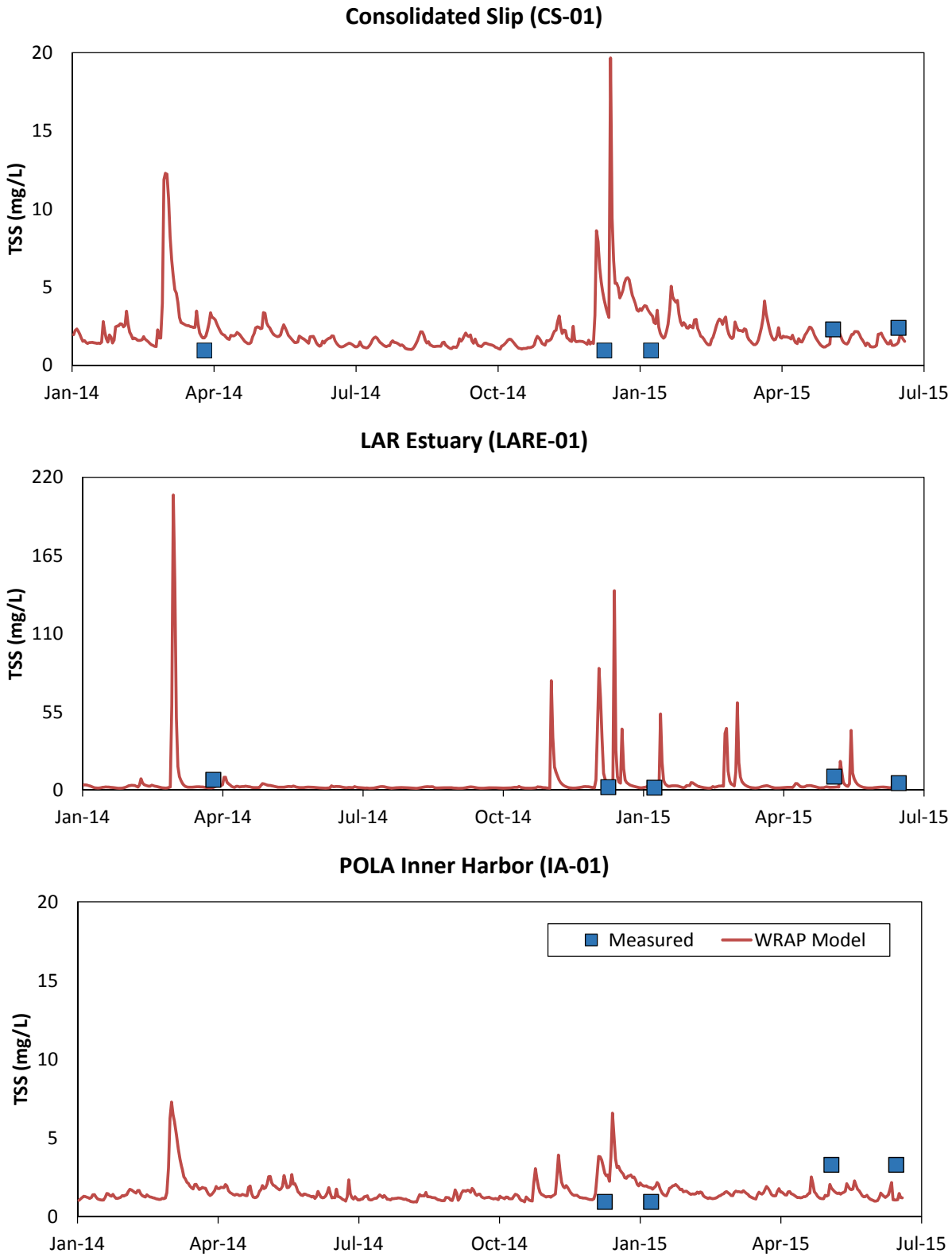

Figure 8.9a TSS Comparisons - Consolidated Slip, LAR Estuary, and POLA Inner Harbor

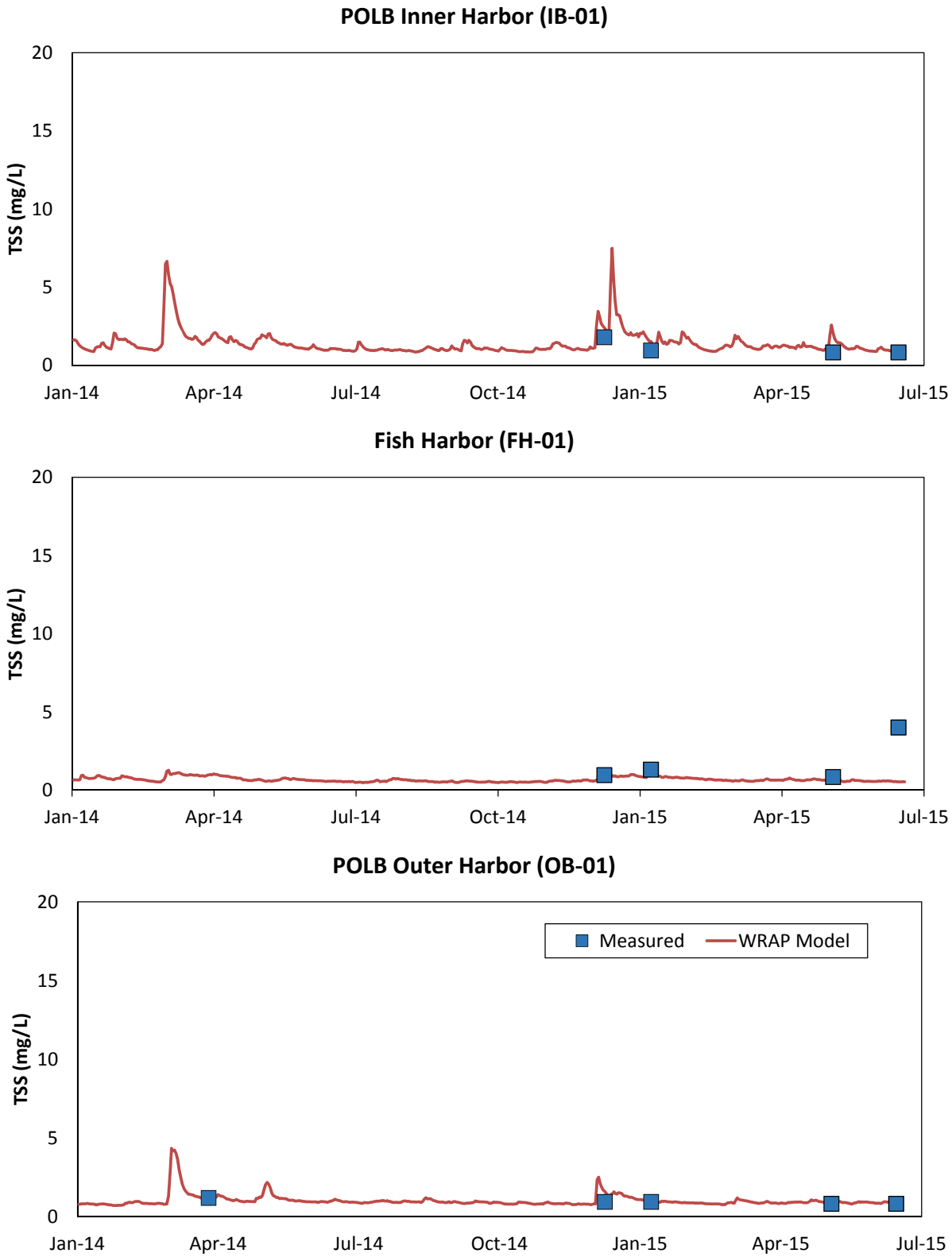

Figure 8.9b TSS Comparisons - POLB Inner Harbor, Fish Harbor, and POLB Outer Harbor

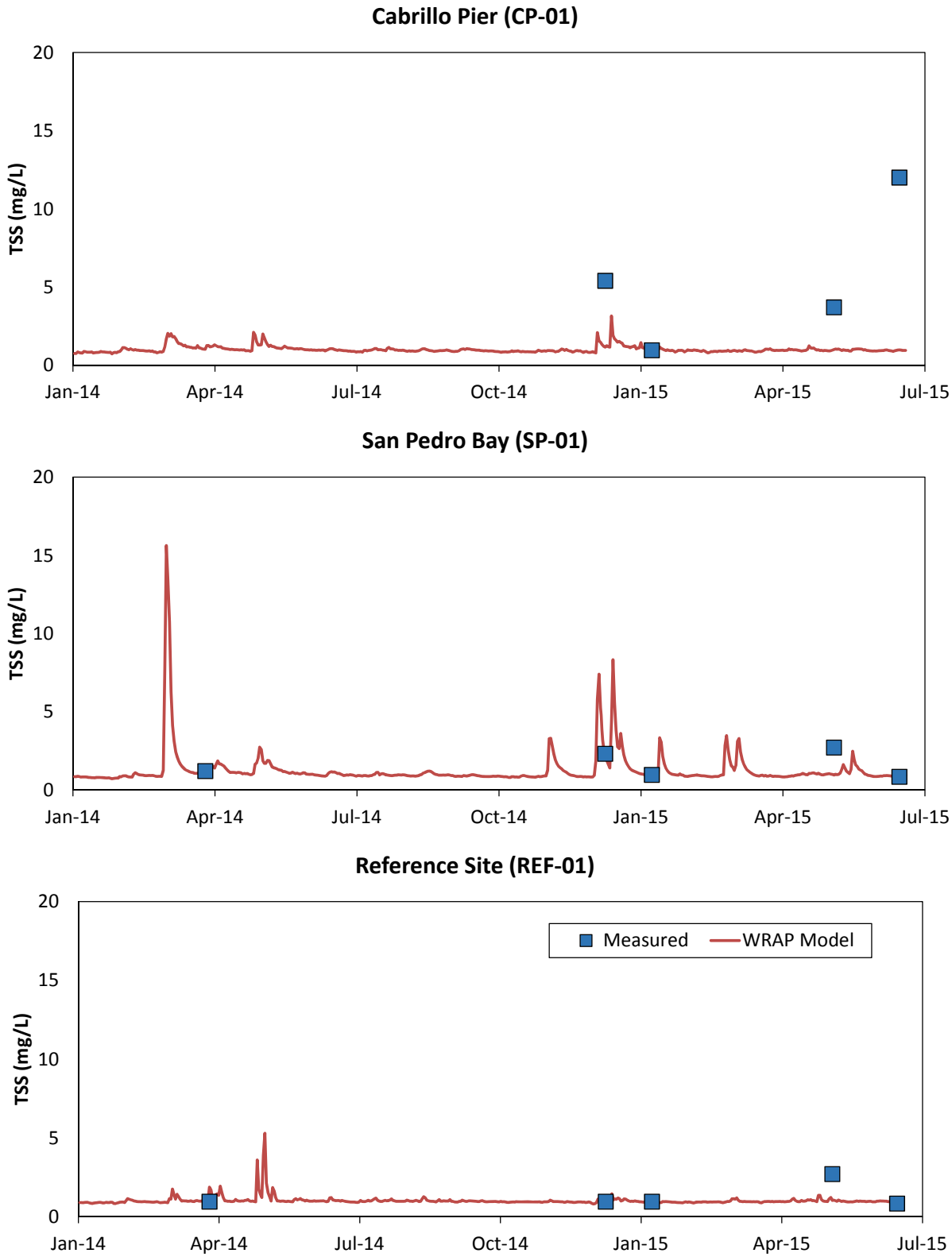

Figure 8.9c TSS Comparisons - Cabrillo Pier, San Pedro Bay, and Reference Site

8.5 EVALUATION OF ORGANIC MODEL PARAMETERS

Numerous simulations were conducted to calibrate the organic model parameters by comparing model predicted freely dissolved concentrations with those measured at the nine LDL Study sampling locations. The organic chemical calibration simulation period was January 2014 through June 2015, plus a two-year spin up period to allow sufficient time for hydrodynamic, sediment, and organic conditions to stabilize. A two-year spin up period was selected based on model simulations conducted below. Evaluation of organic model parameters included the mass transfer coefficient, particle mixing coefficient, and ocean boundary concentration.

Similar to the hydrodynamic and mixing calibration, the calibration of organic chemical model parameters were conducted starting with an initial set of model parameters selected based on site conditions, literature values, and professional engineering judgment. In general, model calibrations started with using a low ocean boundary concentrations to determine the ranges in the mass transfer and particle mixing coefficients that would provide good overall comparison between predicted and measured freely dissolved concentrations at the sampling locations within the harbor. The ocean boundary concentrations were then adjusted to provide a good match between predicted and measured concentrations at the reference site outside of the harbor. Further fine tuning of the mass transfer coefficients and particle mixing coefficients were then made after the change in boundary concentrations, and the process was repeated iteratively until overall best fit between predicted and measured concentrations were found at all nine sampling locations. The final set of calibrated organic model parameters and calibration results are provided in Section 8.6. Below, examples of selected model simulations are presented to illustrate the effects of these model parameters.

8.5.1 Mass Transfer Coefficient

Sediment-water exchange is the transport of organic chemicals between the sediment bed porewater and overlying water column. This is dependent on a mass transfer coefficient and the concentration gradient of the dissolved organic chemical between the bed and water. Sediment-water diffusion tends to be the dominant process in quiescent environments (i.e., hydrodynamically inactive areas), where other processes such as sediment deposition or resuspension are minimal. Quantifying the mass transfer coefficient is typically difficult due to lack of field data and the underestimation of laboratory measurements. Lab measurements can be one to two orders of magnitude lower since laboratory settings cannot properly reproduce turbulent conditions. Alternatively, empirical correlations have been used to estimate the mass transfer coefficients that can be a function of porosity and molecular weight. However, approximations of the mass transfer coefficient are typically determined from model calibration rather than field or laboratory measurements. Typical estimates of mass transfer coefficients range from 1 – 10 cm/day, but have been reported from 0.1 to 40 cm/day (Lick 2009).

In EFDC, the sediment-water diffusion is parameterized by a mass transfer coefficient that accounts for both molecular diffusion and advection. Initial estimates of the mass transfer coefficients were selected based on literature values, as summarized in Table 8.10. Most estimates of the mass transfer coefficient pertain to PCBs with limited reported estimates for DDX. For PCBs, literature estimates of the mass transfer coefficient ranged from 1 to 18.8 cm/day. Estimates of the mass transfer coefficient for DDX were between 0.01 to 1.0 cm/day, lower than the estimates for PCBs.

Table 8.10 Literature Estimates of Organic Chemical Mass Transfer Coefficients

MASS TRANSFER COEFFICIENT (CM/DAY)	STUDY DESCRIPTION
10.2	PCBs in Hudson River, NY (EPA 2000)
1 – 2 (winter) 4 – 5 (summer)	PCBs in Lower Grasse River, NY (Alcoa 2001)
3.5	PCBs in Lower Fox River, WI (WDNR 2001)
1 – 10	PCBs in Housatonic River, MA (USACE and EPA 2004)
2.6 – 18.8	PCBs in Hudson River, NY (Erickson et al. 2005)
0.01 – 1.0	DDXs in Lake Maggiore, Italy (Dueri et al. 2005)

The initial evaluation of the mass transfer coefficients was conducted based on low, mid, and high estimates of 0.17, 1.0, and 10 cm/day, respectively. In order to illustrate differences between TPCB and TDDX, the same range in the mass transfer coefficients were used for both TPCB and TDDX. This range in mass transfer coefficients encompasses the estimates used in the CSM (1 – 10 cm/day), which was based on literature values for TPCB. Simulations with the low, mid, and high estimates were conducted to demonstrate the effects of the mass transfer coefficient on water column concentrations. These simulations were conducted with low estimates of particle mixing coefficient and ocean boundary concentrations, as discussed below. Examples showing the effects of the mass transfer coefficients for TPCB and TDDX are shown in Figures 8.10 and 8.11, respectively.

Comparisons of the freely dissolved TPCB at four selected locations are provided in Figure 8.10. In the figure, the measured concentrations are shown by the blue line, which is the measured mid-water concentration over the SPME sampling duration. The model-predicted mid-water concentrations are shown as a continuous time series of the daily averaged freely dissolved concentrations. Results for the low, mid, and high mass transfer coefficients are indicated by the orange, green, and purple lines, respectively. For easy comparison among different locations, the same vertical scale is used for all locations.

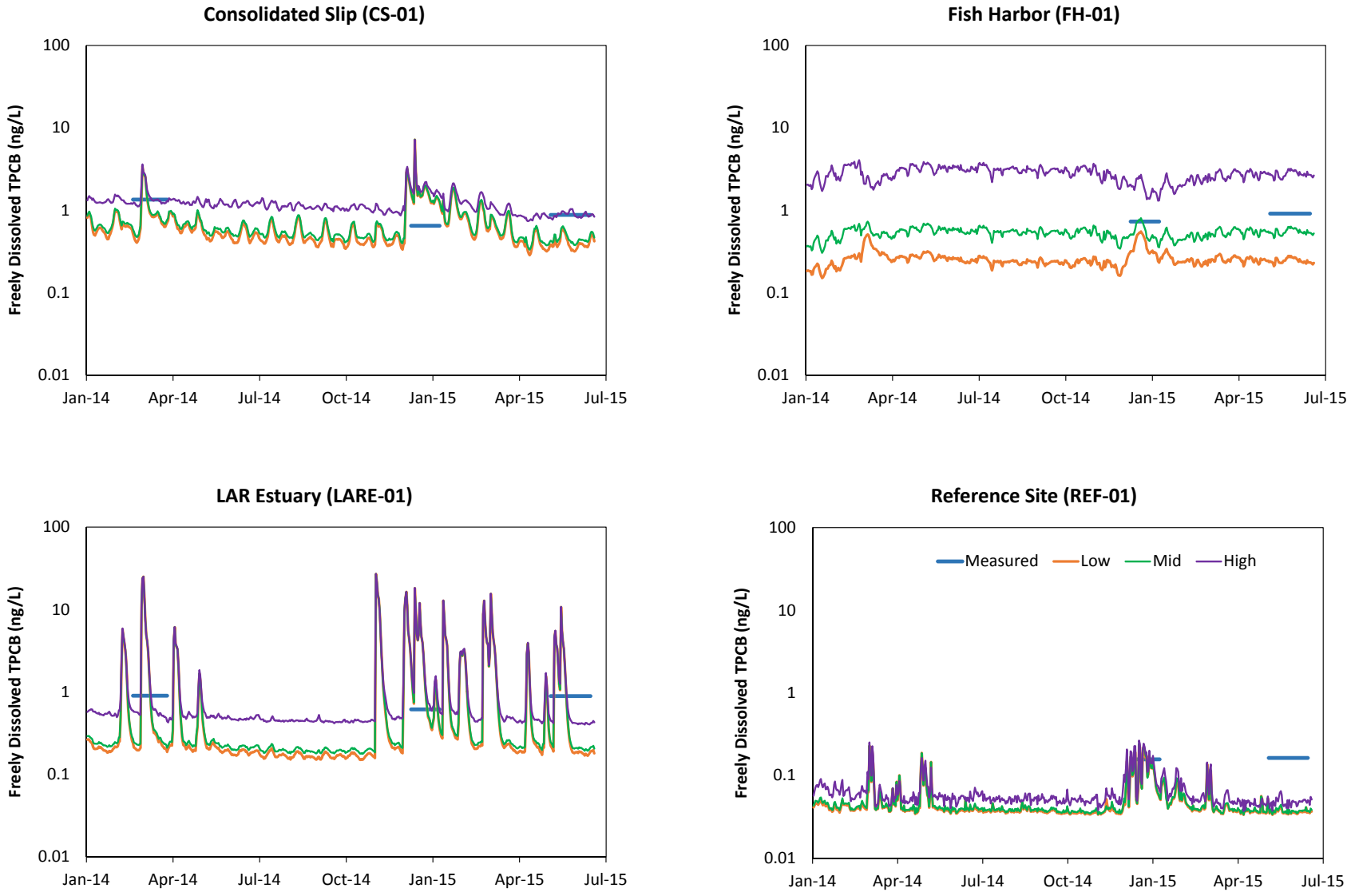

Figure 8.10 Evaluation of Mass Transfer Coefficient for TPCB

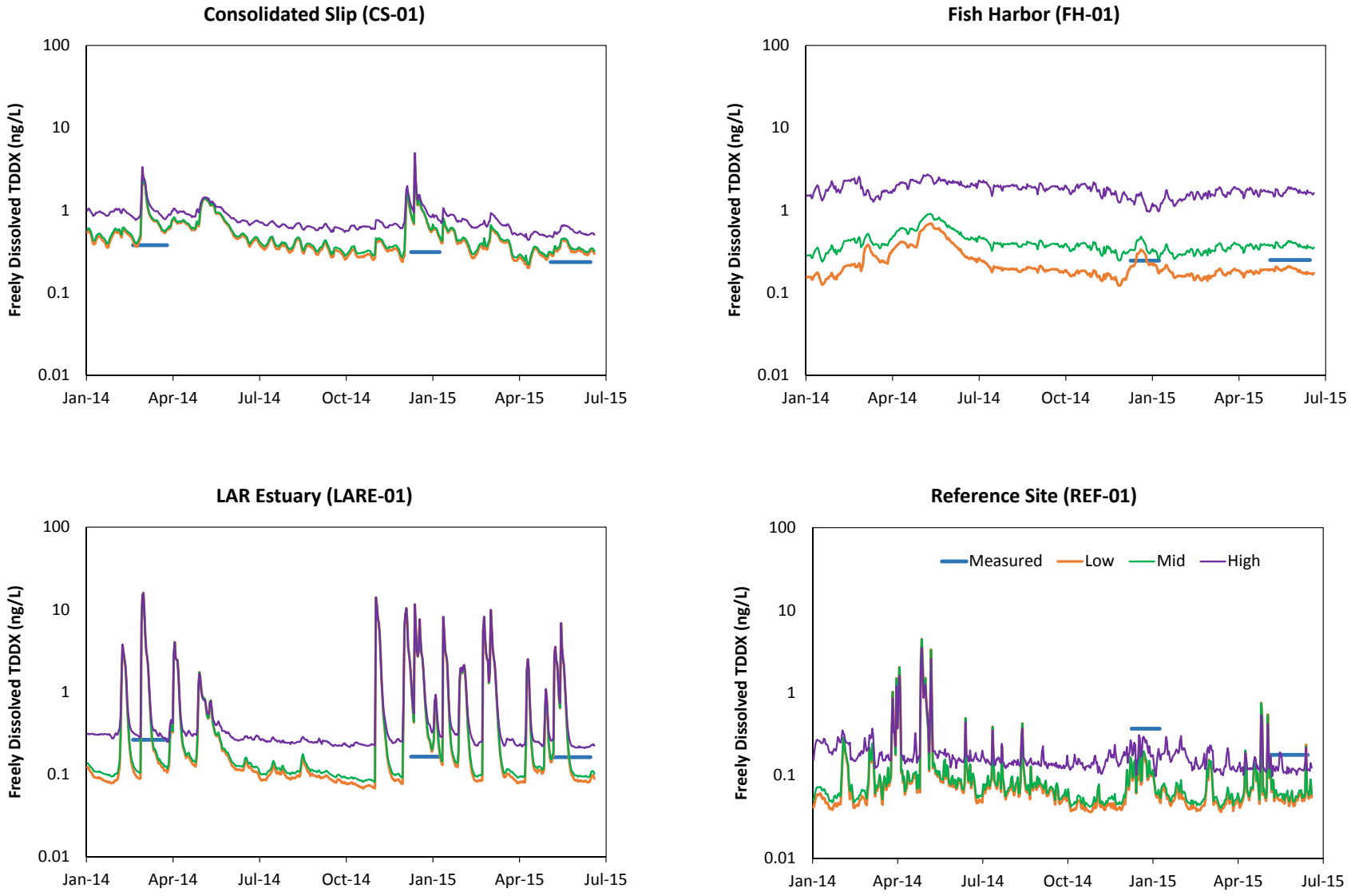

Figure 8.11 Evaluation of Mass Transfer Coefficient for TDDX

Comparisons of the measured and model-predicted TPCB concentrations are provided for the CS (CS-01), LARE (LARE-01), FH (FH-01), and reference site (REF-01). The highest model-predicted concentrations occurred at CS-01 and LARE-01, where concentration spikes corresponding to storm events are shown. The increase in concentrations during storm events may be attributed to higher storm water concentrations and/or erosion of bed sediments due to higher storm water flows. The lowest model-predicted concentrations occur at REF-01, which still shows the influence of storm events, but to a lesser extent than LARE-01 and CS-01. Comparisons of the model-predicted concentrations provided are used to illustrate the effects of the mass transfer coefficients on water column concentrations, which show that the higher the mass transfer coefficient, the higher the water column concentrations. Wet weather concentrations are similar for the three mass transfer coefficient estimates, but differ during dry weather conditions for all locations except for FH (FH-01).

Responses in water column concentration differed at FH (FH-01). The water column concentrations do not show differences between dry and wet weather conditions, indicating less influence of storm events from either storm water sources or erosion of bed sediments. The sediment-water diffusion flux tends to be more dominant when the particulate flux is smaller, such as dry weather conditions or low sediment concentrations, which is the case at FH-01 shown previously in Figures 8.9a – 8.9c. Hence, calibration of the mass transfer coefficient focused on comparisons in FH, which is the least hydrodynamically active area and has the lowest sediment concentrations. In other words, the mass transfer coefficient cannot be calibrated based on any of the other locations because water column concentrations are dominated by other processes (e.g., watershed loadings and sediment re-suspension). To aid in the calibration of the TPCB mass transfer coefficient, the model-predicted concentrations were compared to the measured concentrations at FH-01. The range in model-predicted concentrations illustrates how the mass transfer coefficient can be "adjusted" in order to calibrate the WRAP Model. The measured concentrations fall between the mid and high mass transfer coefficient estimates (1.0 and 10 cm/day). Thus, the TPCB mass transfer coefficient was calibrated by increasing the mass transfer coefficient from 1.0 cm/day until the model predicted concentrations match the measured concentrations. Calibration of the mass transfer coefficient was conducted in conjunction with other model parameters.

Effects of the mass transfer coefficient on TDDX concentrations were also evaluated on the same low, mid, and high mass transfer coefficient estimates, as shown in Figure 8.11. Examples are provided for CS-01, LARE-01, FH-01, and REF-01. The highest model-predicted concentrations were determined for CS-01 and LARE-01, while the lowest concentrations were shown at REF-01. The model-predicted concentrations at CS-01, LARE-01, and REF-01 showed similar responses as TPCB, with the mass transfer coefficients primarily affecting concentrations during dry weather conditions. The calibration of the TDDX mass transfer coefficient was also focused on comparisons at FH-01 by

comparing the model-predicted concentrations to measured concentrations. The low and mid mass transfer coefficient estimates (0.17 and 1.0 cm/day) result in concentrations closest to the measured concentrations. The TDDX mass transfer coefficient was calibrated by adjusting the mass transfer coefficient between 0.17 and 1.0 cm/day in conjunction with other model parameters.

8.5.2 Particle Mixing Coefficient

In the sediment bed, the mixing of sediment particles can be caused by physical or biological processes such as bioturbation. Bioturbation is the mixing of sediment by benthic organisms due to feeding and burrowing activities. The amount and depth of mixing can be highly variable and differs depending on the type of organism. In EFDC, a particle mixing coefficient is used to account for these processes. Estimates of the particle mixing coefficient ranged from 0.03 to 300 cm^2/yr (10^{-13} to 10^{-9} m^2/s) (Thoms et al. 1995, Thibodeaux et al. 2001, USACE and EPA 2004, and Lick 2009).

In general, the particle mixing coefficient increases the surface sediment concentrations, thereby increases water column concentrations. The initial evaluation of the particle mixing coefficients involved low, mid, and high estimates of 0.0, 1.0, and 10 cm^2/yr, respectively. These simulations were conducted only to provide information on the effects of the particle mixing coefficient on water column concentrations. These simulations were conducted with the mid estimate of mass transfer coefficients discussed above, and a low ocean boundary estimate discussed below. Examples of the range particle mixing coefficients for TPCB and TDDX are shown in Figures 8.12 and 8.13, respectively. Water column concentration comparisons are provided for POLA Inner Harbor (IA-01), POLB Outer Harbor (OB-01), FH-01, and REF-01. Responses of the water column concentrations to the particle mixing coefficients are similar for both TPCB and TDDX. The particle mixing coefficient typically affects water column concentrations during dry weather conditions at locations inside of the harbor, as illustrated at IA-01 and OB-01. The various particle mixing coefficients resulted in minimal differences at some locations, as illustrated by FH-01 and REF-01. Overall, the evaluation of the particle mixing coefficients shows that a higher particle mixing coefficient results in higher water column concentrations. The particle mixing coefficient was calibrated in conjunction with other model parameters.

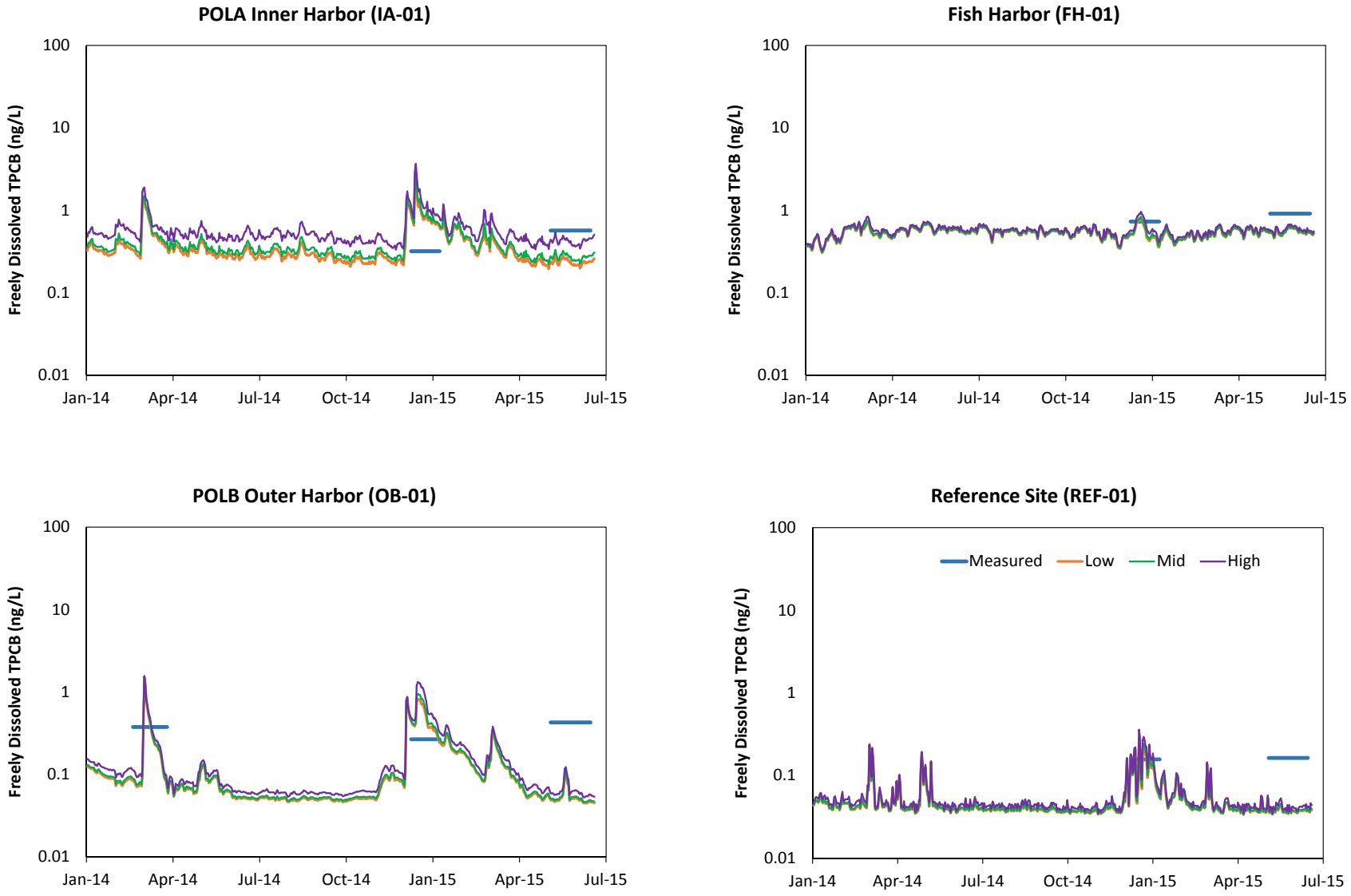

Figure 8.12 Evaluation of Particle Mixing Coefficient for TPCB

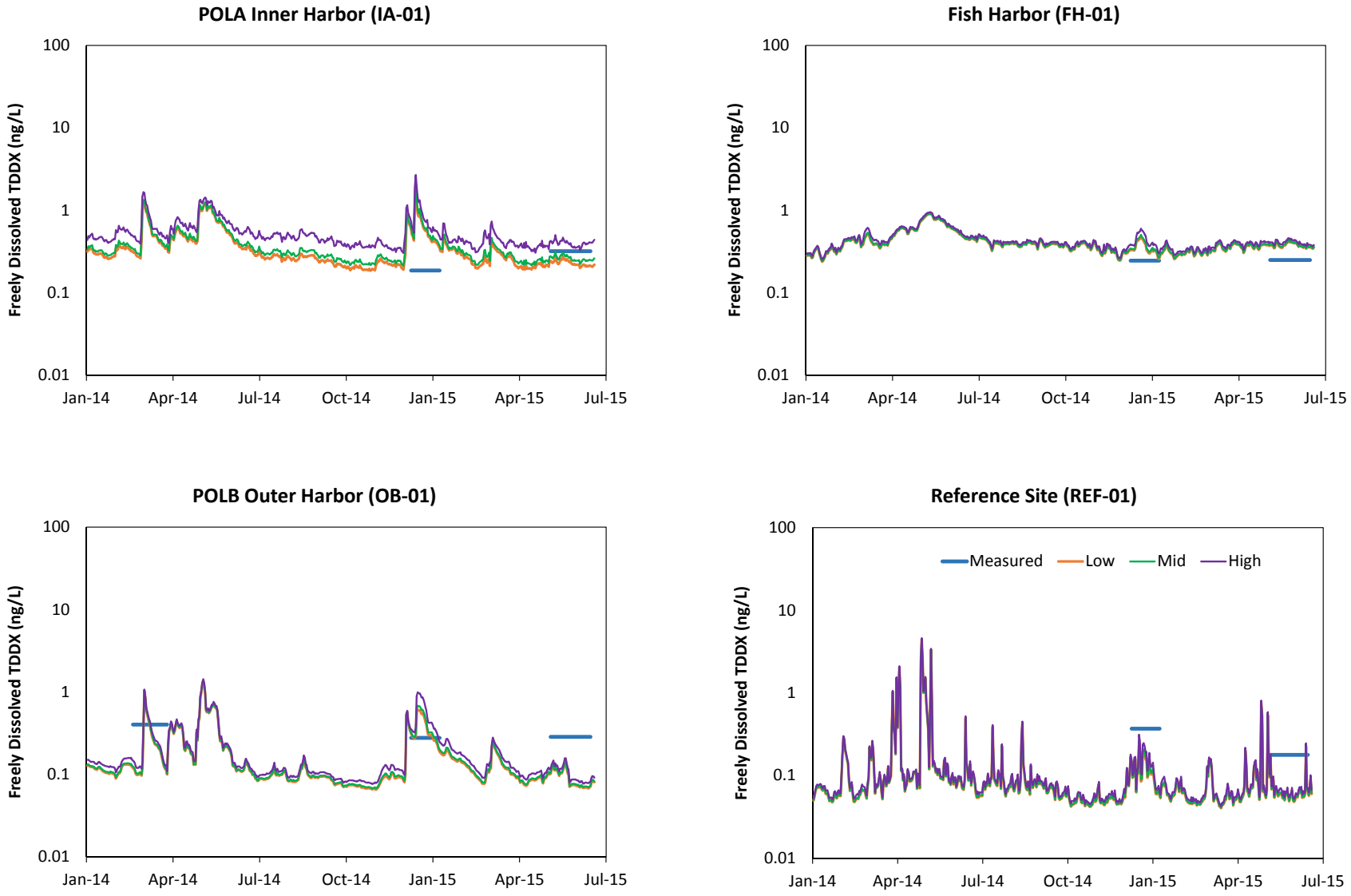

Figure 8.13 Evaluation of Particle Mixing Coefficient for TDDX

8.5.3 Ocean Boundary

In the CSM, tidal-exchange between the harbor and ocean was identified as an important process affecting contaminant concentrations in the harbor. Tidal flushing is the process by which flood tides bring ocean water into the harbor, mix ocean water with harbor waters, and then transport the mixed water out of the harbor during ebb tides. The exchange of contaminants between the harbor and ocean are dependent on hydrodynamics, as well as organic chemical concentrations within the harbor and from the ocean. The ocean boundary represents ocean concentrations near the vicinity of the model boundary.

Initial estimates of the TPCB and TDDX concentrations along the ocean boundary were selected based on measured concentrations from the Palos Verdes Shelf. Sediments of the Palos Verdes Shelf are contaminated with organic chemicals from historical discharges from a wastewater outfall located to the west of Point Fermin, which is located just beyond the model boundary. Prior studies have indicated that this site continues to serve as a source of contaminants, including PCBs and DDTs, to coastal waters (Zeng et al. 2005 and Fernandez et al. 2012). Ocean concentrations were selected from measurements made in 2010, which included both TPCB and TDDX. Dissolved PCB and DDX were measured at nine locations in the vicinity of the outfall and one background station about 24 km southeast of the outfall. SPME measurements of PCBs resulted in concentrations below detection limits, but dissolved TPCB concentrations measured using low-density polyethylene (PE) strips near the outfall ranged from 0.090 to 0.316 ng/L and 0.050 ng/L at the background station. For SPME measurements of DDX congeners, only 2,4-DDE and 4,4-DDE were above detection limits. Dissolved TDDX concentrations near the outfall ranged from 0.041 to 1.14 ng/L and 0.041 ng/L at the background station. The TDDX concentrations near the outfall was consistent with prior SPME measurements taken in 2003 and 2004 ranging from 0.078 to 0.312 ng/L (Zeng et al. 2005).

Effects of the ocean boundary concentrations on water column concentrations were conducted based on low and high estimates. These simulations were conducted to illustrate the calibration process, thus mid estimates of the mass transfer and particle mixing coefficients previously discussed were used to evaluate the effect of ocean boundary concentrations. Low estimates of the ocean boundary concentrations were based on measured background concentrations (Fernandez et al. 2012), which represent a conservative estimate of ocean concentrations. In order to demonstrate the ocean boundary calibration process, the high ocean boundary estimate was specified to provide a good match with Phase 3 concentrations at REF-01. Examples for the evaluation of the ocean boundary are provided in Figures 8.14 and 8.15 for TPCB and TDDX, respectively. Comparisons are shown for CS-01, CP (CP-01), FH-01, and REF-01. Responses of the water column concentrations were similar for both TPCB and TDDX. Overall, the lower ocean boundary estimate resulted in lower water column concentrations compared to the higher estimate indicating the importance of specifying the ocean boundary.

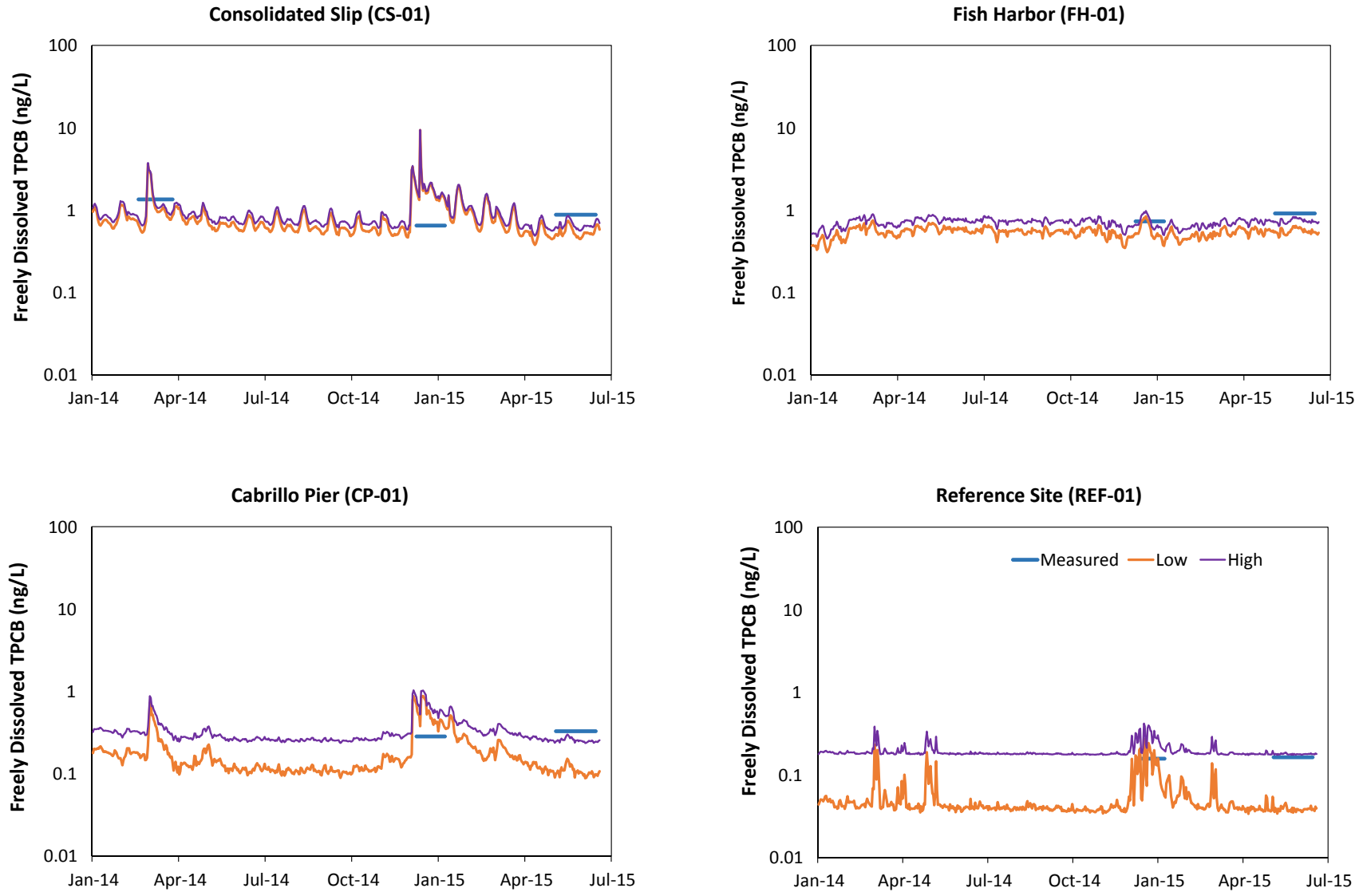

Figure 8.14 Evaluation of Ocean Boundary for TPCB

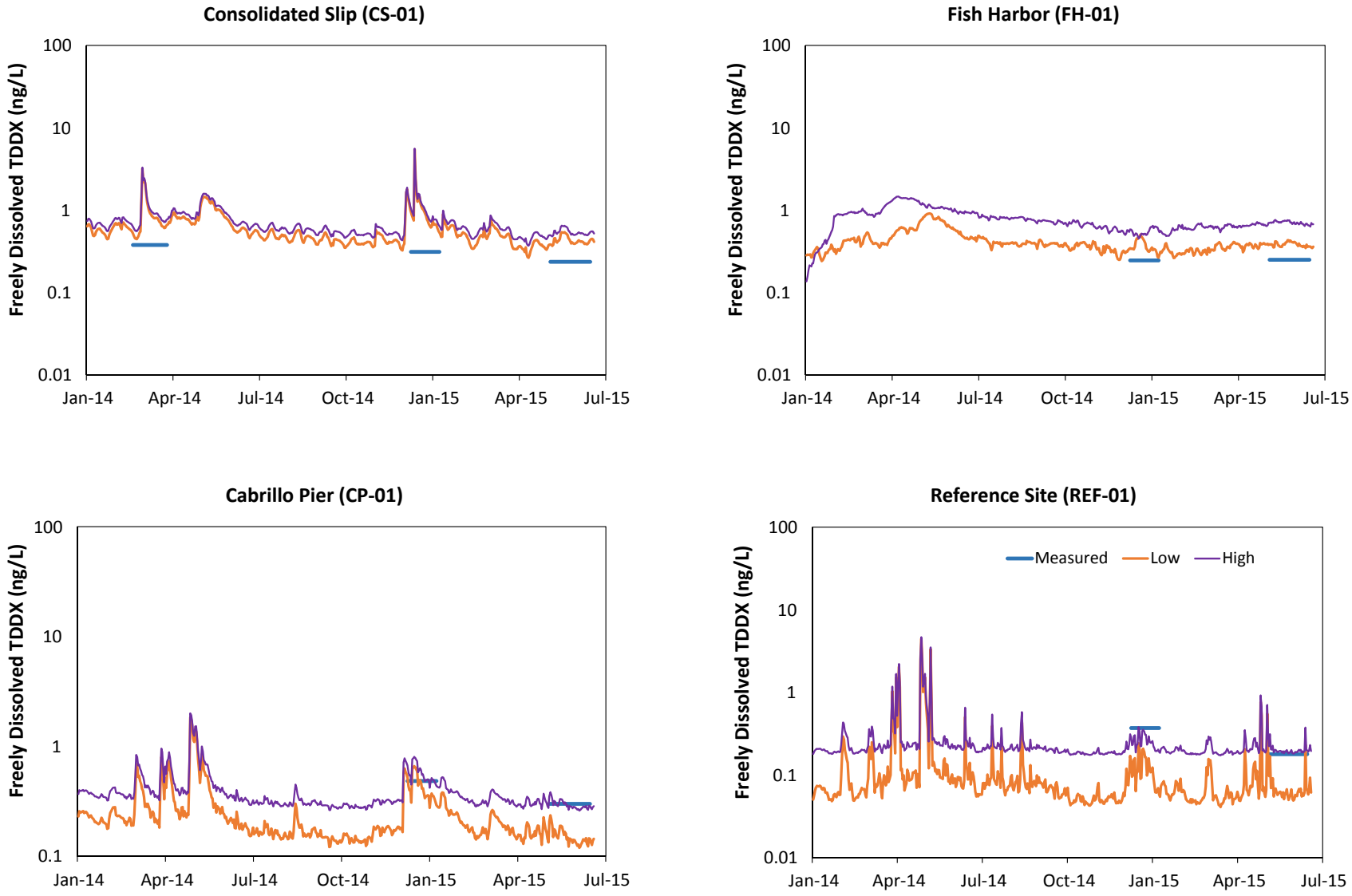

Figure 8.15 Evaluation of Ocean Boundary for TDDX

As expected, the greatest impact to water column concentrations are observed at REF-01, which is located just outside the breakwater and closest to the model boundary. The impact of the ocean boundary decreases into the harbor as illustrated by CP-01 (located in the POLA outer harbor) and CS-01.

The high ocean boundary estimate at REF-01 illustrates the calibration of the ocean boundary concentrations by increasing the concentration to match the measured concentration. The corresponding TPCB concentrations at FH-01 are lower than the measured concentrations. However, these concentrations are based on the mid mass transfer coefficient estimate, which is lower than the calibrated estimate, as discussed previously in Section 8.5.1. A balance between the mass transfer coefficient and ocean boundary will be achieved during the calibration process. Likewise for TDDX, the high ocean boundary estimate matches at REF-01, but under predicts at FH-01. Based on the previous evaluation of the TDDX mass transfer coefficient, the mid mass transfer coefficient estimate will be reduced during the calibration process. This illustrates the iterative process conducted to calibrate the organic model parameters.

8.6 ORGANIC CALIBRATION RESULTS

Based on the evaluation of organic model parameters discussed in Section 8.5, the mass transfer coefficients, particle mixing coefficients, and ocean boundary concentrations were calibrated based on measurements from the LDL Study. The selected organic chemical model inputs and calibrated model parameters are summarized in Table 8.11. These model parameters were judged to provide an overall fit between predicted and measured organic chemical concentrations at all nine sampling locations.

Table 8.11 Selected Organic Model Inputs and Parameters

MODEL PARAMETER	UNITS	TPCB	TDDX
Log K_{poc}	L/kg	6.06	6.16
Log K_{doc}	L/kg	5.61	5.68
Mass Transfer Coefficient	cm/day	3.0	0.35
Particle Mixing Coefficient	cm^2/yr	1.0	1.0
Volatilization Mass Transfer Coefficient	cm/day	13.13	3.10
Ocean Boundary Concentration	ng/L	0.25	0.24

The WRAP Model organic calibration focused on comparison with measured freely dissolved concentrations taken at the nine LDL Study sampling locations. Comparisons of the calibrated WRAP Model and measured freely dissolved TPCB concentrations are provided in Figures 8.16a – 8.16c. In the figures, the WRAP Model daily-averaged, mid-water TPCB concentration (red line) shows the temporal variations in the model-predicted water column concentrations. High fluctuations in the model-predicted concentrations show the responses to storm water discharges from the watersheds. As expected, the highest concentrations were determined at CS-01 and LARE-01, the two locations most affected by watershed discharges from the DC Watershed and LAR Watershed, respectively; and the lowest concentrations were determined at the ocean reference site (REF-01) which is expected to be least influenced by storm water discharges. The measured mid-water TPCB concentrations (blue line) are indicated as a constant concentration over the sampling duration (e.g., Phase 1, Phase 2 and Phase 3) since the SPME measurements represent the average concentration during the instrument deployment. In general, the WRAP Model TPCB concentrations are comparable to the measured concentrations.

Comparisons of the calibrated WRAP Model and measured freely dissolved TDDX concentrations are provided in Figures 8.17a – 8.17c. Similar to TPCBs, the WRAP Model shows fluctuations in TDDX concentrations in response to storm water discharges due to watershed loadings with the highest concentrations observed at CS-01 and LARE-01. At LARE-01, the WRAP Model results show the greatest difference between dry and wet weather concentrations. However, concentrations during dry weather conditions are comparable to the measured concentrations. In general, the WRAP Model TDDX concentrations are comparable to the measured concentrations.

As previously discussed, the calibration of the mass transfer coefficients and ocean boundary concentrations were focused on comparisons to measured concentrations at FH-01 and REF-01, respectively. At these two locations, measurements were made during Phase 2 and 3, with Phase 3 being least affected by storm water flows. The measured and modeled freely dissolved concentrations at the FH and reference site calibration locations are compared in Table 8.12. The WRAP Model concentrations are shown as the average mid-water concentration over the sampling duration to enable a direct comparison to the SPME measurements. For TPCB, the model-predicted concentrations at FH-01 were similar to the measured concentrations including the higher concentration during the drier Phase 3. At REF-01, the model-predicted concentration was higher for Phase 2, but matched the Phase 3 measured concentration. For TDDX, the model-predicted concentration at both FH-01 and REF-01 was also similar to measured Phase 2 concentrations and matched well with Phase 3 concentrations. In general, the organic calibration comparisons at FH-01 and REF-01 best represent the organic model parameter calibration, particularly based on Phase 3 comparisons. Graphical comparisons of the measured and WRAP Model concentrations are provided below.

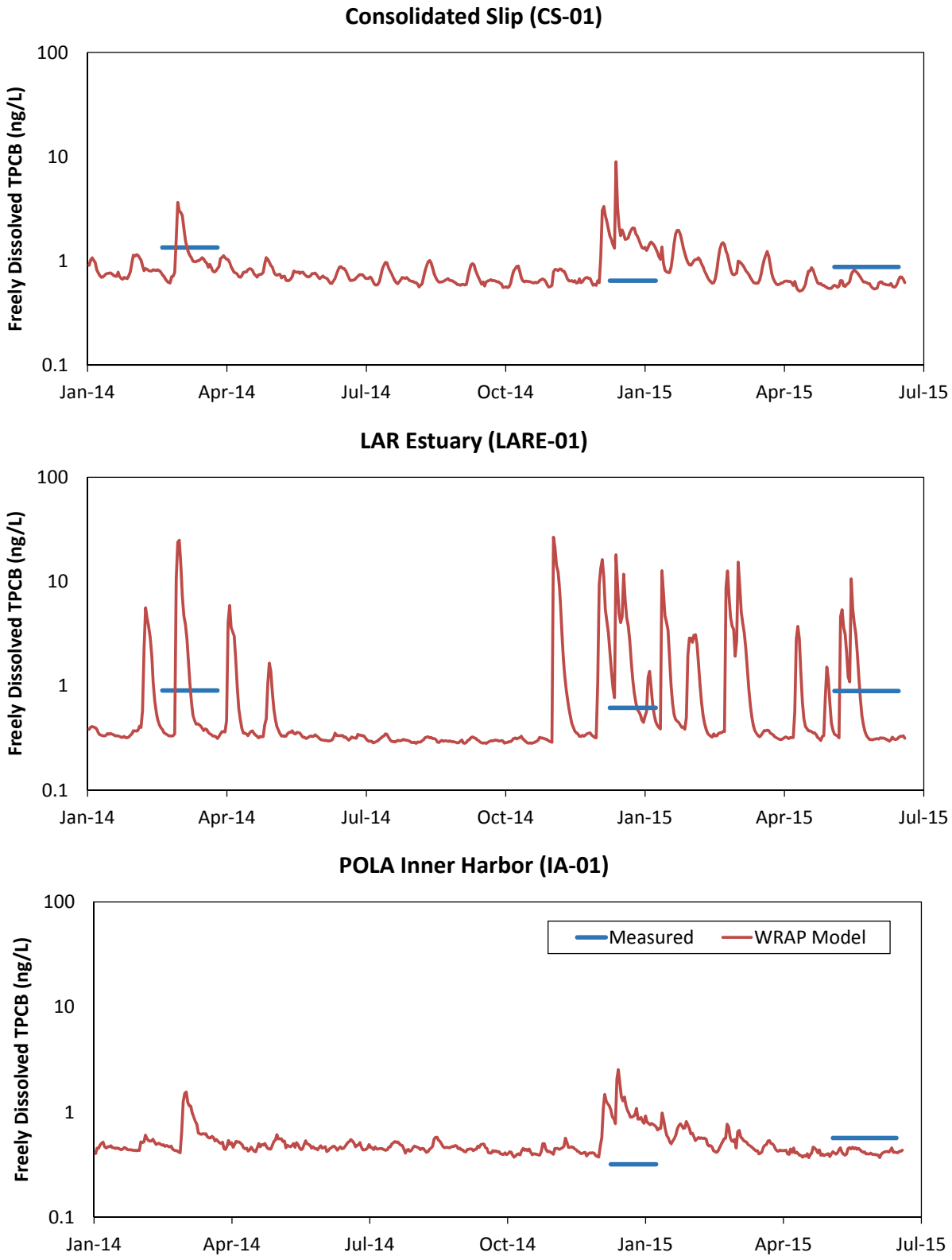

Figure 8.16a TPCB Time Series Comparisons - Consolidated Slip, LAR Estuary, and POLA Inner Harbor

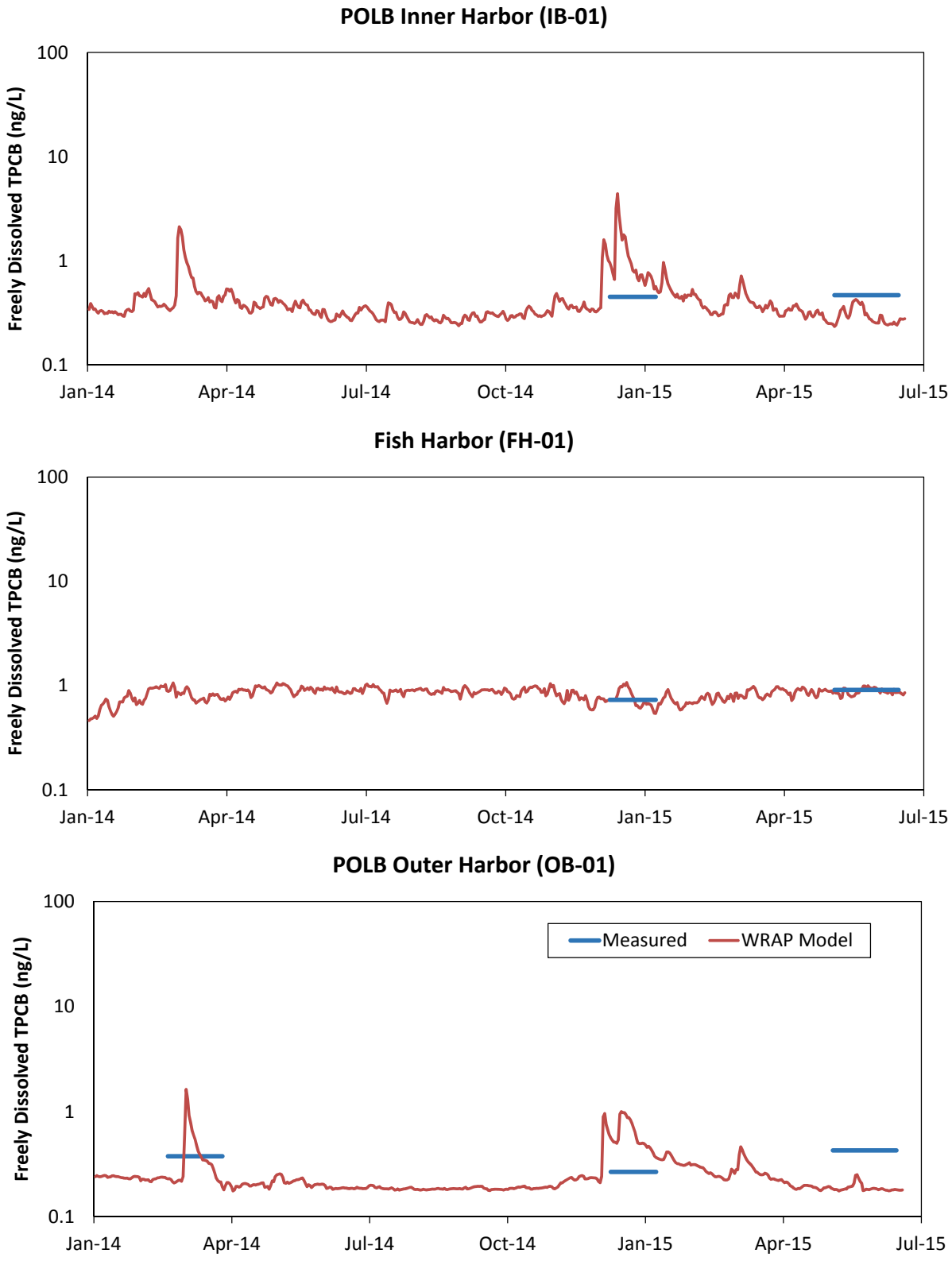

Figure 8.16b TPCB Time Series Comparisons - POLB Inner Harbor, Fish Harbor, and POLB Outer Harbor

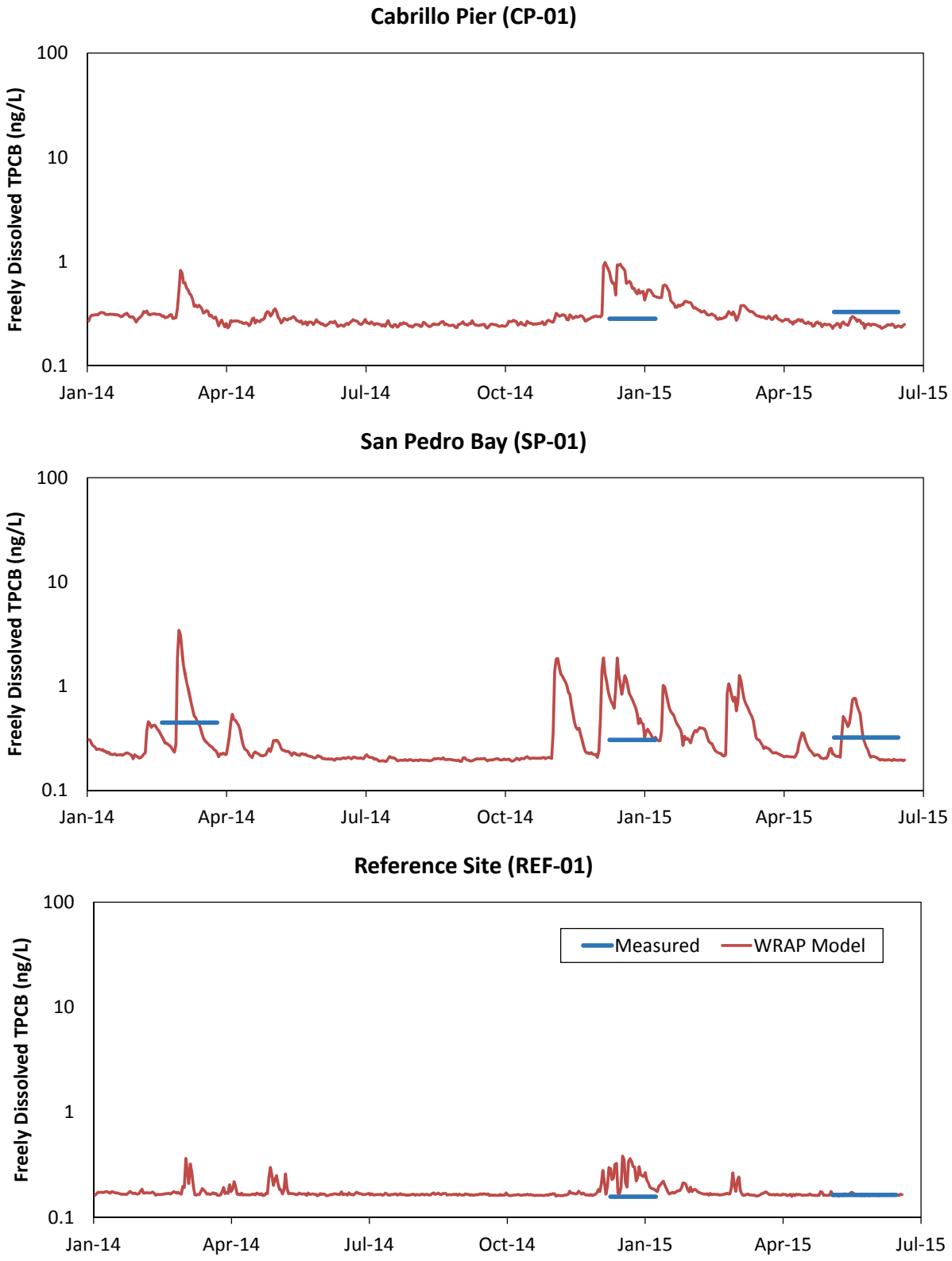

Figure 8.16c TPCB Time Series Comparisons - Cabrillo Pier, San Pedro Bay, and Reference Site

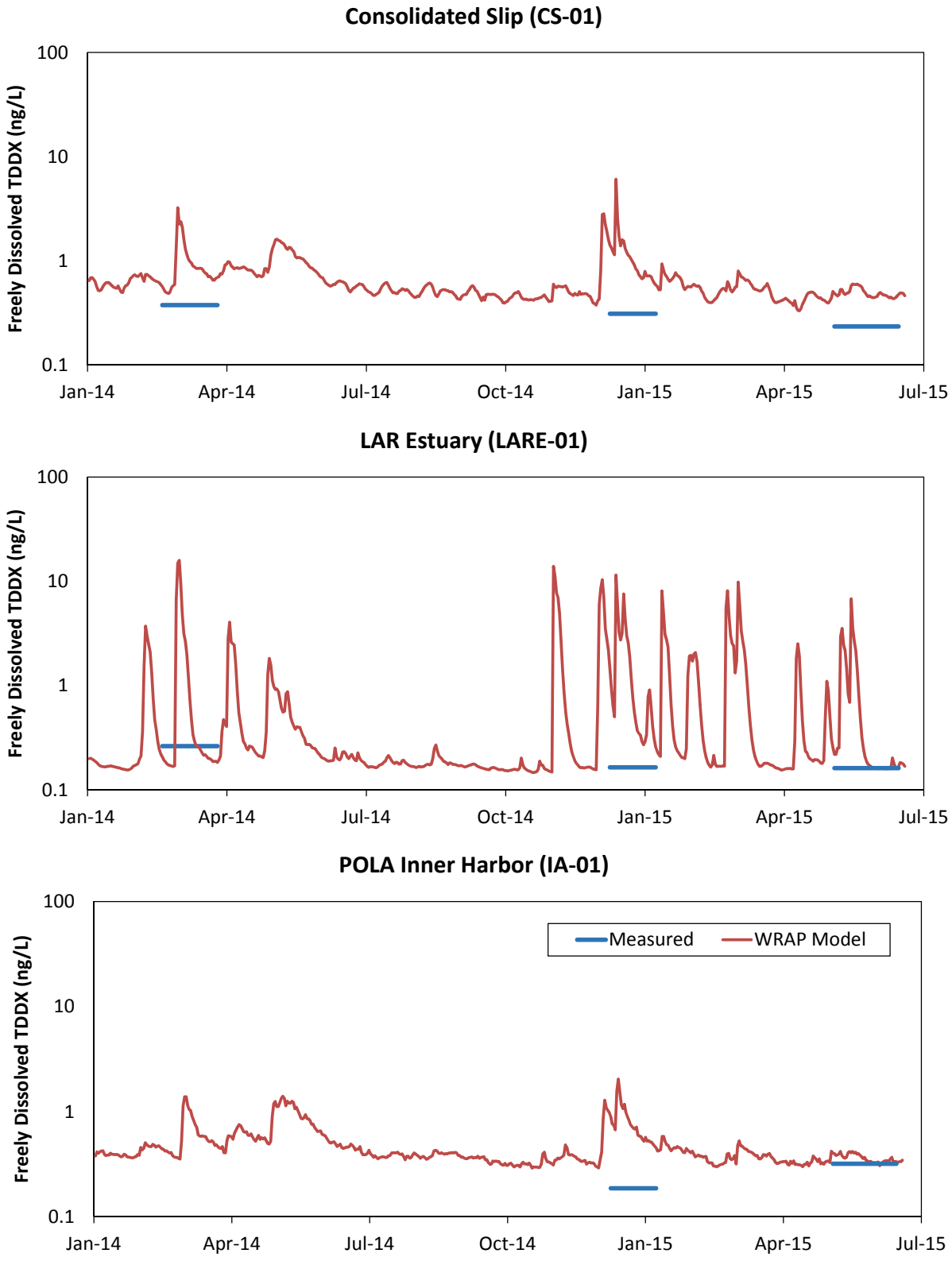

Figure 8.17a TDDX Time Series Comparisons - Consolidated Slip, LAR Estuary, and POLA Inner Harbor

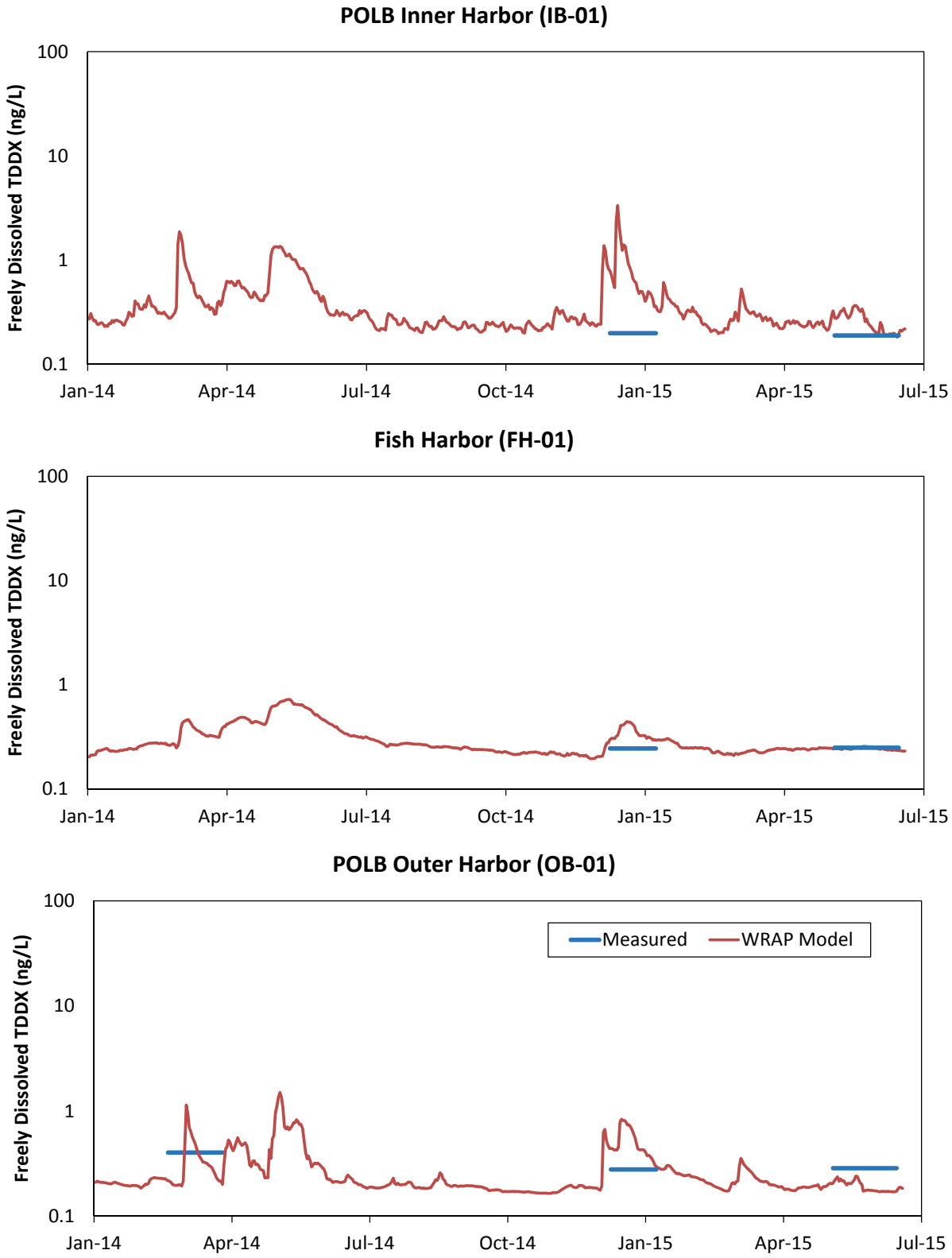

Figure 8.17b TDDX Time Series Comparisons - POLB Inner Harbor, Fish Harbor, and POLB Outer Harbor

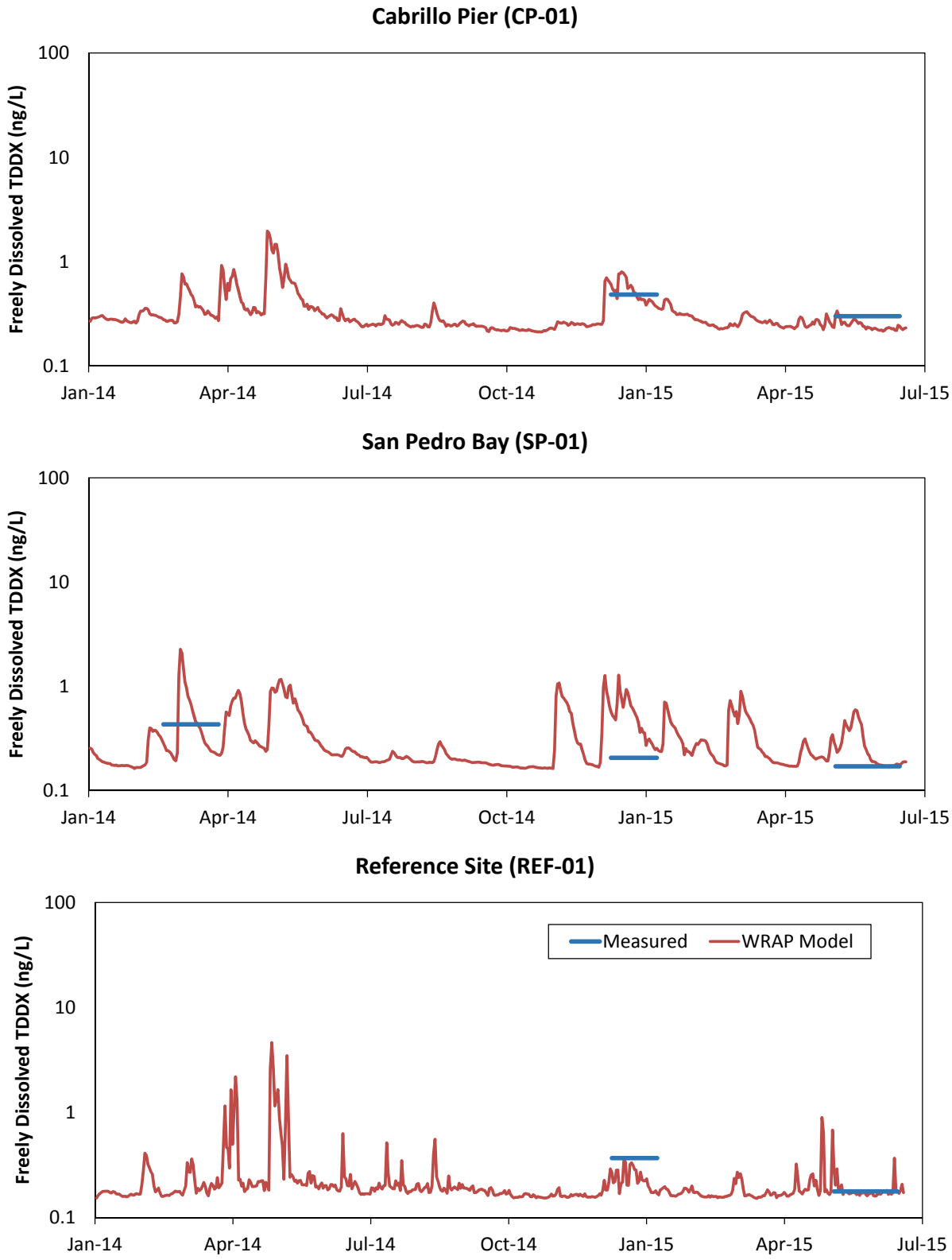

Figure 8.17c TDDX Time Series Comparisons - Cabrillo Pier, San Pedro Bay, and Reference Site

Table 8.12 Organic Chemical Calibration Comparisons for Fish Harbor and Reference Site

ORGANIC CHEMICAL	LOCATION	LDL STUDY PHASE	MEASURED (NG/L)	WRAP MODEL (NG/L)
TPCB	Fish Harbor (FH-01)	2	0.73	0.76
		3	0.91	0.88
	Reference Site (REF-01)	2	0.16	0.25
		3	0.16	0.16
TDDX	Fish Harbor (FH-01)	2	0.25	0.35
		3	0.25	0.25
	Reference Site (REF-01)	2	0.37	0.24
		3	0.18	0.18

Comparisons of the predicted average TPCB and TDDX concentrations over the sampling duration for each of the three phases at all calibration locations are provided in Figure 8.18 and Figure 8.19, respectively. In the figures, the measured concentrations are depicted by the blue bars with colored symbols to illustrate the range in measured concentrations. The orange, magenta, and green symbols correspond to measurements from Phases 1, 2, and 3, respectively. The WRAP Model average concentrations over the sampling period are indicated by the red bars. The black bar indicates the range in daily average concentrations over each sampling period shown in Figures 8.16 and 8.17. The comparisons in Figures 8.18 and 8.19 are arranged by locations from the inner harbor at CS to the ocean at REF. The sampling location labels indicate mid-water depth (-M) or bottom water depth (-B).

Comparisons at the FH and reference site calibration locations best illustrate the calibration of the mass transfer coefficient and ocean boundary, respectively. Comparisons at the other calibration locations demonstrate the overall calibration based on the combined effects of all organic processes. In general, the predicted TPCB and TDDX concentrations were comparable to the measured concentrations at most of the locations except for LARE. At this location, the average TPCB and TDDX are much higher than the measured concentrations, but the lower range in daily average concentrations, indicated by the black bars, extend to concentrations similar to the measured concentrations.

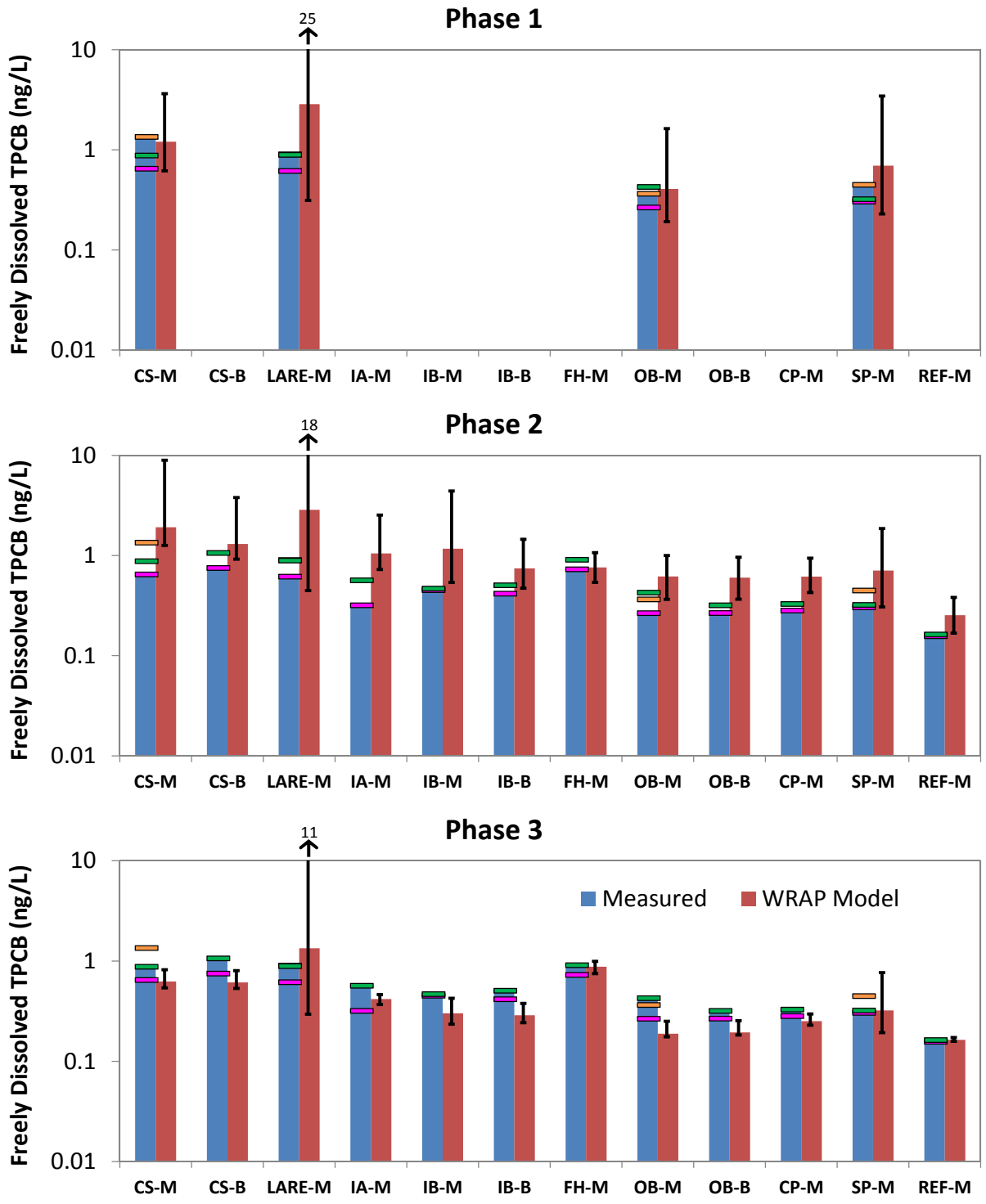

Figure 8.18 TPCB Comparisons

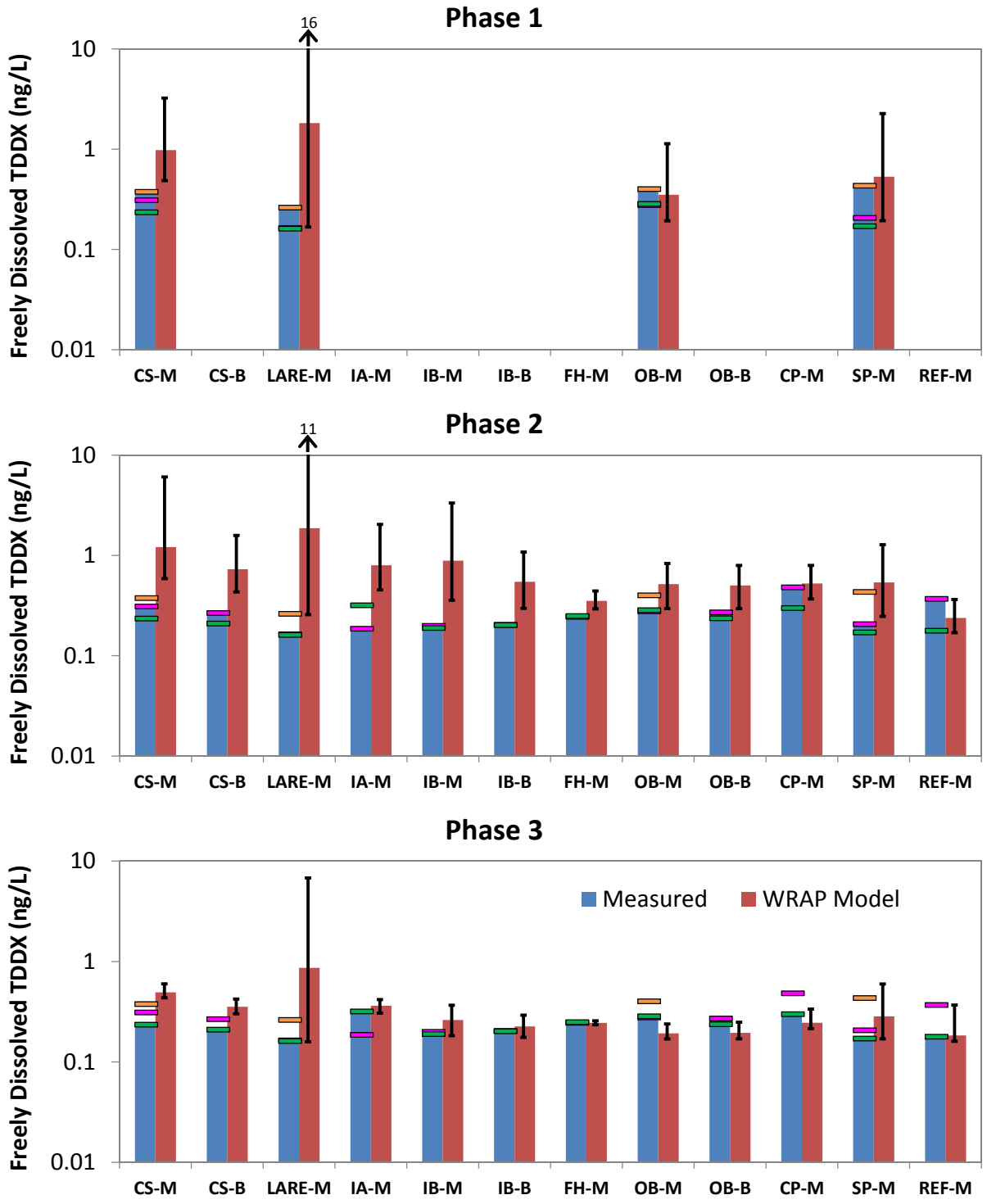

Figure 8.19 TDDX Comparisons

Higher predicted concentrations at LARE may be due to the uncertainty in the estimated watershed loading from the LAR Watershed. As described in Section 3.5, storm water organic concentrations are estimated based on correlation with TSS, the latter is represented by an averaged dry, wet and first flush concentrations. However, the data shows that TSS values for all these three periods can easily vary by more than an order of magnitude; hence, the LAR Watershed inputs can also vary by orders of magnitude. Further discussions of the uncertainty in the model results due to uncertainties in the watershed loadings, as well as other model inputs are provided in Section 9.

9. SENSITIVITY AND UNCERTAINTY ANALYSES

9.1 SENSITIVITY ANALYSIS

A sensitivity analysis was conducted to identify the model input parameters that have the most significant effect on model responses in organic water column and sediment bed concentrations. Ranges in model inputs and parameters were used to evaluate how changes in model inputs would affect model responses (i.e. change in predicted organic concentrations in the water and sediment bed). A sensitivity parameter (defined below) was used to compare the sensitivity of model responses to change in model inputs and rank the relative importance of these tested model input parameters. Based on the uncertainties of the most sensitive model input parameters, the range of potential model predicted organic concentrations are used in the bounding calibration of the bioaccumulation model.

Model inputs and parameters for sensitivity tests included: ocean boundary organic concentrations, initial sediment bed concentrations, watershed loadings, organic carbon partition coefficient (K_{poc}), particulate organic carbon (POC), and two model parameters – mass transfer and particle mixing coefficients. These model inputs and parameters represent model inputs for organic chemicals with the greatest ranges in the data or literature values. Ranges used for sensitivity tests of these model inputs and parameters are summarized in Table 9.1 and are based on the uncertainty in data or literature values. The rationale for selecting the minimum and maximum test values is summarized in Section 9.2.1.

Table 9.1 Ranges in Model Inputs for Sensitivity Analysis

MODEL INPUT	UNITS	RANGE FOR TPCB	RANGE FOR TDDX
Ocean Boundary	ng/L	0.0806 – 0.284	0.0719 – 0.608
Sediment Bed Concentration	ug/kg	½ to 2 times bed concentrations	
Watershed Loadings	kg	5.76 – 29.40	4.13 – 19.07
Organic Carbon Partition Coefficient (K_{poc})	Log L/kg	5.47 – 6.29	5.53 – 6.47
Particulate Organic Carbon (POC)	mg/L	0.013 – 1.09	
Mass Transfer Coefficient	cm/day	0.1 – 10	
Particle Mixing Coefficient	cm^2/yr	0.1 – 10	

The sensitivity analysis was conducted based on the WRAP Model calibration period. Two simulations for each model input were conducted using the high and low estimates shown in Table 9.1. The variation in the model input resulted in changes in the model response (i.e., water column concentrations and sediment bed concentrations). Model responses were evaluated based on the average water column and sediment bed concentrations over the 1.5 year calibration period within the fish movement zones used for the bioaccumulation model, as shown in Figure 9.1. Given the unique hydrodynamic and organic characteristics of each fish movement zone, it is expected that the sensitivity to model inputs will vary by fish movement zones.

The sensitivity of the model inputs was evaluated based on relative changes compared to the WRAP Model calibration simulation. A sensitivity parameter was used to enable comparisons of the effects among different model inputs, as well across the fish movement zones. The sensitivity parameter was defined as the ratio of the percent change in the model response to the percent change in the model input.

$$Sensitivity = \frac{|\%\ Change\ in\ Model\ Response|}{|\%\ Change\ in\ Model\ Input|}$$

For example, the ocean boundary concentration for TDDX was evaluated based on high and low estimates of 0.608 and 0.0719 ng/L, respectively. The high estimate is a 153% increase from the calibrated value of 0.240 ng/L. The corresponding model response within the Outside Harbor Exposure Area was found to result in a 103% increase in the water column concentration; hence a “sensitivity” of 0.67 (103%/153%). Similarly, the low estimate was a 70% decrease resulted in a 47% decrease in the water column concentration, i.e. a sensitivity of also 0.67 (47%/70%).

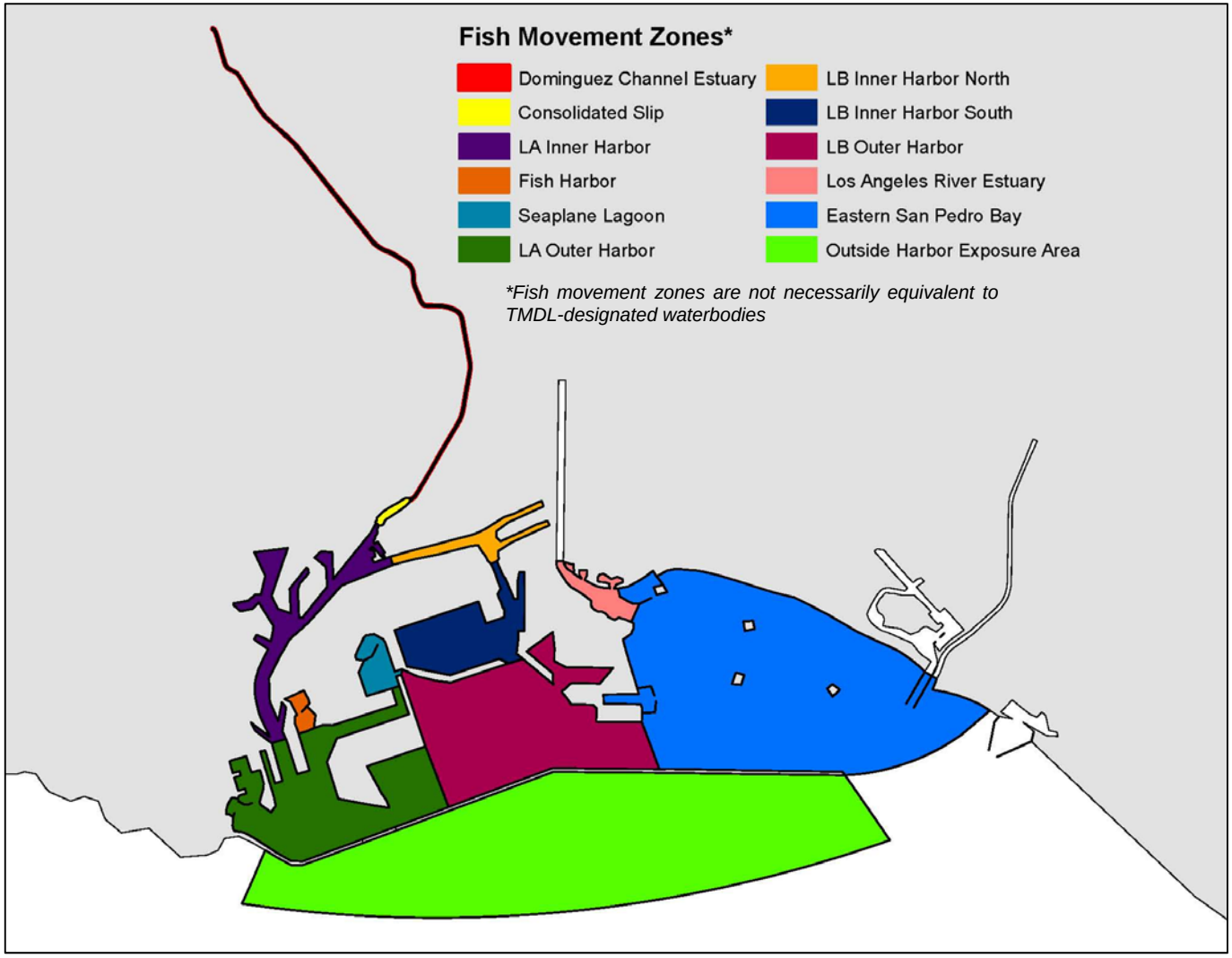

Figure 9.1 Fish Movement Zones for Linkage with Bioaccumulation Model

9.2 SENSITIVITY TEST RESULTS

9.2.1 Sensitivity by Model Inputs

Ocean Boundary

The ocean boundary concentrations were calibrated based on the LDL Study measured concentrations at REF-01, located just outside the harbor breakwater. For the sensitivity analysis, the range in ocean boundary concentrations was established based on the uncertainty in measured concentrations taken outside of the harbor, which is provided in Section 9.3.1.

The sensitivity of the ocean boundary on the model responses is shown in Figure 9.2. In the figure, the sensitivity in the fish movement zones for the freely dissolved water column concentrations and sediment bed concentrations is shown in the top and bottom panels, respectively. By definition, the sensitivity parameter is always positive; a negative sign was used in the figure for the sensitivity response to decreasing model inputs.

Changes in the model responses are only noticeable for the water column concentrations but not the sediment bed concentrations. As expected, the sensitivity of the water column concentrations to the ocean boundary concentrations varies by fish movement zone. The greatest sensitivity to ocean boundary concentrations occurs in the Outside Harbor Exposure Area located closest to the model ocean boundary, followed by the LA and LB Outer Harbors. In general, the sensitivity to the ocean boundary corresponds the relative distance from the model ocean boundary with least impacts observed furthest away from the model ocean boundary (e.g., DC Estuary, CS, and LARE).

Sediment Bed Concentration

The sediment bed concentrations represent ongoing and historical deposition of organic chemicals. As discussed previously in Section 8.2, the initial sediment bed concentrations required utilizing sediment data from multiple studies to provide sufficient spatial coverage throughout the LA/LB Harbor and San Pedro Bay. Sediment bed concentrations vary by up to three orders of magnitude across each fish movement zone, which is discussed in Section 9.3.2. To evaluate the sensitivity of the model response to the initial sediment bed concentrations, the initial bed concentrations were varied from one-half to two times the value of the initial sediment bed concentrations.

The sensitivity of sediment bed concentrations to model responses is provided in Figure 9.3. As expected, sensitivity parameters for the sediment bed concentrations are 1.0 since the change in model inputs were directly specified for the sediment bed concentrations.

Figure 9.2 WRAP Model Sensitivity for Ocean Boundary

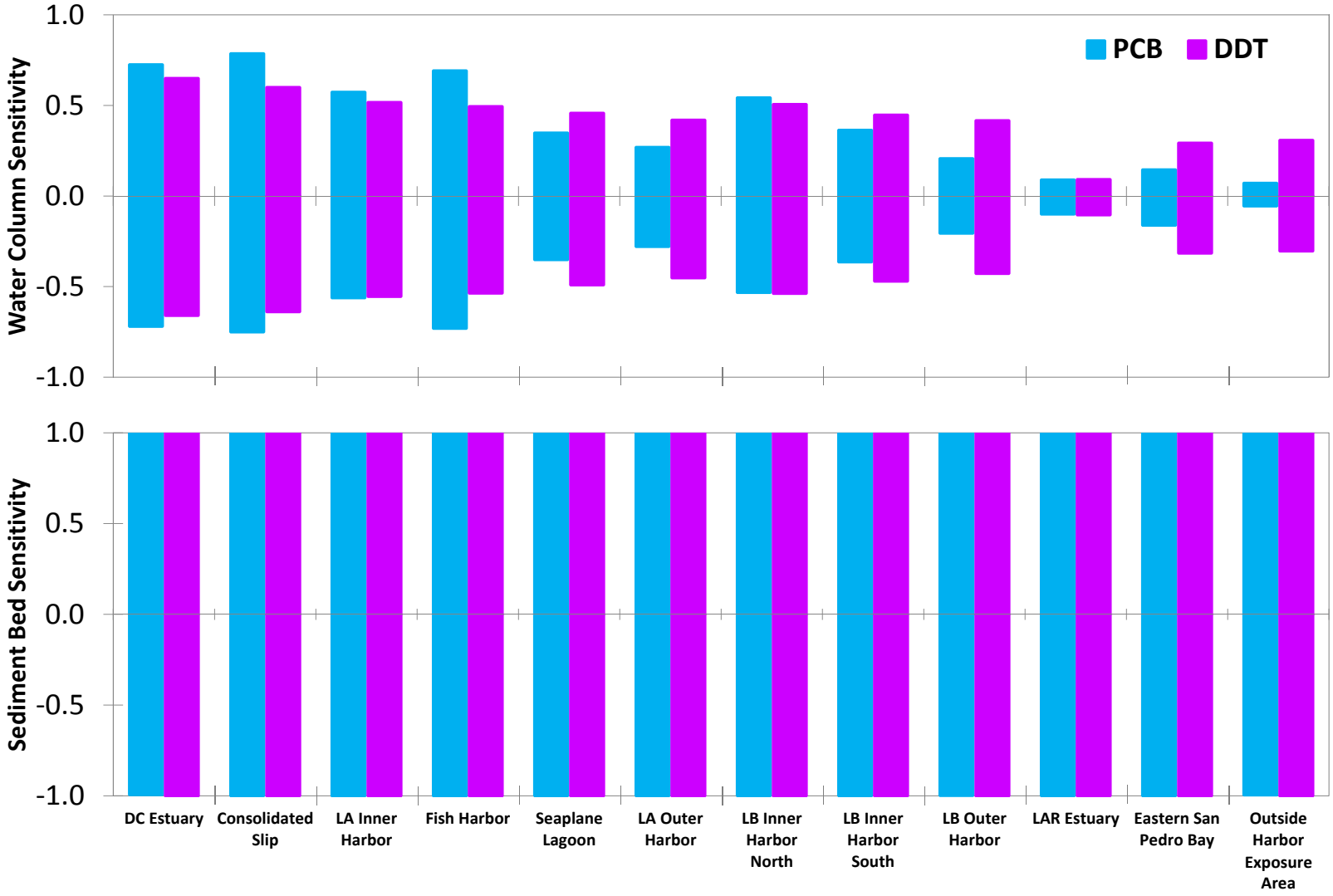

Figure 9.3 WRAP Model Sensitivity for Sediment Bed Concentrations

Thus, the sediment bed sensitivity due to the input sediment bed concentrations is shown for completeness, but was not considered when evaluating the sediment bed sensitivity. In the water column, the sensitivity of sediment bed concentrations varied by fish movement zone. Areas most sensitive to sediment bed concentrations were the DC Estuary, CS, and FH.

Watershed Loadings

Organic chemical watershed loadings were estimated based on correlations between TSS and organic concentrations, as previously discussed in Section 3.5. General storm water data indicated very strong correlations (R^2) of 0.996 and 0.95 for TPCB and TDDX, respectively. The range in watershed loadings for the sensitivity analysis was determined based on the uncertainty of the TSS estimates. The uncertainty of the TSS and organic chemical concentrations are discussed in Section 9.3.1.

Since the spatial distribution of watershed loadings differs for each fish movement zone, the percent change in model input was varied by fish movement zone for the sensitivity tests. Some fish zones receive direct discharges from the one of the watersheds—for example, CS receives loadings directly from the DC Watershed; while other fish zones receive indirect inputs from multiple watersheds—for example, LB likely receives indirect input of loadings from all four watersheds. The watershed loading sensitivity for the LARE fish zone was determined based on the watershed loadings for the LAR only. For the Eastern San Pedro Bay fish movement zone, the watershed loading sensitivity was calculated based on the combined watershed loadings from the LAR and SGR watersheds, which discharge into San Pedro Bay. Watershed loadings from the DC watershed were used for the DC Estuary, CS, LA Inner Harbor, and LB Inner Harbor North fish movement zones. Changes based on the total watershed loadings were used to calculate the sensitivities for the remaining fish movement zones.

The WRAP Model sensitivity to watershed loadings is illustrated in Figure 9.4. The sensitivity to watershed loadings varied for each fish movement zone. The highest sensitivity to water column concentrations was shown for the LARE fish movement zone, corresponding to the highest watershed loadings from the LAR. The next highest sensitivity was observed for Eastern San Pedro Bay, followed by the DC Estuary and CS. Effects of the watershed loadings on sediment bed concentrations were primarily observed for the DC Estuary and LARE and to a lesser extent in the CS.

Figure 9.4 WRAP Model Sensitivity for Watershed Loadings

Organic Carbon Partition Coefficient

The organic carbon partition coefficients (K_{poc}) were determined from the LDL Study Phase 1 data. The K_{poc} was specified as the average value from the four Phase 1 sampling locations, as previously shown in Table 8.6. For the sensitivity analysis, the range in K_{poc} was determined based on the minimum and maximum values of the measured partition coefficients. Decreases in K_{poc} will result in higher freely dissolved concentrations due to the decrease in partitioning to the particulate phase. Conversely, increases in K_{poc} results in lower freely dissolved concentrations.

Sensitivities of the organic carbon partition coefficients are provided in Figure 9.5, which shows that LARE is the most sensitive to K_{poc}, followed by the POLB Inner Harbor. No effects of the water column K_{poc} were observed for the sediment bed concentrations.

Particulate Organic Carbon

Average POC concentrations at the sampling locations were utilized as the model input for water column POC concentrations. The range in POC used for sensitivity test was specified as the minimum and maximum measured POC from each location, representing the uncertainty in the POC data. The ranges in POC data are provided in Section 9.3.1. POC and freely dissolved concentrations are inversely proportional, thus lower POC values result in higher freely dissolved concentrations. For the sensitivity parameter, the percent change in model input was determined based on the average POC concentration in each fish movement zone.

Results of the sensitivity analysis for the water column particulate organic carbon are shown in Figure 9.6. The model responses to POC were similar to K_{poc} with the greatest sensitivity in water column concentrations shown for the LARE and POLB Inner Harbor and no changes in sediment bed concentrations.

Mass Transfer Coefficient

The mass transfer coefficient controls the flux between the sediment bed and water column. This model parameter for TPCB and TDDX were calibrated based on the LDL Study measured concentrations in FH. The range in the mass transfer coefficient for the sensitivity analysis was based on the range in literature values of 0.1 to 10 cm/day for both TPCB and TDDX, which was previously discussed in Section 8.5.1.

The sensitivity for the mass transfer coefficients are shown in Figure 9.7. The most sensitive fish movement zone based on the water column and sediment bed concentrations is FH, which illustrates the importance of the sediment-water exchange in FH. In addition, the sensitivity for TPCB was higher compared to TDDX due to the higher mass transfer coefficient of TPCB.

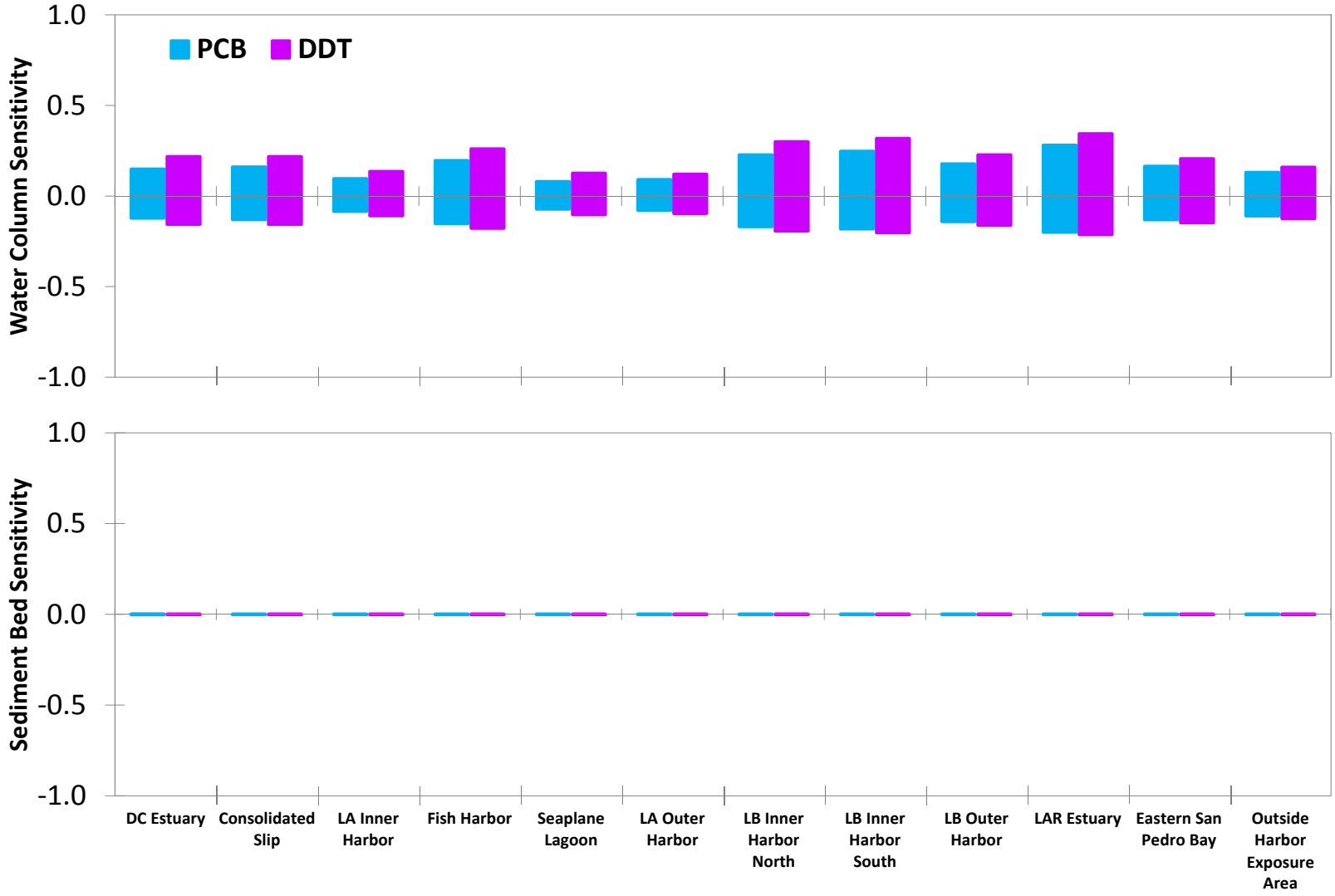

Figure 9.5 WRAP Model Sensitivity for Organic Carbon Partition Coefficient

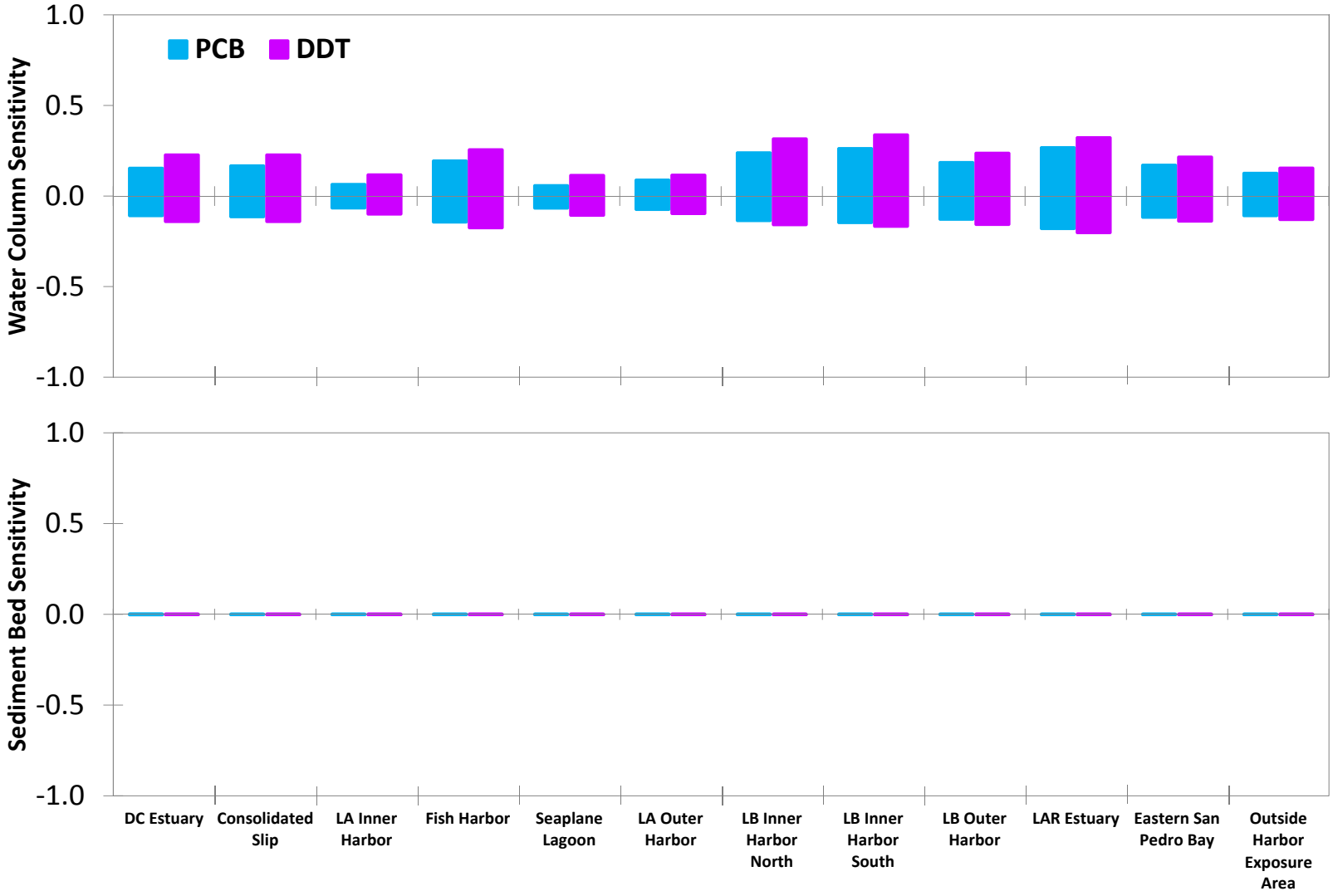

Figure 9.6 WRAP Model Sensitivity for Particulate Organic Carbon

Figure 9.7 WRAP Model Sensitivity for Mass Transfer Coefficient

Particle Mixing Coefficient

The particle mixing coefficient accounts for mixing within the sediment bed. For the sensitivity analysis, the particle mixing coefficient for both TPCB and TDDX was evaluated from 0.1 to 10 cm^2/yr based on literature values, as discussed previously in Section 8.5.2.

Sensitivities of the water column and sediment bed concentrations for the particle mixing coefficient are provided in Figure 9.8. The most sensitive fish movement zones were the DC Estuary and CS for both model responses.

9.2.2 Sensitivity by Fish Movement Zone

The sensitivity of model responses to the test model inputs were also evaluated by fish movement zones, as shown in Figures 9.9 and 9.10 for the water column and sediment bed concentrations, respectively. In the figures, each panel compares the sensitivity for the seven model inputs for that particular fish movement zone. The relative importance of model inputs differed among the fish movement zones. Overall, the changes in model response were greater for water column concentrations compared to sediment bed concentrations. In general, the water column concentrations showed the greatest sensitivity to the ocean boundary, sediment bed concentration, and watershed loadings. For the sediment bed concentrations, changes in model responses were only observed for the watershed loadings, mass transfer coefficient, and particle mixing coefficient.

DC Estuary

For the DC Estuary, water column concentrations are most sensitive to sediment bed concentration, followed by watershed loadings, whereas sediment bed concentrations are most sensitive to the watershed loadings and particle mixing coefficient. Based on the sensitivity analysis, organic concentrations in the DC Estuary are most affected by historical sediment bed concentrations, as well as on-going watershed loadings that deposit in the sediment bed.

Consolidated Slip

In the CS fish movement zone, TPCB water column concentrations are most sensitive to sediment bed concentrations and the organic carbon partition coefficient. TPCB sediment bed concentrations are primarily affected by the mass transfer and particle mixing coefficients, followed by watershed loadings. For TDDX, water column concentrations are most sensitive to the sediment bed concentrations and watershed loadings, while sediment bed concentrations are impacted by watershed loadings and the particle mixing coefficient.

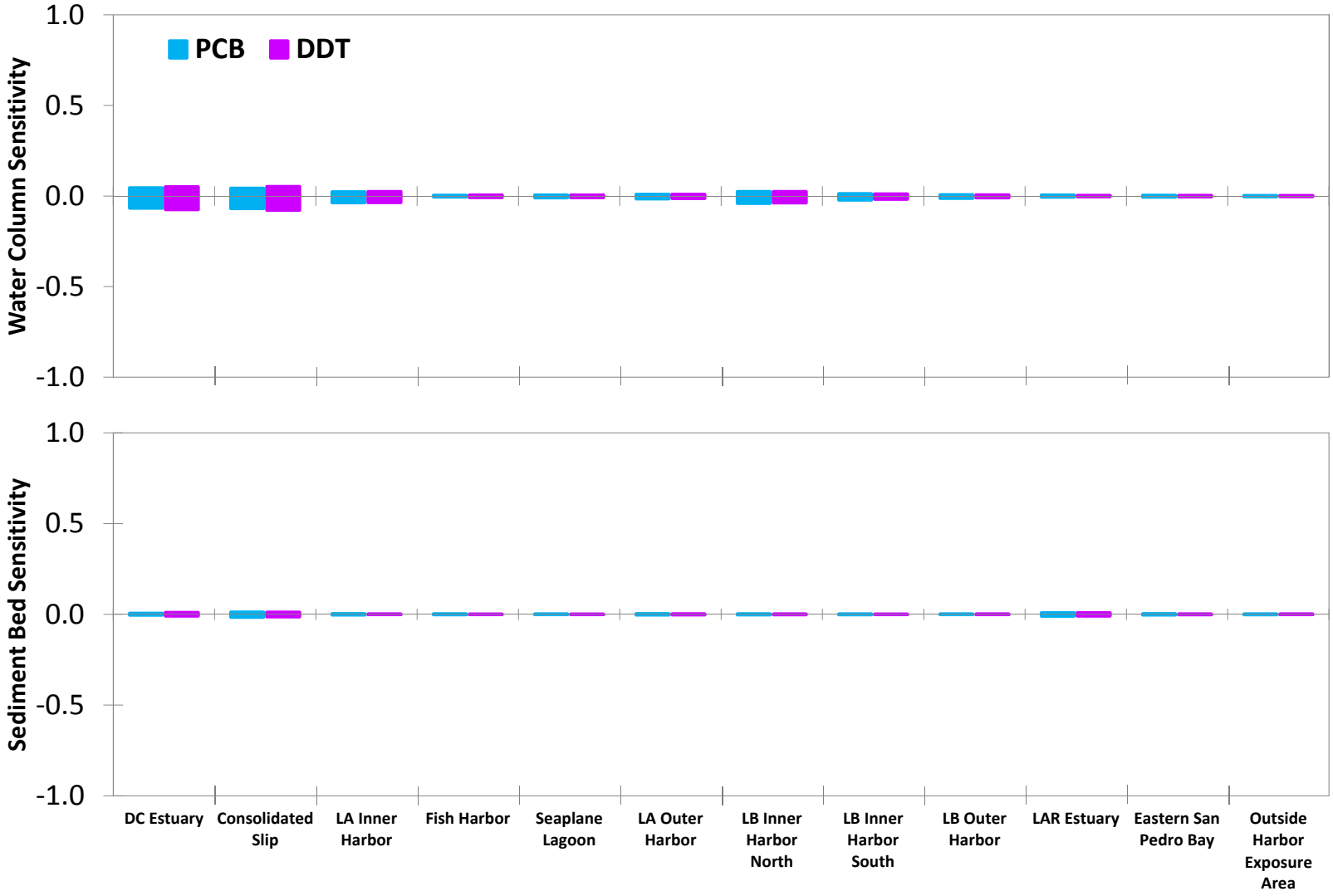

Figure 9.8 WRAP Model Sensitivity for Particle Mixing Coefficient

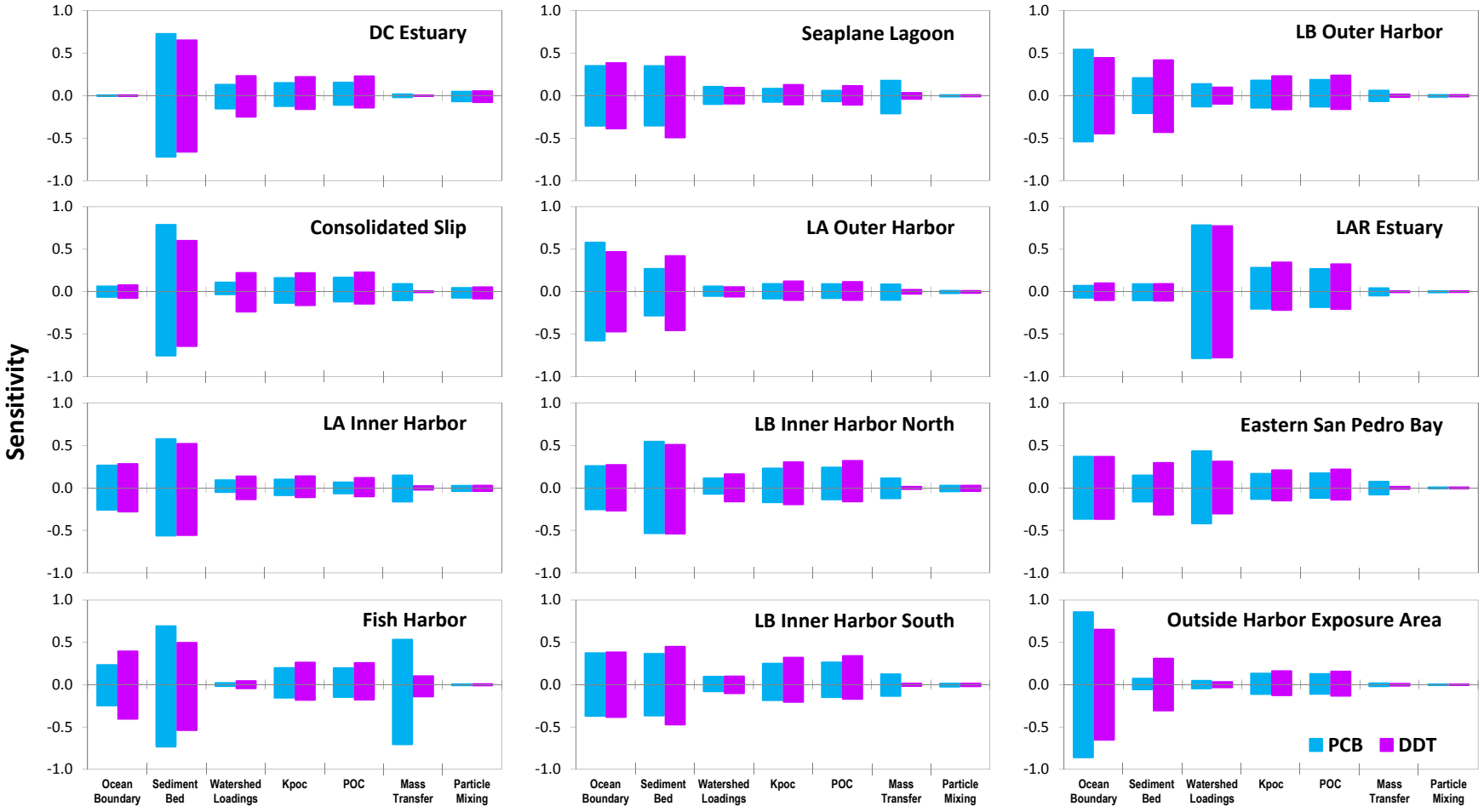

Figure 9.9 WRAP Model Water Column Sensitivity by Fish Movement Zone

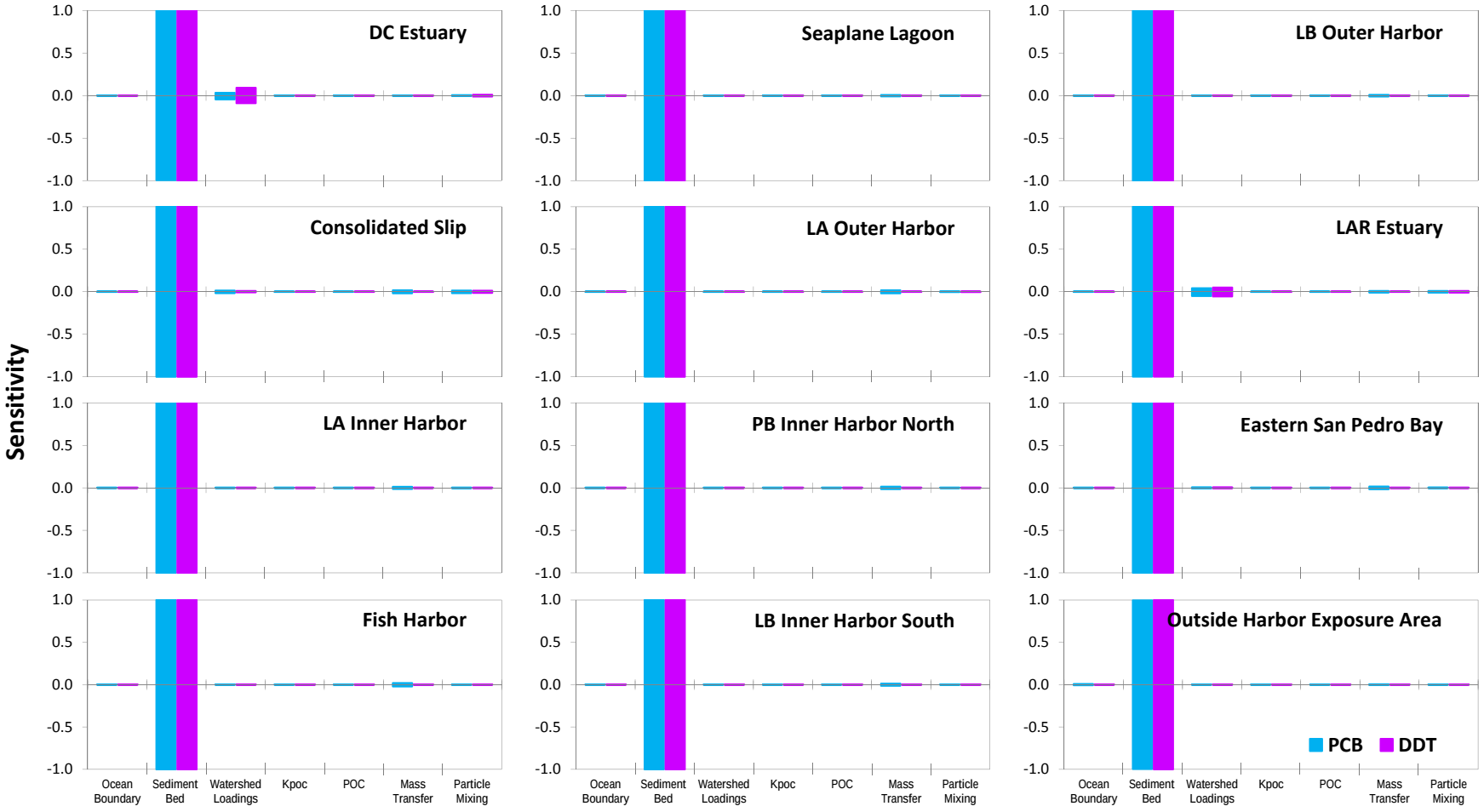

Figure 9.10 WRAP Model Sediment Bed Sensitivity by Fish Movement Zone

LA Inner Harbor

Water column concentrations are most affected by the sediment bed and ocean boundary concentrations in the LA Inner Harbor. Sensitivity to sediment bed concentrations was only observed for the TPCB mass transfer coefficient. The sensitivity analysis indicates organic concentrations are predominantly affected by sediment bed and ocean boundary concentrations in the LA Inner Harbor.

Fish Harbor

In FH, TPCB water column concentrations are most affected by sediment bed concentrations and mass transfer coefficient. TDDX water column concentrations are predominantly affected by sediment bed and ocean boundary concentrations. Differences between TPCB and TDDX are attributed to the higher sediment bed concentrations and mass transfer coefficient for TPCB. Responses to sediment bed concentrations were only observed for mass transfer coefficient for TPCB. Overall, the sensitivity analysis suggests organic concentrations in FH are predominantly controlled by sediment bed concentrations.

Seaplane Lagoon

Organic concentrations are most sensitive to the ocean boundary and sediment bed concentrations in Seaplane Lagoon. Effects to sediment bed concentrations were only observed for the mass transfer coefficient for TPCB.

LA Outer Harbor

For the LA Outer Harbor, the model is most sensitive to the ocean boundary concentrations, followed by the sediment bed concentrations. Effects to sediment bed concentrations were only observed for the TPCB mass transfer coefficient.

LB Inner Harbor North

The most sensitive model input for the LB Inner Harbor North was determined to be the sediment bed concentration with the ocean boundary as the next most sensitive model input. Minor effects to sediment bed concentrations were found for the TPCB mass transfer coefficient.

LB Inner Harbor South

The ocean boundary and sediment bed concentrations were the most sensitive model inputs for the LB Inner Harbor South. Again, only minor effects to sediment bed concentrations were found for the TPCB mass transfer coefficient.

LB Outer Harbor

In the LB Outer Harbor, the ocean boundary and sediment bed concentrations were the most sensitive model inputs. Effects to sediment bed concentrations were only observed for the mass transfer coefficient for TPCB.

LAR Estuary

For the LAR Estuary fish movement zone, watershed loadings were found to have the greatest impact on both the water column and sediment bed concentrations. The organic partition coefficient was the next most important model input.

Eastern San Pedro Bay

The most sensitive model inputs were found to be the watershed loadings and ocean boundary for Eastern San Pedro Bay. The most sensitive model inputs to sediment bed concentrations were watershed loadings and mass transfer coefficient.

Outside Harbor Exposure Area

In the Outside Harbor Exposure Area, the ocean boundary was the most sensitive model input, which corresponds to the greatest sensitivity among all the fish movement zones. The next most sensitive model input was K_{poc} for TPCB and sediment bed concentration for TDDX. Effects to sediment bed concentrations were only observed for the mass transfer coefficient for TPCB.

Summary

The two most sensitive model inputs to model-predicted water column concentrations were identified for each fish zone and summarized in Figure 9.11. In the figure, the two most sensitive model inputs for each fish zone are indicated by two circles – blue for PCB and red for DDT. As shown in the figure, the most sensitive model inputs for the WRAP Model are the ocean boundary, sediment bed concentrations, and watershed loadings. These model inputs correspond to the three most important processes that were identified in the CSM – tidal exchange, sediment-water exchange, and watershed loadings.

Fish Movement Zone	Ocean Boundary	Sediment Bed	Watershed Loadings	Kpoc	POC	Mass Transfer	Particle Mixing
DC Estuary							
Consolidated Slip							
LA Inner Harbor							
Fish Harbor							
Seaplane Lagoon							
LA Outer Harbor							
LB Inner Harbor North							
LB Inner Harbor South							
LB Outer Harbor							
LAR Estuary							
Eastern San Pedro Bay							
Outside Harbor							

Figure 9.11 WRAP Model Sensitivity Rankings of Model Inputs

9.3 UNCERTAINTY ANALYSIS

The uncertainty analysis was conducted to assess the variation in model predictions attributed to uncertainties in the WRAP Model inputs that were determined based on field data; these include: ocean boundary organic concentrations, initial sediment bed concentrations, watershed loadings, organic carbon partition coefficient and particulate organic carbon. These model inputs showed the greatest ranges in the data and correspond to the most sensitive parameters from the sensitivity analysis. The effect of the uncertainty in the field data to model response was evaluated based on the calibration comparisons, and the uncertainties in the WRAP Model predictions were considered in the bounding calibration of the bioaccumulation model (Anchor QEA 2016).

9.3.1 Uncertainty in Model Inputs

Ocean Boundary

The ocean boundary represents the background concentration outside the harbor. The uncertainty in the ocean boundary was selected from measured concentrations taken outside the harbor, as summarized in Table 9.2. In the table, measured freely dissolved concentrations were converted to TPCB and TDDX based on data from the LDL Study REF sampling location. Water column concentrations from the Palos Verdes Shelf were taken in 2010 (Fernandez et al. 2012). Total PCB concentrations in the vicinity of the outfall ranged from 0.145 to 0.510 ng/L. Total DDX concentrations near the outfall varied from 0.0719 to 2.035 ng/L. From the same study, background concentrations taken about 24 km southeast of the outfall measured concentration of 0.0806 and 0.0719 ng/L for TPCB and TDDX, respectively. Water column concentrations measured just outside the harbor during the LDL Study showed concentrations ranging from 0.241 to 0.284 ng/L for TPCB and 0.340 to 0.608 ng/L for TDDX. Based on measurements taken outside the harbor, the uncertainty for the ocean boundary ranged from the lowest, background concentrations to the maximum measured just outside the harbor at the LDL reference site (REF-01).

Table 9.2 Measurements of Water Column Concentrations Outside of Harbor

LOCATION	TOTAL PCB (NG/L)	TOTAL DDX (NG/L)
Palos Verdes Shelf	0.145 – 0.510	0.0719 – 2.035
Background	0.0806	0.0719
REF-01	0.241 – 0.284	0.340 – 0.608

**Measured data for freely dissolved concentrations converted to total*

Sediment Bed Concentration

As discussed previously in Section 8.2, initial sediment bed concentrations were determined using sediment data from multiple studies conducted between 2002 and 2014. It was shown in Section 8.2 that sediment bed concentrations vary widely throughout the harbor. Ranges in sediment bed concentrations in each fish movement zone are summarized in Table 9.3. Sediment bed concentrations vary from one to three orders of magnitude in each zone. To represent the possible range in sediment bed concentrations for the uncertainty analysis, bed concentrations were varied from half to two times the value of the measured sediment bed concentrations.

Table 9.3 Range of Sediment Bed Concentrations

FISH MOVEMENT ZONE	TPCB (UG/KG)	TDDX (UG/KG)
LA Outer Harbor	0.80 – 92.9	1.12 – 161
LA Inner Harbor	1.10 – 2,370	0.64 – 2,048
Consolidated Slip (CS)	6.80 – 16,800	3.80 – 1,922
LB Inner Harbor North	1.10 – 105	2.40 – 56.1
LB Inner Harbor South	1.00 – 611	0.50 – 77.8
LB Outer Harbor	0.90 – 52.7	0.60 – 93.1
Fish Harbor (FH)	6.10 – 812	1.90 – 285
Seaplane Lagoon	16.4 – 23.8	0.90 – 24.1
Eastern San Pedro Bay	0.10 – 207	1.00 – 63.2
LAR Estuary	207*	47.3*
Outside Harbor Exposure Area	1.28 and 13.9**	10.3 and 449**
DC Estuary	5.4 – 2,270	9.3 – 2,539

* *Concentrations for LARE based on nearest data in San Pedro Bay*
** *Two average concentrations used to define ocean bed concentrations*

Watershed Loadings

Organic chemical watershed loadings were estimated based on correlations between TSS and organic concentrations, as previously discussed in Section 3.5. General storm water data indicated very strong correlations for TPCB and TDDX with TSS, but TSS data showed significant variability about the mean TSS concentrations. Given there is little correlation between TSS and flow, the TSS concentration is likely a stochastic process with random variability, resulting in uncertainty in the TSS estimates. Thus, the range in watershed loadings was determined based on the uncertainty in the sediment loading estimates.

The uncertainty in the sediment loading estimates was established based on the probability distributions of the TSS data. The uncertainty ranges of the seasonal average concentrations (i.e., low and high TSS concentrations) were determined as plus and minus one standard deviation. This corresponds to the 16^{th} and 84^{th} quantiles of the probability distribution. Most of the TSS data followed a log-normal distribution, with a few exceptions in

which the data fits better with a normal distribution. In Figure 9.12, the TSS data for LAR is used as an example to show the use of the probability distributions of the data to evaluate the uncertainty of the data. In the figure, the top left panel shows a scatter plot of the TSS data with solid lines indicating the seasonal average concentrations. The other panels contain the distribution of TSS data for the dry, first flush, and wet weather. In each panel, the red line shows either a log-normal or normal distribution based on the mean and standard deviation of the data. The mean of the data is indicated by the solid-black line, while the uncertainty range is shown by the dashed-black line. A summary the seasonal average TSS uncertainty ranges is provided in Table 9.4.

Table 9.4 Seasonal Average TSS Uncertainty Ranges

LOCATION	DRY WEATHER (MG/L)	FIRST FLUSH (MG/L)	WET WEATHER (MG/L)
Los Angeles River (LAR)	12 – 96	330 – 1,751	77 – 471
Coyote Creek (CC)	5 -72	369 – 1,431	53 – 316
Dominguez Channel (DC)	6 – 67	222 – 725	60 – 204
Torrance Lateral	17 – 56	402 – 914	42 – 336
Port Land Uses	2 - 31	24 – 183	20 – 163
Machado Lake	--	--	6 – 26

Organic Carbon Partition Coefficient

The organic carbon partition coefficients (K_{poc}) were determined from the LDL Study Phase 1 data. The K_{poc} was specified as the average value from the four Phase 1 sampling locations, as previously shown in Table 8.6. The uncertainty in K_{poc} was determined based on the minimum and maximum values. The Log K_{poc} for TPCB ranged from 5.47 to 6.29 L/kg. The Log K_{poc} for TDDX ranged from 5.53 to 6.47 L/kg.

Particulate Organic Carbon

Water column POC concentrations were collected throughout the LDL Study during deployment and retrieval of SPME instruments. The uncertainty range in POC was specified as the minimum and maximum measured POC from each location, as summarized in Table 9.5.

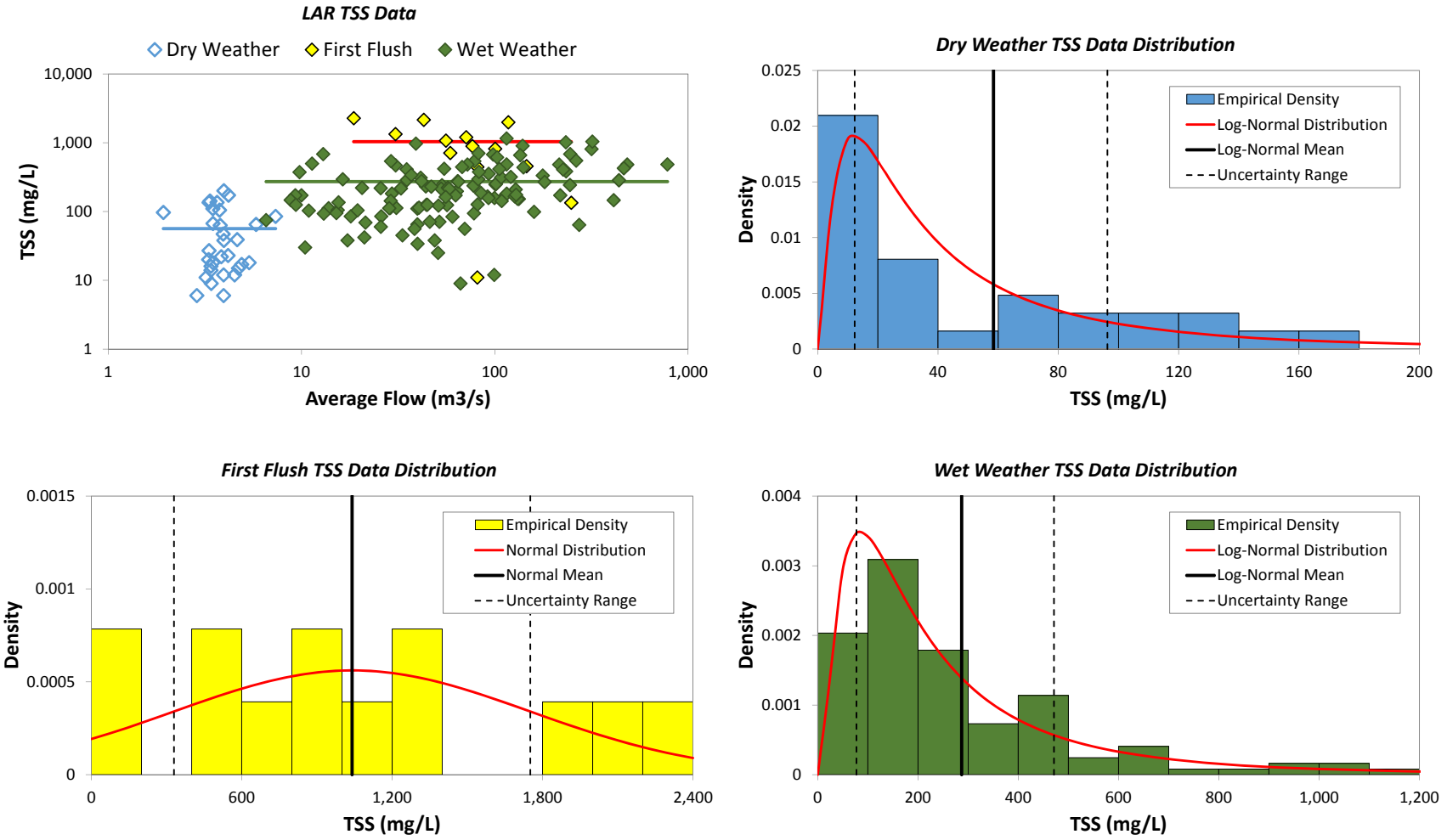

Figure 9.12 Probability Distributions of TSS Data for Los Angeles River

Table 9.5 Particulate Organic Carbon Uncertainty Ranges

LOCATION	SAMPLE ID	MINIMUM POC (MG/L)	MAXIMUM POC (MG/L)
Cabrillo Pier (CP)	CP-01	0.0128	0.1912
Consolidated Slip (CS)	CS-01	0.0150	0.7253
Fish Harbor (FH)	FH-01	0.0963	0.6438
POLA Inner Harbor	IA-01	0.1040	0.2353
POLB Inner Harbor	IB-01	0.0209	1.0855
LARE	LARE-01	0.1940	1.0200
POLB Outer Harbor	OB-01	0.0199	0.4618
Reference Site	REF-01	0.0751	0.2865
San Pedro Bay	SP-01	0.0182	0.3507

9.3.2 Uncertainty Analysis for WRAP Model Calibration

For the uncertainty analysis, the calibration period was repeated with the uncertainty ranges in the model inputs, as discussed previously in Section 9.3.1. The resulting model responses produce an upper and lower bounds in water column concentrations attributed to uncertainties in the model inputs. Ranges in the model inputs are summarized in Table 9.6. The lower bound model inputs were selected to determine the lower estimates of organic concentrations due to the uncertainty in the model inputs. Model inputs for the ocean boundary, sediment bed concentrations, and watershed loadings were based on the lower estimates. For the lower bound, model inputs for the organic carbon partition coefficients and POC were based on the higher estimates since these inputs are inversely proportional to the freely dissolved organic concentrations. In other words, higher values result in lower freely dissolved organic concentrations. Likewise, the higher bound model inputs were selected to determine the higher estimates of organic concentrations. For the higher bound, model inputs for the ocean boundary, sediment bed concentrations, and watershed loadings were based on the higher estimates. The organic carbon partition coefficients and POC were based on the lower estimates, which results in higher freely dissolved organic concentrations.

Table 9.6 Ranges in Model Inputs for Uncertainty Analysis

MODEL INPUT	UNITS	LOWER BOUND	HIGHER BOUND
Ocean Boundary	ng/L	TPCB = 0.0806 TDDX = 0.0719	TPCB = 0.284 TDDX = 0.608
Sediment Bed Concentration	ug/kg	½ bed concentrations	2 x bed concentrations
Watershed Loadings	kg	TPCB = 5.76 TDDX = 4.13	TPCB = 29.40 TDDX = 19.07
Organic Carbon Partition Coefficient (K_{poc})	Log L/kg	TPCB = 6.29 TDDX = 6.47	TPCB = 5.47 TDDX = 5.53
Particulate Organic Carbon (POC)	mg/L	0.1912 – 1.0855	0.0128 – 0.194

The upper and lower range in model predicted water column concentrations were compared to the organic calibration data to illustrate that the uncertainty in the WRAP Model predictions encompasses the measured organic chemical concentrations. The WRAP Model calibration uncertainty for TPCB and TDDX are shown in Figures 9.13 and 9.14, respectively. In the figure, model-predicted freely dissolved concentrations are compared to the measured data for the three phases of the LDL Study. The measured data are shown by the blue bars with black bars to indicate the range in the data. The WRAP Model calibration concentrations are shown by the red bars with green and yellow bars indicating the upper and lower bounds in concentrations due to the uncertainty in the model inputs. For Phase 1, the TPCB calibration was consistent with the measured concentrations except for LARE. However, the lower estimate is shown to be similar to the measured concentrations. Similarly for Phase 2, the WRAP Model TPCB lower bound generally corresponds to the measured concentrations. However for Phase 3, the TPCB upper bound matches the measured concentrations.

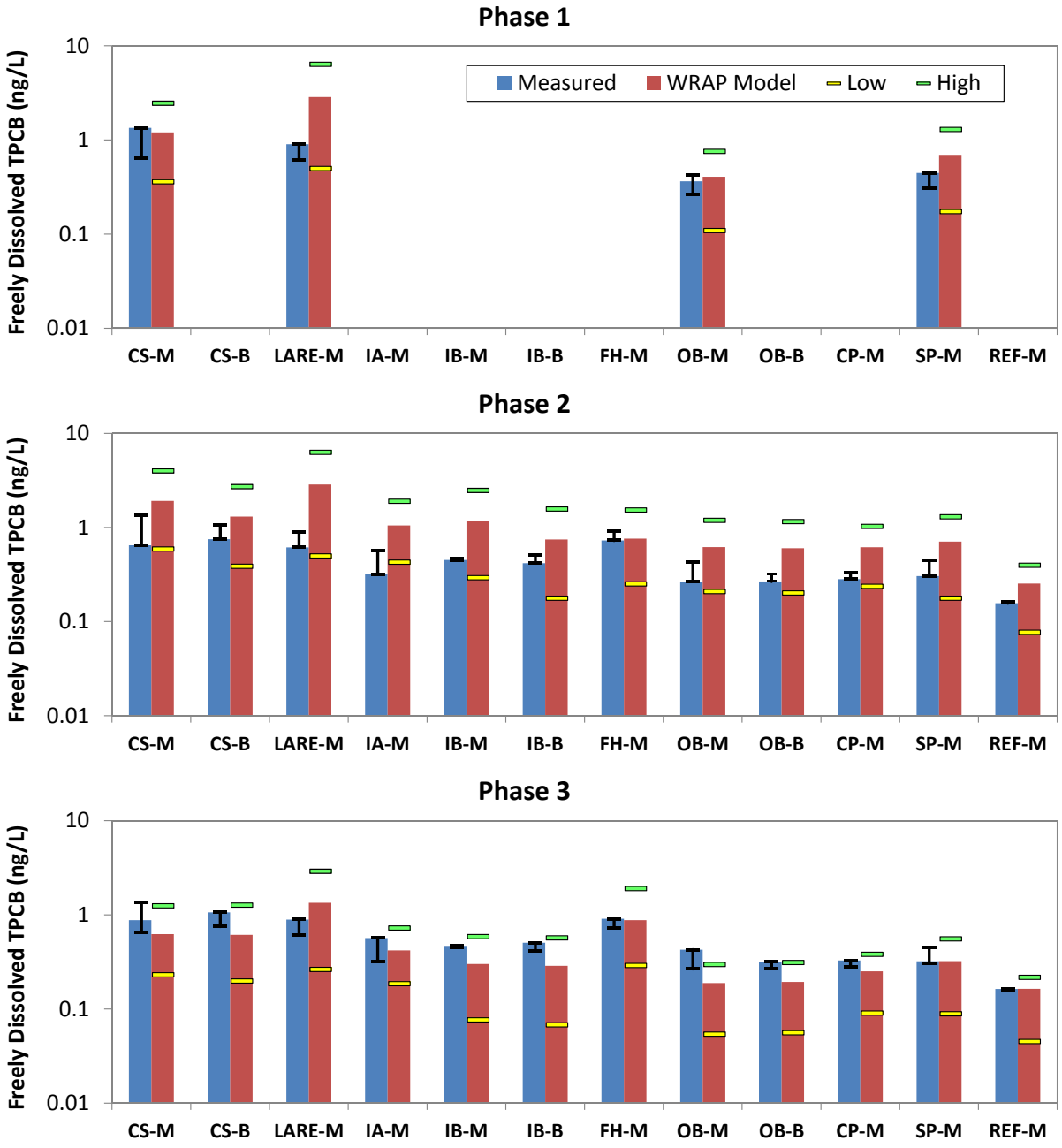

Figure 9.13 WRAP Model Calibration Uncertainty for TPCB

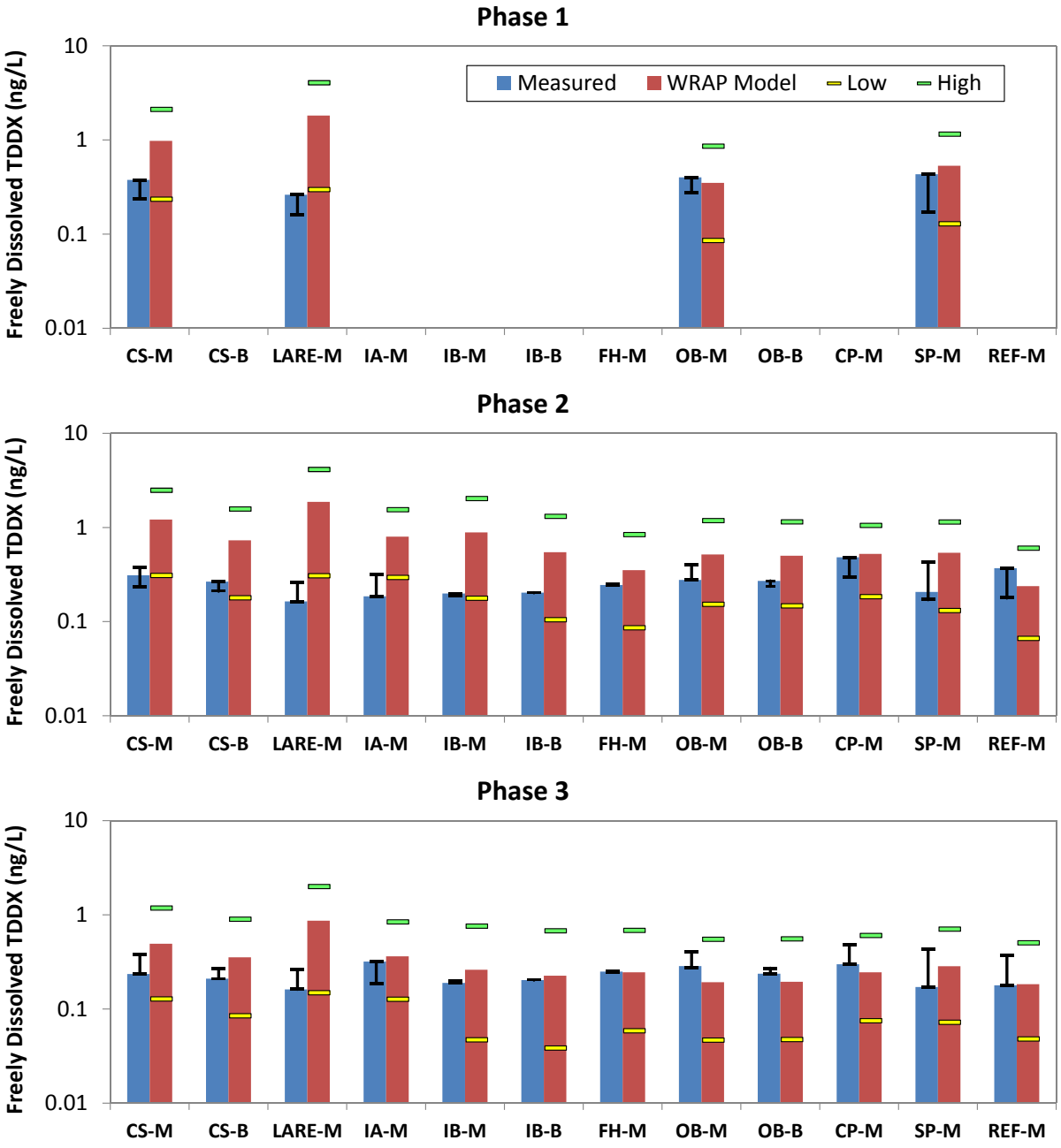

Figure 9.14 WRAP Model Calibration Uncertainty for TDDX

For TDDX, the measured concentrations generally fall in between the WRAP Model upper and lower predicted concentrations. In general, the range in model-predicted concentrations cover the range in measured concentrations for both TPCB and TDDX, thus illustrating that the WRAP Model predictions are within the uncertainties of the input data. For some comparisons, the lower bound provided a better match to the measured concentration, while other comparisons the upper bound provided a better match.

The WRAP Model inputs were estimated from best available data and averages used to represent inputs that may vary temporally such as watershed loadings. However, the methodologies for estimating model inputs were not adjusted to match the measured data to avoid any bias, given that the measured data only provides a comparison for a limited time period. For example at LARE, the overestimated model predictions are most likely attributed to watershed loading estimates since this area is most sensitive to watershed loadings. The comparisons with measured concentrations indicate the low estimate of watershed loadings best represent loadings during the Phase 1 and 2 comparison periods, but not Phase 3. Although, the watershed loadings for individual rain events during each comparison period could be adjusted to provide for a better match with the measured data, there would be no justification for adjusting watershed loadings outside of the data comparison periods.

10. SUMMARY

The LA/LB Harbor and San Pedro Bay is an extremely complex system comprised of estuarine and coastal waters with continuous anthropogenic activities. This report documents the development of the WRAP Model – a 3D hydrodynamic, sediment transport, and chemical fate model, to simulate movement of organic chemicals (TPCB and TDDX) in the greater harbor waters, accounting for ongoing storm water discharges from four major watersheds, tidal exchange between TMDL receiving waterbodies, and re-suspension of existing contaminated sediments caused by fluvial and tidal currents as well as vessel traffic. The WRAP Model was calibrated with a comprehensive set of hydrodynamic, dye, salinity, sediment, and organic chemical data, as illustrated previously in Figure 4.1. The data included measurements from prior studies and new special studies designed to augment existing data. The overall calibration showed that the WRAP Model can accurately simulate the physical processes including tidal exchange, storm water discharges, and sediment transport, as well as chemical processes of organic chemicals. The WRAP Model provides a greater understanding of the organic chemical transport in the LA/LB Harbor and supports findings from the CSM. Organic chemicals in the harbor waters are primarily affected by ocean concentrations and existing sediment bed concentrations with a few locations affected by watershed loadings.

The WRAP Model was linked with a site-specific food chain bioaccumulation model, as illustrated in Figure 1.2. The linkage describes the transfer of TPCB and TDDX from the water and sediment to the food web. The linkage between the WRAP Model and the bioaccumulation model consists of daily averaged concentrations within fish movement zones (shown previously in Figure 9.1) that are used as exposure inputs to the bioaccumulation model. The EFDC source code was modified to output model-wide organic concentrations in the water column and sediment bed. Organic concentrations included three-phase partitioning concentrations, as well as total organic concentrations on a carbon-normalized basis. Water column and sediment bed concentrations were averaged over the fish movement zones to provide continuous time series of exposure concentrations for the bioaccumulation model. Volume-weighted water column concentrations were provided for freely dissolved and carbon-normalized particulate concentrations. Sediment bed concentrations consisted of area-weighted surface sediment freely dissolved (i.e., pore water) and carbon-normalized total concentrations.

In the future, the linked WRAP Model and bioaccumulation model will be used to support the proposed SQO Tier III site assessment and to evaluate potential management scenarios to attain TMDL targets. It is anticipated that the WRAP Model will also be utilized to provide an understanding of sediment and chemical fate transport and technical support for the TMDL re-opener.

11. REFERENCES

ABC 2014. San Gabriel River Regional Monitoring Program 2012 Annual Report. Prepared by Aquatic Bioassay & Consulting Laboratories. Prepared for Council for Watershed Health. August 2014.

ACTA 2001. Alameda Corridor Currents and Tracer Study Revised Final Report. Prepared for Alameda Corridor Transportation Authority. Prepared by Moffatt & Nichol Engineers and Reed International. May 31, 2001.

Alcoa 2001. Comprehensive Characterization of the Lower Grasse River. Alcoa, Inc. Amended April 2001.

AMEC 2003. Supplemental Report Consolidated Slip Restoration Project Concept Plan. Prepared by AMEC Earth & Environmental, Inc. Prepared for Regional Water Quality Control Board Los Angeles Region and Port of Los Angeles. October 2003.

AMEC 2009. Draft Cabrillo Dredge Monitoring Special Study Report. Prepared by AMEC Earth & Environmental, Inc. in association with Everest International Consultants, Inc. Prepared for Port of Los Angeles. November 2009.

AMEC 2011. Port of Los Angeles Dominguez Channel/Consolidated Slip Erosion Study Phase 1 Draft. Prepared by AMEC Earth & Infrastructure, Inc. Prepared for Port of Los Angeles. November 2011.

AMEC 2013. Draft Sediment Characterization Report for Berth 36 Cabrillo Beach Yacht Club Maintenance Dredging Project Los Angeles Harbor. Prepared by AMEC Environmental & Infrastructure, Inc. Prepared for Port of Los Angeles, Environmental Management Division. August 2013.

AMEC Foster Wheeler 2015a. Draft Report Harbor Toxics TMDL: Bight 2013 Monitoring Program Los Angeles and Long Beach Harbors. Prepared by AMEC Foster Wheeler Environmental & Infrastructure, Inc. Prepared for Port of Los Angeles Environmental Management Division and Port of Long Beach Environmental Planning. June 2015.

AMEC Foster Wheeler 2015b. Harbor Toxics Total Maximum Daily Loading Estimation – Storm Water Monitoring. Prepared by AMEC Foster Wheeler Environmental & Infrastructure, Inc. Prepared for Port of Los Angeles and Port of Long Beach. August 2015.

Anchor QEA 2011. Installation Restoration Site 7 (West Basin) Sediment Remediation Implementation Report. Prepared by Anchor QEA, L.P. Prepared for Port of Long Beach. April 2011.

Anchor QEA 2012. Technical Memorandum. Sampling and Analysis of Sediments within Fish Harbor at the Port of Los Angeles. Prepared by Anchor QEA, LLC. Prepared for Port of Los Angeles. September, 2012.

Anchor QEA 2013a. Compilation of Sediment, Fish Tissue, and Mussel Tissue Datasets for the TMDL Support Program. Memorandum to State Water Resources Control Board and Los Angeles Regional Water Quality Control Board. From Port of Long Beach and Port of Los Angeles. Prepared by Anchor QEA, LLC. April 16, 2013.

Anchor QEA 2014a. Development of a Chemical Fate Conceptual Site Model for the Greater Los Angeles and Long Beach Harbor Waters. Technical Memorandum to Port of Los Angeles and Port of Long Beach. March 19, 2014.

Anchor QEA 2014b. Data Gaps Analysis for Bioaccumulation Model Development Greater Los Angeles and Long Beach Harbor Waters. Prepared by Anchor QEA, LLC. Prepared for Port of Long Beach and Port of Los Angeles. August 2014.

Anchor QEA 2016. Draft Bioaccumulation Model Report Greater Los Angeles and Long Beach Harbor Waters. Prepared by Anchor QEA, LLC. Prepared for Port of Long Beach and Port of Los Angeles. June 2016.

Blumberg, Alan F. and Mellor, George L. 1987. A Description of a Three-Dimensional Coastal Ocean Circulation Model. *In Three Dimensional Coastal Ocean Models. Norman S. Heaps, editor*. American Geophysical Union. Washington, DC.

Bopp, R. 1983. *Revised parameters for modeling the transport of PCB components across an air water interface*. J. Geophys. Res. Journal of Geophysical Research, 2521-2521.

Chapra, S.C. 1997. Surface Water-Quality Modeling. New York: McGraw-Hill.

City of Long Beach 2007. Stormwater Monitoring Report 2006/2007 NPDES Permit No. CAS004003 (CI 8052). Prepared for City of Long Beach. Prepared by Kinnetic Laboratories Incorporated. July 2007.

City of Los Angeles 2002. Ken Malloy Harbor Regional Park Development Program. Volume II Machado Lake Watershed Management Plan. Prepared for City of Los Angeles Department of Recreation and Parks and Palos Verdes/Southbay Audubon Society. Prepared by Parsons.

City of Los Angeles 2009. Machado Lake Ecosystem rehabilitation Project Wilmington Drain Multi-Use Project Pre-Design Report Executive Summary. City of Los Angeles Department of Public Works Bureau of Engineering. July 2009.

Dietrich, E.W. 1982. Settling velocity of natural particles. *Water Resources Research*, 18 (6).

Dueri, S., Zaldivar, J.M., and Olivella, A. 2005. Dynamic modeling of the fate of DDT in Lake Maggiore: preliminary results. Institute for Environment and Sustainability. 2005.

EMAP 2008. Environmental Monitoring and Assessment Program 2005 Sediment Chemistry. Excel file. Provided to Ports of Long Beach and Los Angeles by the Southern California Coastal Water Research Project.

Environ 2015a. Sampling and Analysis Report for Port of Los Angeles and Port of Long Beach Geochronology Core Sampling. Prepared by Ramboll Environ US Corporation. Prepared for Port of Los Angeles and Port of Long Beach. June 22, 2015.

Environ 2015b. Sampling and Analysis Report for Surface Sediment Characterization and Polychaete Tissue Collection Program at the Greater Los Angeles and Long Beach Harbor Waters. Prepared by Ramboll Environ US Corporation. Prepared for Port of Los Angeles and Port of Long Beach. June 29, 2015.

Environ 2015c. Low Detection Limit Water Column Special Study. Prepared by Ramboll Environ US Corporation. Prepared for Port of Los Angeles and Port of Long Beach. In press.

EPA 1996. Soil Screening Guidance: Technical Background Document Second Edition. Office of Solid Waste and Emergency Response, U.S. Environmental Protection Agency. EPA-500-R95-128. May 1996.

EPA 2000. Phase 2 Report – Review Copy Further Site Characterization and Analysis Volume 2D – Revised Baseline Modeling Report Hudson River PCBs Reassessment RI/FS. Prepared for U.S. Environmental Protection Agency, Region 2 and U.S. Army Corps of Engineers, Kansas City District. Prepared by TAMS Consultants, Inc., Limno-Tech, Inc., Menzie-Cura & Associates, Inc., and Tetra Tech, Inc. January 2000.

EPA 2007a. The Environmental Fluid Dynamics Code User Manual US EPA Version 1.01. Prepared for U.S. Environmental Protection Agency. Prepared by Tetra Tech, Inc. June 2007.

EPA 2007b. The Environmental Fluid Dynamics Code Theory and Computation Volume 1: Hydrodynamics and Mass Transport. Prepared for U.S. Environmental Protection Agency. Prepared by Tetra Tech, Inc. June 2007.

EPA 2007c. The Environmental Fluid Dynamics Code Theory and Computation Volume 2: Sediment and Contaminant Transport and Fate. Prepared for U.S. Environmental Protection Agency. Prepared by Tetra Tech, Inc. June 2007.

EPA 2015. BASINS 4.1 (Better Assessment Science Integrating Point & Non-point Sources) Modeling Framework. National Exposure Research Laboratory, RTP, North Carolina.

EPA 2016. Montrose Chemical Corporation Superfund Site Description. https://yosemite.epa.gov/r9/sfund/r9sfdocw.nsf/3dec8ba3252368428825742600743733/b7db9903773ec74188257007005e93ed!OpenDocument Updated May 5, 2016.

EPA and RWQCB 2011a. Los Angeles-Long Beach Harbors and San Pedro Bay Hydrodynamic and Sediment-Contaminant Transport Model Report. Prepared for U.S. Environmental Protection Agency, Region 9 and Los Angeles Regional Water Quality Control Board. Prepared by Tetra Tech, Inc. May 2011.

EPA and RWQCB 2011b. LSPC Watershed Model Development for Simulation of Loadings to the Los Angeles/Long Beach Harbors Final. Prepared for U.S. Environmental Protection Agency, Region 9 and Los Angeles Regional Water Quality Control Board. Prepared by Tetra Tech, Inc. May 2011.

Erickson, M.J., Turner, C.L., and Thibodeaux, L.J. 2005. Field Observation and Modeling of Dissolved Fraction Sediment-Water Exchange Coefficients for PCBs in the Hudson River. *Environ Sci. Technol*, 39, 549-556.

Everest 2007. Dominguez Channel Estuary Model Study: Model Data, Calibration, and Verification Report. Prepared for Port of Los Angeles. Prepared by Everest International Consultants, Inc. January 2007.

Everest 2009. Los Angeles and Long Beach Harbor Model Development for the Water Resources Action Plan Final Report. Prepared for Port of Los Angeles and Port of Long Beach. Prepared by Everest International Consultants, Inc. July 2009.

Everest 2010. Los Angeles Dredge Material Management Plan Environmental Tracers Investigation Final Report. Prepared for U.S. Army Corps of Engineers, Los Angeles District. Prepared by Everest International Consultants, Inc. June 2010.

Fernandez, Loretta A., Lao, Wenjian, Maruya, Keith A., White, Carmen, and Burgess, Robert M. 2012. Passive Sampling to Measure Baseline Dissolved Persistent Organic Pollutant Concentrations in the Water Column of the Palos Verdes Shelf Superfund Site. *Environmental Science & Technology*. American Chemical Society. 2012, 46, pp 11937-11947.

LACDPW 2004. Final Dominguez Watershed Management Master Plan. Prepared for County of Los Angeles Department of Public Works. Prepared by MEC Analytical Systems, Inc. April 2004.

LACDPW 2005. Los Angeles County 1994-2005 Integrated Receiving Water Impacts Report Final Report. Prepared for Los Angeles County Department of Public Works. Prepared by Weston Solutions, Inc. August 2005.

LACDPW. 2006. A Common Thread Rediscovered San Gabriel River Corridor Master Plan. Prepared for County of Los Angeles Department of Public Works. Prepared and produced by Moore Iacofano Goltsmand, Inc. June 2006.

LACDPW 2010a. Flow data for F319, F42B, and F354, October 1994 to September 2009 provided by Los Angeles County Department of Public Works, Water Resources Division. April 14, 2010.

LACDPW 2010b. Flow and water quality data for S28, 2003-2009 provided by Los Angeles County Department of Public Works, Watershed Management Division. April 21, 2010.

LACDPW 2011. Los Angeles County 2010-2011 Annual Stormwater Monitoring Final Report. Los Angeles County Department of Public Works Watershed Management Division and Los Angeles County Flood Control District. August 2011.

LACDPW 2012a. Flow and water quality data for S28, 2009-2012 provided by Los Angeles County Department of Public Works, Watershed Management Division. July 12, 2012.

LACDPW 2012b. Hydrologic Report 2011-2012. County of Los Angeles Department of Public Works, Water Resources Division.

LACDPW 2013a. Flow data for F319, F42B, F354, October 2009 to April 2013 and F38C, October 1994 to April 2013 provided by Los Angeles County Department of Public Works, Water Resources Division. May 17, 2013.

LACDPW 2013b. Los Angeles County 2012-2013 Annual Stormwater Monitoring Final Report. Los Angeles County Department of Public Works Watershed Management Division. December 2013.

LACDPW 2015. Flow data for F319, F42B, F354, and F38C, April 2013 to May 2015 and flow data for S28, July 2012 to May 2015 provided by Los Angeles County Department of Public Works. June 18, 2015.

LACSD 2013. Pales Verdes Shelf Historical Sediment Chemistry, 1998-2011. Summer Surveys. Excel file. Provided to Anchor QEA by Los Angeles County Sanitation Districts, Ocean Monitoring and Research, Technical Services Department.

Lick, Wilbert 2009. Sediment and Contaminant Transport in Surface Waters. Wilbert J. Lick. CRC Press. 2009.

Liss, P.S., and Slater, P.D. 1974. *Flux of gases across the air-sea surface*. Nature, 247, 181.

NOAA 2004a. NOAA Nautical Chart 18749 San Pedro Bay. US Department of Commerce, National Oceanic and Atmospheric Administration, Nation Ocean Survey.

NOAA 2004b. NOAA Nautical Chart 18751 Los Angeles and Long Beach Harbors. US Department of Commerce, National Oceanic and Atmospheric Administration, Nation Ocean Survey.

NOAA 2011. Bench Mark Sheet for 9410660, Los Angeles, Outer Harbor, CA. National Ocean Service, National Oceanic and Atmospheric Administration. Publication Date 10/12/2011.

NOAA 2013a. Descriptive Report to Accompany Survey H12617. US Department of Commerce, National Oceanic and Atmospheric Administration, Nation Ocean Survey.

NOAA 2013b. Descriptive Report to Accompany Survey H12618. US Department of Commerce, National Oceanic and Atmospheric Administration, Nation Ocean Survey.

NOAA 2013c. Descriptive Report to Accompany Survey H12619. US Department of Commerce, National Oceanic and Atmospheric Administration, Nation Ocean Survey.

NOAA 2013d. Descriptive Report to Accompany Survey H12620. US Department of Commerce, National Oceanic and Atmospheric Administration, Nation Ocean Survey.

POLA 2005. Water quality data from Maritime Museum, Torrance Lateral, Pier A, and Forest provided by Port of Los Angeles and Southern California Coastal Water Research Project. October 2005.

POLA 2006. Dominguez Channel Berth 200H-I to Victoria Street. Port of Los Angeles, Construction Division, Survey Section. March 6, 2006.

POLA 2007. Bathymetry data files provided by Port of Los Angeles, July 2007.

POLA 2010a. Special Study POLA Tenant Facility and Tributary Watershed Monitoring Investigation 2008 – 2010. Prepared by Weston Solutions, Inc. Prepared for Port of Los Angeles. June 2010.

POLA 2010b. GIS data provided by Port of Los Angeles December 2010.

POLA 2012. Al Larson Boat Shop Improvement Project Final Environmental Impact Report. Prepared by Los Angeles Harbor Department Environmental Management Division with assistance from CDM Smith. July 2012.

POLA and POLB 2009. Water Resources Action Plan. Port of Los Angeles and Port of Long Beach. Prepared in participation and cooperation with U.S. Environmental Protection Agency and Los Angeles Regional Water Quality Control Board. August 2009.

POLA and POLB 2010. Final 2008 Biological Surveys of Los Angeles and Long Beach Harbors. Prepared for Port of Los Angeles, Environmental Management Division and Port of Long Beach. Prepared by Science Applications International Corporation. In association with Seaventures, Keane Biological Consulting, Tenera Environmental, ECORP Consulting Incorporated, and Tierra Data Incorporated. April 2010.

POLA and USACE 2007. Berth 136-147 [TraPac] Container Terminal Project Final Environmental Impact Statement/Final Environmental Impact Report (FEIS/FEIR). Los Angeles Harbor Department, Environmental Management Division and U.S. Army Corps of Engineers. 2007.

POLB 2000. Final Environmental Impact Report and Application Summary Report – The Port of Long Beach Piers G and J Terminal Development. Prepared for Port of Long Beach. Prepared by URS/Dames & Moore. SCH No. 2000-021021. September 2000.

POLB 2010. Annual Report Storm Water Discharge Monitoring Port of Long Beach. June 2010. Prepared for Port of Long Beach Planning Division. Prepared by MBC Applied Environmental Sciences.

POLB 2011. Ambient Water Quality Characterization Long Beach Harbor 2010-2011. Prepared for Port of Long Beach, Planning Division. Prepared by MBC Applied Environmental Sciences. August 2011.

POLB 2013a. Port of Long Beach Storm Water Geodatabase. Provided by Port of Long Beach May 2, 2013.

POLB 2013b. City of Long Beach Geodatabase of Storm Drain Network. Provided by Port of Long Beach May 7, 2013.

POLB and POLA 2002. Ports of Long Beach and Los Angeles Year 2000 Biological Baseline Study of San Pedro Bay. Prepared for Port of Long Beach and Port of Los Angeles. Prepared by MEC Analytical Systems, Inc. In association with Science

Applications International Corporation, Merkel & Associates, Inc., Keane Biological Consulting, and Everest International Consultants, Inc. June 2002.

POLB and USACE 2011. Pier S Marine Terminal + Back Channel Improvements Project Draft Environmental Impact Statement (DEIS)/Draft Environmental Impact Report (DEIR). Prepared for Port of Long Beach and U.S. Army Corps of Engineers Los Angeles District. Prepared by AECOM.

RWQCB 2007. Watershed Management Initiative Chapter. California Regional Water Quality Control Board, Los Angeles Region. December 2007.

RWQCB 2011. Final Basin Plan Amendment: Attachment A to Resolution No. R11-008. Amendment to the Water Quality Control Plan – Los Angeles Region to Incorporate the Total Maximum Daily Load for Toxic Pollutants in Dominguez Channel and Greater Los Angeles and Long Beach Harbor Waters. California Regional Water Quality Control Board, Los Angeles Region. Adopted May 5, 2011.

Sabin, L., K. Maruya, W. Lao, D. Diehl, D. Tsukada, K. Stolzenbach, and K. Schiff 2011. A pilot study of air-water exchange of organochlorine compounds at three coastal estuaries in southern California. Prepared for Southern California Coastal Water Research Project 2011 Annual Report.

SAIC 2010. Final Sediment Quality Report. Prepared by Science Applications International Corporation. Prepared for Port of Los Angeles. April 2010.

SCCWRP 2003. Southern California Bight 1998 Regional Monitoring Program Volume VI: Sediment Chemistry. Southern California Coastal Water Research Project. February 2003.

SCCWRP 2007. Southern California Bight 2003 Regional Monitoring Program. Technical Report.

SCCWRP 2012. Southern California Bight 2008 Regional Monitoring Program. Excel file. B08DataRequest_10_22_2012. Sediment Chemistry Data from the Southern California Bight. Provided to Anchor QEA by SCCWRP.

Stein, E. and Ackerman, D. 2007. Dry Weather Water Quality Loadings in Arid, Urban Watersheds of the Los Angeles Basin, California, USA. *Journal of American Water Resources Association*, 43(2), pp 398-413.

SWRCB 2005. California Sediment Quality Objectives Database. State Water Resources Control Board. September 2, 2005.

Thibodeaux, Louis J., Valsaraj, Kalliat T., Reible, Danny D. 2001. Bioturbation-Driven Transport of Hydrophobic Organic Contaminants from Bed Sediment. *Environmental Engineering Science*. Volume 18, Number 4. 2001.

Thoms, S.R., Matisoff, G., McCall, P.L., and Wang, X. 1995. Models for Alteration of Sediments by Benthic Organisms. Project 92-NPS-2. Water Environment Research Foundation. Alexandria, Virginia.

USACE 1957. Reservoir Regulation Manual for Whittier Narrows Flood Control Reservoir. U.S. Army Corps of Engineers, Los Angeles District. October 1, 1957.

USACE 2002. Coastal Engineering Manual Part III-1 Coastal Sediment Properties. . U.S. Army Corps of Engineers, Coastal and Hydraulics Laboratory. EM 1110-2-1100. April 30, 2002.

USACE 2004. Los Angeles Regional Dredged Material Management Plan Feasibility Study Baseline Conditions (F3) Report Technical Appendix. U.S. Army Corps of Engineers, Los Angeles District. August 2004.

USACE 2005. Seaplane Lagoon Bathymetry Survey May 2005. U.S. Army Corps of Engineers, Los Angeles District.

USACE 2008. Los Angeles River Estuary Pre-dredge Survey January 11, 2008. U.S. Army Corps of Engineers, Los Angeles District.

USACE 2010. Sampling and Analysis Report Los Angeles River Estuary Maintenance Dredging. U.S. Army Corps of Engineers, Los Angeles District. September 2010.

USACE 2012. Whittier Narrows Dam and Reservoir Los Angeles County, California Pertinent Data. U.S. Army Corps of Engineers, Los Angeles District. January 2012.

USACE and EPA 2004. Model Calibration: Modeling Study of PCB Contamination in the Housatonic River. Prepared by Weston Solutions, Inc. Prepared for U.S. Army Corps of Engineers, New England District and U.S. Environmental Protection Agency, New England Region. December 2004.

USACE and POLA 2014. Notice of Intent (NOI)/Notice of Preparation (NOP) of the Draft Environmental Impact Statement/Environmental Impact Report and Public Scoping Meeting for the Berths 121-131 [Yang Ming] Container Terminal Redevelopment Project. U.S. Army Corps of Engineers and City of Los Angeles Harbor Department. April 2014.

USACE and POLB 2009. Middle Harbor Redevelopment Project Final Environmental Impact Statement (FEIS)/Final Environmental Impact Report (FEIR) and Application Summary

Report (ASR). Prepared for U.S. Army Corps of Engineers Los Angeles District and Port of Long Beach. April 2009.

USACE and POLB 2015. Port of Long Beach Deep Draft Navigation Project Review Plan. U.S. Army Corps of Engineers Los Angeles District and Port of Long Beach. 2015.

USGS 2001. The Search for Reliable Aqueous Solubility (Sw) and Octanol-Water Partition Coefficient (Kow) Data for Hydrophobic Organic Compounds: DDT and DDT as a Case Study. James Pontolillo and Robert P. Eganhouse. U.S. Geological Survey. Water-Resources Investigation Report 01-4201. 2001.

Weston 2007. Final Report Characterization of Sediment Contaminant Flux for the Inner Harbor and Outer Harbor Waterbodies to Support Sediment TMDL Implementation. Prepared by Weston Solutions. Prepared for Port of Los Angeles and Port of Long Beach. Revised May 2007.

Weston 2008. Draft Report Sediment Characterization in Support of the Water Resources Action Plan, Port of Los Angeles. Weston Solutions, Inc. September 2008.

Weston 2013. Work Order 13-01-0847. POLA SQO Phase II, Supplemental Report 2. Weston Solutions, Inc. Analyzed by Calscience Environmental Laboratories, Inc. April 3, 2013.

WDNR 2001. Lower Fox River/Green Bay Remedial Investigation and Feasibility Study Development and Application of a PCB Transport Model for the Lower Fox River. Prepared by Wisconsin Department of Natural Resources. June 15, 2001.

Zeng, Eddy Y., Tsukada, David, Diehl, Dario W., Peng, Jian, Schiff, Kenneth, Noblet, James A., and Maruya, Keith A. 2005. Distribution and Mass Inventory of Total Dichlorodiphenyldichloroethylene in the Water Column of the Southern California Bight. *Environmental Science & Technology*. American Chemical Society. 2005, Vol. 39, No. 21, pp 8170-8176.

APPENDIX A

EFDC OVERVIEW

A.1 BACKGROUND

EFDC is a surface water modeling system developed and distributed by the EPA Center for Exposure Assessment Modeling. The model was originally developed by Dr. John Hamrick at the Virginia Institute of Marine Science. EFDC has been designed to quantify movement and concentrations of contaminants in lakes, rivers, stratified estuaries, and coastal environments to support environmental assessment and management and regulatory requirements. The EFDC modeling system includes hydrodynamic, sediment, contaminant, and eutrophication components that can simulate geometrically and dynamically complex water bodies (EPA 2007a).

A.2 HYDRODYNAMIC COMPONENT

The EFDC hydrodynamic component simulates water levels and velocities, as well as dispersion coefficients for mixing and transport. EFDC is capable of simulating time and spatially varying environmental forcing functions such as tides and winds, as well as an arbitrary number of inflows (e.g., rivers and storm drain discharges). User-specified inputs can be generated to allow integration of inputs from other models such as a watershed model (EPA 2007a).

The physics and computational scheme are similar to the Princeton Ocean Model (Blumberg and Mellor 1987). EFDC solves the 3D Reynold-Averaged Navier-Stokes equations assuming incompressible flow and hydrostatic pressure distribution. A time variable transformation of the vertical coordinate is applied to provide uniform resolution in the vertical direction, which is aligned with the gravitational vector and bounded by the bottom topography and free surface. Details of the transformation can be found in Vinokur (1974), Blumberg and Mellor (1987) or Hamrick (1986). The applied transformation of the vertically hydrostatic boundary layer form of the turbulent equations of motion and utilization of the Boussinesq approximation for variable density results in the following momentum, continuity, and transport equations:

$$\partial_t(\mathrm{mHu}) + \partial_x(\mathrm{m_y Huu}) + \partial_y(\mathrm{m_x Hvu}) + \partial_z(\mathrm{mwu}) - (\mathrm{mf} + \mathrm{v}\partial_x \mathrm{m_y} - \mathrm{u}\partial_y \mathrm{m_x})\mathrm{Hv} \quad (1)$$

$$= -\mathrm{m_y H}\partial_x(\mathrm{g}\zeta + \mathrm{p}) - \mathrm{m_y}(\partial_x \mathrm{h} - \mathrm{z}\,\partial_x \mathrm{H})\partial_z \mathrm{p} + \partial_z(\mathrm{mH^{-1}A_v}\partial_z \mathrm{u}) + \mathrm{Q_u}$$

$$\partial_t(\mathrm{mHv}) + \partial_x(\mathrm{m_y Huv}) + \partial_y(\mathrm{m_x Hvv}) + \partial_z(\mathrm{mwv}) - (\mathrm{mf} + \mathrm{v}\partial_x \mathrm{m_y} - \mathrm{u}\partial_y \mathrm{m_x})\mathrm{Hu} \quad (2)$$

$$= -\mathrm{m_x H}\partial_y(\mathrm{g}\zeta + \mathrm{p}) - \mathrm{m_x}(\partial_y \mathrm{h} - \mathrm{z}\,\partial_y \mathrm{H})\partial_z \mathrm{p} + \partial_z(\mathrm{mH^{-1}A_v}\partial_z \mathrm{v}) + \mathrm{Q_v}$$

$$\partial_z \mathrm{p} = -\mathrm{gH}(\rho - \rho_o)\rho_o^{-1} = -\mathrm{gHb} \quad (3)$$

$$\partial_t(\mathrm{m}\zeta) \; + \; \partial_x\left(\mathrm{m}_y\mathrm{Hu}\right) \; + \; \partial_y(\mathrm{m}_x\mathrm{Hv}) \; + \; \partial_z(\mathrm{mw}) = 0 \tag{4}$$

$$\partial_t(\mathrm{mHC}) + \; \partial_x\left(\mathrm{m}_y\mathrm{HuC}\right) + \; \partial_y(\mathrm{m}_x\mathrm{HvC}) + \; \partial_z(\mathrm{mwC}) = \; \partial_z(\mathrm{mH}^{-1}\mathrm{A_b}\partial_z\mathrm{C}) + \; \mathrm{Q_C} \tag{5}$$

Where:

$\mathrm{u, v}$ = horizontal velocity components in the coordinates x and y
w = vertical velocity component in the dimensionless vertical coordiante z
$\mathrm{m}_x, \mathrm{m}_y$ = square roots of the diagonal components of the metric tensor
$\mathrm{m} = \mathrm{m}_x\mathrm{m}_y$ = square root of the metric tensor determinant
$\mathrm{H} = \mathrm{h} + \zeta$ = total depth
h = depth below free surface
ζ = free surface displacement relative to physical vertical coordinate origin
b = buoyancy
g = gravitaitonal constant
p = pressure in excess of reference density hydrostatic pressure
ρ_o = reference density
f = Coriolis parameter
$\mathrm{A_v}$ = vertical turbulent eddy viscosity
$\mathrm{A_b}$ = vertical turbulent diffusivity
$\mathrm{Q_u}, \mathrm{Q_v}$ = momentum source and sink terms
ρ = density, which is a function of temperature and salinity
C = generic transport variable (temperature, salinity, suspended sediment)
$\mathrm{Q_C}$ = source and sink term of generic transport variable

The system of equations (1-5) includes the momentum equations (1-2), vertical pressure distribution (3), continuity equation (4), and the generic transport equation (5). Integrating the continuity equation with respect to z produces the depth integrated continuity equation, and provides a closed system for the variables u, v, w, p, ρ, ζ, and C, provided that the vertical turbulent viscosity and diffusivity and the source and sink terms are specified. The second moment turbulence closure model developed by Mellor and Yamada (1982) and modified by Galperin *et al.* (1988) is used to provide the vertical turbulent viscosity and diffusivity. Therefore, the EFDC hydrodynamic model provides spatially varying velocity predictions in three dimensions, as well as the mass transport of environmental variables such as salinity, temperature, dye, dissolved, and suspended concentrations. Equations of motion (1-4) are solved using a combination of finite volume and finite difference techniques on a staggered grid, commonly referred to as the C grid (Arakawa and Lamb 1977) or the MAC grid (Peyret and Taylor 1983). The use of this spatial averaging scheme to represent

the Coriolis and curvature accelerations also guarantees energy conservation. The mass transport equation (5) is integrated over a cell layer and solved using a three time level fractional step with periodic insertion of a two time level correction step (EPA 2007b).

A.3 SEDIMENT TRANSPORT

The hydrodynamic component provides the dynamics for the sediment transport processes, which include settling, deposition, resuspension, and bed consolidation mechanisms. The dynamic coupling between the sediment and hydrodynamics components account for both changes in bed topography and water depth due to sediment deposition or erosion. EFDC is capable of simulating multiple sediment classes of cohesive and/or noncohesive sediments. For the WRAP Model, sediments were simulated with three cohesive and two noncohesive sediment classes. For each sediment class, the sediment settling velocities were calculated externally from EFDC based on representative grain size diameters (Dietrich 1982).

Sediment transport in EFDC is governed by the generic mass transport equation (5) solved for suspended sediment (6) with vertical boundary conditions (7 and 8). The sediment transport equation (6) is solved using a high order upwind difference solution scheme for the advective terms (Hamrick 1992 and Tetra Tech 2002). A small amount of horizontal numerical diffusion remains inherent to the scheme, so the physical horizontal diffusion terms are omitted. Here, J_{jo} is the net water column-bed exchange flux defined as positive into the water column.

$$\partial_t(mHS_j) + \partial_x(m_y HuS_j) + \partial_y(m_x HvS_j) + \partial_z(mwS_j) - \partial_z(mw_{sj}S_j) \tag{6}$$

$$= \partial_z\left(m\frac{K_v}{H}\partial_z S_j\right) + Q_{sj}^E + Q_{sj}^I$$

$$-\frac{K_v}{H}\partial_z S_j - w_{sj}S_j = J_{jo} : z \approx 0 \tag{7}$$

$$-\frac{K_v}{H}\partial_z S_j - w_{sj}S_j = 0 : z = 1 \tag{8}$$

Where:

S_j = concentration of the j^{th} sediment class
Q_{sj}^E = external source or sink of sediment (point or nonpoint source loads)
Q_{sj}^I = internal source or sink of sediment (decay of sediment or exchange between classes)
K_v = vertical turbulent diffusion coefficient
w_{sj} = positive settling velocity
J_{jo} = net water column-bed exchange

The numerical solution of (6) uses a fractional step procedure for 1) advection and external sources and sinks, 2) settling, 3) resuspension and deposition, and 4) diffusion. The advection step computes the concentration due to advection and volumetric sources and sinks using the anti-diffusive MPDATA scheme (Smolarkiewcz and Clark 1986) with optional flux corrected transport (Smolarkiewicz and Grabowski 1990). The settling step (10) is solved by a fully implicit upwind difference scheme from the top layer downward. The third step (11) accounts for resuspension and deposition. The diffusion step (12) is for an implicit vertical turbulent diffusion with zero diffusive fluxes at the bed and water surface. Combining (10-12) determines the water column-bed exchange flux accounting for settling, resuspension, deposition, and diffusion (13). In EFDC, components for the water column-bed exchange are modeled differently depending on the sediment class, as summarized below.

$$H^{n+1}\,S^{*} = H^{n}S^{n} + \frac{\theta}{m}\left(Q_{sj}^{E}\right)^{n+1/2} \tag{9}$$

$$-\frac{\theta}{m}\left(\partial_x\left(m_y(Hu)^{n+1/2}S^{n}\right) + \partial_y\left(m_x(Hv)^{n+1/2}S^{n}\right) + \partial_z\left(mw^{n+1/2}S^{n}\right)\right)$$

$$S^{**} = S^{*} + \frac{\theta}{H^{n+1}}\partial_z(w_s S^{**}) \tag{10}$$

$$S^{***} = S^{*} + \frac{\theta}{\Delta_z H^{n+1}} L_o J_o^{***} \tag{11}$$

$$S^{n+1} = S^{***} + \theta\partial_z\left(\left(\frac{K_v}{H^2}\right)^{n+1}\partial_z S^{n+1}\right) \tag{12}$$

$$S^{*} = S^{n+1} - \frac{\theta}{H^{n+1}}\partial_z(w_s S^{n+1}) - \theta\partial_z\left(\left(\frac{K_v}{H^2}\right)^{n+1}\partial_z S^{n+1}\right) \tag{13}$$

Noncohesive Sediment

For noncohesive sediment, settling depends on the settling velocity. At low concentrations, the settling velocity equals the settling velocity of a discrete particle, which is based on sediment density, effective grain diameter, and fluid kinematic viscosity. The settling velocity can be user specified or computed internally (van Rijn 1984b).

For noncohesive sediment resuspension, sediment is then either transported as bed or suspended load. Initiation of transport occurs when the bed shear stress, τ_b, exceeds a critical stress known as the Shield's stress, τ_{cs}. Bed shear stresses are calculated internally based on predicted flow velocities near the bed, and τ_{cs} is provided from external calculations. In EFDC, transport via bedload and/or suspended load is based on an

approach by van Rijn (1984a), the latter was specified in the WRAP Model. When the bed shear stress velocity exceeds the settling velocity and critical Shield's shear stress velocity, noncohesive sediment will be resuspended and transported as suspended load. For noncohesive sediment, deposition occurs when the bed shear stress is less than the settling velocity and critical Shield's shear stress velocity. The bed flux to the water column is then:

$$J_{jo} = w_{sj}(\overline{S}_{jeq} - \overline{S}_j) \tag{14}$$

$$\overline{S}_{jeq} = \frac{\ln(z_{eq}^{-1})}{(z_{eq}^{-1} - 1)} S_{jeq} : R = 1 \tag{15}$$

$$\overline{S}_{jeq} = \frac{(z_{eq}^{R-1} - 1)}{(1 - R)(z_{eq}^{-1} - 1)} S_{jeq} : R \neq 1 \tag{16}$$

Where:

S_{jeq} = equilibrium near bed sediment concentration (no net flux)
$\overline{S}_{jeq}$ = model layer mean, near bed equilibrium sediment concentration
$\overline{S}_j$ = model layer mean sediment concentration
z_{eq} = reference height for equilibrium concentration
R = the Rouse number

Equations (14-16) show that the water column-bed flux for non-cohesive sediments depends on the near bed equilibrium concentration and its corresponding reference distance above the bed. In the WRAP Model, S_{jeq} and z_{eq} are calculated based on the formulations of Garcia and Parker (1991).

Cohesive Sediment

Settling for cohesive sediment uses semi-empirical methods based on an effective settling velocity. EFDC offers several options to determine the effective settling velocity based on a reference settling velocity, particle size, and/or sediment concentration. The WRAP Model uses a widely used empirical expression relating effective settling velocity to the reference settling velocity and sediment concentration (Ariathurai and Krone 1976).

The water column-bed exchange for cohesive sediment is dependent on bed shear stress and bed geomechanical properties. Cohesive sediment deposition occurs when the bed shear stress is less than a critical stress for deposition and the near bed depositing sediment concentration. The critical depositional stress is an input model parameter. Cohesive sediment deposition is based on a probability of deposition and settling velocity:

$$J_{jo}^{d} = -w_s S_d \left(\frac{\tau_{cd} - \tau_b}{\tau_{cd}}\right) : \tau_b \leq \tau_{cd} \tag{17}$$

For the water column-bed flux, resuspension can either occur as bulk or surface erosion; the latter was considered for the WRAP Model. Surface erosion occurs when the bed shear stress, τ_b, is less than the bed shear strength, but greater than the critical erosion stress, τ_{ce}. The critical stress for surface erosion was calculated externally. Surface erosion of cohesive sediment is calculated as:

$$J_{jo}^{r} = \frac{dm_e}{dt}\left(\frac{\tau_b - \tau_{ce}}{\tau_{ce}}\right)^a : \tau_b \geq \tau_{ce} \tag{18}$$

Where:

$\frac{dm_e}{dt}$ = surface erosion rate per unit surface area of the bed
a = exponent determined for laboratory or field experiments

Sediment parameters for the WRAP Model were based on literature values and initial discussions with the EFDC model developer. These values were indirectly validated through the sediment transport and organics calibration process.

A.4 CONTAMINANT FATE AND TRANSPORT

The hydrodynamic and sediment transport components are linked with the contaminant component, which can simulate an arbitrary number of contaminants (e.g., metals or organic chemicals). Sorptive contaminants can be specified to include chemical interactions for contaminants sorbed to material effectively dissolved in the water phase and/or contaminants sorbed to suspended particles. The contaminant transport is based on the same advection-diffusion scheme used for salinity and temperature. The sorption kinetics are based on the Langmuir isotherm (Chapra 1997).

The general mass transport equation (5) can be solved for a contaminant that is dissolved in the water phase (19), sorbed to a dissolved material (20), and sorbed to sediment particles (21):

$$\partial_t(mHC_w) + \partial_x\left(m_y HuC_w\right) + \partial_y(m_x HvC_w) + \partial_z(mwC_w) \tag{19}$$

$$= \partial_z\left(m\frac{A_b}{H}\partial_z C_w\right) + mH\left(\sum_j K_{dS}^j C_s^j + \sum_i K_{dD}^i C_D^i\right)$$

$$- mH\left(\sum_i K_{aS}^j S^j \left(\psi_w \frac{C_w}{\emptyset}\right)\left(\hat{X}_S^j - X_S^j\right) + \sum_i K_{aD}^i D^i \left(\psi_w \frac{C_w}{\emptyset}\right)\left(\hat{X}_D^i - X_D^i\right) + \gamma C_w\right)$$

$$\begin{aligned} &\partial_t\left(mHC_D^i\right) + \partial_x\left(m_y HuC_D^i\right) + \partial_y\left(m_x HvC_D^i\right) + \partial_z\left(mwC_D^i\right) \\ &= \partial_z\left(m\frac{A_b}{H}\partial_z C_D^i\right) + mH\left(K_{sD}^i D^i\right)\left(\psi_w \frac{C_w}{\emptyset}\right)\left(\hat{X}_D^i - X_D^i\right) - mH(K_{dD}^i + \gamma)C_D^i \end{aligned} \quad (20)$$

$$\begin{aligned} &\partial_t\left(mHC_S^j\right) + \partial_x\left(m_y HuC_S^j\right) + \partial_y\left(m_x HvC_S^j\right) + \partial_z\left(mwC_S^j\right) + \partial_z\left(mw_s^j C_S^j\right) \\ &= \partial_z\left(m\frac{A_b}{H}\partial_z C_S^j\right) + mH\left(K_{aS}^j S^j\right)\left(\psi_w \frac{C_w}{\emptyset}\right)\left(\hat{X}_S^j - X_S^j\right) - mH(K_{dS}^j + \gamma)C_S^j \end{aligned} \quad (21)$$

Where:

$C_w =$ contaminant concentration freely dissolved in water phase
$C_D^i = D^i X_D^i =$ contaminant concentration sorbed to dissolved material *i*
$C_S^j = S^j X_S^j =$ contaminant concentration sorbed to suspended material *j*
$D^i =$ dissolved material concentration of material *i*
$S^j =$ suspended particle concentration of sediment class *j*
$X_D^i =$ mass of contaminant sorbed to dissolved material *i* per unit mass of material
$X_S^j =$ mass of contaminant sorbed to suspended material *j* per unit mass of material
$\emptyset =$ porosity
$\psi_w =$ fraction of the water dissolved contaminant available for sorption
$K_a =$ adsorption rate for suspended (S) or dissolved material (D)
$K_d =$ desoption rate for suspened (S) or dissolved material (D)
$\gamma =$ linearized decay rate coefficient
$\hat{X} =$ denotes saturation sorbed mass per carrier mass for suspended or dissolved material

EFDC employs equilibrium partitioning balancing adsorption and desorption terms, resulting in the following equilibrium partition coefficients based on the ratio of sorbed to water phase concentrations.

$$P_D^i = \frac{\psi_w K_{aD}^i \hat{X}_D^i}{K_{dD}^i} \quad (22)$$

$$P_S^j = \frac{\psi_w K_{aS}^j \hat{X}_S^j}{K_{dS}^j} \quad (23)$$

The linear equilibrium partitioning requires the three phases to sum to unity, which is a generalization of Chapra's (1997) formulation for sorption to dissolved organic carbon (DOC) and particulate organic carbon (POC).

$$f_w + f_D + \sum_j f_S^j = 1 \tag{24}$$

$$f_w = \frac{C_w}{C} = \frac{\emptyset}{\emptyset + \sum_j P_S^j S^j + \sum_i P_D^i D^i} \tag{25}$$

$$f_D = \frac{C_D}{C} = \frac{P_D^i D^i}{\emptyset + \sum_j P_S^j S^j + \sum_i P_D^i D^i} \tag{26}$$

$$f_S^j = \frac{C_S^j}{C} = \frac{P_S^j S^j}{\emptyset + \sum_j P_S^j S^j + \sum_i P_D^i D^i} \tag{27}$$

Combining equations (19-21) with the equilibrium partition equations (22-23) results in a single transport equation describing the total contaminant concentration in the water column:

$$\partial_t(mHC) + \frac{1}{m}\partial_x\left(m_y Hu C\right) + \frac{1}{m}\partial_y(m_x Hv C) + \partial_z(mwC) \tag{28}$$

$$-\partial_z\left(m\sum_i w_S^j f_S^j C\right) = \partial_z\left(m\frac{A_b}{H}\partial_z C\right) - mH\gamma C$$

In the WRAP Model, a three-phase equilibrium partitioning was used for organic chemicals. The sorption to dissolved material was specified for DOC, while the sorption to suspended material was specified for POC. The three phases for organic chemicals included freely dissolved, DOC-complexed, and particulate phases. The partitioning coefficients are provided externally to EFDC, which are based on the physical properties of the contaminants. The contaminant transport equation for the total contaminant concentration is solved using a fractional step procedure. The procedure sequentially treats advection; settling, deposition, and resuspension; porewater advection and diffusion; and then chemical reactions. For details on the solution scheme, see Tetra Tech (2002).

A.5 REFERENCES

Arakawa, A. and Lamb, V.R. 1977. Computational design of the basic dynamical processes of the UCLA general circulation model. *Methods in Computational Physics, Volume 17, Academic Press, 174-265*.

Ariathurai,R. and Krone, R.B. 1976. Finite element model for cohesive sediment transport. *J. Hyd. Div. ASCE, 102, 323-338*.

Blumberg, Alan F. and Mellor, George L. 1987. A Description of a Three-Dimensional Coastal Ocean Circulation Model. *In Three Dimensional Coastal Ocean Models. Norman S. Heaps, editor*. American Geophysical Union. Washington, DC.

Chapra, S.C. 1997. Surface Water-Quality Modeling. New York: McGraw-Hill.

Dietrich, W. E. 1982. Settling Velocity of Natural Particles, *Water Resour. Res., 18(6), 1615–1626*. December 1982.

EPA 2007a. The Environmental Fluid Dynamics Code User Manual US EPA Version 1.01. Prepared for U.S. Environmental Protection Agency. Prepared by Tetra Tech, Inc. June 2007.

EPA 2007b. The Environmental Fluid Dynamics Code Theory and Computation Volume 1: Hydrodynamics and Mass Transport. Prepared for U.S. Environmental Protection Agency. Prepared by Tetra Tech, Inc. June 2007.

Galperin, B., Kantha, L., Hassid, S., and Rosati, A. 1988. A Quasi-equilibrium Turbulent Energy Model for Geophysical Flows. American Meteorological Society. *Journal of the Atmospheric Sciences, Volume 45, No. 1, pp 55-62*. January 1988.

Garcia, M., and G. Parker, 1991. Entrainment of bed sediment into suspension. *J. Hyd.Engrg*., *117, 414-435.*

Hamrick, J. M., 1986. Long-term dispersion in unsteady skewed free surface flow. *Estuar. Coast. Shelf Sci., 23, 807-845.*

Hamrick, J. M., 1992. A three dimensional Environmental Fluid Dynamics Computer Code: theoretical and computational aspects. *Special Report No. 317 in Applied Marine Science and Ocean Engineering*.

Mellor, George and Yamada, Tetsuji. 1982. Development of a Turbulence Closure Model for Geophysical Fluid Problems. *Reviews in Geophysics and Space Physics, Volume 20, No. 4, pp 851-875*. November 1982.

Peyret, R. and Taylor, T.D. 1983. Computational methods for fluid flow, Springer-Verlag, 358 pp.

Smolarkiewcz, P.K. and Clark, T.L. 1986. The multidimensional positive definite advection transport algorithm: further development and applications. *J. Comp. Phys., 67, 396-438*.

Smolarkiewicz, P.K. and Grabowski, W.W. 1990. The multidimensional positive definite advection transport algorithm: non-oscillatory option. *J. Comp. Phys., 86, 355-375*.

Tetra Tech 2002. Theoretical and Computational Aspects of Sediment and Contaminant Transport in the EFDC Model. *Technical Memorandum 2002*

van Rijn, L.C. 1984a. Sediment transport, Part I: Bed load transport. *J. Hyd. Engrg., 110, 1431-1455*.

van Rijn, L.C. 1984b. Sediment transport, Part II: Suspended load transport. *J. Hyd. Engrg., 110, 1613-1641*.

Vinokur, M., 1974. Conservation equations of gas dynamics in curvilinear coordinate systems. *J. Comp. Phys., 50, 71-100.*

APPENDIX B

INCORPORATING VOLATILIZATION INTO THE WRAP MODEL

B.1 BACKGROUND

Volatilization is the process by which freely dissolved organic chemicals are vaporized and transported to the surrounding atmosphere. Volatile emissions from the water column to the atmosphere can be an important process in the fate and transport of persistent organic chemicals (e.g. PCBs, DDT, and PAHs). A study of atmospheric fluxes in the LA/LB Harbor (Sabin et al. 2011) measured a net positive flux of TPCB and TDDX from the water to the air, which is consistent with the LA/LB Harbor Conceptual Site Model (CSM) that estimated volatilization to be a moderate sink (Anchor QEA 2014). Thus, to account for losses due to volatilization, the EFDC source code was updated to incorporate the volatilization mechanism. This appendix documents the development and incorporation of volatilization in the WRAP Model.

B.2 MODELING VOLATILIZATION

Chemical volatilization at the air-water interface is typically estimated using a two-layer film resistance approach (Liss and Slater 1974). According the film resistance model, the flux across the air-water interface is represented by the equation (Bopp 1983):

$$F = K_l\left(C_w - C_g/H\right) \quad (1)$$

Where:

F = flux of constituent across the air-water interface $\left(\mathrm{g/cm^2 \cdot sec}\right)$
C_w = constituent concentration in water $\left(\mathrm{g/cm^3}\right)$
C_g = constituent concentration in bulk gas phase $\left(\mathrm{g/cm^3}\right)$
H = Henry's law constant (dimensionless)
K_l = mass transfer coefficient $(\mathrm{cm/sec})$

Consequently, the volatilization (F) is proportional to the concentration gradient between air and water and the mass transfer coefficient (K_l). When applying Eq. 1, the constituent water concentration (C_w) is typically defined as the constituent concentration at the air-water interface (i.e., water surface). For environmental conditions where the water concentration is much greater than the gaseous concentration (e.g., $C_w >> C_g$), Eq. 1 can be simplified further to:

$$F \approx K_l(C_w) \quad (2)$$

In the LA/LB Harbor, TPCB and TDDX water concentrations are much greater than gaseous concentrations, as shown in Table B.1. Measured gas phase concentrations (Sabin et al. 2011) are three-orders of magnitude smaller than measured water concentrations (Environ 2015). Therefore, Eq. 2 is applicable when the gaseous term (C_g/H) is negligible compared to the water concentration, which is applicable for the LA/LB Harbor. This simplification enables the estimation of the volatilization flux based solely on the volatilization mass transfer coefficient.

Table B.1 Measured Water and Gaseous Concentrations in LA/LB Harbor

VARIABLE	PCB	DDT
C_g (ng/L)	0.000156	0.000054
H	0.0063	0.000861
C_g / H	0.0248	0.0627
C_w (ng/L)	0.539	0.264

B.3 VOLATILIZATION MASS TRANSFER COEFFICIENT

The mass transfer coefficient (K_l) represents the ease of constituent transport across the air-water interface. In environmental systems, the ease of transport is primarily related to the diffusivity of the constituent and turbulent mixing at the air-water interface. Diffusivity is a function of physical-chemical properties and temperature, whereas turbulent mixing can be characterized by wind or water velocities. By assuming K_l is constant, we neglect changes in mass transfer due to fluctuations in temperature and turbulent mixing (Bopp 1983):

$$\frac{1}{K_l} = \frac{\mu_l}{D_l} + \frac{\mu_g}{D_g H} \tag{3}$$

Where:

D_l = liquid phase diffusion coefficient (cm^2/sec)
D_g = gas phase diffusion coefficient (cm^2/sec)
μ_l = liquid boundary layer thickness (cm)
μ_g = gaseous boundary layer thickness (cm)

In Eq. 3, the total resistance to transport $(1/K_l)$ is the sum of the resistance to transport through the liquid and air boundary layers. Determination of the volatilization mass transfer

coefficient requires characterization of the liquid and gaseous boundary layer thicknesses, chemical diffusivity, and Henry's law constants, as characterized by methods specified by Bopp (1983). Parameters used to determine the volatilization mass transfer coefficient are provided in Table B.2.

Table B.2 Parameters for Volatilization Mass Transfer Coefficient

VARIABLE	UNITS	PCB	DDT
μ_l	cm	0.018	0.018
μ_g	cm	1.0	1.0
D_l	cm^2/s	5.10E-6	4.73E-6
D_g	cm^2/s	5.20E-2	4.85E-2
H	--	6.30E-3	8.61E-4
K_l	cm/s	1.52E-4	3.59E-5

The liquid boundary layer thickness was specified based on an empirical correlation to wind speed developed by Emerson (1975) for average summer conditions in the Hudson River, New York where the air-water concentration gradient was negligible. This estimate is similar to values estimated for San Francisco Bay (Hammond and Fuller 1979). Therefore, while Eq. 3 does not explicitly account for changes in wind speed, the effect of wind on the mass transfer coefficient is considered in determining the liquid boundary layer thickness. The corresponding gaseous boundary layer thickness was derived based on evaporation rates (Defant 1961).

The aqueous and gaseous diffusion coefficients are chemical-specific based on empirical relationships. Aqueous diffusion coefficients were determined from the Wilke-Chang equations (Wilke and Chang 1955) as modified by Hayduk and Laudie (1974), which is based on the molecular weight, temperature, viscosity, and molar volume. Les Bas volumes were used for the molar volumes at the boiling point. Gas phase diffusion coefficients were determined from the Fuller, Schettler, and Giddings correlation (Reid et al. 1987). Both the aqueous and gaseous diffusion coefficients were calculated for 35% saline water at 25^o C. Physical-chemical properties used in the aqueous and gaseous calculations were taken from Mackay et al. (2006). The properties vary by congener, thus the physical-chemical properties were based on the dominant PCB and DDX congeners found in harbor waters (Environ 2015). TPCB properties were specified based on properties for the tetrachlorobiphenyl homologs. Chemical properties for p,p'-DDE were used to characterize TDDX.

Estimates of the Henry's law constant vary widely based on the method used to determine the Henry's law constant and also vary for congeners of similar chemical species. The dominant PCB and DDX congeners were used to specify the Henry's law constant. For PCB, the Henry's law constant was selected based on the tetrachlorobiphenyl homologs determined by Brunner et al. (1990) as reported in Mackay et al. (2006). The value (6.3E-3) is the average of the individual tetra-congeners and fall within the acceptable range found in literature ranging from 6.3E-4 to 7.5E-3. For DDT, the Henry's law constant of 8.61E-4 was obtained for p,p'-DDE (USEPA 1996), which are within the literature range of 1.4E-4 to 3.26E-3.

Based on the liquid and gaseous boundary layer thicknesses, chemical diffusivity, and Henry's law constants, the volatilization mass transfer coefficients were calculated as 1.52E-6 m/s (13.13 cm/d) for TPCB and 3.59E-7 m/s (3.10 cm/d) for TDDX. The volatilization mass transfer coefficient was determined to be higher for TPCB compared TDDX, which is consistent with prior estimates from the CSM.

B.4 EFDC MODIFICATIONS

The EFDC source code was modified to incorporate the volatilization mechanism into the model computations. The total contaminant concentration in the water surface layer was adjusted by:

$$C_v = C_{nv} - K_l\,(F_w \times C_{nv})L^{-1}dt \qquad (4)$$

Where:

C_v = total concentration of contaminant in top layer after volatilization (ug/L)
C_{nv} = total concentration of contaminant in top layer before volatilization (ug/L)
K_l = mass transfer coefficient (m/s)
F_w = fraction of total concentration in aqueous phase (dimensionless)
L = thickness (depth) of top layer (m)
dt = time step (s)

The loss due to volatilization was quantified by subtracting the estimated volatilization flux based on the freely dissolved (aqueous) phase concentration from the total contaminant concentration in the water surface layer. The mass transfer coefficient was defined as a user-specified parameter for each contaminant.

To demonstrate the effects of volatilization, the WRAP Model organic chemical calibration period was simulated with and without volatilization. These simulations were conducted prior to the completion of the model parameter calibration and are not meant to show calibrated

organic concentrations. Comparisons of the mid-water concentrations were made at the nine organic calibration locations to illustrate the loss due to volatilization. The effects of volatilization for TPCB are shown in Figures B.1a – c. In each panel, the freely dissolved concentration with no volatilization (orange line) is compared to the freely dissolved concentration with volatilization (purple line). At all comparison locations, effects of volatilization show an overall reduction in TPCB concentrations reflecting the loss due to volatilization. For TDDX, the effects of volatilization are less apparent, as shown in Figures B.2a – c. The volatilization mass transfer coefficient for TDDX was estimated to be significantly less than TPCB, hence reductions in TDDX concentrations are observed, but to a lesser extent than TPCB.

B.5 VOLATILIZATION FLUX RATES

To validate the estimated volatilization mass transfer rates for the WRAP Model, volatilization flux rates were compared with prior estimates for the LA/LB Harbor. The WRAP Model volatilization flux for TPCB and TDDX are compared to other estimates in Table B.3. The WRAP Model volatilization flux was determined based on the average surface concentrations over the calibration period. Average surface concentrations ranged from 0.183 to 2.065 ng/L for TPCB and 0.248 to 1.912 ng/L for TDDX. Estimates of volatilization fluxes from the CSM were made based on measured and literature values. Atmospheric fluxes in the LA/LB Harbor were previously measured by Sabin et al. 2011. The fluxes were estimated based on water concentrations measured 1-m above the sediment bed in the Consolidated Slip. The water concentrations ranged from 0.414 to 0.700 ng/L for TPCB and 0.416 to 0.570 ng/L for TDDX. The comparisons of volatilization fluxes are also graphically compared in Figure B.3. Comparison between the WRAP Model and measured fluxes illustrates comparable water column concentrations and corresponding volatilization flux rates. Therefore, the updated WRAP Model can reasonably account for losses due to volatilization.

Table B.3 Comparisons of Volatilization Fluxes

ESTIMATE	TPCB (NG/M^2/D)	TDDX (NG/M^2/D)
WRAP Model	24 – 271	7.7 – 59
CSM	10 – 1,000	0.5 – 50
Measured	49 – 135	13 – 32

B.6 REFERENCES

Anchor QEA 2014. Development of a Chemical Fate Conceptual Site Model for the Greater Los Angeles and Long Beach Harbor Waters. *Technical Memorandum March 19, 2014.*

Bopp, R. 1983. *Revised parameters for modeling the transport of PCB components across an air water interface*. J. Geophys. Res. Journal of Geophysical Research, 2521-2521.

Brunner, S., Hornung, E., Santl, H., Wolff, E., Piringer, O. G., Altschuh, J., & Brueggemann, R. 1990. Henry's law constants for polychlorinated biphenyls: experimental determination and structure-property relationships. *Environmental science & technology*, *24*(11), 1751-1754.

Defant, A. 1961. Physical oceanography; volume 2.

Emerson, S. 1975. Gas exchange rates in small Canadian Shield lakes.*Limnology and Oceanography*, *20*(5), 754-761.

Environ 2015. Low Detection Limit Water Column Special Study. Prepared by Ramboll Environ US Corporation. Prepared for Port of Los Angeles and Port of Long Beach. In press.

Hammond, D. E., & Fuller, C. 1979. The use of radon-222 to estimate benthic exchange and atmospheric exchange rates in San Francisco Bay.

Hayduk, W., & Laudie, H. 1974. Prediction of diffusion coefficients for nonelectrolytes in dilute aqueous solutions. *AIChE Journal*, *20*(3), 611-615.

Liss, P.S., and Slater, P.D. 1974. *Flux of gases across the air-sea surface*. Nature, 247, 181.

Mackay, D., Shiu, W. Y., Ma, K. C., & Lee, S. C. 2006. *Handbook of physical-chemical properties and environmental fate for organic chemicals*. CRC press.

Reid, R. C., Prausnitz, J. M., & Poling, B. E. 1987. The properties of gases and liquids, p 11.10

Sabin, L. D., Maruya, K., Lao, W., Diehl, D., Tsukada, D., Stolzenbach, K. D., & Schiff, K. C. 2011. A pilot study of air-water exchange of organochlorine compounds at three coastal estuaries in southern California.

USEPA 1996. Soil screening guidance technical background document. *Office of Solid Waste and Emergency Response, Washington, DC EPA/540*,*95*.

Wilke, C. R., & Chang, P. 1955. Correlation of diffusion coefficients in dilute solutions. *AIChE Journal*, *1*(2), 264-270.

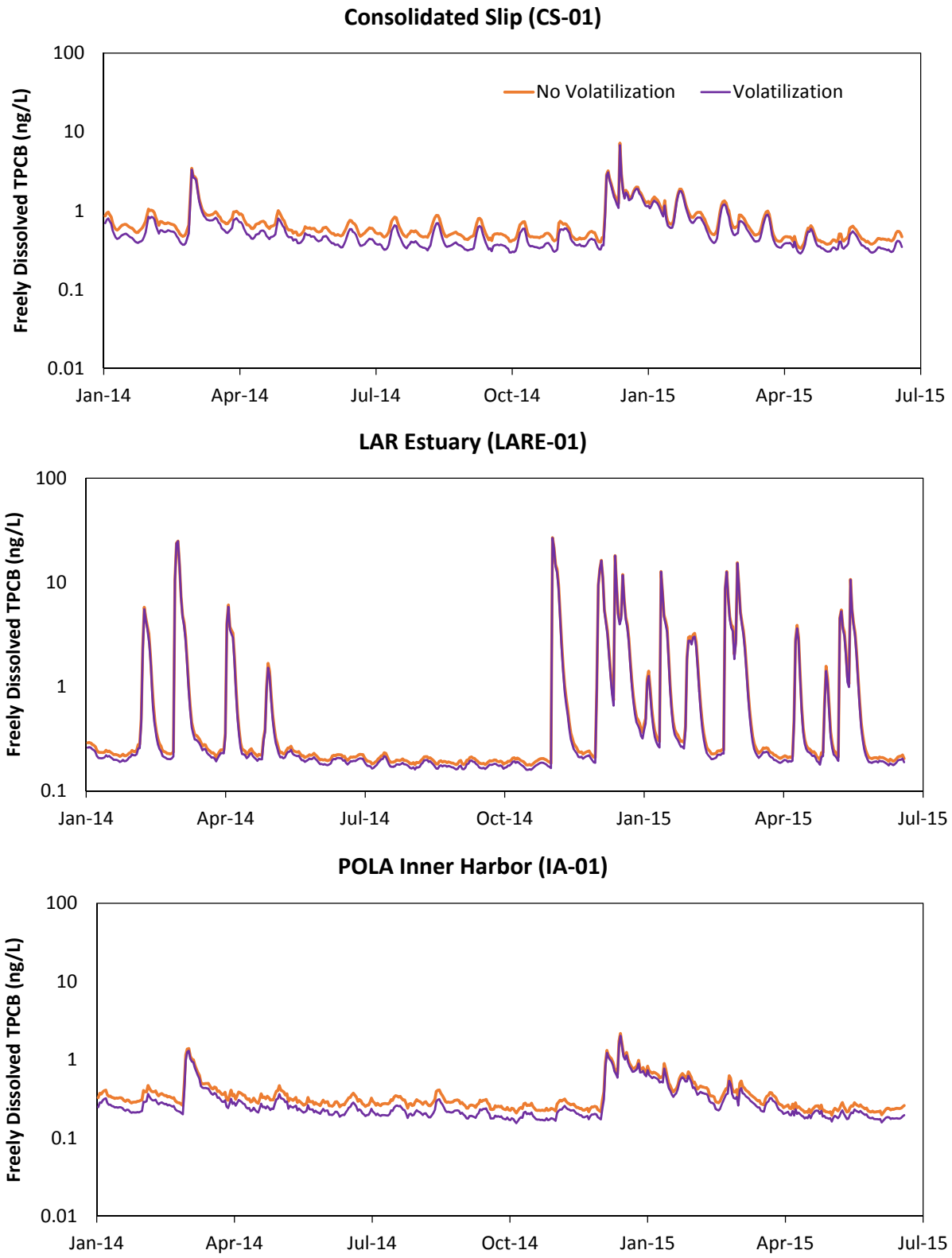

Figure B.1a Evaluation of Volatilization for TPCB

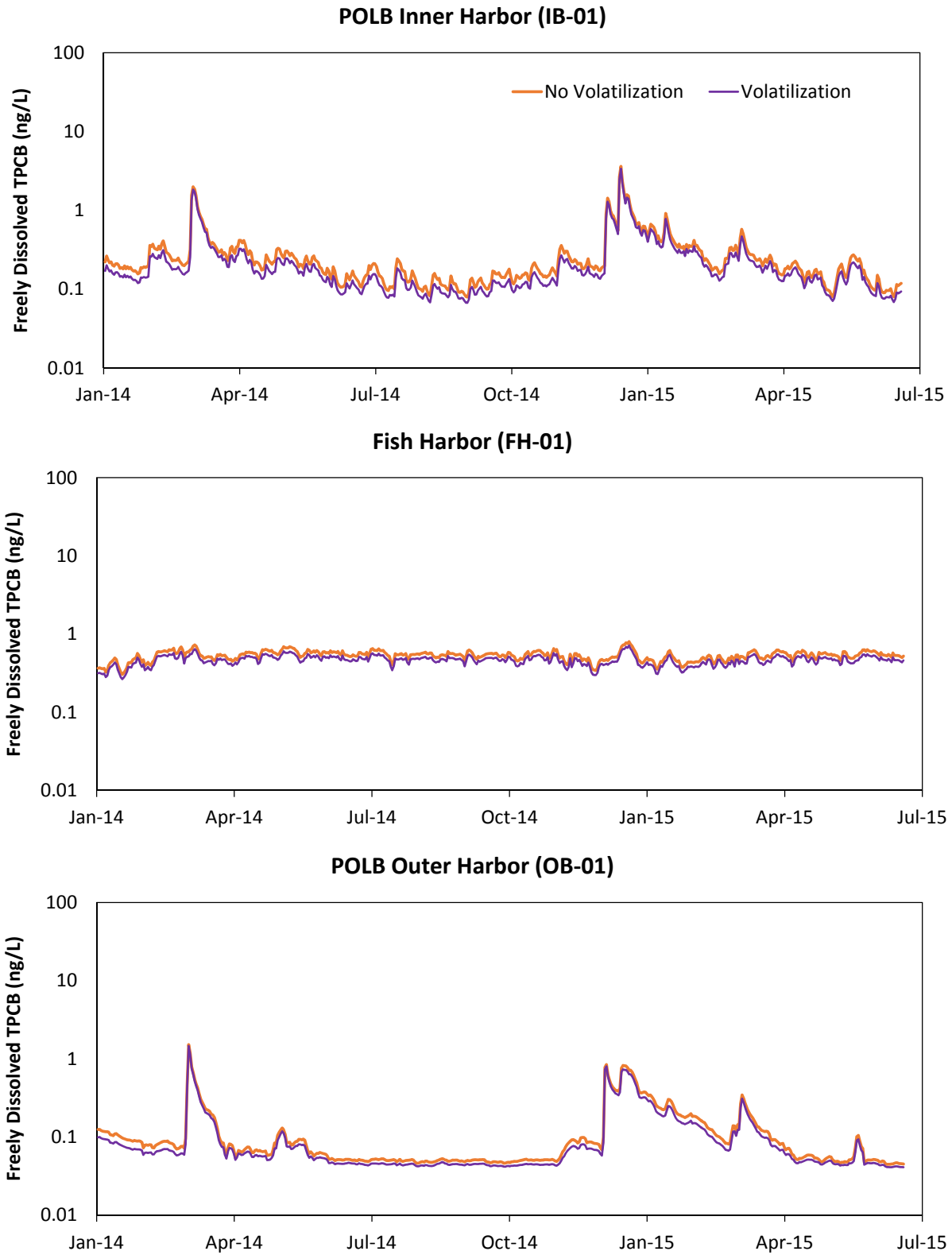

Figure B.1b Evaluation of Volatilization for TPCB

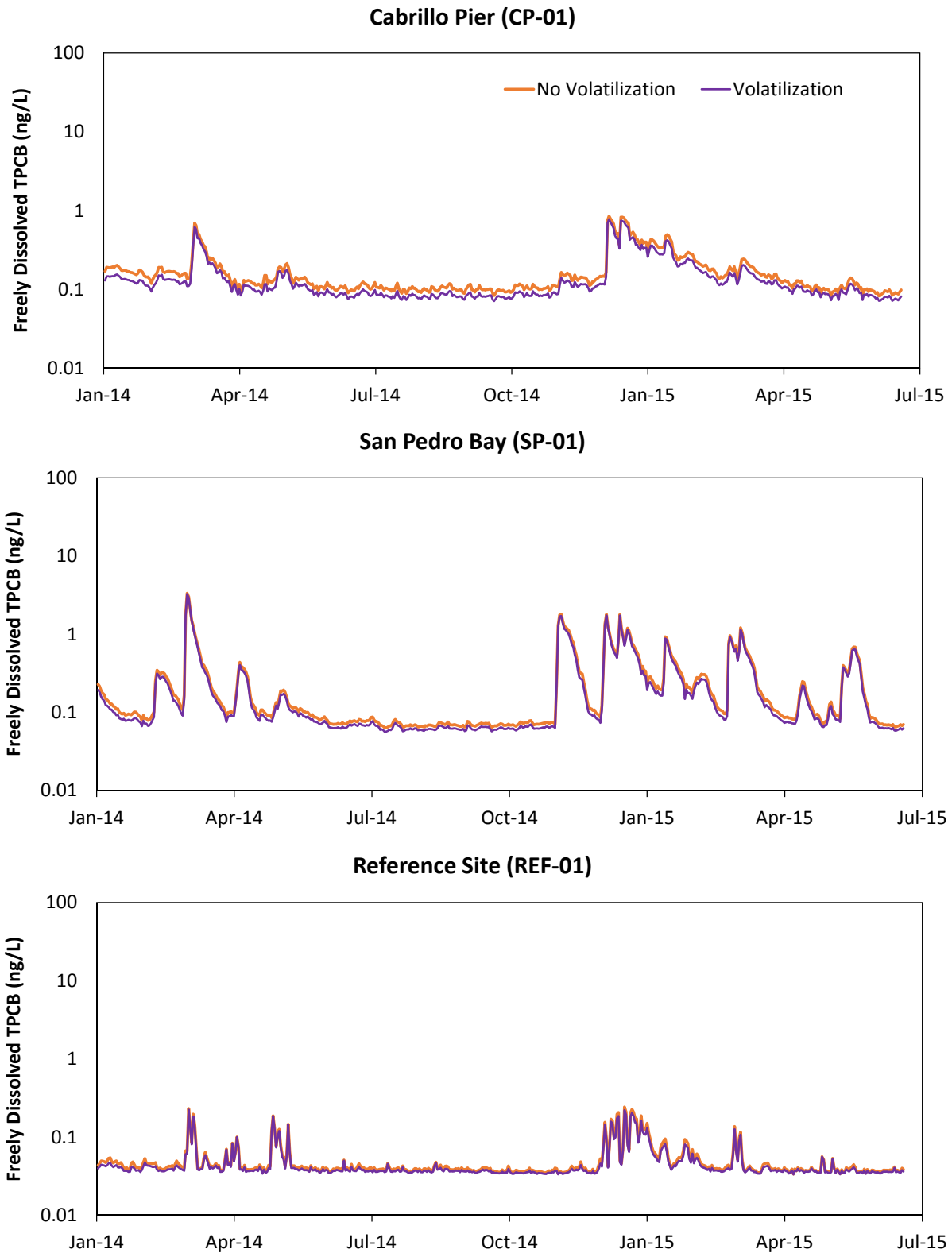

Figure B.1c Evaluation of Volatilization for TPCB

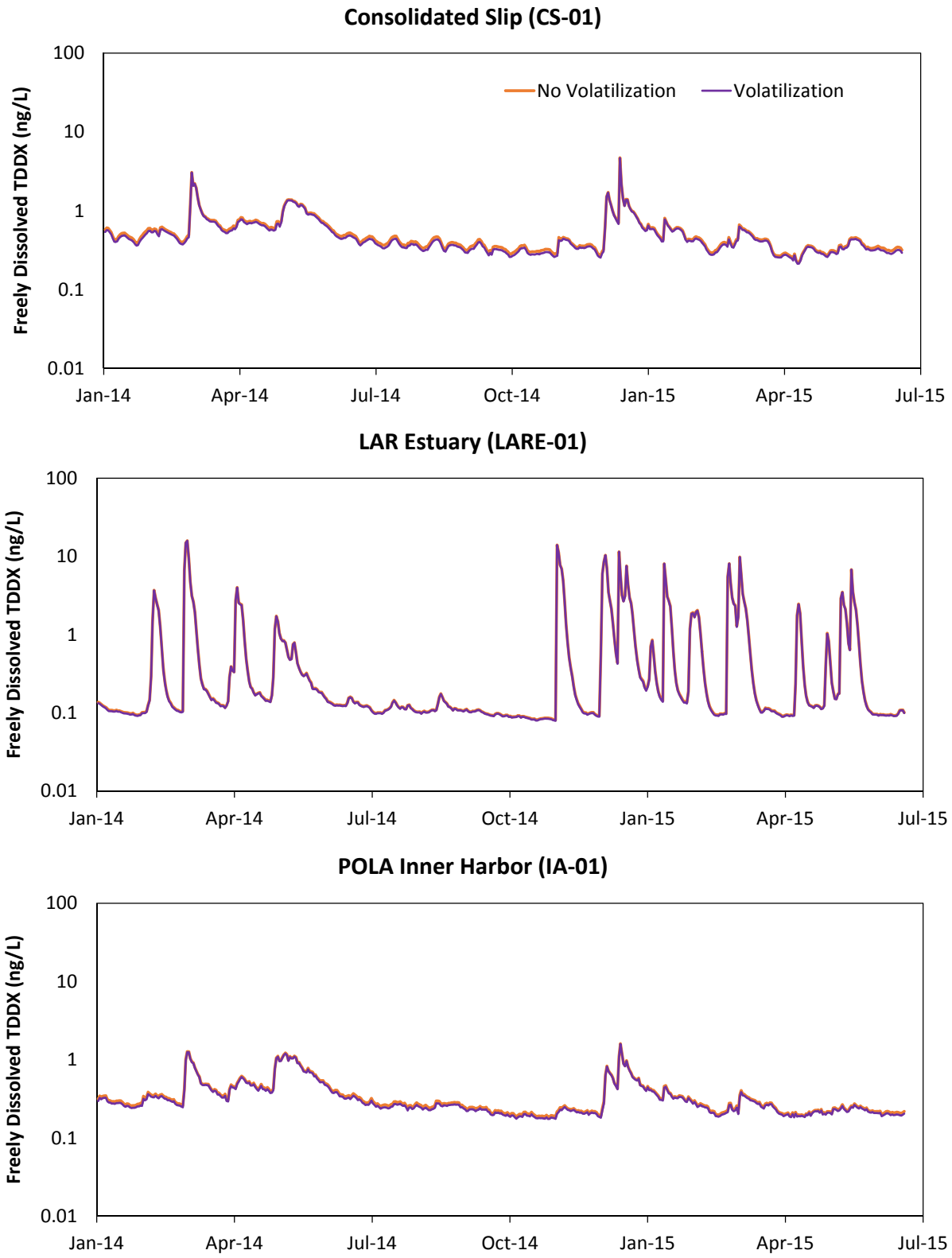

Figure B.2a Evaluation of Volatilization for TDDX

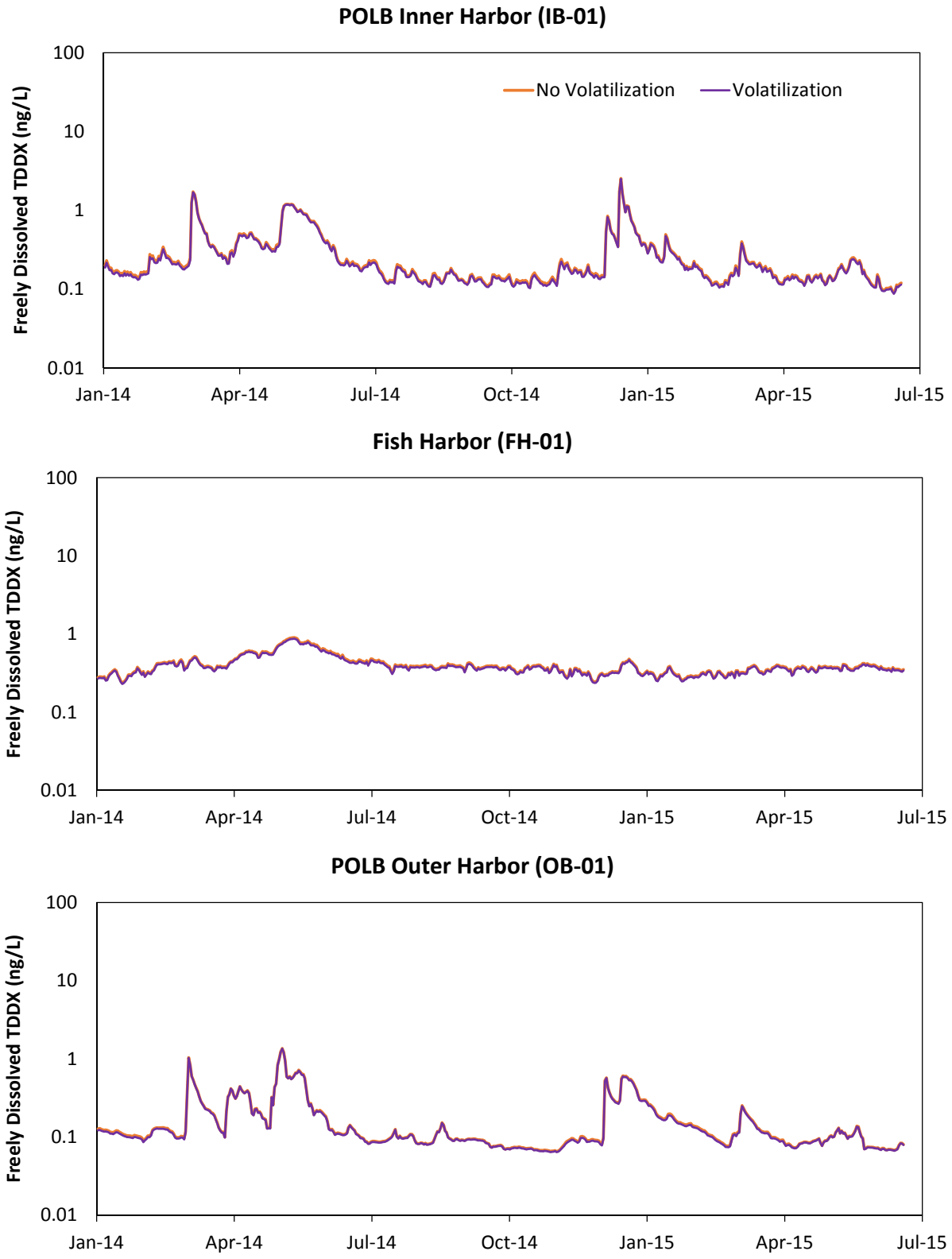

Figure B.2b Evaluation of Volatilization for TDDX

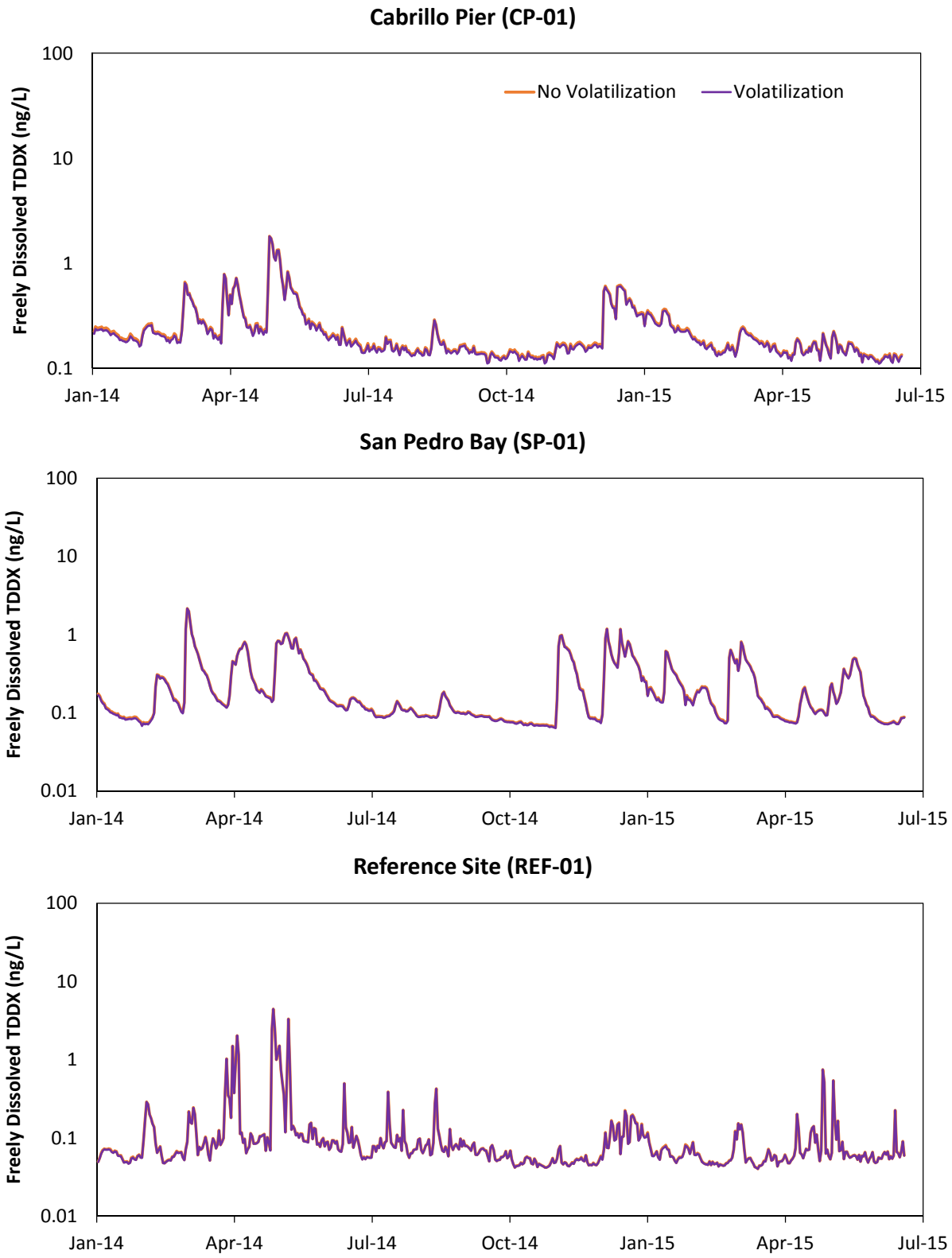

Figure B.2c Evaluation of Volatilization for TDDX

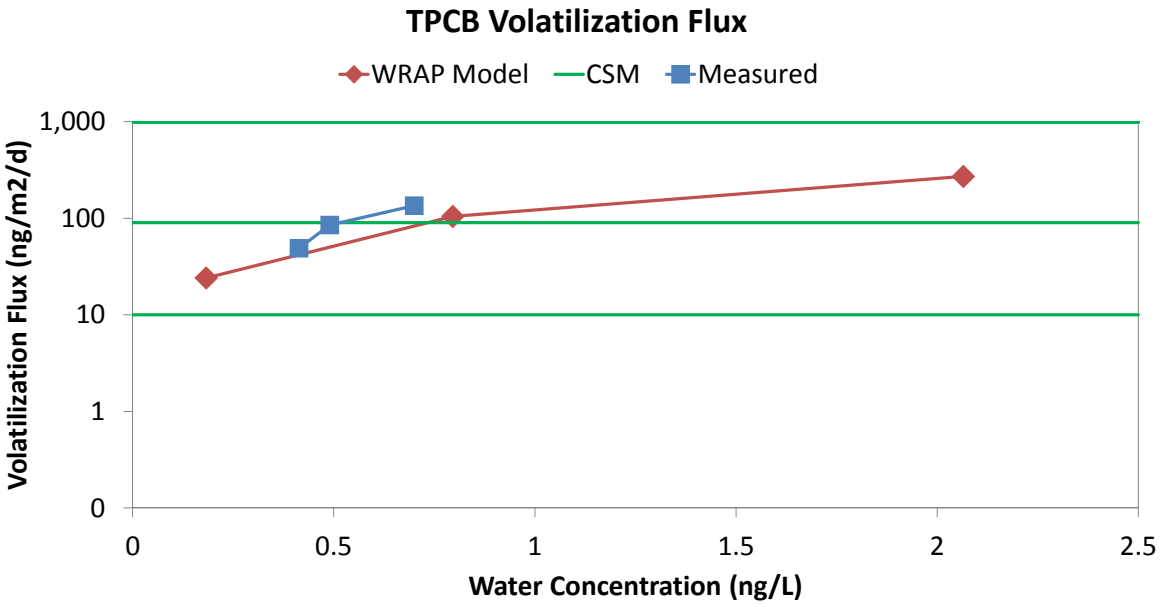

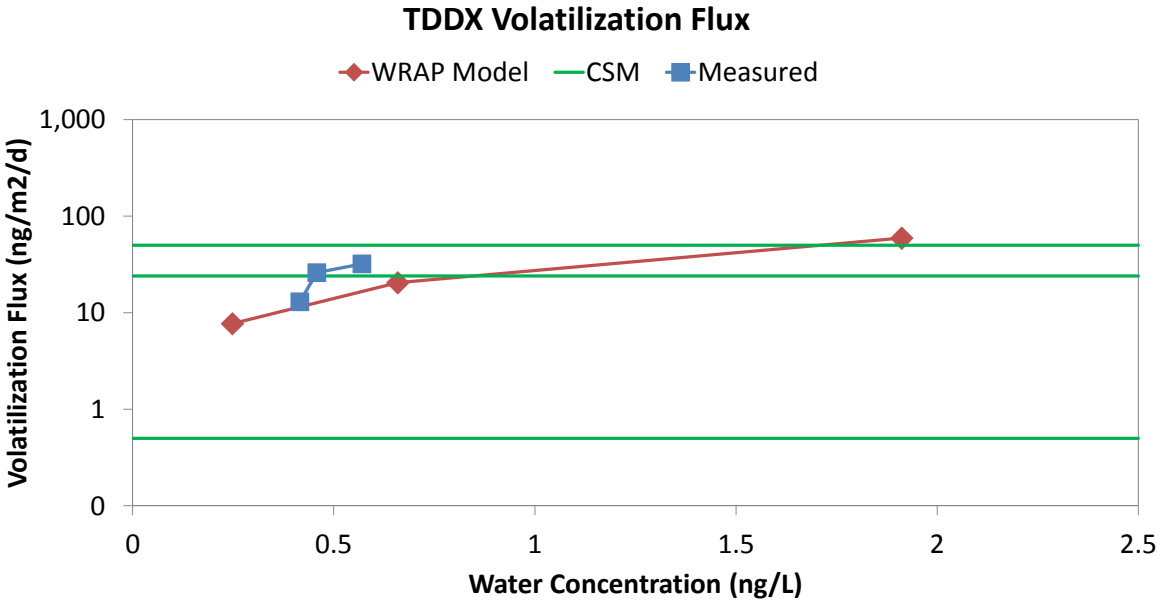

Figure B.3 Comparison of Volatilization Fluxes

APPENDIX C

INCORPORATING PROPELLER INDUCED RE-SUSPENSION OF SEDIMENT IN THE WRAP MODEL

C.1 BACKGROUND

Propeller induced re-suspension of sediment, referred to as propwash, occurs when vessel propeller currents generate high bed shear stresses sufficient to re-suspend sediment. Consequently, sediment and associated contaminants are eroded from the bed and re-suspended into the water column, enabling the movement and redistribution of sediment and contaminants. Hence, propwash may contribute to the transport of sediment bed contaminants in active port environments. Combined, the Port of Los Angeles (POLA) and Port of Long Beach (POLB) complex is the busiest port in the United States with widespread depositions of legacy pollutants. Due to the frequent vessel traffic within the harbor and potential transport of contaminants, the propwash effects were incorporated into the WRAP Model. Although EFDC is capable of simulating the typical processes involved in chemical fate and transport, the standard code does not account for anthropogenic mechanisms of transport such as propwash. Propwash was incorporated into the WRAP Model by first defining the propwash bed shear stresses of different vessels operating in the ports based on vessel characteristics (e.g., engine power, propeller diameter, etc.) and water depths along vessel routes. Next, the effects of propwash were characterized by representing the frequency, duration, and locations of propwash bed shear stresses. The procedure to incorporate the effects of propwash into the WRAP Model is summarized as follows:

1. Analyze traffic data to determine common vessel characteristics and frequently traveled routes
2. Estimate propwash bed shear stresses based on vessel types and water depth
3. Develop propwash exposure times along vessels paths
4. Modify EFDC code to allow user to supply time series of bed shear stresses and to adjust sediment flux along vessel paths

C.2 PROPWASH BED SHEAR STRESS

The propeller-induced velocity fields are determined using methods from Blaauw and van de Kaa (1978), Blaauw et al. (1984), and Verhey (1983):

$$V_{x,r} = M \times C_1 \times \left(\frac{P_d}{{D_p}^2}\right)^{1/3} \left(C_2 \frac{D_p}{x}\right)^{1.1} \exp\left(C_3 \left(\frac{r}{x}\right)^2\right) \quad (1)$$

Where:

$V_{x,r}$ = velocity of propeller jet at longitudinal distance,x, and radial distance, r (m/s)
x = distance behind vessel (m)
r = radial distance from propeller shaft to bed (m)
M = multi-propeller factor (unitless)
P_d = engine power applied (W)

D_p = propeller diameter (m)
C_1, C_2, C_3 = empirical constants (unitless)

Application of Eq.1 results in a velocity field at the bed as a function of water depth and vessel characteristics. The resulting velocity field is then converted into propeller-induced bed shear stress using Prandtl's universal velocity distribution for turbulent flow over hydraulically rough conditions, which logarithmically relates velocity and shear stress based on fluid density, height above bed, and sediment size. An example of the propeller-induced velocity field and shear stress for a 4-8k TEU container is shown in Figure C.1.

To determine propwash properties of vessels operating in the ports, characteristics of vessels were assembled from harbor vessel data. Given the large diversity of vessels, the data were grouped into 10 vessel types. For each vessel type, information was gathered for vessel and port operation characteristics. Vessel characteristics included engine horsepower, propeller diameter, and propeller depth needed for computing the propwash velocity and shear stress fields. Port operations characteristics were summarized by vessel type, vessel route, terminal destinations, and engine load factors for inbound and outbound operating conditions. Information on vessels and port operations was obtained from the Southern California Marine Exchange, manufacturer websites, port facility maps, and Starcrest Consulting, LLC (air quality consultants for the ports).

A preliminary assessment of vessels operating in the ports was conducted to identify vessels types that are capable of re-suspending sediment. Since sediment re-suspension is dependent on vessel characteristics, port operation characteristics, and water depths, 15 cases were defined to combined vessel characteristics and routes, as summarized in Table C.1. Examples of the container and liquid bulk vessel routes are shown in Figure C.2 to illustrate vessel travel routes.

Table C.1 Vessels Considered in Preliminary Assessment

CASE	VESSEL	DESCRIPTION	VESSEL ROUTE
1	Automobile Carrier	POLB 734	POLB Pier B
2	Breakbulk	POLB 722	POLB Channel No. 3
3	Yang Ming Mega-Container	8,600 TEU	POLA Berth 121-131
4	Yang Ming Container	5,500 TEU	POLA Berth 121-131
5	Yang Ming Small Container	2,000 TEU	POLA Berth 121-131
6	Hanjin Small Container	2,000 TEU	POLB Pier T
7	Maersk Mega-Container	14,770 TEU, E-Class, 2 propellers	POLB Pier G
8	Hanjin Container	5,500 TEU	POLB Pier T
9	Dry Bulk	Typical dry bulk vessel	POLB Pier B
10	Liquid Bulk	Oil Tanker	POLB Pier B
11	Catalina Jet Cat	Jet Cat Express, high speed catamaran, 4 propellers	POLA WorldPort 93
12	Passenger Cruise	Carnival Cruise Ship, 2 propellers	POLB Queen Mary
13	Recreational Sailboat	Recreational sailboats	POLA Berth 29-40
14	POLA Tug	Tug “American Spirit”, 2 propellers	POLA terminal areas
15	POLB Tug	Pacific Tug “Lillian G”, 2 propellers	POLB terminal areas

For each case, the propwash sediment re-suspension potential was evaluated by comparing the propwash velocity to the minimal velocity required for re-suspension of sediment based on the Hjulstrom curve, which correlates velocity, sediment size, and erosion. Propwash velocities were determined for three water depths along each vessel route at the entrance channel, access channel, and terminal. The re-suspension potential was also evaluated based on a range of sediment bed sizes. A summary of the propwash resuspension potential is provided in Table C.2, which identifies the 11 vessel types (shown in **bold**) that were incorporated into the WRAP Model propwash.

Table C.2 Summary of Propwash Resuspension Potential

CASE	VESSEL	ENTRANCE CHANNEL	ACCESS CHANNEL	TERMINAL
1	**Automobile Carrier***	Maybe	Yes	Yes
2	**Breakbulk***	Unlikely	Yes	Yes
3	**Yang Ming Mega-Container***	Yes	Yes	Yes
4	**Yang Ming Container***	Maybe	Yes	Yes
5	**Yang Ming Small Container***	Maybe	Yes	Yes
6	**Hanjin Small Container***	Maybe	Maybe	Yes
7	**Maersk E-Class Mega-Container***	Yes	Yes	Yes
8	**Hanjin Container***	Maybe	Maybe	Yes
9	**Dry Bulk***	Unlikely	Yes	Yes
10	**Liquid Bulk***	Unlikely	Yes	Yes
11	Catalina Jet Cat	Unlikely	Unlikely	Maybe
12	**Passenger Cruise***	Yes	Yes	Yes
13	Recreational Sailboat	Unlikely	Unlikely	Unlikely
14	POLA Tug	Unlikely	Unlikely	Maybe
15	POLB Tug	Unlikely	Unlikely	Maybe

**Vessel type incorporated into WRAP Model propwash*

C.3 VESSEL TRAFFIC ANALYSIS

Once the bed shear stresses were determined for individual vessels, the challenge then becomes characterizing the long term impact of the propwash bed shear stress, which must be estimated under the wide range of vessel types, vessel routes, and water depths that occur as part of typical port operations. In addition, propwash occurs intermittently and sporadically throughout the year. It is impractical to simulate the propwash effect of each individual vessel. Hence, detailed vessel traffic data were analyzed to categorize representative vessel characteristics and travel routes to identify high traffic regions of the Ports.

Available vessel traffic statistics for the LA/LB Harbor from 2012 to 2013 were used for the vessel traffic analysis. The data describes vessel type, travel route, number of arrivals (sea to berth), number of departures (berth to sea), number of shifts (berth to berth), average travel time, maximum average main engine power, actual vessel engine power used, and vessel draft. The two-year dataset was analyzed to categorize vessels by type to identify the most frequently used vessel types and routes. The eight most common vessel types, ranked by total number of movements per year, were considered for the propwash analysis. For each common vessel types, the range of vessel characteristics—including applied engine power, propeller diameter, and vessel draft—was summarized by their median values in Table C.3. These median values were used to calculate propeller-induced bed velocities and bed shear stresses.

Table C.3 Vessel Characteristics for Propwash Analysis

Vessel Characteristics	Auto Carrier	Breakbulk	Container (<4K TEU)	Container (4-8K TEU)	Container (>8K TEU)	Dry Bulk	Liquid Bulk	Cruise
POLA P_d (kW)	2,030	430	2,180	4,170	5,660	410	430	6,650
POLB P_d (kW)	840	370	2,500	4,070	5,990	410	510	7,060
D_p (m)	7.6	7.0	9.1	9.1	9.6	6.1	5.8	3.8
Draft (m)	12.3	14.5	12.5	14.0	15.0	11.4	11.5	8.1

For vessel traffic analysis, the travel paths taken to and from adjacent berths were consolidated into a number of common vessel travel paths. Common vessel travel paths were determined by grouping travel paths to adjacent berths. A total of 13 travel paths, as shown in Figure C.3, were identified for the POLA. The common vessel travel paths were compared based on the total travel time vessels spent on each path, as illustrated by the pie chart. Similarly, 12 common vessel travel paths, as shown in Figure C.4, were identified for the POLB. To further simplify the propwash analysis procedure, vessel travel paths with less than 5% of the total travel time were excluded from further analysis. These results in 14 most traveled paths to represent vessel traffic for both ports, as shown in Figure C.5. These 14 paths include the main channel path at each port, in addition to the most traveled offshoots from these main channel paths.

Since the propwash-induced bed shear stress is dependent on water depth, each of the vessel travel path has to be further divided into regions with similar water depths. Model cells in the WRAP Model grid with relatively constant bathymetry intersected by selected paths were grouped into 19 regions, as shown in Figure C.6. Within each region, the

average depth was computed to define the distance from propeller shaft to bed for vessels traveling within the region.

C.4 PROPWASH EXPOSURE TIMES

The next step towards simulating the propwash effect in the WRAP Model is quantifying the yearly exposure times of the propwash shear stresses. The detailed vessel traffic data were used to determine frequency and duration that propwash occurs in high traffic regions. The yearly time exposure to bed shear stresses was approximated on a cell by cell basis for each vessel type (Eq. 2). It was necessary to include each vessel type in this calculation, due to the unique bed shear caused by each vessel. After the exposure was estimated for each cell, the cell times were averaged between previously defined regions (Eq. 3).

$$E_{v,c} = \sum_{p=1}^{N_p} T_{v,p} \times t_{avg,p} \times \left(\frac{L_c}{L_p}\right) \quad (2)$$

Where:

$E_{v,c}$ = exposure time to vessel v at cell c in a given year (hrs/year)
p = path overlapping model cell
N_p = number of paths overlapping model cell
$T_{v,p}$ = trips made by vessel v along path *p* in an average year
$t_{avg,p}$ = average maneuvering time along path *p* (hrs)
L_c = length of path overlapping model cell c (m)
L_p = total length of path (m)

$$T_{R,v} = \sum_{c=1}^{N_c} E_{v,c} \times \left(\frac{1}{N_c}\right) \quad (3)$$

Where:

$T_{R,v}$ = average cell exposure to vessel v within region R $(\mathrm{hrs/year})$
N_c = number of cells within region R

Eq. 2 results in cell exposure time to specific vessels in an average year. However, since the propwash shear stress was calculated for depth averaged regions, not unique cells in the modeling domain, Eq. 3 was applied so that exposure time is estimated over depth-averaged regions. Figure C.7 shows an example of the yearly exposure times for a 4-8k TEU container vessel. In the figure, the dark blue indicates the greatest time exposed to

propwash by 4-8k TEU container vessels. Blank regions indicate regions not traveled by this type of vessel.

The regional exposure to shear stress represents the average time per year a cell within the region is exposed to vessel shear stresses. This total exposure time was divided into 30-minute increments and randomly distributed amongst a one-year period. Thirty minutes represents the estimated average time vessels spend within regions during a single maneuver, so a 30-minute regional "pulse" of shear stress approximates the regional exposure during a single movement. Figure C.8 shows the random distribution of vessel shear stresses within Region 15, which is exposed to multiple vessel types. In this example, propwash shear stresses representing four vessel types (auto carrier, breakbulk, <4k TEU container, and 4-8k TEU container) were combined into a single shear stress time series that will be applied to Region 15. A similar time series is available for all regions, providing the estimated yearly exposure to propwash bed shear.

C.5 EFDC MODIFICATIONS

Sediment re-suspension from hydrodynamics is typically modeled by comparing the hydrodynamic bed shear stress to the critical shear stress of the sediment. If the hydrodynamic shear stress is greater than the critical shear stress, then erosion begins to occur and sediment is re-suspended and introduced into the water column. In EFDC, and most sediment transport models, the hydrodynamic shear stress is dependent on fluid velocity predicted by the numerical model, where fluid velocities represent tidal currents, riverine flows, or wind-induced currents. Therefore, re-suspension of sediment is usually modeled as a function of naturally occurring hydrodynamics.

To simulate propwash effects, the propwash shear stress can be simulated in EFDC by replacing the hydrodynamic shear with the propwash shear stress. The higher propwash shear stress effectively results in EFDC computing a greater sediment flux. The following modifications were made to the EFDC source code to incorporate propwash into the WRAP Model:

- Enable user-specified time series of bed shear stresses and bed shear areas
- Allow propwash shear stress to replace hydrodynamic shear stress when propwash is active
- Scale EFDC sediment flux from propwash based on shear area and cell area

The first modification to the EFDC source code enabled specification of time varying bed shear stress and bed shear areas for each propwash region. The bed shear stress time series represents the propwash "pulse" and set to zero between pulses when the propwash is not active. The corresponding bed shear areas were also specified based on the vessel type.

In the modified version of EFDC, during time steps when user-supplied bed shear stresses are greater than zero, the propwash shear stress replaces the EFDC-calculated hydrodynamic shear stress, and is used in the subsequent calculations of sediment flux to the water column. Essentially, this modification acts as a switch between hydrodynamic- and propeller-induced shear: If propwash is active, EFDC calculates sediment flux based on user supplied shear stress. Otherwise, EFDC calculates the sediment flux based on the hydrodynamic shear stress.

In EFDC, the shear stress is applied to the entire model cell to compute the sediment flux. However, the area of vessel-induced bed shear stresses is typically smaller than a model cell, thus the propwash shear stress should not be applied to the entire model cell (i.e., applying the propwash shear stress directly would result in over estimating the sediment flux). Hence, the sediment flux based on the propwash shear stress was scaled based on the propwash bed shear stress area. When the propwash is active, the sediment flux is scaled by the ratio of the shear stress area to the cell area. This modification does not account for the hydrodynamic sediment flux when the propwash is active. However, propwash is active for a relatively short time during the year-long simulations, and propwash shear stresses are much greater than hydrodynamic shear stresses. Thus, the sediment flux due to hydrodynamic shear stress is negligible when the propwash shear stresses are active.

To demonstrate the propwash effects, the WRAP Model organic chemical calibration period was simulated with and without propwash. An example of the effect of propwash at one location in Region 1 is shown in Figure C.9. In the figure, the comparison location is depicted in the lower left panel. The other panels show the comparison of TSS, PCB, and DDT concentrations for the bottom water layer adjacent to the sediment bed with and without propwash (blue line for no propwash and red line for with propwash). As shown in the figure, at the comparison location, TSS, PCB and DDT concentrations in the water column are relative stable under hydrodynamic only conditions (no propwash). With propwash, the water concentrations behave as expected, with large spikes in TSS, PCB, and DDT concentrations occurring when propwash is active. The water concentrations also show that TSS, PCB, and DDT concentrations rapidly decrease following the active propwash to the “no propwash” levels. This demonstrates that sporadic exposure to propwash does not lead to a significant sustained increase in sediment and organic contaminant concentrations. Comparison of the PCB and DDT concentrations indicate higher DDT concentrations for the same propwash spike because the sediment bed DDT concentration is significantly higher than the sediment bed PCB concentration at the comparison location. This illustrates that the propwash mechanism appropriately simulates the re-suspension of organic chemicals from the sediment bed.

C.6 REFERENCES

Blaauw, H.G. and van de Kaa, E.J. 1978. Erosion of bottom and sloping banks caused by the screw race of maneuvering ships. 7th International Harbour Congress, Antwerp, Belgium. May 22-26, 1978.

Blaauw H.G., van der Knaap, F.C.M., de Groot, M.T., and Pilarcyk, K.W. 1984. Design of Bank Protection of Inland Navigation Fairways. Publication No. 320, Delft Hydraulics Laboratory.

Verhey, H.J. 1983. The stability of bottom and bank subjected to the velocities in the propeller jet behind ships. 8th International Harbour Congress, Antwerp, Belgium, June 13-17, 1983.

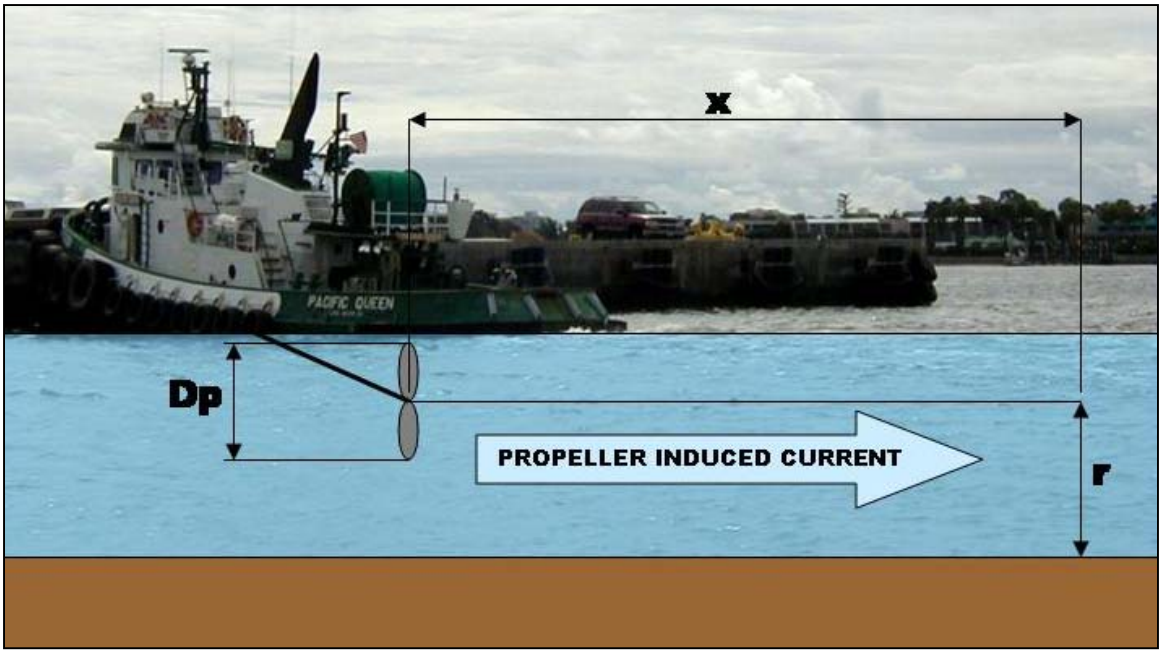

a) Vessel Properties for Propeller Induced Velocity

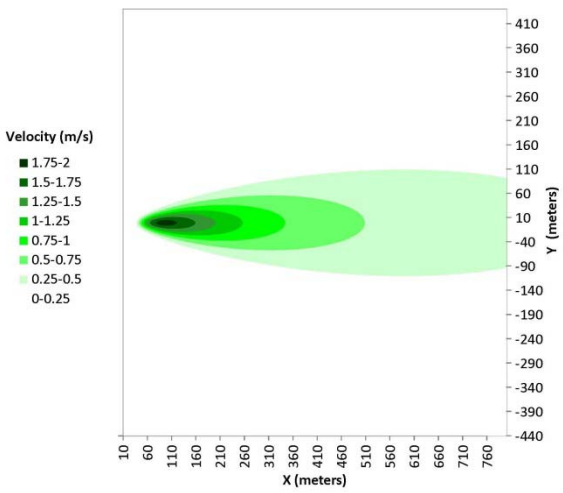

b) Propeller Induced Velocity Field for Container (4-8k TEU) Region 5

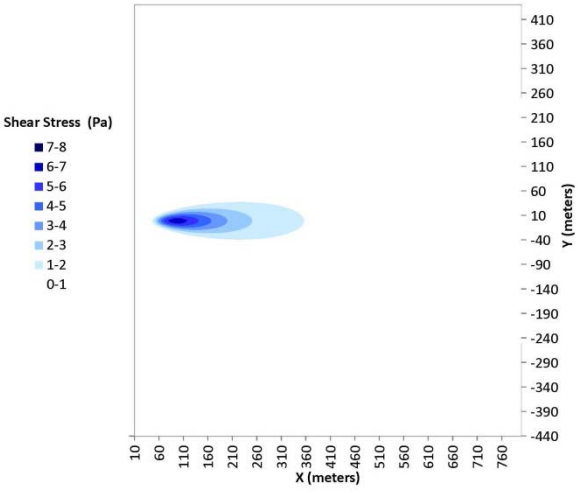

c) Propeller Induced Shear Stress Field for Container (4-8k TEU) Region 5

Figure C.1 Example of Propwash Velocity and Shear Stress Fields

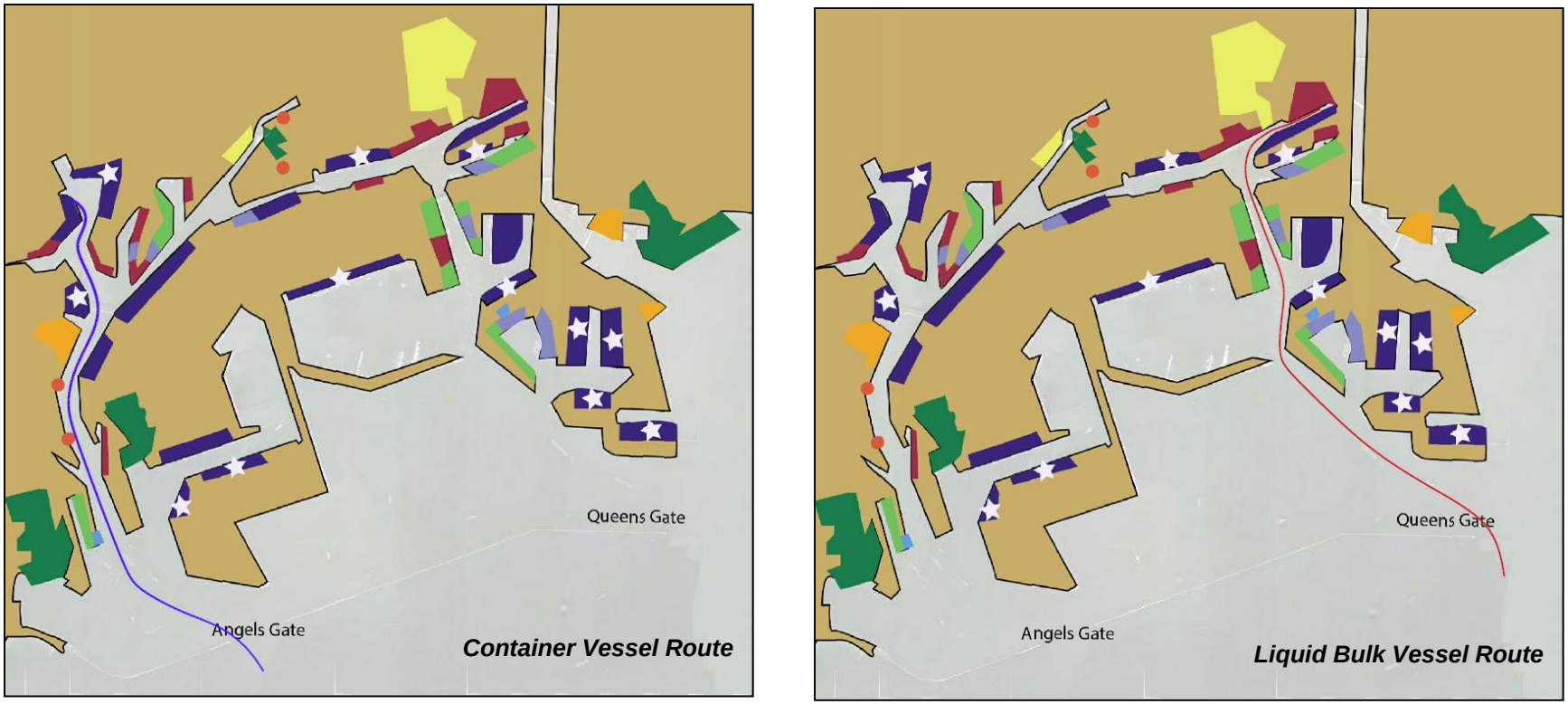

Figure C.2 Example Vessel Routes

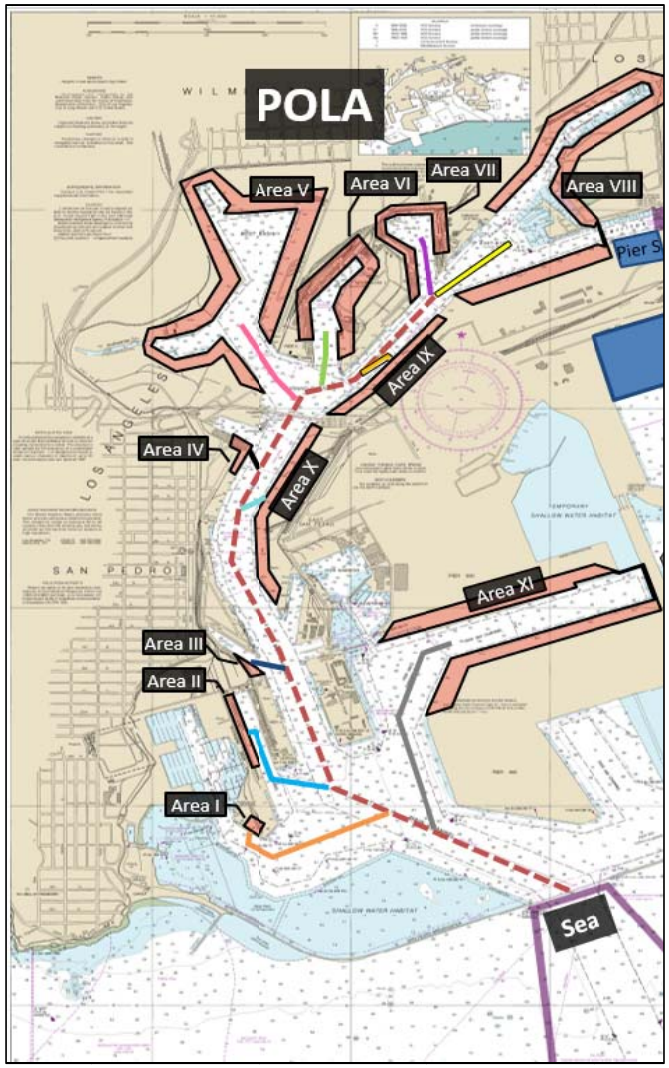

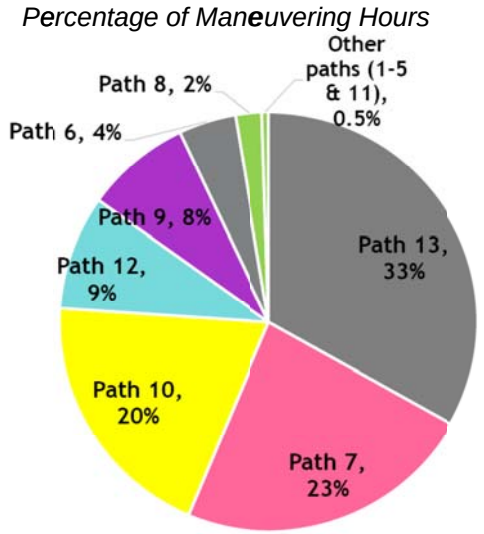

Path No.	To/From Area IDs			Berths
Path 1	Sea	↔	Anchor B	--
Path 2	Sea	↔	Anchor D	--
Path 3	Sea	↔	I	46
Path 4	Sea	↔	II	52,54-55
Path 5	Sea	↔	III	73A
Path 6	Sea	↔	IV	91-93A
Path 7	Sea	↔	V	100,118-149
Path 8	Sea	↔	VI	154-168
Path 9	Sea	↔	VII	176-189
Path 10	Sea	↔	VIII	196-198,207-214
Path 11	Sea	↔	IX	216-224
Path 12	Sea	↔	X	227-230,238
Path 13	Sea	↔	XI	301-305,401-406

Figure C.3 POLA Vessel Traffic Summary

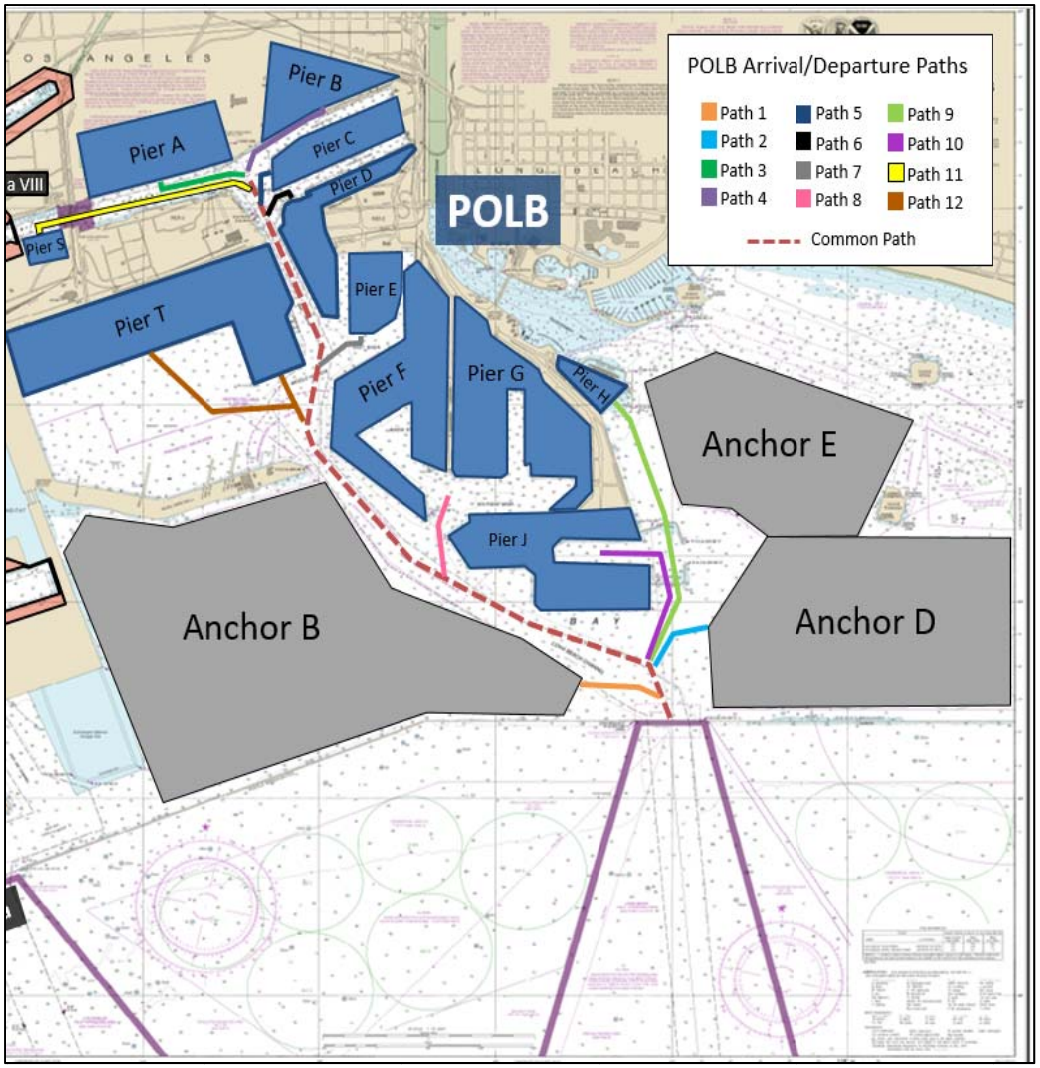

Percentage of Maneuvering Hours

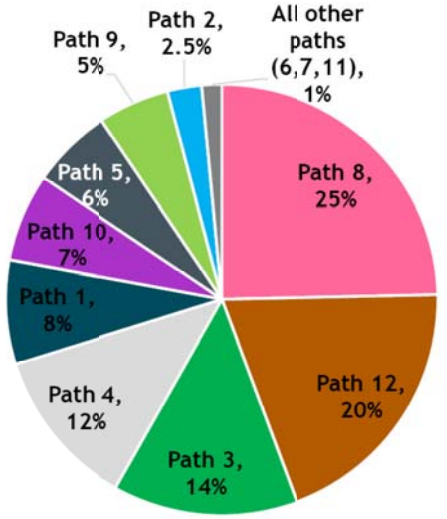

Path No.	To/ From Areas		
Path 1	Sea	↔	Anchor B
Path 2	Sea	↔	Anchor D
Path 3	Sea	↔	Pier A
Path 4	Sea	↔	Pier B
Path 5	Sea	↔	Pier C
Path 6	Sea	↔	Pier D
Path 7	Sea	↔	Pier E
Path 8	Sea	↔	Pier F/G
Path 9	Sea	↔	Pier H
Path 10	Sea	↔	Pier J
Path 11	Sea	↔	Pier S
Path 12	Sea	↔	Pier T

Figure C.4 POLB Vessel Traffic Summary

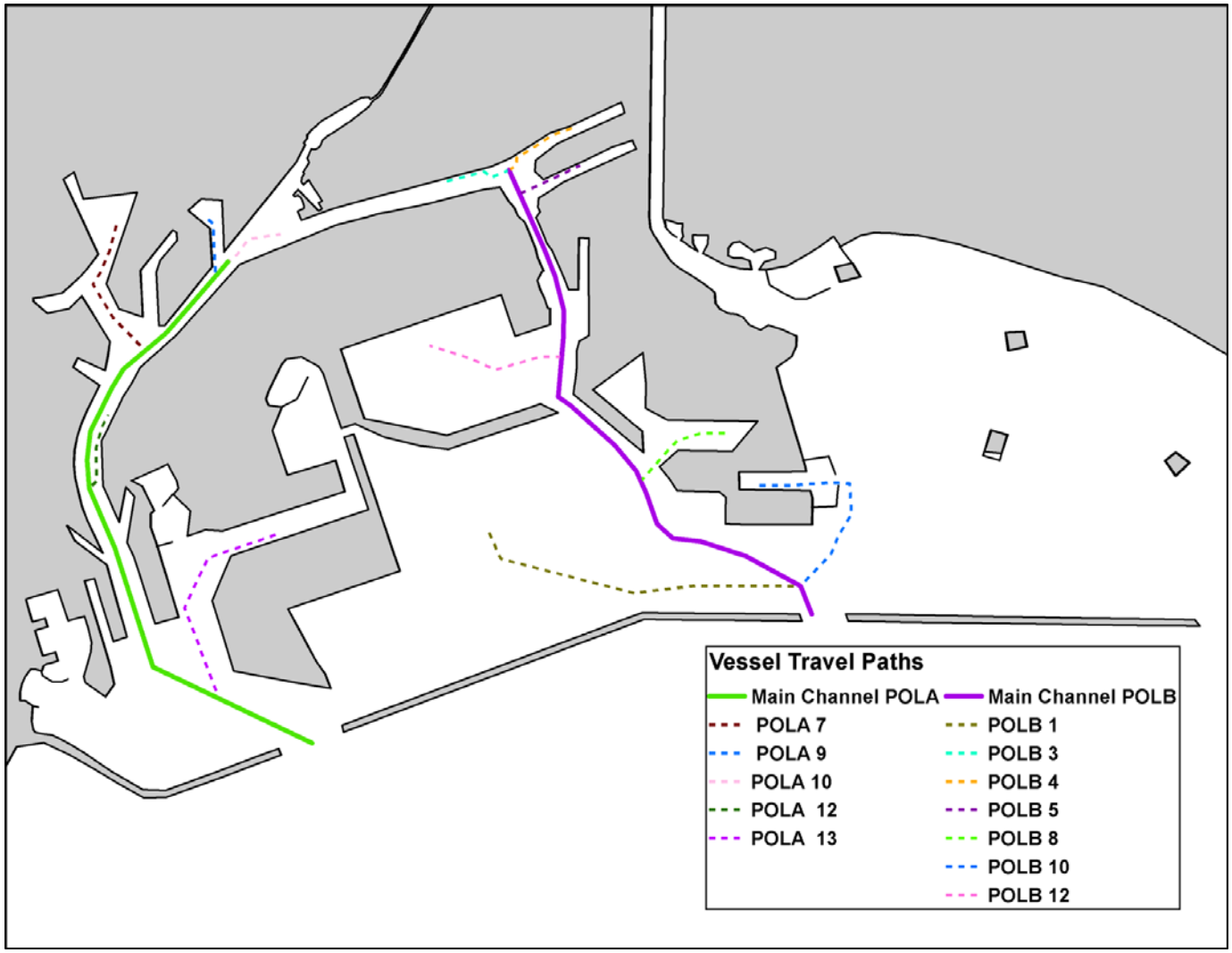

Figure C.5 Vessel Travel Paths

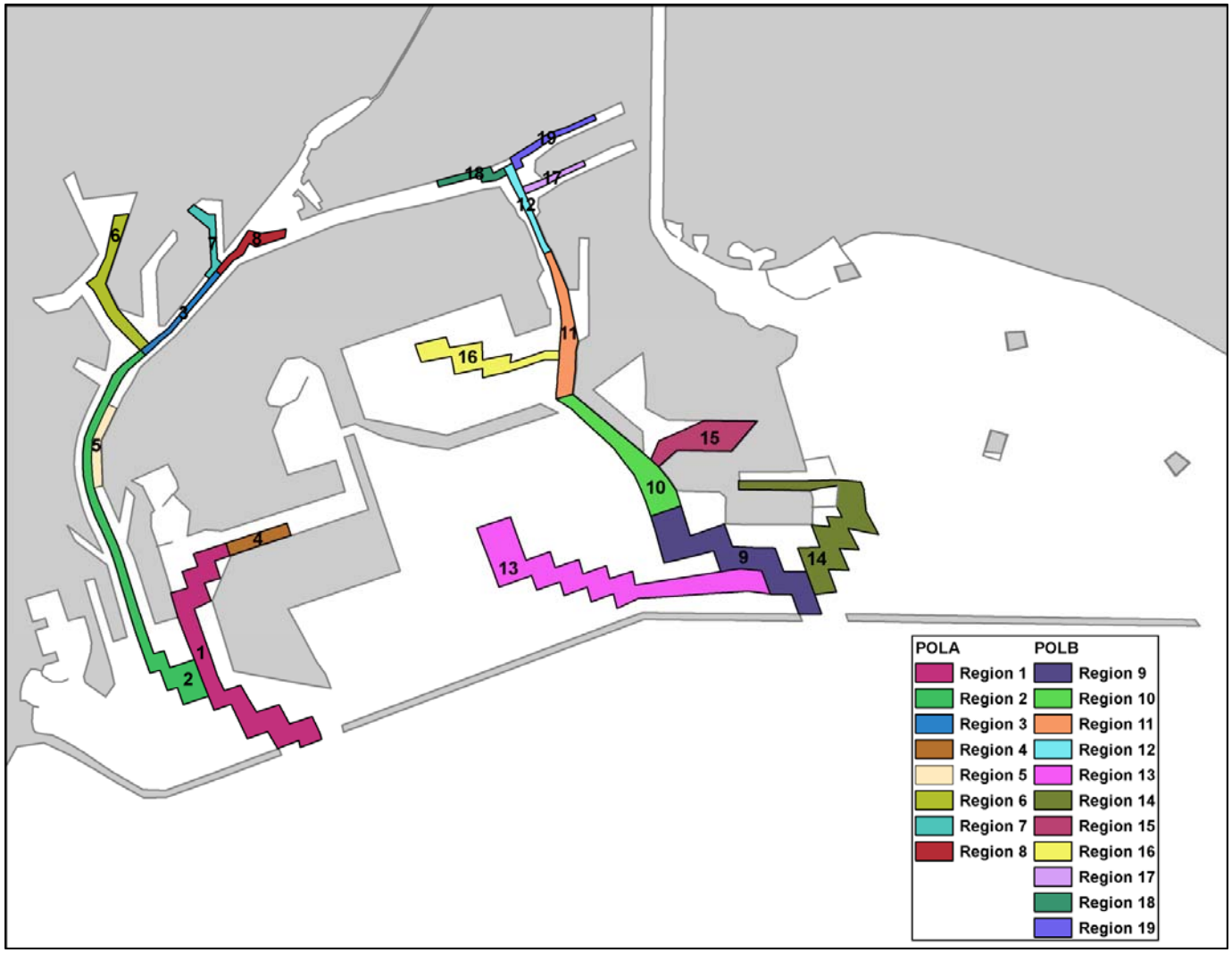

Figure C.6 Propwash Regions

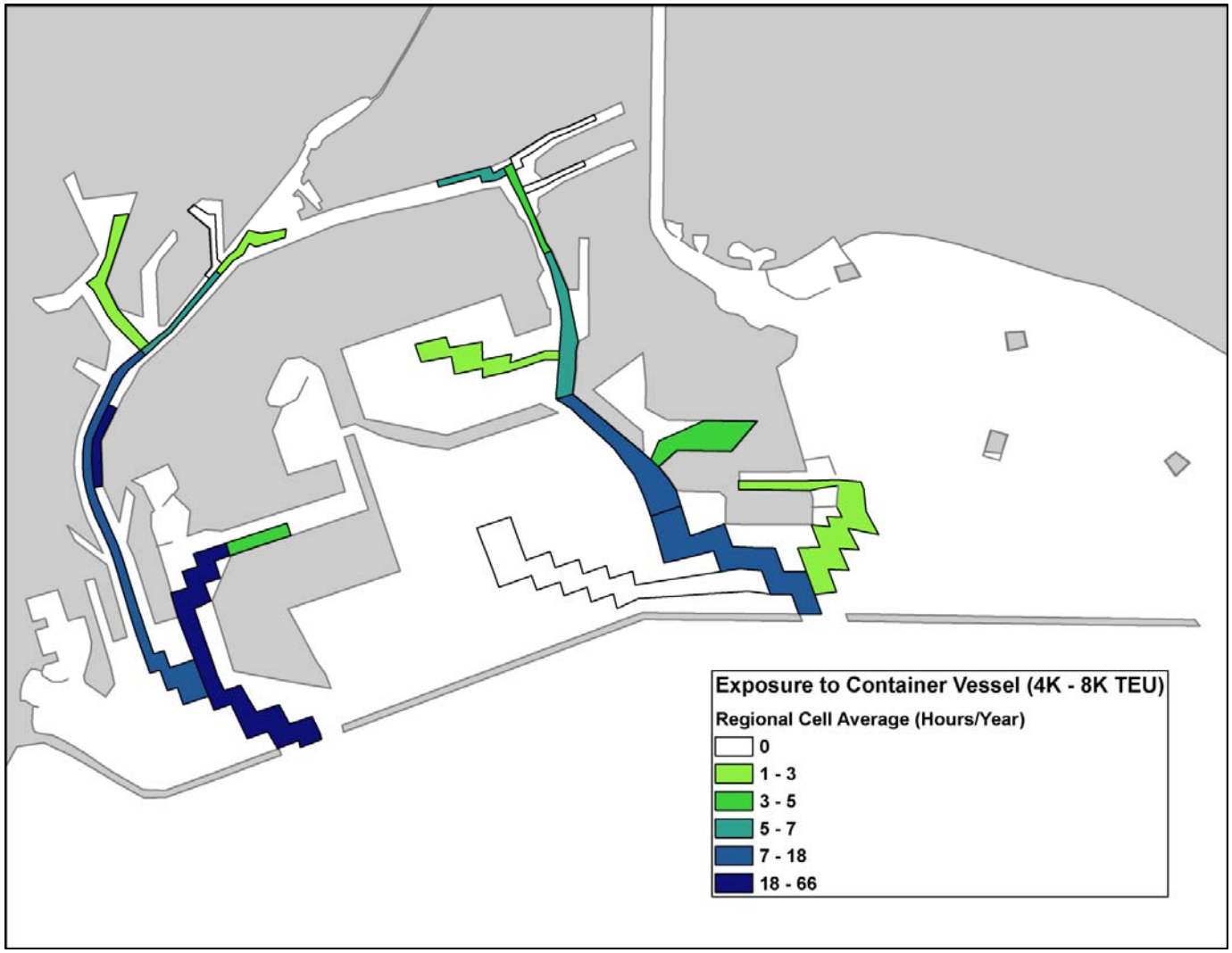

Figure C.7 Yearly Exposures by Region for Container (4-8k TEU) Vessel

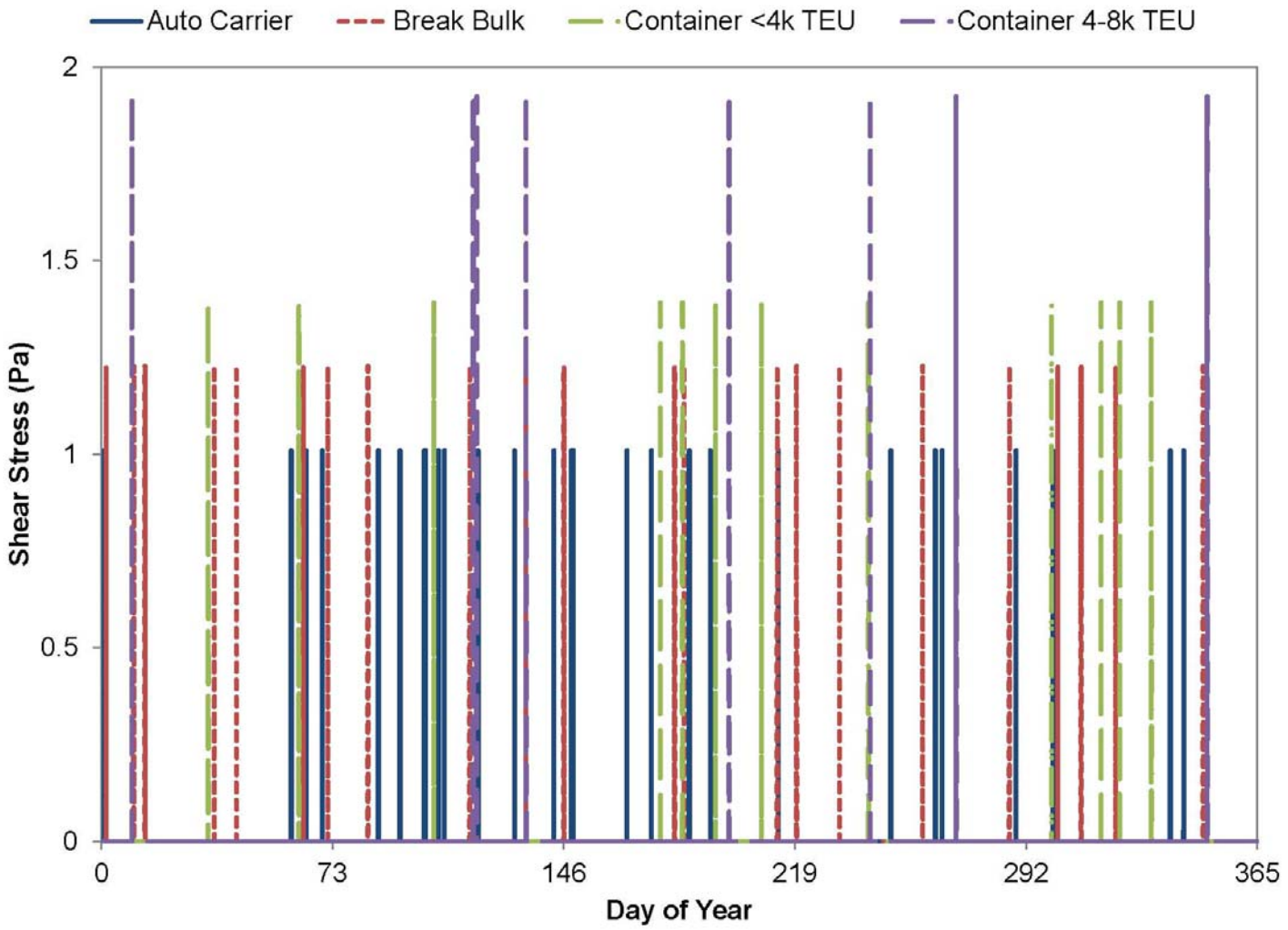

Figure C.8 Propwash Shear Stress for Region 15

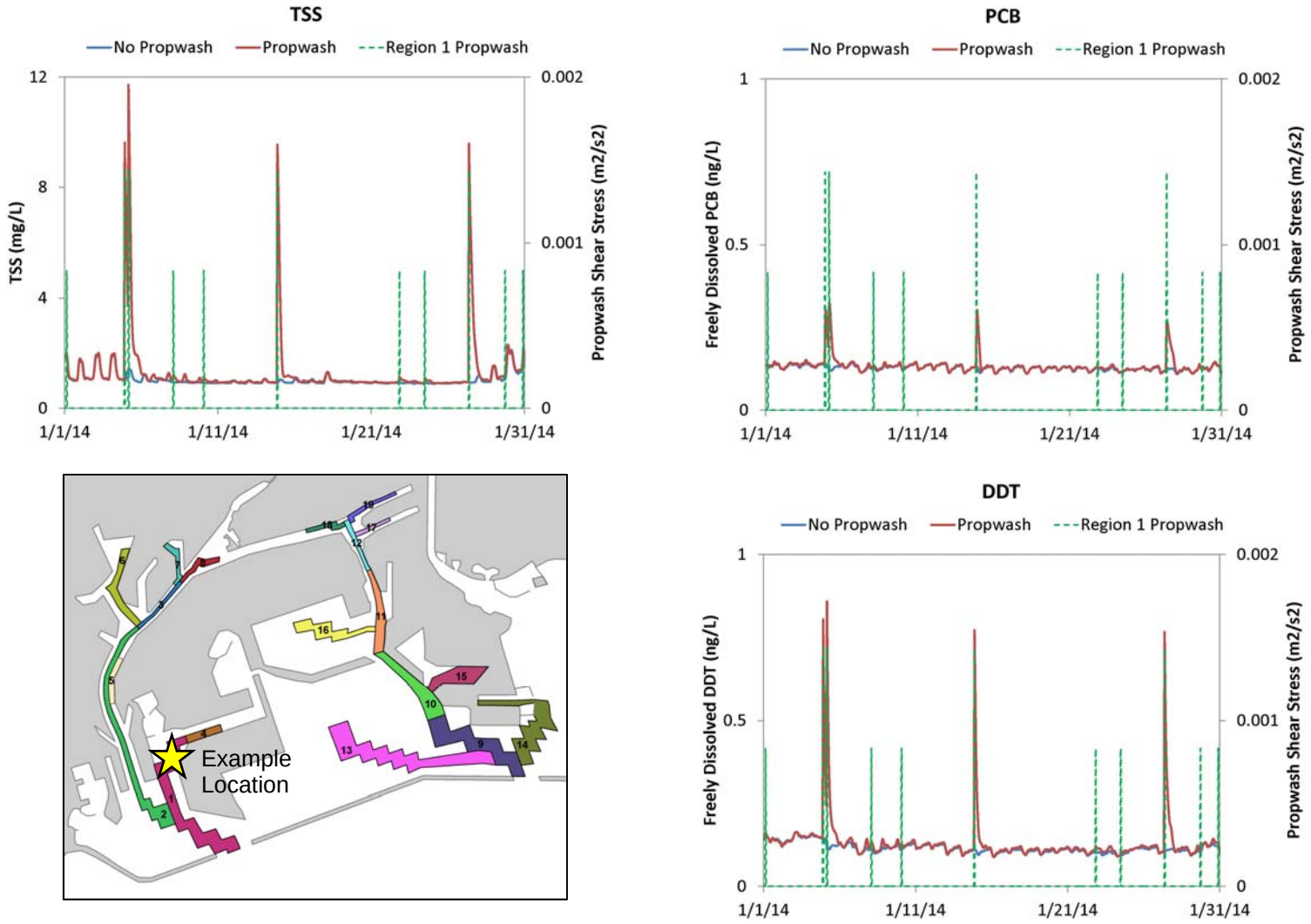

Figure C.9 Region 1 Example of Propwash Re-suspension

APPENDIX D

QUALITY CONTROL TESTS FOR ORGANIC TRANSPORT

D.1 BACKGROUND

The presence of errors in a model source code is difficult to evaluate in the context of a complex simulation and is easier to assess using simple test setup. Hence, several quality control tests were conducted on the WRAP Model to verify the key aspects of the model in simulating organic transport. These quality control tests, as summarized in Table D.1, focus on assessing the conservation of mass and sediment-water exchange of organics. These test simulations were conducted prior to the WRAP Model organics calibration, hence do not necessarily have the same calibrated model parameters shown in Section 8.

Table D.1 Summary of Quality Control Tests

QUALITY CONTROL TEST	PURPOSE
Conservation of Mass #1	Conservation of chemical mass to maintain mass
Conservation of Mass #2	Conservation of chemical mass with steady in increasing mass
Chemical Dissolved Phase Depuration	Evaluate chemical sediment-water exchange based on dissolved phase
Chemical Sorbed Phase Depuration	Evaluate chemical sediment-exchange based on particulate phase
Chemical Mass Balance – Water Column	Verify chemical mass in water column
Chemical Mass Balance – Sediment	Verify chemical mass in sediment bed

D.2 CONSERVATION OF MASS #1

This test was conducted to evaluate that chemical mass is conserved with a constant input of chemical mass into the model domain. For this test, a 60-day simulation was conducted with constant inflow with chemical concentrations of 1 ug/L. Initial water column, initial porewater, and boundary concentrations were all specified as 1 ug/L. In order to isolate effects to the dissolved phase, sorption (K_{poc} = 0 and K_{doc} = 0) and other chemical sinks (e.g., volatilization or degradation) were not simulated. This quality control test case was used to verify that both the water column and porewater concentrations remain constant (i.e. 1 ug/L). As illustrated in Figure D.1, both the water column concentrations (see upper left panel) and the porewater freely dissolved concentrations (see lower left panel) at 10 selected locations (see inset figure) remain stable throughout the simulation period.

D.3 CONSERVATION OF MASS #2

The second conservation of mass test was conducted based on increasing the chemical mass to reach a constant. A 120-day simulation was conducted with constant inflow and boundary chemical concentrations of 1 ug/L. Initial water column and initial porewater concentrations were specified as 0 ug/L. Again, sorption was not simulated (K_{poc} = 0 and K_{doc} = 0) and other chemical sinks (e.g., volatilization or degradation) were not simulated. Effectively, the chemical was added into the model domain via storm water inflows and the tidal exchange from the ocean boundary. This quality control test case was used to verify that water column and porewater concentrations will steadily increase to near steady state conditions, as shown in Figure D.2. In the figure, the daily averaged freely dissolved concentrations in the water column and porewater were determined for the same 10 locations as the earlier test. The water column concentrations show an increase in concentration over time to approach 1 ug/L in 120 days. The rate of increase differs for each zone due to varying mixing conditions. The faster increases in concentration are shown for the LARE, San Pedro Bay, POLA Outer, and POLB Outer, corresponding to area closest to storm water inflows (e.g., LAR) or the ocean boundary. The slowest increase in concentration was observed for Fish Harbor, which is more isolated from inflows and ocean boundary. For the porewater concentrations, increases in concentration occur more slowly compared to water column concentrations since porewater concentrations depend on the mass transfer coefficient between the sediment bed and water. Differences in the rate of increasing porewater concentrations correspond to varying mixing conditions in each zone.

D.4 CHEMICAL DISSOLVED PHASE DEPURATION

A 60-day simulation was conducted to verify that porewater concentrations follow an exponential decay as chemicals are diffused out of the sediment bed into the water column. For this test, an initial chemical mass was specified in the sediment bed such that the porewater concentration would have a value of 1 ug/L. The chemical within the sediment bed was allowed to equilibrate with no other chemical sources or sinks. Initial water column and all boundary concentrations were specified as 0 ug/L. Sorption (K_{poc} = 0 and K_{doc} = 0) and other chemical sinks (e.g., volatilization or degradation) were not simulated. This test case was designed to isolate the flux from the sediment bed into the water column, thus porewater concentrations should follow an exponential decrease over time, as shown in Figure D.3. As illustrated in the lower left panel, porewater concentrations at the 10 output locations decrease over time exponentially as expected. The corresponding water column concentrations are shown in the upper left panel.

D.5 CHEMICAL SORBED PHASE DEPURATION

The prior chemical depuration test was repeated to evaluate the sorbed phase depuration. An initial chemical mass was specified in the sediment bed such that the porewater concentration would have a value of 1 ug/L and the sediment bed was allowed to equilibrate with no other chemical sources or sinks. Initial water column and all boundary concentrations were specified as 0 ug/L. For this test, a hypothetical particulate organic carbon partition coefficient (K_{poc} = 0.1 mg/L) was used to allow sorption. Partitioning to dissolved organic carbon (K_{doc} = 0) and other chemical sinks (e.g., volatilization or degradation) were not simulated. This test case was designed to isolate the flux from the sediment bed into the water column, thus porewater concentrations should follow an exponential decrease over time, as shown in Figure D.4. Similar to the dissolved phase depuration test, the porewater concentrations also show an exponential decrease over time.

D.6 CHEMICAL MASS BALANCE – WATER COLUMN

This test was conducted to check that the total chemical mass in the model domain remains constant. For this test, an initial chemical mass of 1 kg was specified in the water column of an arbitrary cell located inside the harbor with little tidal mixing. The initial water column concentration was specified such that the total mass was 1 kg. All other initial water column and initial porewater concentrations were specified as 0 ug/L. Model inflow and boundary conditions were specified as 0 ug/L. Sorption (K_{poc} = 0 and K_{doc} = 0) and other chemical sinks (e.g., volatilization or degradation) were not simulated. A 10-day simulation was conducted to evaluate the transport and dispersion of the initial chemical mass, as illustrated in Figure D.5. A spatial map of the water column concentrations after 10 days is provided in the upper panel, which shows the dispersion of the initial chemical mass. The chemical mass balance is shown in the lower panel that indicates the chemical mass in the water column within the model domain remains constant.

D.7 CHEMICAL MASS BALANCE – SEDIMENT BED

A similar mass balance test was conducted with an initial chemical mass in the sediment bed. An initial chemical mass of 1 kg was specified in the surface sediment bed of an arbitrary cell located inside the harbor where little tidal mixing occurs. All other initial water column and sediment bed concentrations were specified as 0 ug/L. Model inflow and boundary conditions were specified as 0 ug/L. Sorption (K_{poc} = 0 and K_{doc} = 0) and other chemical sinks (e.g., volatilization or degradation) were not simulated. The transport and dispersion of the initial chemical mass was evaluated over a 10-day period, as shown in Figure D.6. Over time the chemical mass slowly moves from the sediment bed (orange line) into water column (blue line), as shown in the lower panel. The total chemical mass in the model domain is indicated by the black line and chemical mass transport out of the model

domain by the red line. The test result again indicates that the chemical mass within the model domain remains constant. The upper panel of the figure shows the spatial variation of the water column concentrations at the end of the 10-day simulation, illustrating the spreading of chemicals from the initial location through tidal mixing.

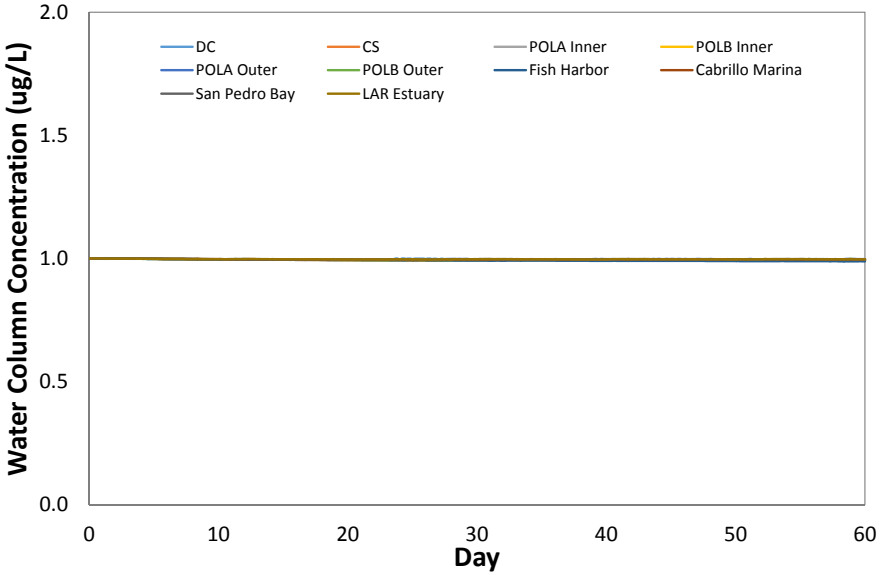

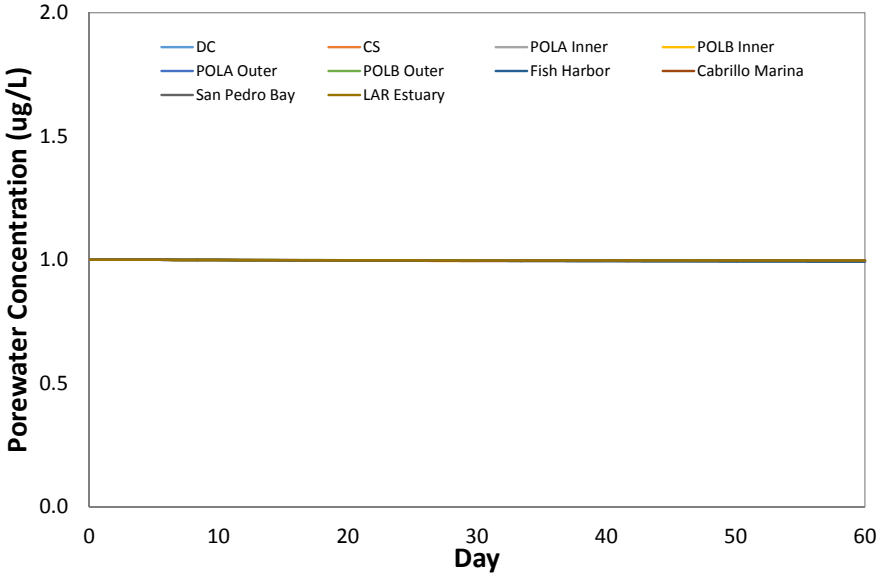

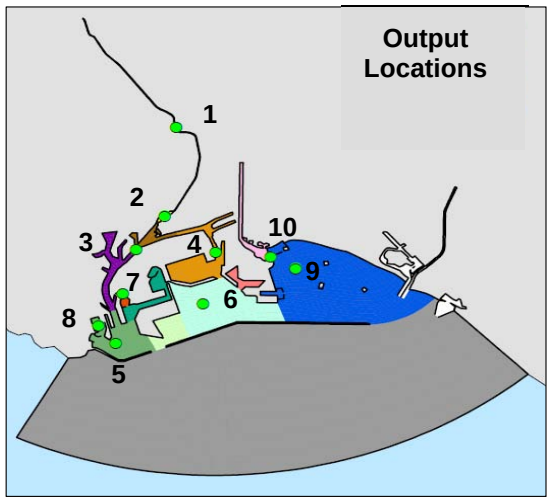

Output Locations

1 - Dominguez Channel (DC)
2 - Consolidated Slip (CS)
3 - POLA Inner
4 - POLB Inner
5 - POLA Outer
6 - POLB Outer
7 - Fish Harbor
8 - Cabrillo Marina
9 - San Pedro Bay
10 - LAR Estuary

Figure D.1 Quality Control Test: Conservation of Mass #1

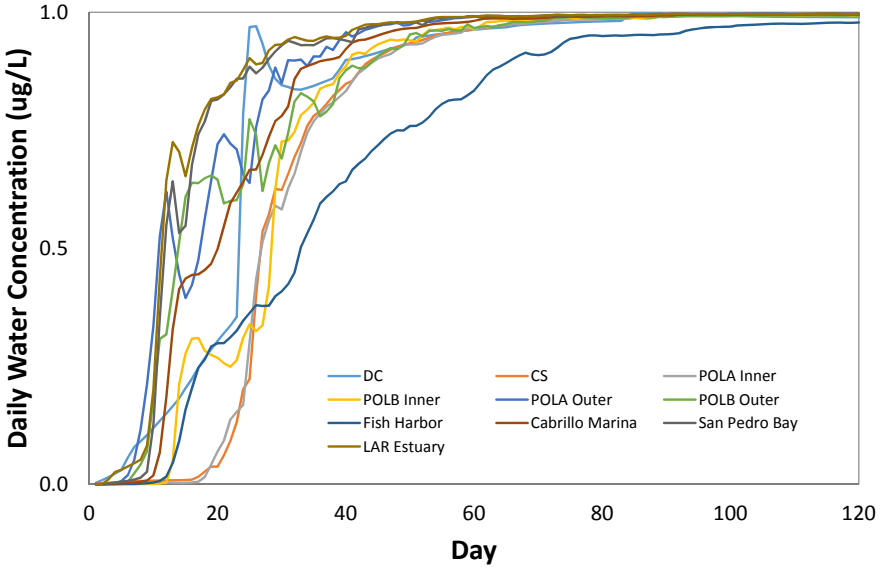

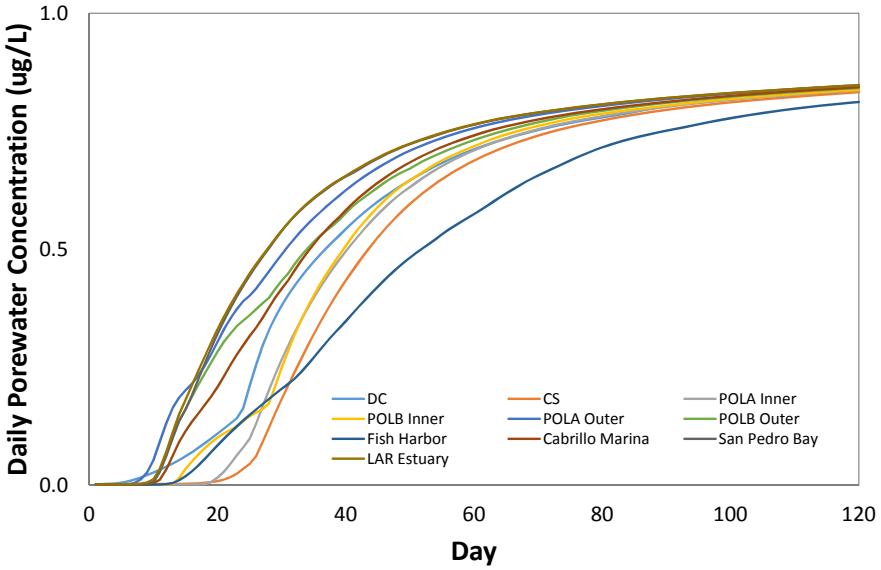

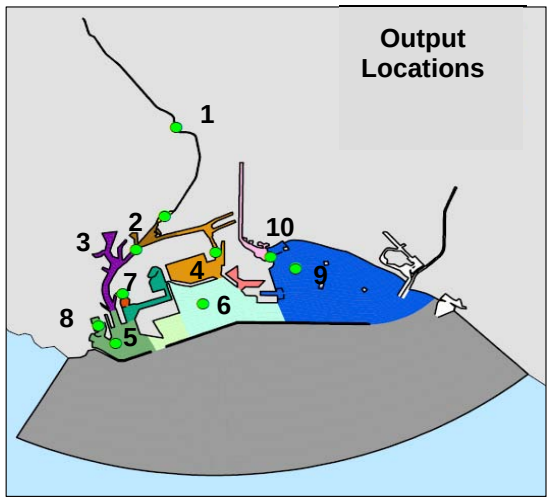

Zones

1 - Dominguez Channel (DC)
2 - Consolidated Slip (CS)
3 - POLA Inner
4 - POLB Inner
5 - POLA Outer
6 - POLB Outer
7 - Fish Harbor
8 - Cabrillo Marina
9 - San Pedro Bay
10 - LAR Estuary

Figure D.2 Quality Control Test: Conservation of Mass #2

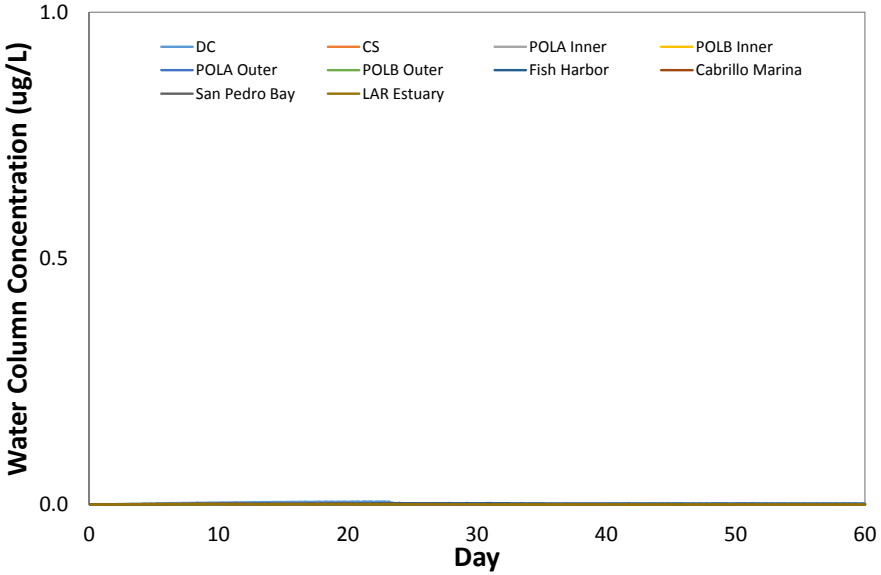

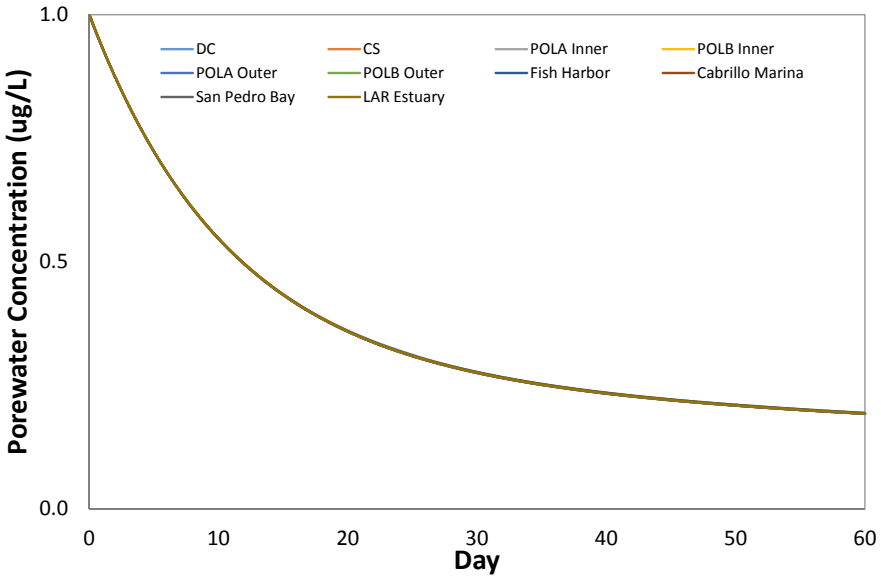

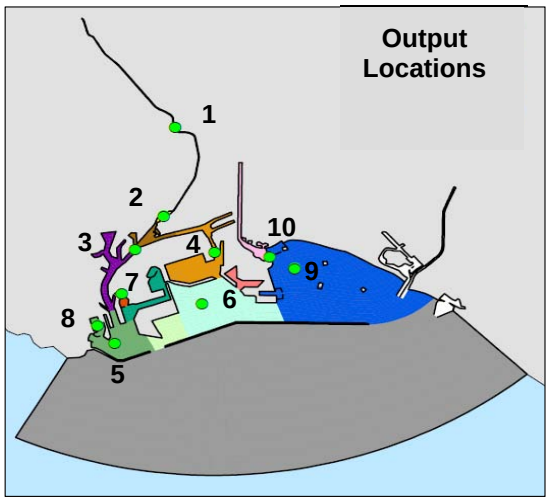

Output Locations

1 - Dominguez Channel (DC)
2 - Consolidated Slip (CS)
3 - POLA Inner
4 - POLB Inner
5 - POLA Outer
6 - POLB Outer
7 - Fish Harbor
8 - Cabrillo Marina
9 - San Pedro Bay
10 - LAR Estuary

Figure D.3 Quality Control Test: Chemical Dissolved Phase Depuration

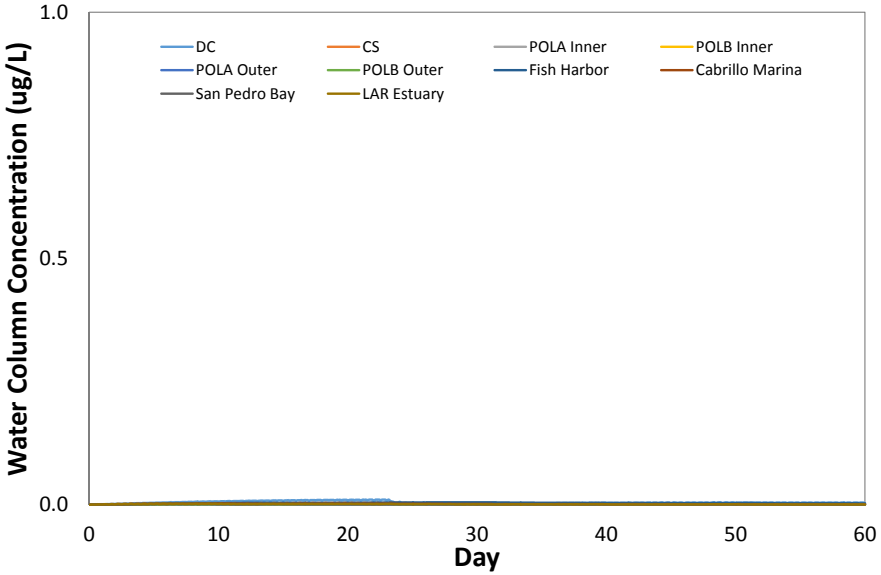

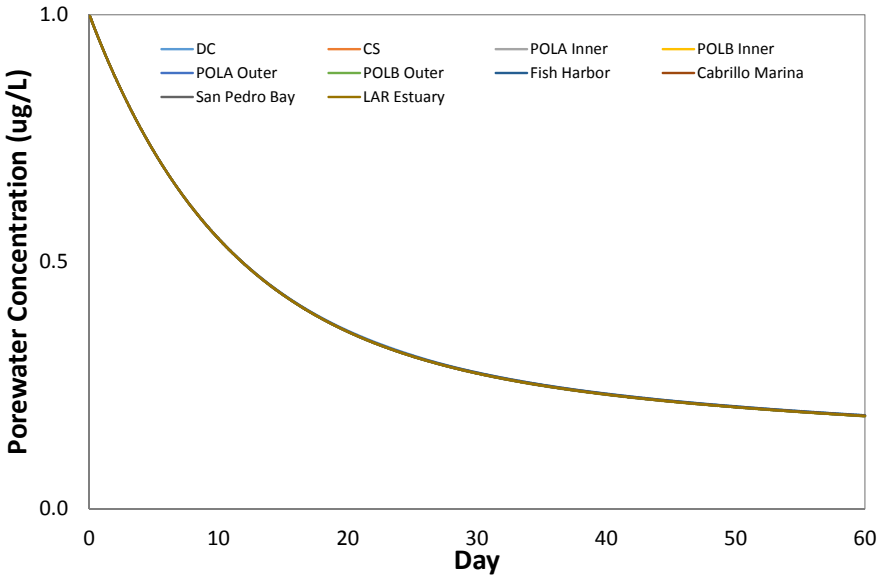

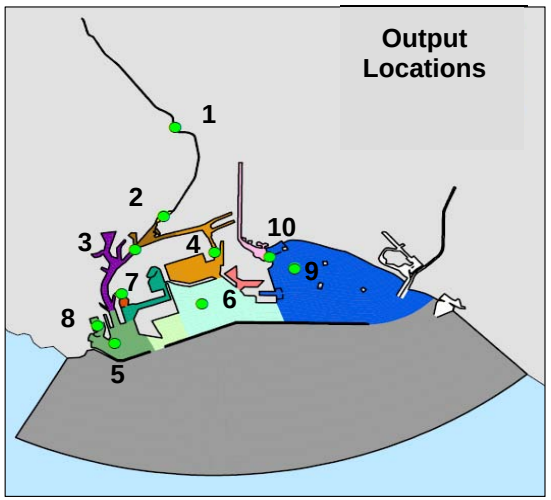

Output Locations

1 - Dominguez Channel (DC)
2 - Consolidated Slip (CS)
3 - POLA Inner
4 - POLB Inner
5 - POLA Outer
6 - POLB Outer
7 - Fish Harbor
8 - Cabrillo Marina
9 - San Pedro Bay
10 - LAR Estuary

Figure D.4 Quality Control Test: Chemical Sorbed Phase Depuration

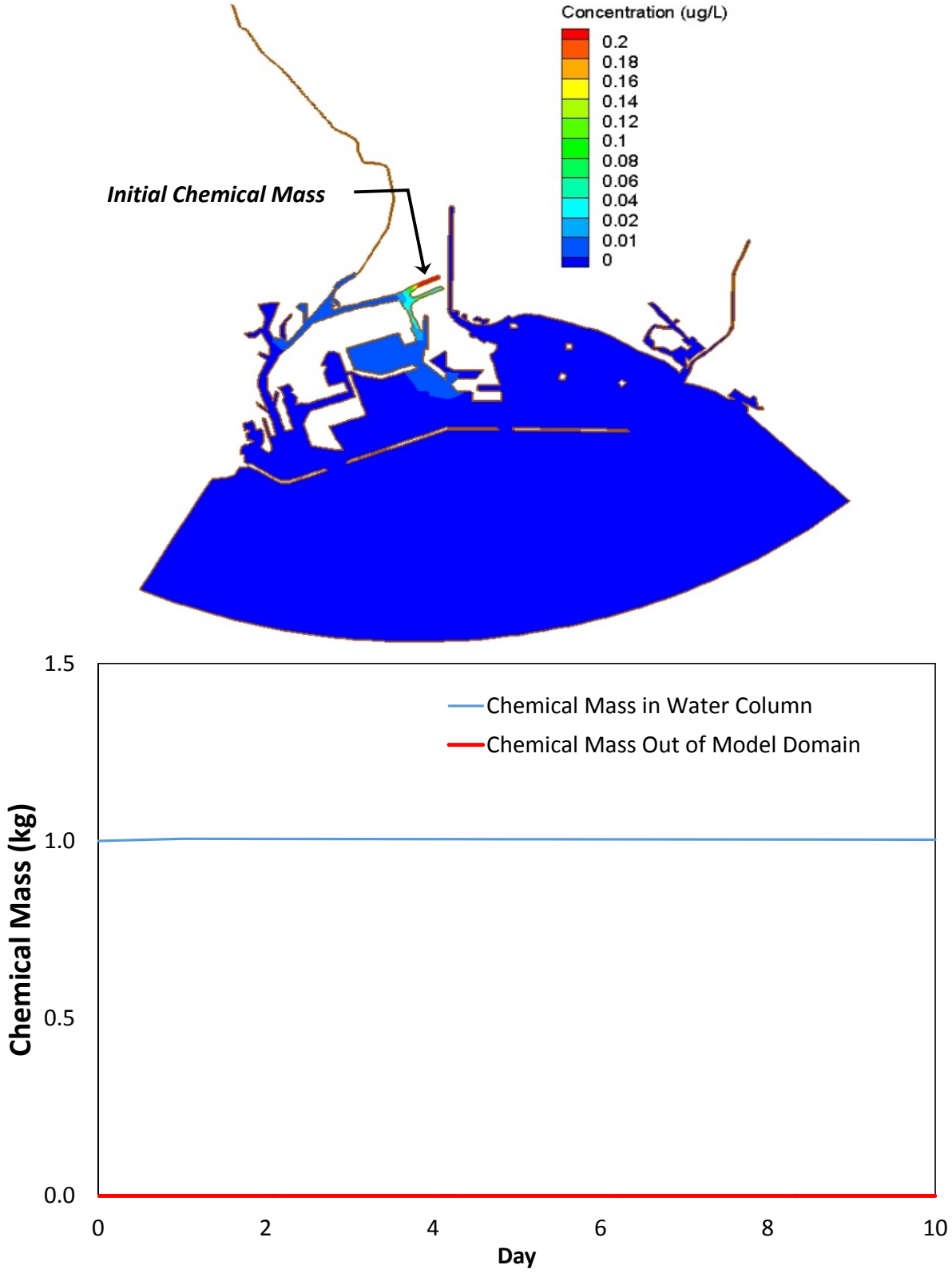

Figure D.5 Quality Control Test: Chemical Mass Balance - Water Column

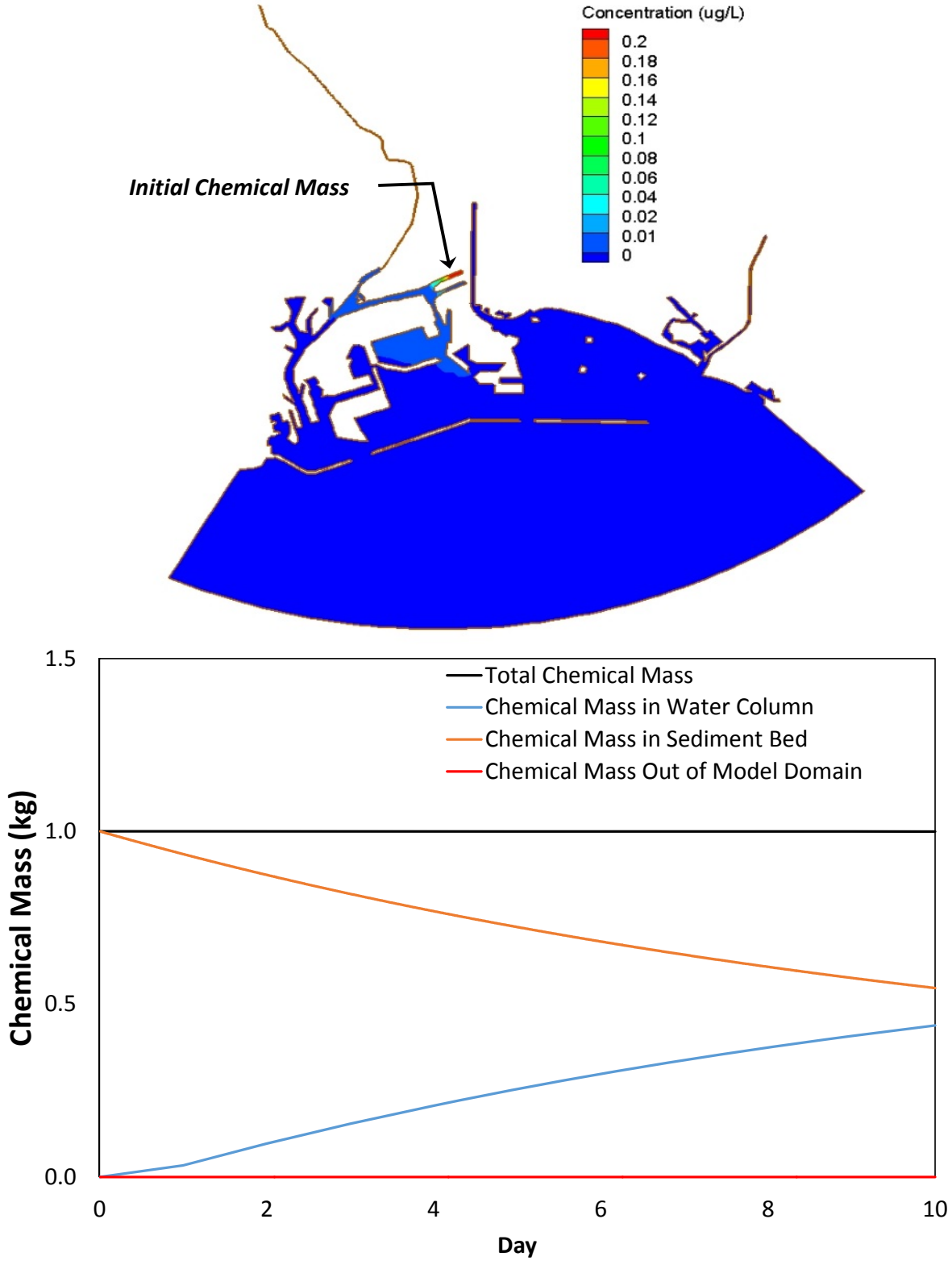

Figure D.6 Quality Control Test: Chemical Mass Balance - Sediment Bed